Unified Design Criteria for Steel Cantilever Plate Connection Elements

by

Pouya Salem

A thesis submitted in partial fulfillment of the requirements for the degree of

Doctor of Philosophy

in

STRUCTURAL ENGINEERING

Department of Civil and Environmental Engineering

University of Alberta

ABSTRACT

Steel cantilever plate connection elements are rectangular steel plates that are distinguished from other connection plates by their two opposite unrestrained edges. The increased length of cantilever plate connection elements in some connection configurations raises concern regarding the potential of instability of the plate. Fearing that the plate may buckle due to its increased length has led engineers to utilize stiffeners at the plate free edges, which results in a significantly increased fabrication cost.

The behaviour of steel cantilever plate connection elements is investigated through experiments and numerical simulation. Two connection configurations, including extended shear tabs and double-coped beams, are considered. The behaviour of the steel cantilever plate connection elements is evaluated by considering limit states, shear load eccentricity, and plasticity sequence. The effects of various variables on the response of the connection are also discussed.

Based on the studies, recommendations are provided to be used in the design of steel cantilever plate connection elements.

DEDICATION

To my dear parents and my loving wife

ACKNOWLEDGEMENTS

I wish to express my deepest gratitude to my dear parents for their endless and unconditional love. Words cannot describe my heartfelt feelings for them.

I am deeply grateful to my supervisor, Dr. Robert Driver, for his utmost sincere guidance, support, and kindness. He has had a great influence on my both personal and professional life. I was honoured to get the chance to achieve my Ph.D. degree under his supervision.

I would like to thank Dr. Matthew Eatherton from Virginia Polytechnic Institute and State University (Virginia Tech.) for serving as my external committee member. The suggestions and recommendations of other committee members, Dr. Roger Cheng, Dr. Carlos Cruz-Noguez, Dr. Ming Lu, and Dr. John A. Nychka are highly acknowledged.

I am greatly thankful to all my fellow graduate students in our research group, especially Dr. Amirhoushang Jamshidi, for their constructive comments and help.

Tests specimen donation by Waiward Steel LP. of Edmonton is highly appreciated.

Last but not the least, I am grateful to my dear wife, Saeideh, whose mental, emotional, and technical support has always been an invaluable gift in my life.

TABLE OF CONTENTS

LIST OF TABLES

LIST OF FIGURES

LIST OF SYMBOLS AND ABBREVIATIONS

A_b	=	nominal area of an individual bolt
BCK	=	buckling limit state
BF	=	bolt fracture limit state
c	=	cope length
C_b	=	moment gradient coefficient for lateral–torsional buckling
CFP	=	cope face plasticity limit state
CWT	=	column web tearing limit state
D	=	fillet weld leg size
d	=	beam depth
d_{bh}	=	bolt hole diameter
d_c	=	cope depth
d_p	=	extended shear tab depth
E	=	modulus of elasticity
e_{eff}	=	effective eccentricity
$e_{eff\text{-}cs}$	=	clear span effective eccentricity
e_g	=	geometric eccentricity
e_s	=	shear load eccentricity w.r.t. support
F_{cr}	=	flexural local buckling stress
f_d	=	adjustment factor for various effects in cope beams
F_u	=	ultimate stress
F_v	=	shear stress of an individual bolt
F_y	=	specified minimum yield stress
FY	=	flexural yielding limit state
GSP	=	gross section plasticity limit state
h_0	=	reduced beam depth in double-coped beams
L	=	extended shear tab unbraced length
M^B	=	moment at bolt line
M_{BG}	=	moment about the centroid of the bolt group
M^B_{Max}	=	maximum moment developed at bolt line
M_{max}	=	moment strength of bolt group in shear
M_n	=	nominal flexural strength

M_p	=	plastic moment
M_{pv}	=	plastic moment accounting for shear load
M_r	=	required moment
M^S	=	moment at support
M^S_{Max}	=	maximum moment developed at support
M_y	=	yield moment
N	=	nominal applied axial load
N_F	=	factored applied axial load
n_h	=	number of horizontal bolt lines
NSP	=	net section plasticity limit state
OPD	=	out-of-plane deformation limit state
PB	=	plate buckling limit state
P_r	=	required axial load
P_y	=	axial yield load
Q	=	yield stress reduction factor for plate buckling
R_r	=	required end reaction
R_y	=	factor to approximate probable yield stress
S	=	elastic section modulus
s	=	bolt spacing in horizontal direction
SC	=	shear capacity limit state
SFP	=	support face plasticity limit state
T	=	clear distance between W-shape web-to-flange fillets
t_{max}	=	maximum permitted plate thickness
t_p	=	plate thickness
t_w	=	web thickness
V	=	vertical load
V_{BG}	=	shear capacity of bolt group
V_{CW}	=	column web shear yielding capacity
V_{LTB}	=	nominal shear load in absence of stabilizer plates
V_{Max}	=	peak vertical load
V_{MN}	=	flexural shear capacity of the plate
V_n	=	shear yield strength
V_r	=	required shear
w	=	column web thickness

WR	=	weld rupture limit state
X_u	=	ultimate tensile strength of weld filler metal
Z	=	plastic section modulus
λ	=	slenderness parameter
σ_n	=	normal stress
ϕ	=	plate resistance factor
ϕ_b	=	bolt resistance factor, flexure resistance factor
ϕ_v	=	shear resistance factor

CHAPTER 1: INTRODUCTION

1.1 Statement of Problem

In steel structures, different connection configurations are designed to satisfy specific expectations. In a vast range of conventional steel frames, connections designed to transfer only gravity loads from beams to columns (shear or simple connections) are by far the most common. As a result, the design efficiency of these connections has a significant impact on the cost efficiency of the whole structure and a thorough understanding of their behaviour is critical to the safety of the occupants. A number of different configurations are proposed for shear connections, namely, single angles, double angles, shear tabs (single-plate shear connections), etc. Amongst the several configurations possible, shear tabs have gained considerable popularity in design and practice due to their relatively low fabrication cost and erection simplicity. They consist of a single plate welded vertically to the support and bolted to the beam web. A typical shear tab is shown in Figure 1-1.

Figure 1-1: Typical shear tab
Source: www.microstran.com.au

In many common cases, however, problems arise when framing the beam into the web of the column or when the beam is framed into the web of a girder of the same size. As illustrated in Figure 1-2, in these cases, either the shear tab must be extended

or the beam should be coped to move the supported member clear of the support and simplify the framing. The modified configurations are called “extended shear tab” (Figure 1-2(a)) and “double-coped beam” (Figure 1-2(b)), respectively.

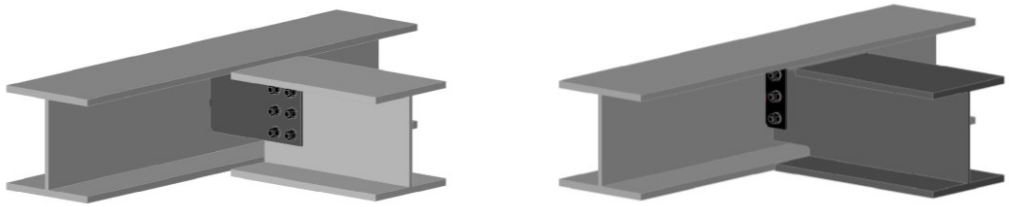

(a) (b)

Figure 1-2: Beam framing into the web of a similarly sized beam using:
(a) Extended shear tab; (b) Double-coped beam

The two configurations are examples of steel connections where cantilever plate connection elements are being used. Cantilever plate connection elements are steel plates, which are distinguished from other connection plates by their two opposite unrestrained edges. The increased length of cantilever plate connection elements in some connection configurations raises concern regarding the potential of instability of the plate. Fearing that the plate may buckle due to its increased length has led engineers to utilize stiffeners at the plate free edges, which results in an increased fabrication cost. Moreover, recent research at the University of Alberta (Thomas et al. 2014) has revealed that these stiffeners alter the behaviour of the connection substantially, and in some situations can even be detrimental to the performance of the connection.

According to the aforementioned discussion, the behaviour of cantilever plate connection elements is investigated both experimentally and through computer simulations. A detailed and comprehensive finite element model is generated, validated and justified by comparison to the results of full-scale tests from a recent Master’s research project (Thomas et al. 2014) on extended shear tabs conducted at the University of Alberta. The model is then used to study the influences of numerous design parameters on the behaviour of cantilever plate connection elements through a

comprehensive parametric investigation. A new full-scale test program that answers additional questions related to the failure modes, ultimate capacity, ductility, and the load–deflection relationship of the connections is developed and conducted.

To extend the scope of the study, a broader range of steel connections is considered. Test results of a Master's research project on the behaviour of double-coped beams (Johnston et al. 2015) are used to identify the similarities in the behaviour of cantilever plate connection elements as components of double-coped beams. Again, a finite element model is developed and verified using available test data. Comprehensive parametric analyses are conducted on double-coped beams.

1.2 Objectives and Scope

The main objective of this research is to evaluate the behaviour of cantilever plate connection elements, which can be used as a part of a variety of steel connections. Two major configurations are considered in this study—extended shear tabs and double-coped beams—in both of which cantilever plate connection elements act as the principal connection element. The results of this study are used to propose guidelines to be considered in the design of cantilever plate components in steel connections.

The scope of the research consists of:

- developing a finite element model to study the behaviour of extended shear tabs and using the available test data to verify and validate the modelling procedure and results;
- defining and conducting a new full-scale test program on extended shear tabs to identify the effect of some key parameters not investigated previously on the behaviour of the connection, and using the results to further verify the finite element model;
- using the verified finite element model to investigate different parameters affecting the behaviour of extended shear tabs;

- developing and validating finite element models to study the performance of cantilever plate connection elements as components of double-coped beams using the available test data;
- conducting an extensive parametric study on the parameters affecting the behaviour of double-coped beams;
- identifying the similarities of the behaviour of cantilever plate connection elements in different connection configurations;
- unifying the results acquired from investigations of the behaviour of cantilever plate connection elements as components of different connection configurations; and
- proposing recommendations for the design of cantilever plate connection elements applicable to a wide range of such elements present in steel connections.

1.3 Organization of Chapters

This report is organized into seven chapters. Chapter 2 covers the relevant available literature on both extended shear tabs and double-coped beams. In addition, current design recommendations for these two types of cantilever plate connections are reviewed.

The new test program conducted on extended shear tabs is discussed in Chapter 3. Test specimen details, including geometry and material properties, are presented, followed by descriptions of the test set-up, instrumentation, and loading procedure. The results achieved from the tests are also presented in this chapter, including the extended shear tab behaviour, vertical load–vertical displacement response, observed limit states, plasticity development along the plate, and shear load eccentricity. The effects of key variables on the behaviour of extended shear tabs are discussed, followed by comparisons between of the test results and the predictions of two current design recommendations.

Chapter 4 includes the development of a finite element model capable of accurately capturing the nonlinear behaviour of extended shear tabs. Complex aspects of the

model development are addressed. The model is validated using the existing test data. A comprehensive parametric study is then conducted on extended shear tabs using the developed model. Selected model details, including geometry and material properties, are presented, followed by introducing the model assembly, loading, analysis procedure, and data extraction. The results achieved from the parametric study are presented, including the extended shear tab behaviour, vertical load–vertical displacement response, observed limit states, plasticity development along the plate, and shear load eccentricity. The effects of key variables on the behaviour of extended shear tabs are discussed, followed by a comparison between the analysis results and recently proposed design recommendations.

Chapter 5 covers the finite element model development for double-coped beams and the comprehensive parametric study performed on this connection type. Chapter details are the same as those of Chapter 4.

Chapter 6 summarizes the results achieved from the test program and finite element studies on extended shear tabs and double-coped beams. Similarities between the behaviour of the two types of connections are discussed and recommendations are provided for a unified design procedure for cantilever plate connection elements. These design recommendations are compared with test results from the current study, as well as two previous studies on extended shear tabs and double-coped beams.

Conclusions achieved through this study are summarized in Chapter 7, and recommendations for further research on this topic are provided.

CHAPTER 2: BACKGROUND AND LITERATURE REVIEW

2.1 Introduction

The main purpose of this research program is to evaluate the behaviour of extended shear tabs and double-coped beams and to define the similarities between the behaviour of these two connection configurations. Comprehensive background information is needed to be able to identify the gap in the current knowledge and identify the shortcomings of current design methods. In this chapter, a number of previous research programs on extended shear tabs and double-coped beams are reviewed. Emphasis is placed on the more recent research studies. Finally, current significant design recommendations adopted widely within the steel industry for both connections are discussed.

2.2 Extended Shear Tabs

2.2.1 Sherman and Ghorbanpoor (2002)

One of the most comprehensive studies on extended shear tabs was performed by Sherman and Ghorbanpoor (2002) at the University of Wisconsin-Milwaukee. The main purpose of this study was to develop a design procedure for extended shear tabs. The aims of the study were to:

- evaluate the capacity of extended shear tabs;
- determine the critical limit states associated with conventional shear tabs that are applicable to extended shear tabs;
- identify any additional limit states;
- define the location of the point of inflection along the extended shear tab; and
- recommend a uniform design procedure for extended shear tabs.

All specimens had one vertical bolt line. The test matrix consisted of 31 full-scale tests conducted in three phases. In the first phase, 17 tests were performed in two groups: stiffened and unstiffened shear tabs. Four tests were conducted on unstiffened

shear tabs, including two on specimens welded to a column web and two welded to a plate girder web. The remaining 13 tests were divided into five and eight tests with stiffened plates welded to a column web and plate girder web, respectively. The behaviour and capacity of the connections were studied as a function of the following parameters: span-to-depth ratio of the supported beam, width-to-thickness ratio of the support member web, shear tab depth, thickness and length, number of bolts, hole type (standard or short slots) and existence of lateral bracing of the beam.

The second phase of the study, which consisted of four tests, focused on the effect of bolt tightening, use of either one or two stiffeners, and the stiffener plate behaviour on the capacity and behaviour of the extended shear tabs.

Ten tests were conducted in the third phase. This phase aimed to investigate the effect of the same parameters as in the first phase, but in deeper connections having six and eight bolts.

For each test, the shear load–displacement, shear load–twist, and shear load–rotation curves were derived. The curves were used to identify the point at which the connection behaviour became nonlinear, the ultimate shear capacity, and the primary failure mode. A number of conditions including shear distortion of the shear tab, twisting of the shear tab, and the yield line mechanism of the support member were observed to trigger connection nonlinear behaviour. The researchers investigated shear load eccentricity, ultimate shear load and the failure mode of the connection.

Eccentricity is defined as the distance from a reference point to the point of zero moment. The reference point is usually taken as the bolt line or centre of the bolt group. The reaction eccentricity is dependent on a number of factors including the number of bolts, the relative flexibility or rigidity of the supporting member, the thickness and proportions of the shear tab, the extent of bolt tightening and the amount of rotation at the support. It was observed that the eccentricities obtained for both unstiffened and stiffened connections do not correlate well with the values recommended by AISC (1994) for either rigid or flexible supports. Moreover, the AISC eccentricity values were in most cases greater than those obtained from the experiments. Using greater eccentricities led to a more conservative design.

The ultimate connection shear capacity was considered to be reached when the shear distortion curves reached their peak load or when the connection underwent considerable yielding without any further load increase. The anticipated failure modes for plate connections include bolt shear, bolt bearing, gross section yield, net section rupture, block shear and weld shear (Sherman and Ghorbanpoor 2002). However, new failure modes were observed during the tests including weld failure by tearing, plate buckling, tearing of the extended plate, bolt fracture, web shear and column web mechanism.

A number of observations and conclusions were made resulting from this study:

- Using measured eccentricities resulted in a much better calculation of the connection capacity compared to the capacities achieved by using the AISC recommended design eccentricity (to the face of the support).
- AISC eccentricities always produced bolt shear as the critical limit state, whereas measured eccentricities often predicted plate yielding as the critical limit state.
- Using AISC eccentricities produced conservative capacity results.
- Changing the design eccentricity can change the critical limit state.
- An additional limit state, web mechanism failure, must be considered for slender-web column supports.
- Another additional limit state, twisting of the shear tab, was identified as either the primary or secondary failure mode for nearly all the unstiffened tests.
- In the stiffened tests, the stiffeners' characteristics, such as thickness and welding details, did not affect the connection capacity.

Based on the results of this study, a design procedure considering the new observations was provided by the researchers.

2.2.2 Goodrich (2005)

The behaviour of stiffened extended shear tabs was investigated by Goodrich (2005). The study was primarily conducted to determine the role of stabilizer plates in extended shear tabs. The objectives of this study could be listed as:

- evaluating the practice of shear tab design at the time (AISC 2005);
- proposing a design method for extended shear tabs;
- testing full-scale extended shear tabs designed based on the proposed method;
- conducting finite element analyses on the test specimens;
- evaluating the test data and finite element analysis results; and
- making recommendations on the design of extended shear tabs.

Goodrich suggested three main points for the design of extended shear tabs:

- using the standard shear tab design tables to determine the shear plate thickness, number of bolts and plate-to-column weld size;
- sizing the stabilizer plate thickness to be at least 1.5 times the shear tab thickness; and
- sizing the stabilizer plate weld size to be 75% of the stabilizer plates' thickness and to be at least twice the plate-to-column weld size.

A series of six tests was conducted. The test setup consisted of a beam bolted to the shear tab, loaded using a series of concentrated loads defined such that they represent a uniformly distributed load applied to the beam span. Connection capacity and failure mode were investigated. A number of specimens failed due to buckling of the shear tab. Numerical modelling of the connections was also performed and validated by comparison to the test data.

2.2.3 Metzger (2006)

The performance of shear tabs designed in accordance with the 13th edition of the *Steel Construction Manual* (AISC 2005) was investigated by Metzger (2006). The study consisted of eight full-scale tests, including four conventional and four

extended shear tabs. The points of concern were the connection capacity, failure mode and rotational ductility. The test results were compared with the values predicted by the AISC method.

The specimens were loaded through a simulated uniformly distributed load on the beam. In the first test, the rotation of 0.03 radians, which was considered as the goal for connection ductility, was achieved. Significant vertical deflection occurred in the beam. No deformation was observed in the bolts or at the bolt holes. No yielding was observed in the shear plate. In the second test, failure occurred when the plate-to-column flange weld ruptured. Significant deformations occurred in the beam; however, like the previous test, no deformation occurred in the bolts, at the bolt holes, or in the plate. Based on the experimental results, the researchers concluded that in most cases the capacity predictions made by AISC are overly conservative and a more realistic bolt group shear load eccentricity should be defined to achieve a more economical design.

2.2.4 Rahman et al. (2007)

A 3D finite element model was developed by Rahman et al. (2007) to validate the test results of Sherman and Ghorbanpoor (2002). This model could be used to analyze a number of different connection configurations and other loading scenarios.

Four element types were used in the model:

- three dimensional, 8-node, brick elements to model the beam, supporting members and the shear tab;
- three dimensional, 10-node, tetrahedral elements to model the bolts;
- pretensioning elements to model the pretension force in the bolts;
- contact elements to simulate contact surfaces between connection components.

The load was applied in three steps:

1. applying pretension force to the bolts in order to establish contact between the surfaces. Several pretensioning forces were applied starting from 22 kN

(5 kips) and ending with 133 kN (30 kips). The optimum pretensioning force was chosen as the force that correlates the finite element results with the experimental results.

2. converting the stresses due to pretensioning force into strain.
3. applying shear load to the connection.

Several parameters were considered in studying the behaviour of unstiffened extended shear tabs. The parameters included: vertical displacement of the connection along the bolt line, shear load eccentricity relative to the connection bolt line, twisting of the connection plates, nonlinearity and failure modes.

Shear load–vertical displacement curves were used to determine the connection ultimate capacity. They were also used to indicate the point at which the connection behaviour became nonlinear.

The eccentricity was determined at each shear value. It was observed that eccentricity obtained from finite element models correlated well with the experimental values except for the early loading steps in which eccentricity was subjected to fluctuations due to bolt slip.

Twisting of the connection plates was significant in unstiffened connections. Shear load-twist curves were plotted to study the twist in the shear tab. Twisting was observed as the primary failure mode in many cases.

Nonlinearity was studied by considering the shear load–displacement curves and by calculating the stresses and plastic deformations at different locations. Plastic deformations occurred in the supporting columns at the top and bottom tip of the shear tab causing the column web failure mechanism. Failure modes were observed using extracted curves and visual inspection. The primary failure modes for the three-bolt connections were bolt shear, web mechanism and shear tab twist.

2.2.5 Mahamid et al. (2007)

Mahamid et al. (2007) conducted a finite element study on stiffened extended shear tabs. The same procedure and details as the research conducted by Rahman et al. (2007) were used.

Shear load–deflection curves were within an acceptable deviation compared to experimental results by Sherman and Ghorbanpoor (2002). Plate twisting was recognized as the secondary failure mode for some models. A yield line mechanism was also observed for stiffened extended shear tabs.

According to the two studies on unstiffened and stiffened extended shear tabs, it was recommended that unstiffened extended shear tabs be avoided due to the significant twist which reduced the connection capacity.

2.2.6 Muir and Hewitt (2009)

Despite the significant advantages offered by the use of extended shear tabs, some aspects of the connection behaviour have been a grey area for designers. The rigidity of the connection at the support may induce unanticipated moment to the connection. This extra moment may result in either a moment delivered to the column that it has not been designed for or a sudden rupture of the weld or bolts. Muir and Hewitt (2009) addressed each of the concerns and presented a general design procedure for extended shear tabs. They also discussed the outline and background of the 13th edition of *Steel Construction Manual* (AISC 2005) procedure for the design of extended shear tabs. A summary of the design procedure suggestions is reported here.

The moment applied to the connection depends on many factors, including the extended shear tab length, relative stiffness of the supported beam, the connection and the support. After discussing different models to come up with a model that more realistically represents the moment transfer to the connection, the pinned-end beam model was proposed as the most logical one for the connection design. Based on this

assumption, the bolt group was subjected to a moment equal to the shear reaction multiplied by the distance from the support to the centre of the bolt group.

The connection must have sufficient ductility to be able to redistribute the loads. To achieve this, the plate should act as a fuse and should yield prior to any other failure modes. To define the minimum thickness for the plate, the limit states of gross shear yielding, net shear rupture, gross flexural yielding and net flexural rupture and block shear should be satisfied. Additionally, a stability check to avoid plate buckling was proposed.

A modified requirement for the weld was also defined. In order for the plate to act as a fuse, the plate should yield before the weld ruptures. If the weld size is designed to be greater than 5/8 times the plate thickness, this requirement is satisfied.

The plate should also yield prior to bolt shear failure. To achieve this, a maximum plate thickness was defined based on the concept that the yield moment of the plate should be less than the bolt group moment capacity.

Since the AISC design procedure sizes the components to resist the full eccentricity at the bolted connection, the connection components accommodate for the rotation applied to the connection and therefore the rotational resistance of the support is not required to resist the design load. Thus, the column web mechanism is assumed to be prevented and there is no need for it to be checked as a limit state.

The design procedure was compared with the test results by Sherman and Ghorbanpoor (2002). It was observed that the design procedure provides a good margin of safety.

2.2.7 Thornton and Fortney (2011)

The 13th edition of the *Steel Construction Manual* (AISC 2005) contains many design checks. However, it does not discuss the lateral-torsional stability of the extended shear tab. Thornton and Fortney (2011) proposed the use of the stability equation used for coped beams to check the lateral stability of extended shear tabs. They recommended a check to investigate the need for stiffeners to avoid lateral-torsional

instability of the extended shear tabs and evaluated the proposed equation through some examples.

2.2.8 Muir and Thornton (2011)

A modified design procedure for conventional shear tabs was developed by Muir and Thornton (2011). Since some of the results and recommendations are applicable to extended shear tabs, this study is discussed here.

The 13th edition of the *Steel Construction Manual* (AISC 2005) design procedure is based on nominal bolt shear values that are 20% lower than the theoretical bolt values. This reduction was considered to account for the uneven force distribution among the bolts. Another function of this reduction was to justify the practice of neglecting eccentricity in the bolt group. Studies have shown that this practice is no longer appropriate. Thus, the 14th edition of *Steel Construction Manual* (AISC 2011) design procedure increased the nominal bolt shear, necessitating a revised design procedure for single-plate shear tabs. This revision was done in this study.

To establish a new design model a number of details should be taken into account. The primary consideration is to accommodate simple beam end rotations and ductility to allow for unanticipated moments established in the connection. To achieve this, a target end rotation must be determined. The 0.03 radians rotation has been accepted to provide a reasonable upper bound for the beam end rotation. Theoretically, the rotational demand is accommodated through a combination of plate flexural yielding; bolt plowing; bolt deformation and support rotation. However, since yielding can occur over a very small area of the plate, it is excluded as a means of rotational capacity. The support rotation is not applicable to rigid supports and is omitted, consequently. Doing some calculations in the study, it was proved that relying on bolt deformation only is not sufficient for the rotational demand. To be able to account for bolt plowing to provide ductility requires an upper limit placed on the stiffness and strength of the shear plate and beam web. According to the results of tests by Sarkar and Wallace (1992), limiting the plate and beam web thickness to half of the bolt diameter allows the activation of bolt plowing.

The bolt group in a shear tab connection experiences some eccentricity. However, the eccentricity is not equal to the distance from the weld to the bolt group centre (a-distance). This distance varies between 5 to 267% of the a-distance (Muir and Thornton 2011). Reanalysis of the test results by Creech (2005) and Metzger (2006) was done, and it was concluded that in most cases if the bolt group capacity is defined based on eccentricities larger than half of the a-distance, good agreement with the test results could be observed. In this design procedure, the recommended eccentricities provided by the 14th edition of *Steel Construction Manual* (AISC 2011) were used.

2.2.9 Marosi et al. (2011)

The current design procedure for shear tabs in the *Handbook of Steel Construction* (CISC 2010) is based on rather old studies. Marosi et al. (2011) conducted a research program that aimed to develop an up-to-date design procedure for single and double row bolted shear tabs for use in Canada. Since the results are applicable to extended shear tabs, this study is discussed.

The program consisted of 16 full-scale tests. Bolt configurations varied between one vertical line of three bolts to two vertical lines of ten bolts each. The summary of test results is presented here:

- All the connections having a single vertical line of three bolts failed at a load higher than the predicted capacity. The targeted beam end rotation was exceeded in the tests. Significant shear deformations were observed in the shear tab. Weld rupture occurred at the plate-to-column weld.
- The performance of the connections with a single vertical line of six bolts was quite satisfactory. The target beam rotation was met. Shear yielding occurred in the shear plate along the bolt line. Following that, bolt bearing and finally shear fracture of the net area were observed.
- The connections with a single vertical line of ten bolts performed adequately. Flexural and shear yielding followed by bearing deformations at the bolt holes were observed. The shear tab fractured between some of the bolt holes and weld fracture occurred at the plate-to-column weld.

- The connections with two vertical bolt lines performed almost the same as the connections with a single vertical bolt line.
- According to the results, the *Handbook of Steel Construction* (CISC 2010) was found to be outdated in design of shear tabs since it is based on old procedures and resistance factors that have been superseded. Moreover, as the *Handbook* does not address the design of multi-row connections, the applicability of the design procedure is limited. The capacity values calculated based on the method in the *Handbook* were found to be overly conservative.

2.2.10 Suleiman et al. (2013)

The expected failure mode of extended shear tabs was evaluated by Suleiman et al. (2013). In this study, a numerical model was developed and the failure mode of the unstiffened extended shear tabs was investigated. The test results by Sherman and Ghorbanpoor (2002) and Metzger (2006) were used to verify the model. The focus of the study was to examine whether twisting can be a governing limit state for the extended shear tabs.

In order to identify whether twisting is a primary mode of failure or not, two curves were plotted: shear load–vertical displacement and angle of twist. It was observed that the shear load–vertical displacement curve started to level-off before any significant nonlinearity occurred in the shear load–twist angle curve. Therefore, twisting was excluded as a governing failure mode. Yielding was observed in the bolts and around the bolt holes. Bolt shear was identified as the primary failure mode. The finite element analysis also captured the local deformations. The capacity resulting from finite element models were on average 9% larger than the capacity based on the 14th edition of *Steel Construction Manual* (AISC 2011).

The most specific result of this study was that twisting did not control the design of unstiffened extended shear tabs. As a result, it was recommended that stabilizer plates are not needed provided that the connection satisfies all other design limit states.

2.2.11 Mirzaei et al. (2013)

Axial load can be developed in shear tabs as a result of earthquake or wind loads and column out-of-plumbness. Mirzaei et al. (2013) investigated the effect of axial load on the behaviour of shear tabs through a series of tests.

The research was aimed at improving the current design provisions for shear tabs in Canada. In this study, parameters such as the member size, plate size, number and size of the bolts, number of bolts per row and support conditions were varied. Each shear tab was tested under a combination of shear and axial load. To be compatible with experimental results by Marosi et al. (2011), the same vertical displacement-based loading was utilized.

The failure modes observed in the tests were flexural and shear yielding of the plate followed by rupture in the connecting plate-to-column fillet weld. However, after the fracture initiation, the connections were still able to carry additional shear loads. By further loading of the connection, additional cracks developed in the net area of the plate between the bolt holes.

Regarding the connection capacity, it was observed that application of axial compressive force increased the shear resistance, whereas tensile axial load resulted in capacity reduction.

2.2.12 Thomas et al. (2014)

One of the most recent and extensive research programs on extended shear tabs was performed by Thomas et al. (2014) at the University of Alberta. The main objective of this study was to evaluate the behaviour of extended shear tabs with and without the presence of axial load. The study consisted of 23 full-scale extended shear tab specimens welded to the web of stub columns. The specimens were categorized into two main groups of stiffened and unstiffened extended shear tabs. Each group of specimens varied in plate depth, plate thickness, bolt group configuration and magnitude of applied axial load. All the specimens had two vertical bolt lines and 6 mm plate-to-column web welds. The number of horizontal bolt lines varied among

2, 3 and 5. The extended shear tab length was constant in all specimens. Connections were tested under different axial loads and the effect of axial load on the connection capacity was evaluated.

Several observations were made in the unstiffened extended shear tab tests:

- Weld rupture was observed in all specimens. The rupture initiated from the tension tip of the weld and propagated towards the compression tip. Weld rupture size was more severe in the specimens with tensile axial load. For the specimens under the combination of compressive axial and shear loads the compression tended to have a counteracting effect, hindering the weld rupture. However, when a tensile load was applied combined with the shear load, extensive weld rupture was always the failure mode.
- Bolt fracture was identified as the main mechanism contributing to the decrease in shear load for many specimens. In some cases, bolt fracture occurred before weld rupture, which made bolt fracture the primary failure mode. In other cases, it happened after weld rupture as the secondary failure mode.
- Column web yielding occurred during all 13 unstiffened extended shear tab tests. This observation is consistent with the phenomenon observed by Sherman and Ghorbanpoor (2002).
- Localized plate yielding was observed in many specimens along the vertical bolt line. However, this minor yielding was not responsible for a decrease in vertical load.
- Bolt bearing deformations were observed in all the unstiffened specimens. This phenomenon contributed to the overall ductility of the connection and was not a critical failure mode in any of the specimens.
- Out-of-plane deformation was not observed in any of the unstiffened specimens.

The specimens were evaluated based on some current design methods, including the method recommended in the 14th edition of the *Steel Construction Manual* (AISC 2011). The AISC method is discussed in detail in section 2.4.1.

It was observed that in all cases the test-to- predicted strength ratio was considerably higher than one, which is indicative of the current design methods inefficiency and conservatism. Moreover, current design methods were found to wrongly predict the failure mode of the connection in most cases.

In the case of stiffened extended shear tabs, the stiffeners significantly improved the connection capacity. Column web yielding and weld rupture were not observed; however, out-of-plane deformation was the critical failure mode for all cases. Bolt fracture was the secondary failure mode for some specimens. Gross section yielding was also observed in all cases, even though it was not the critical failure mode. A photo of out-of-plane deformation observed in the study is shown in Figure 2-1.

Figure 2-1: Out-of-plane deformation (Thomas et al. 2014)

Based on the results gained by this study, a design method was developed to predict the capacity and failure mode of extended shear tabs more effectively than previously developed methods. Since this design method is considered as the base point for the current study, it is discussed here. According to the design method several limit states should be checked to evaluate the capacity and ductility of the extended shear tabs.

Sizing the bolt group is the initial step in the design of unstiffened extended shear tabs. Since the load is applied eccentrically, the instantaneous centre of rotation method is used to calculate the bolt group shear load capacity, V_{BG}. The details of the instantaneous centre of rotation method to evaluate the bolt group capacity are addressed in several references, including Thomas et al. (2014). Thomas et al. (2014) proposed that the bolt group shear load eccentricity be taken as 75% of the geometric eccentricity.

In the design of extended shear tabs, the plate should act as a fuse, implying that the plate should fail before any failure occurs in connection fasteners or any buckling happens in the plate itself. Moreover, the plate should satisfy ductility requirements that allow the plate to rotate, consistent with the assumption of simple connection. Based on the two criteria, two limits for the plate thickness are defined. To ensure sufficient strength against any failure due to buckling, a minimum plate thickness was proposed as (symbols are defined in the prefatory pages of this report):

2-1
$$t_{min} = 0.663\sqrt{\frac{F_y d_p L}{E}}$$

To achieve sufficient ductility, plate thickness was limited to the value calculated as follows:

2-2
$$t_{max} = \frac{6\phi_b M_{BG}}{R_y F_y {d_p}^2} + \frac{N}{R_y F_y d_p}$$

In this equation, the moment capacity of the bolt group, M_{BG}, is calculated by multiplying the shear capacity of the bolt group by the effective eccentricity of the load, taken equal to 75% of the geometric eccentricity:

2-3
$$M_{BG} = V_{BG} e_{eff}$$

In cases where the column web capacity is limited by the formation of a flexural yield mechanism, the shear capacity of the column web, V_{CW}, is:

2-4 $$V_{CW} = \frac{F_{yc} w^2 d_p}{0.5 e_g}\left[\frac{T}{2d_p} + \frac{d_p}{T} + \sqrt{3}\right]$$

The minimum weld size to prevent weld rupture from happening before plate yielding was defined as follows:

2-5 $$D \geq 1.155 \frac{F_y}{X_u} t_p$$

To resist the applied shear and/or axial loads, the extended shear tab should satisfy strength requirements. The shear resistance of the section is taken as the lesser of the capacity determined based on the gross section yielding and net section fracture limit states. Therefore, the shear capacity is the lesser of the values predicted by Equations 2-6 and 2-7.

2-6 $$\phi V_{GS} = 0.66 \phi F_y t_p d_p$$

2-7 $$\phi V_{NS} = 0.6 \phi F_u t_p (d_p - n_h d_{bh})$$

The section flexural capacity should also be checked under the application of shear and axial loads. To check this limit state, the flexural capacity is determined in terms of the shear load causing the plate to reach its section plastic moment:

2-8 $$\phi V_{MN} = \frac{\phi \sigma_n t_p d_p^2}{4 e_{eff-cs}} - \frac{N_F^2}{4 \sigma_n t_p e_{eff-cs}}$$

The specimens' capacities were calculated based on the proposed design method and an average test-to-predicted capacity ratio of 1.02 was observed.

At the end of this comprehensive study, several recommendations were suggested for further research. A parametric study was recommended to validate the design recommendations. Moreover, some additional parameters were recommended to be investigated, namely plate length, presence of back-to-back extended shear tabs and support stiffness.

2.3 Double-Coped Beams

Previous research on double-coped beams is scarce. In this section, three major studies on double-coped beams are discussed.

2.3.1 Cheng et al. (1984)

Cheng et al. (1984) conducted one of the earliest and most comprehensive research studies on double-coped beams. They examined the behaviour of double-coped beams having various coping details, both numerically and experimentally.

In the numerical part of the study, finite element software was used to assess the performance of different cope geometries. Since the program could only solve linear-elastic buckling problems, the onset of material yielding was considered to be the upper limit of capacity. Initially, two top-flange coped beams with different lengths were modelled and loaded using a point load at the centre of the span. In the short beam, the buckling capacity was controlled by the coped section. However, for the long beam, the capacity reached almost 90% of the lateral-torsional buckling capacity of the beam. Based on these observations, a preliminary design model was developed that considered the interaction of the coped and uncoped regions of the beam in predicting the buckling capacity of the top-flange coped beam. A parametric study was then conducted on the proposed design model to investigate the effect of span length, cope length and cope depth on the design model behaviour. Based on the results of the parametric study, appropriate modifications were applied to the design model. In the next phase of study, a similar procedure was used to develop and modify a design model for bottom-flange coped beams. The third phase of the

numerical study was an investigation of the behaviour of double-coped beams, which was found to be similar to that of the top-flange coped beams. However, the resistance of double-coped beams against buckling was considerably lower than that of top-flange coped beams. An equation considering the interaction of the buckling load of the rectangular section in the coped region and the I-section over the uncoped region was proposed.

In the first phase of the experimental part of the study, six top-flange coped beams were tested to verify and check the reliability of the finite element model and the proposed design method. It was concluded that both led to conservative results. Moreover, the program captured the buckled shapes of the specimens quite satisfactorily. The conclusions of this study are:

- The lateral buckling capacity of coped beams was governed by the interaction between the coped and uncoped sections of the beam. Beams with short copes tended to behave similar to uncoped beams. The behaviour of beams with long copes was dominated by the buckling capacity of the coped region.
- Bottom-flange coped beams showed more resistance to buckling than top-flange and double-coped beams.
- The behaviour of double-coped beams was similar to top-flange coped beams. The difference between the behaviour of the two was caused due to the shape of the coped section.
- Using theoretical lateral-torsional buckling equations always led to conservative, yet reasonable, results compared to the test results. The source of conservatism was explained as the effect of restraints from adjacent spans and restraints caused by test fixtures.

The second and third phases of the study included tests on top-flange and bottom-flange coped beams, but not double-coped beams. Therefore, these phases are not discussed here.

At this stage of the study, a design procedure was proposed for each of the three cases of top-flange coped beams, bottom-flange coped beams and double-coped beams.

The research was expanded by conducting a comprehensive parametric study for each cope configuration separately, with various cope geometries. Since the current study deals with double-coped beams, only the section on double-coped beams is discussed here. The work not discussed included additional numerical parametric studies on top-flange and bottom-flange coped beams, but not double-coped beams.

The elastic local web buckling of double-coped beams was studied considering a double-coped beam with three different cope lengths. Observation of buckled shapes suggested that web buckling could be modelled as a lateral-torsional buckling problem of a rectangular section.

Based on the results of this research program, several design equations were proposed to evaluate the critical stress of coped beams. Since all the equations were derived based on elastic buckling, the critical stresses were limited to F_y. Moreover, the applicability of the design equations was limited to specific cope dimensions.

2.3.2 Dowswell and Whyte (2014)

Dowswell and Whyte (2014) investigated the local stability of double-coped beams and proposed modification factors for the equations recommended by the AISC Specification (2010) Section F11, "Rectangular bars and rounds". The study aimed to address three specific issues:

- Cope depths greater that 20% of the beam depth.
- Unequal cope depths at top and bottom.
- Unequal cope lengths at top and bottom.

In this numerical study, 54 elastic finite element models were constructed, including 30 models with equal top and bottom cope lengths and 24 with unequal top and bottom cope lengths.

All the models buckled in the same manner. The tension edge of the coped cross-section experienced lateral translation, while the shear centre of the section underwent both lateral displacement and rotation. The buckling mode was identified to be a combination of modes, including local buckling, lateral-torsional buckling, shear

buckling, and distortional buckling. However, different cope geometries experienced different dominant buckling modes. Shear buckling was dominant for short copes, while long copes were dominated by lateral-torsional buckling.

The design model developed in this study was proposed based on lateral-torsional buckling, which was found to be the dominant buckling mode over the critical variable range. A modification factor was introduced that incorporated the effect of other buckling modes. It was also proposed that the simultaneous actions of normal and shear stresses be accounted for in the calculation of flexural strength. This method is based on the plastic capacity of a rectangular section under the simultaneous actions of shear, axial load and moment about one axis as developed by Neal (1961):

2-9
$$\frac{M_r}{M_p} + \left(\frac{P_r}{P_y}\right)^2 + \frac{\left(\frac{R_r}{V_n}\right)^4}{1 - \left(\frac{P_r}{P_y}\right)^2} \leq 1.0$$

If no axial load is applied to the section, the plastic moment strength can be calculated by rearranging Equation 2-9 as follows:

2-10
$$M_{pv} = M_p \left[1 - \left(\frac{R_r}{V_n}\right)^4\right]$$

2.3.3 Johnston et al. (2015)

Johnston et al. (2015) evaluated the performance of double-coped beams through a comprehensive testing program. The primary objective of the study was to investigate the local strength and behaviour of double-coped beams having a variety of geometries and boundary conditions. The secondary objective was to investigate the behaviour of the connections under combined axial and shear loading.

The study consisted of 29 full-scale tests on double-coped beams with equally coped top and bottom flanges. The cope length and beam section (which accounted for both

net web depth and thickness) were considered as test variables. Four end-supports were utilized in the research, which represented a range of potential support conditions with different rotational stiffnesses. The specimens were tested under various combinations of axial and shear loads, with the axial load being either compressive, tensile or zero.

Several failure modes were observed in the tests, including yielding, out-of-plane deformation, buckling, and tearing. Generally, the tested specimens behaved in a ductile manner and were subjected to yielding at early stages of loading. All specimens experienced out-of-plane deformation, defined as a ductile failure associated with gradual deformation of the coped region out of the plane of the beam web. This failure mode was distinguished from buckling by being ductile gradual. Buckling was also observed in some specimens, defined by a large out-of-plane deformation accompanied by a sudden and significant drop in the vertical load. Tearing was observed in a number of specimens after large out-of-plane deformation had already occurred and therefore was not regarded as the primary failure mode in these specimens. However, tearing was identified as the primary failure mode for two specimens only. Five of the specimens failed during the application of horizontal load and before any vertical load was applied. Although these specimens were able to resist horizontal load in the absence of vertical load, they were unable to sustain the horizontal load in combination with vertical load.

The in-plane bending moment developed at the cope face and the support face were calculated and the moment distribution along the cope length was investigated. The moment distribution was significantly affected by the end-support condition.

The linear moment distribution along the cope length was used to track the location of the inflection point. The effective eccentricity, which was defined as the distance between the location of the inflection point and the face of the cope, was calculated and it was observed that it varied quite significantly during each test.

Some specific conclusions were made from this study:

- Heavier sections had higher capacities due to their increased cross-sectional depth and thickness.

- As the length of the coped region increased, the connection capacity decreased. This was due to the greater moment developed at the cope face.
- Horizontal tensile load tended to stabilize the coped region and increased the connection capacity. Conversely, horizontal compressive load destabilized the coped region and resulted in a decrease in capacity.
- Higher support rotational stiffness increased the connection capacity.
- The inflection point moved significantly along the cope length during the application of vertical load, making it impossible to propose an accurate single value for the eccentricity for all the tests.

Based on the results achieved from this study, it was suggested that a parametric study be conducted on double-coped beams with additional geometric variables to investigate the individual effects of cope dimensions on the overall behaviour. Moreover, a parametric investigation of the effect of support conditions on the behaviour of double-coped beams was recommended.

2.4 AISC Design Manual

The *Handbook of Steel Construction* (CISC 2010) does not include any explicit design method for extended shear tabs or double-coped beams and therefore is not discussed here. In this section, the design methods recommended by the 14th edition of *Steel Construction Manual* (AISC 2011) for extended shear tabs and double-coped beams are discussed.

2.4.1 Extended Shear Tabs

Both the 13th and the 14th editions of the *Steel Construction Manual* (AISC 2005; 2011) address the design of extended shear tabs. Since the 14th edition is more comprehensive than the 13th edition, only the design method recommended by the 14th edition of *Steel Construction Manual* (AISC 2011) is discussed here.

First, the bolt group required for the design shear load is defined. The eccentricity applied to the bolt group is considered as the distance from the support to the centroid

of the bolt group. However, other values could be considered, provided they are justified by rational analysis.

The maximum plate thickness is calculated such that the plate moment strength does not exceed the bolt group moment strength.

2-11
$$t_{max} = \frac{6M_{max}}{F_y {d_p}^2}$$

where

2-12
$$M_{max} = \frac{F_v}{0.9}(A_b C')$$

The plate should be checked for the limit states of shear yielding, shear rupture, and block shear rupture. The plate should also be checked for the limit states of shear yielding, shear buckling, and yielding due to flexure according to:

2-13
$$\left(\frac{V_r}{\phi_v V_p}\right)^2 + \left(\frac{M_r}{\phi_b M_p}\right)^2 \leq 1.0$$

The buckling limit state should be checked using the double-coped beam procedure, discussed in Section 2.4.2.

The design procedure for extended shear tabs allows the support column to be designed for an axial force without eccentricity. However, more economic design could be achieved by allowing some moment to transfer to the support. Therefore, the shear load eccentricity applied to the bolt group could be reduced, provided that the moment transferred to the column is considered in the design of the column.

Stabilizer plates should be considered in the design to avoid lateral displacement, if critical. Thornton and Fortney (2011) evaluated the need for stabilizer plates and concluded that stabilizer plates are not required when the required shear strength is limited to the value given by:

2-14 $$V_{LTB} = 1500\pi \frac{d_p {t_p}^3}{L^2}$$

The connection resistance to torsion is evaluated based on equations developed by Thornton and Fortney (2011). They proposed that the torsional resistance of the connection be calculated considering the effect of the torsional capacity of the plate and the resistance provided by the beam bearing against the concrete slab, in case the slab is present. The connection is considered to be sufficiently resistant to torsion if the resistance is equal to or higher than the torsional moment caused by the lateral eccentricity of the lap splice. However, Thornton and Fortney (2011) showed that the capacities of conventional connections were much higher than the required resistance, and therefore the check can be neglected in most cases.

2.4.2 Double-Coped Beams

The applicable code recommendations for double-coped beams could be discussed in two categories: the recommendations specifically addressing double-coped beams and those addressing strength and stability of rectangular plates.

The 14th edition of the *Steel Construction Manual* (AISC 2011) recommends the following equations for the design of double-coped beams.

If $c \leq 2d$ and $d_c \leq 0.2d$, and the cope lengths are equal, Equations 2-15 and 2-16, which are the equations recommended by Cheng et al. (1984), are used to calculate the critical buckling stress.

2-15 $$F_{cr} = 0.62\pi E f_d \frac{{t_w}^2}{ch_0}$$

2-16 $$f_d = 3.5 - 7.5\frac{d_c}{d}$$

For all other cases, Equations 2-17 to 2-21, which are based on the plate buckling model recommended by Muir and Thornton (2004), are used.

2-17 $$F_{cr} = F_y Q$$

The reduction factor for plate buckling, Q, is calculated based on the slenderness parameter, λ.

If $\lambda \leq 0.7$:

2-18 $$Q = 1.0$$

If $0.7 < \lambda \leq 1.41$

2-19 $$Q = 1.34 - 0.486\lambda$$

If $\lambda > 1.41$

2-20 $$Q = \frac{1.30}{\lambda^2}$$

where the slenderness parameter, λ, is:

2-21 $$\lambda = \frac{h_0}{10t_w}\sqrt{\frac{F_y}{475 + 280\left(\frac{h_0}{c}\right)^2}}$$

The AISC Specification (2010), Section F11, recommends that the following equations be used for evaluation of strength and stability of rectangular plates. Since the coped region of a double-coped beam could be treated as an individual rectangular plate, the following equations are applicable to the coped section.

For yielding, $\frac{ch_0}{{t_w}^2} \leq \frac{0.08E}{F_y}$:

2-22 $$M_n = M_p = F_y Z \leq 1.6 M_y$$

For inelastic lateral-torsional buckling, $\frac{0.08E}{F_y} < \frac{ch_0}{{t_w}^2} \leq \frac{1.9E}{F_y}$:

2-23 $$M_n = C_b \left[1.52 - 0.274 \left(\frac{ch_0}{{t_w}^2}\right) \frac{F_y}{E}\right] M_y \leq M_p$$

For elastic lateral-torsional buckling, $\frac{ch_0}{{t_w}^2} > \frac{1.9E}{F_y}$:

2-24 $$M_n = F_{cr} S \leq M_p$$

where the critical stress is:

2-25 $$F_{cr} = \frac{1.9EC_b}{\frac{ch_0}{{t_w}^2}}$$

2.5 Summary

Extended shear tabs and double-coped beams are two commonly used examples of cantilever plate connection elements.

Several research programs have been conducted on extended shear tabs and some recommendations were provided; however, limited physical testing has been carried out. Thomas et al. (2014) performed an experimental program on extended shear tabs with flexible support, but the effect of support stiffness on the behaviour was not addressed. As such, additional study is needed to further investigate the behaviour of extended shear tabs.

Research on the behaviour of double-coped beams is scarce. Some previous numerical studies did not incorporate the inelastic effects in the connection behaviour. Therefore, numerical study accounting for the inelastic behaviour of double-coped beams is necessary to obtain a better understanding of the connection behaviour. Results from a recent experimental study that incorporated a wide range of double-coped beams (Johnston et al. 2015) contributed extensive physical evidence about the behaviour and failure modes of double-coped beams, but a comprehensive numerical study covering a wider range of dimensions and boundary conditions was recommended for further research.

CHAPTER 3: EXPERIMENTAL PROGRAM

3.1 Introduction

A comprehensive full-scale testing program was designed and conducted to achieve a better and broader understanding of extended shear tab behaviour. The specific goal of the experimental program was to investigate the behaviour of extended shear tabs with rigid supports to complement previous tests at the University of Alberta that made use of relatively flexible supports. To achieve this, a total of 17 extended shear tab specimens were considered, varying in extended shear tab length, thickness, bolt configuration, weld size and application of axial load.

In the upcoming sections, specimen specifications are presented followed by a summary of material properties, test configuration, instrumentation and loading scheme. In the end, tests results are summarized and discussed in detail.

3.2 Test Specimens

A total of 17 specimens were designed according to the procedure developed by Thomas et al. (2014). Typical specimens' drawings are presented in Figure 3-1. The specimens were donated for testing by Waiward Steel LP of Edmonton, Alberta. Each specimen consisted of an extended shear tab welded to either a 25 mm (1 in.) thick 700 mm×250 mm plate or the stiffened web of a W310×107 column stub. A W530×165 beam was reused as the loading beam for all tests. The beam was sized to be compatible with the test set-up and to preclude any beam failure. An extra beam was also ordered so that the loading beam could be replaced by an intact beam in case the beam underwent excessive local deformations during the tests.

The specimens vary in extended shear tab length, thickness, bolt configuration, support condition and application of horizontal load. The naming scheme of the specimens consists of numbers and letters. The first two characters indicate the number of horizontal bolt lines. In all the specimens there were three horizontal bolt lines; therefore, all specimen identifications (IDs) begin with "3B". The next letter

implies whether the specimen support was a rigid plate (R) or a flexible (column web) support was modified using stabilizer plates to form a relatively rigid support (M). The reason behind using stabilizer plates was to be able to identify the extent of improvement in connection behaviour with respect to some specimens tested by Thomas et al. (2014). For the specimens with the "M" support condition, the extended shear tabs were welded to the web of a column using 6 mm fillet welds. The size of the weld was defined based on the assumption of pure shear at the support. For the specimens with the "R" support condition, the extended shear tabs were welded to a 25 mm (1 in.) plate using 8 mm and 10 mm welds for the specimens with 9.5 mm and 12.7 mm extended shear tabs, respectively.

The next number indicates the extended shear tab thickness rounded up to the closest millimeter. Finally, the magnitude of axial load applied to the specimen is specified in kilonewtons. The letter adjacent to the axial load defines whether the axial load was compressive (C) or tensile (T). The term just after the axial load, if any, depicts the variation in specimen geometry from the base case (see Figure 3-1(a)) that impacts the flexibility of the connection. The base case consisted of a 348 mm extended shear tab in which the distance between the support and the centreline of the first vertical line of bolts was 233 mm. Specimens with a shorter length are identified by "L" and specimens with one vertical bolt line are identified by "V1". As an example, specimen 3BR-10-200C is a 9.5 mm thick extended shear tab with three horizontal bolt lines, attached to a rigid plate as the support, under 200 kN compressive axial load. As another example, specimen 3BM-10-0-V1 is a 9.5 mm thick extended shear tab with three horizontal bolt lines and one vertical bolt line, attached to a stiffened column web as the support, under no axial load. Since the specimen geometry is not altered in the specimens with axial load, only the drawings for the specimens without axial load are presented in Figure 3-1. Moreover, only the specimens with 9.5 mm thick extended shear tabs are shown in the figure. The as-built dimensions of the specimens were measured for all specimens to ensure that they were fabricated as requested. Since the measured-to-specified specimens' dimensions were within an acceptable tolerance, the specified dimensions were used to calculate section properties in the forthcoming sections.

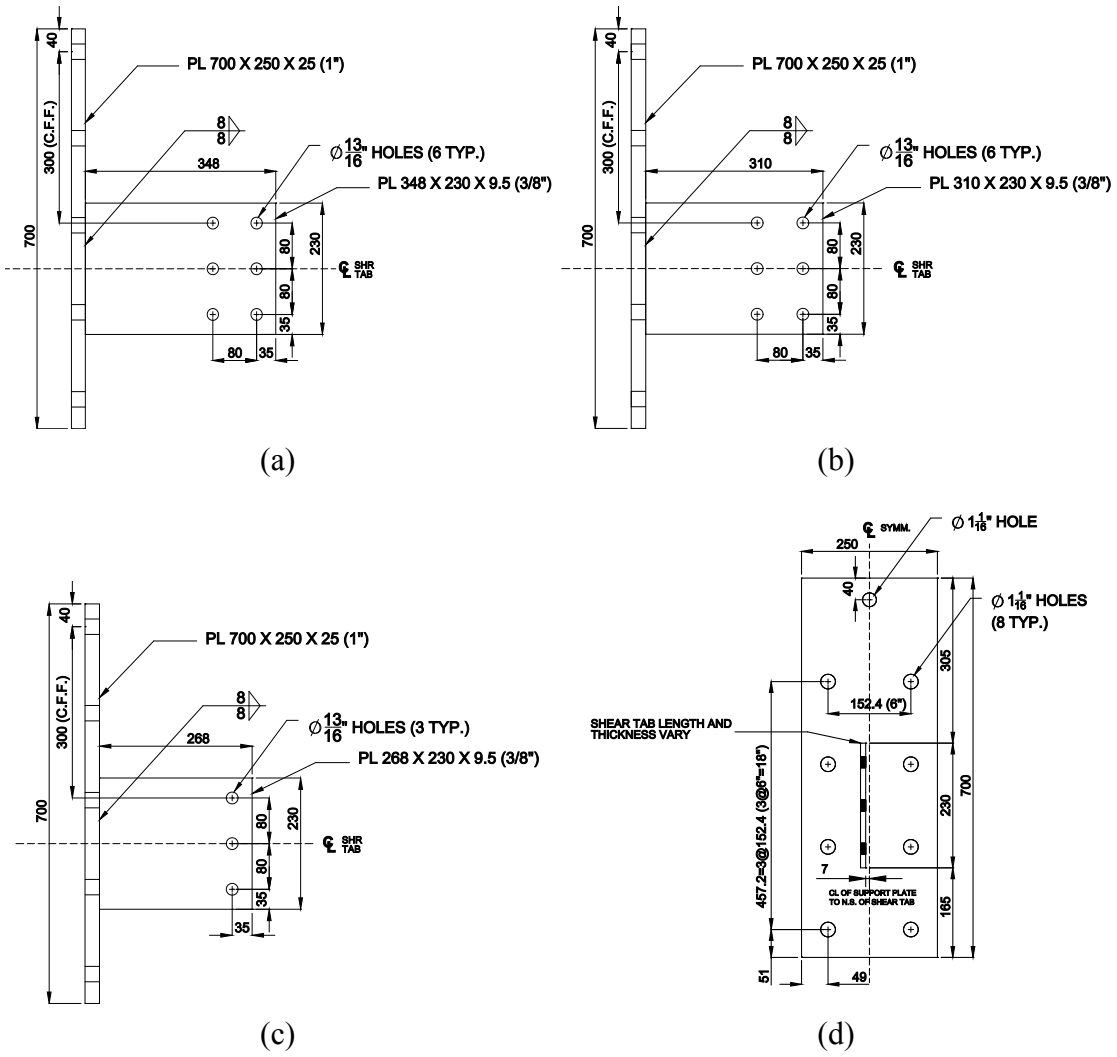

Figure 3-1: Details and dimensions of specimens:
(a) 3BR-10-0; (b) 3BR-10-0-L; (c) 3BR-10-0-V1 and (d) Typical elevation view

The dimensions of the specimens were selected such that one-to-one comparisons could be made with some specimens tested by Thomas et al. (2014). In addition to the parameters investigated by Thomas et al. (2014), specimens with shorter length were considered to investigate the effect of extended shear tab length on the connection behaviour. Moreover, specimens with one vertical bolt line were considered in the test matrix to investigate the effect of bolt configuration. Finally, contrary to all unstiffened extended shear tab specimens tested by Thomas et al. (2014), all the

specimens' supports were stiff. The geometrical specifications and horizontal loading conditions for the specimens are reported in Table 3-1.

Table 3-1: Specimens specifications

Specimen ID	Plate Thickness (mm)	Plate Depth (mm)	Plate Length (mm)	No. of Vertical Bolt Lines	Horizontal Load (kN)	Compressive or Tensile (C/T)
3BR-10-0	9.5	230	348	2	0	-
3BR-13-0	12.7	230	348	2	0	-
3BR-10-0-L	9.5	230	310	2	0	-
3BR-13-0-L	12.7	230	310	2	0	-
3BR-10-0-V1	9.5	230	268	1	0	-
3BR-13-0-V1	12.7	230	268	1	0	-
3BR-10-100C	9.5	230	348	2	100	C
3BR-13-100C	12.7	230	348	2	100	C
3BR-10-200C	9.5	230	348	2	200	C
3BR-13-200C	12.7	230	348	2	200	C
3BR-10-200T	9.5	230	348	2	200	T
3BR-13-200T	12.7	230	348	2	200	T
3BM-10-0	9.5	230	348	2	0	-
3BM-13-0	12.7	230	348	2	0	-
3BM-10-200C	9.5	230	348	2	200	C
3BM-13-200C	12.7	230	348	2	200	C
3BM-10-0-V1	9.5	230	348	1	0	-

3.3 Material Properties

3.3.1 Plate Coupon Tests

All steel materials used in this study were ordered to be from CAN/CSA-G40.20/G40.21 grade 350W steel. Tension coupons were cut from the same plate used to fabricate the extended shear tabs. Six coupons were taken from each plate thickness: three in the longitudinal direction and three in the transverse direction. The reason behind the orientation of coupon cuts was to incorporate the effect of steel grain orientation on the material properties. The coupon plate cut-out pattern, as well as the coupon cut-out pattern and typical coupon dimensions, are shown in Figure 3-2.

Coupons were tested in accordance with ASTM standard A370-14 (ASTM 2014). Initial cross-sectional dimensions were accurately measured for each coupon individually. The engineering stress was calculated by dividing the force at each step by the initial area resulting from the measured dimensions. During each test, loading was paused at three different points during the yield plateau. Pausing the test resulted in an abrupt drop in the load until the load reached a steady value. The three values were recorded and averaged to find the static yield stress. After the three pauses, loading was pursued until it reached close to the ultimate load. Another static point was recorded at the ultimate load using the described procedure. A sample stress–strain curve for a coupon cut from the 9.5 mm thick plate is shown in Figure 3-3. The stress–strain curves for all the coupons are presented in Appendix A. A summary of the results is presented in Table 3-2, where “L” and “T” in the coupon ID indicate longitudinal and transverse, respectively, to the extended shear tab plate axis.

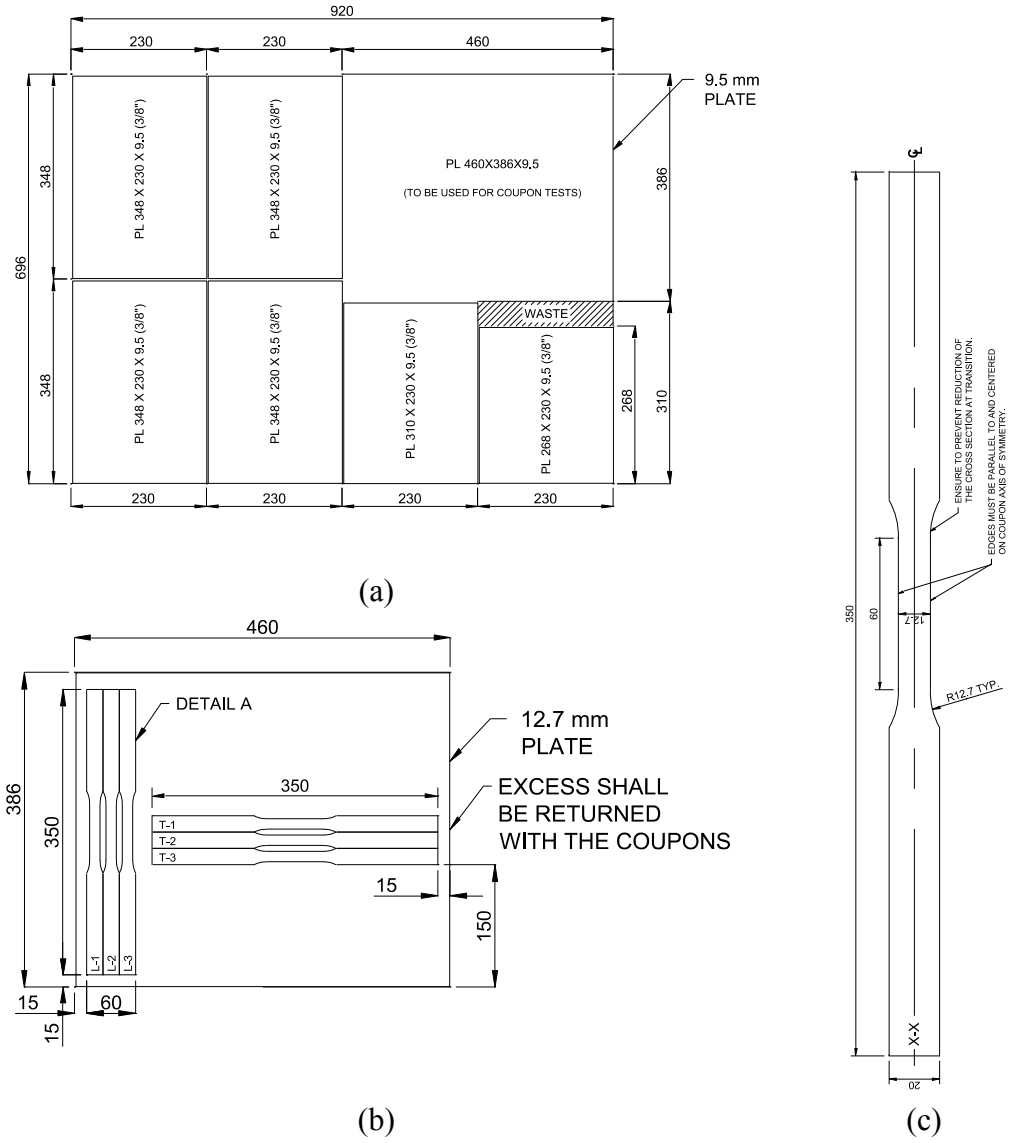

Figure 3-2: Tension coupons:
(a) Plate cut-out pattern; (b) Coupon cut-out pattern; (c) Coupon dimensions

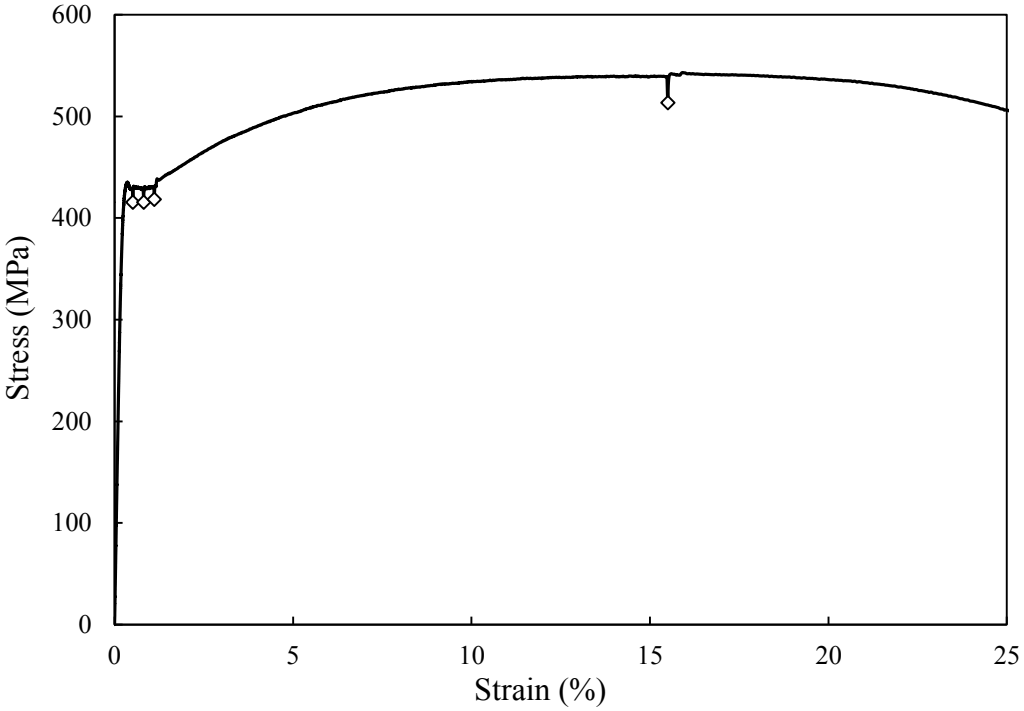

Figure 3-3: Sample coupon test stress–strain curve (Coupon T-2, 9.5 mm plate)

Table 3-2: Coupon tests results summary

Plate Thickness (mm)	Coupon ID	Yield Stress§ (MPa)	Ultimate Stress§ (MPa)	Elastic Modulus (MPa)
9.5	L-1	434	527	203,900
	L-2	437	529	198,700
	L-3	433	528	201,600
	T-1	423	519	197,000
	T-2	417	513	208,400
	T-3	421	519	204,900
	Average	428	523	202,400
12.7	L-1	354	490	198,300
	L-2	349	490	205,600
	L-3	352	490	200,000
	T-1	349	486	197,000
	T-2	352	488	201,700
	T-3	352	487	194,800
	Average	351	489	199,600

§Static stresses; yield values are average of three measurements.

As noticed from Table 3-1, although all plates were ordered to be grade 350W steel, the 9.5 mm (3/8 in) plates' steel showed a considerably higher yield strength compared to 350 MPa, where the steel of the 12.7 mm (1/2 in.) plates was very close to the nominal value.

3.3.2 Bolt Shear Tests

To evaluate the shear strength of the bolts used in the extended shear tab connections, bolts were tested in shear. A simple test set-up was developed, as shown in Figure 3-4, and used to test three bolts in single shear. The bolts were picked randomly from the same bolt lot used in the extended shear tab tests. The plates were sized such that the shear plane was intercepted at the exact same location along the bolt shank as in the extended shear tabs tests. The bolt capacities are reported in Table 3-3 and the load–displacement curves for the three tests are shown in Figure 3-5. The mean measured bolt shear capacity was used to calculate the connection predicted capacities based on different design methods discussed in Section 3.9.

Table 3-3: Bolt test results summary

Test No.	Shear Load Capacity (kN)
1	180
2	176
3	176
Average	177

(a) (b)

Figure 3-4: (a) Bolt shear test set-up; (b) Deformed bolt

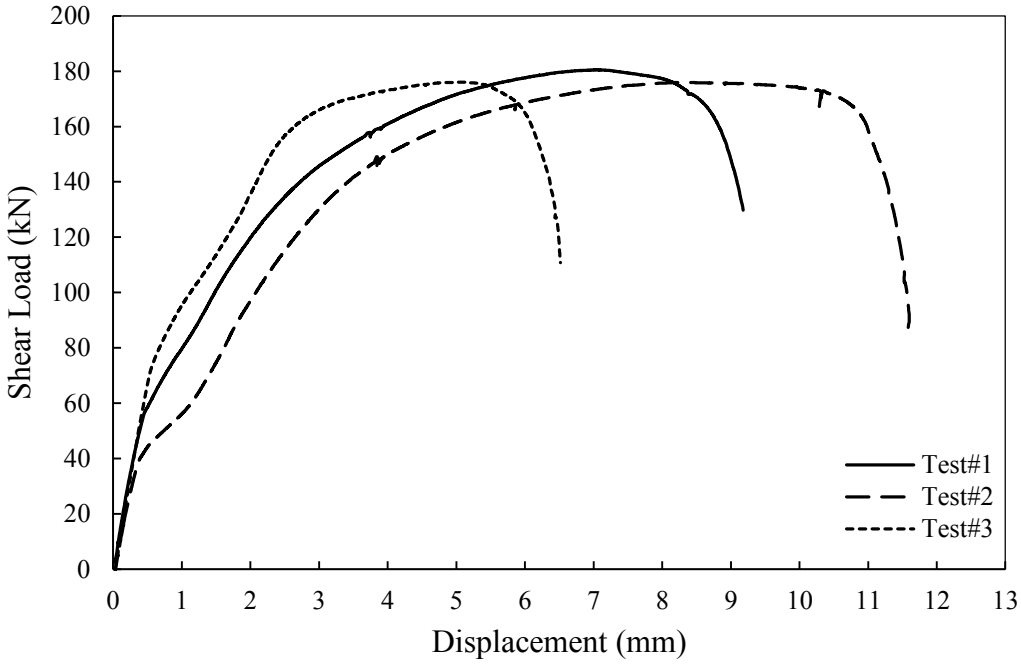

Figure 3-5: Bolt load–displacement curves

3.4 Test Set-up

Extended shear tab tests were conducted in the I.F. Morrison structural engineering laboratory at the University of Alberta using the test apparatus specifically designed to test steel connections. The existing set-up was modified to meet the specific research needs. The test set-up is shown schematically in Figure 3-6. Actuators 1 and 2 were mainly used to apply shear load and rotation, respectively, to the specimen. The purpose of actuator 3 was to apply axial load to the specimens, while accounting for the axial load that may be developed in the specimen due to any inclination in actuators 1 and 2.

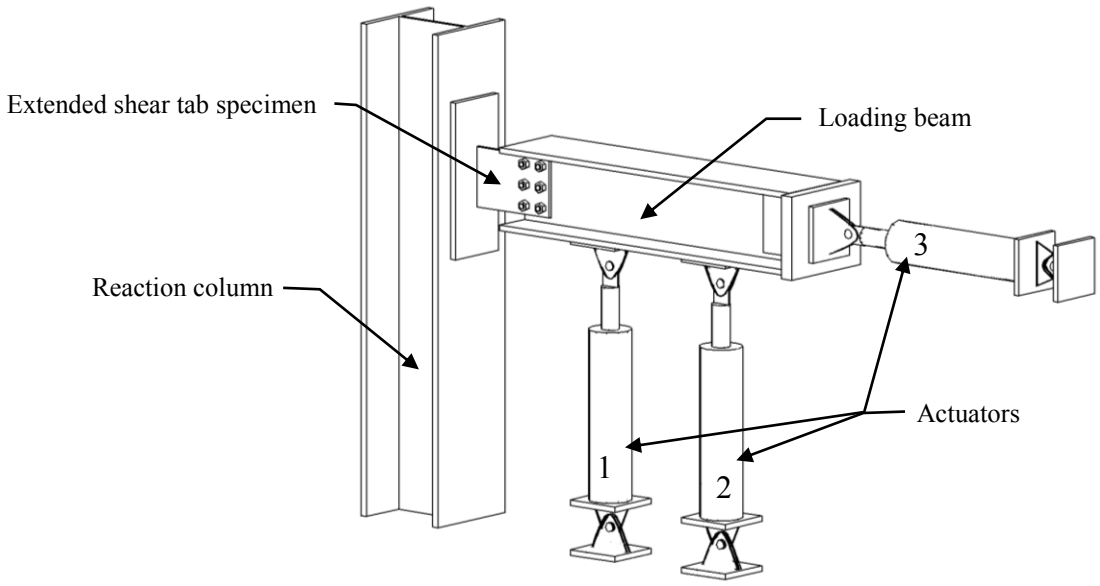

Figure 3-6: Schematic test apparatus

A typical shear tab specimen consisted of an extended shear tab plate shop-welded to a 25 mm (1 in.) thick support plate, which was intended to provide a stiff support condition, as shown in Figure 3-6. Alternatively, it was welded to the stiffened web of a column stub, as discussed previously. Typical 3BR-10 and 3BM-10 specimens are shown in Figure 3-7.

(a) (b) (c)

Figure 3-7: Typical test specimens:
(a) 3BR-10, (b) 3BM-10 (front view) and (c) 3BM-10 (back view)

The reaction column was anchored to the lab strong floor using a base plate and four pre-stressed anchor rods. Moreover, the reaction column was restrained against in-plane displacement using a diagonal brace bolted to the strong floor at the back of the column (base plate, strong floor and brace are not shown in the figure). The loading beam (loaded using three actuators) was bolted to actuators 1 and 2 using eight 22 mm (7/8 in.) diameter pretensioned ASTM A325 bolts. The beam was connected to actuator 3 using a 13 mm (1/2 in.) lap plate on each side of the beam web. Installation of the extended shear tab itself is discussed in Section 3.6.

To eliminate lateral displacement of the loading beam during the tests, thereby simulating a braced-beam condition, a short column was installed on each side of the beam close to the connection location. These columns were anchored to the lab strong floor using pretensioned anchor rods. The gap between the beam flanges and each side column were filled using two Teflon® sheets attached to two steel plates. The

plates were then slid between the side column and the loading beam flanges such that the Teflon® sheets lightly touched the beam flanges. The test set-up before conducting a typical test is shown in Figure 3-8.

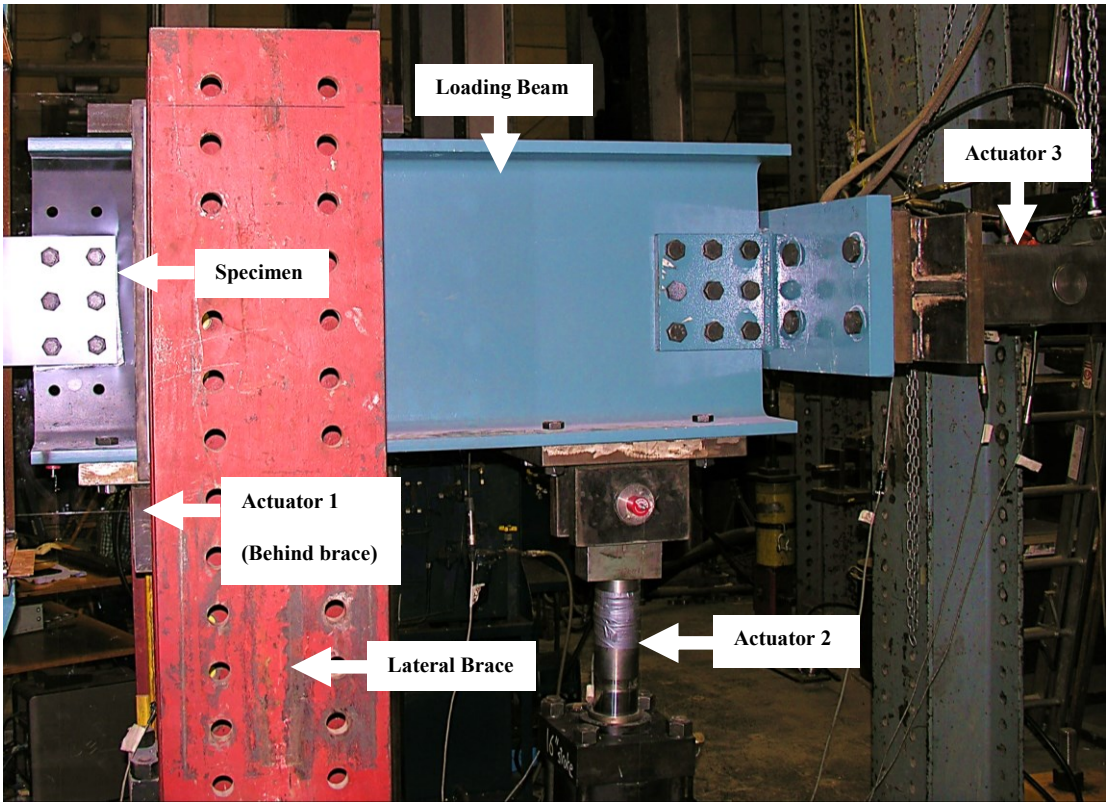

Figure 3-8: Test assembly before conducting the test

3.5 Instrumentation

Several measurement instruments were used in the test set-up to capture and record the desired parameters. Cable transducers were used to measure the actuator extensions from the initial position. A cable transducer was also used to measure the vertical displacement of the connection at the bolt group centreline. A linear variable differential transformer (LVDT) was used to measure the connection slip with respect to the reaction column. Another LVDT was used to measure the axial deformation of the connection. Clinometers were mounted on the three actuators as well as the beam and were used to measure rotations. Load cells were installed on the actuators, and

pressure transducers were also installed in the hydraulic lines to enable independent redundant load evaluations.

Beam rotation was calculated using the actuators' inclination angles as well as their extension. The calculated beam rotation was compared with the rotation measured directly by the beam clinometer to ensure the validity of the measurements.

The load applied by each actuator was calculated by multiplying the pressure in the hydraulic jack by the area of the piston. The calculated load was compared to the load cell measurement during the test to confirm that all measurement devices are operating properly and consistently.

Horizontal and vertical components of the loads applied by the three actuators were calculated using the cable transducers and clinometers mounted on the actuators. The values were utilized to determine the total horizontal and vertical loads applied to the connection.

3.6 Test Procedure

The specimens were lifted using a chain hoist and moved to the appropriate location on the reaction column. They were bolted to the reaction column using eight 25 mm (1 in.) diameter ASTM A325 pretensioned bolts. The specimens were then bolted to the beam using six or three 19 mm (3/4 in.) diameter ASTM A325 snug-tight bolts. The tests were conducted by application of three loading stages. In the first stage, the loading beam was rotated incrementally using actuator 2 (see Figure 3-6). The rotation was increased until the beam inclination angle with respect to the horizon reached 0.03 radians. The rotation of 0.03 radians is widely used to represent a typical rotation in shear connections at the flexural ultimate limit state, i.e., when the first plastic hinge is formed in the beam. During the application of rotation, the shear load was kept close to zero using actuator 1 to counteract the shear imposed by pushing with actuator 2. After the rotation phase, the horizontal load, if applicable, was applied to the specimen using actuator 3. Once the horizontal loading phase was complete, the shear load was applied mainly using actuator 1. During this stage, the beam inclination angle was kept constant at 0.03 radians using small modifications of

the load in actuator 2. Shear load was increased until the load–displacement curve reached a plateau and the load subsequently started to decline, or one of the specimen components fractured. It is recognized that in reality the shear load and rotation would normally be applied to the connection simultaneously; however, the rotation of 0.03 radians provides a reasonable upper limit of connection rotation at the ultimate limit state and permits the evaluation of the strength of the connection to be made as a pure shear load. Based on the high level of connection ductility observed, the impact of the loading sequence is considered negligible. For interpreting the results in the following section, it is important to note that the connections were tested in an inverted orientation for convenience; i.e., the loading beam was pushed up rather than pulled down.

3.7 Safety

To assure compliance with the university's health and safety act, certain criteria had to be satisfied. The purpose was to prevent any injury to the people present in the lab and/or loss and damage to the equipment and instrumentation. Different potential hazard sources were identified and evaluated and the necessary precautions were considered. One major source of hazard was the possibility of sudden bolt fracture accompanied by a projectile detachment of the bolt shank into two pieces. To avoid any issue caused by this phenomenon, a Plexiglas® shield barrier was set up between the testing area and the person conducting the test, as well as any other person working in the lab. Although the barrier hindered direct access to the specimen for visual inspection, a camera system was installed near the specimen in the hazard area to capture and record the specimen deformations during the test. Any access to the testing area was banned during the test using hazard strips.

3.8 Test Results

General observations from the 17 tests are reported in Table 3-4. The maximum vertical load that each specimen was able to sustain is reported as the connection capacity. Out-of-plane deformation of the plate was visually examined, as well as bolt

fracture and weld rupture. In Table 3-4, "Y" indicates that the specific phenomenon occurred during the test and "N" indicates the contrary. Each column of the table is discussed in detail in the following subsections.

Table 3-4: Connection shear capacities and limit states

Specimen ID	Connection Capacity (kN)	Out-of-plane Deformation (Y/N)	Bolt Fracture (Y/N)	Weld Rupture (Y/N)
3BR-10-0	430	Y	N	N
3BR-13-0	524	Y	Y	N
3BR-10-0-L	467	Y	Y	N
3BR-13-0-L	590	Y	Y	N
3BR-10-0-V1	323	Y	Y	N
3BR-13-0-V1	442	Y	Y	N
3BR-10-100C	350	Y	N	N
3BR-13-100C	455	Y	Y	N
3BR-10-200C	234	Y	N	N
3BR-13-200C	418	Y	Y	N
3BR-10-200T	459	Y	Y	N
3BR-13-200T	522	Y	Y	N
3BM-10-0	255	Y	N	Y
3BM-13-0	275	N	Y	Y
3BM-10-200C	275	Y	N	N
3BM-13-200C	358	N	Y	Y
3BM-10-0-V1	318	N	N	Y

3.8.1 Connection Capacity

The vertical load–vertical displacement curve for specimen 3BR-10-0-L is presented in Figure 3-9. The response curve was derived for every test and was used to evaluate the connection capacity. As noticed from the figure, a number of spikes were formed in the curve due to the incremental application of loading and maintaining the rotation during the test. To capture the capacity more accurately, a horizontal line was fitted to the maximum vertical load of the curve eliminating the effect of spikes. The capacity

of the connection was evaluated at the point right before the vertical load started to decline. In the specific case shown in Figure 3-9, the capacity was evaluated as 467 kN. The vertical load–vertical displacement curves for all the tested specimens are presented in Appendix B.

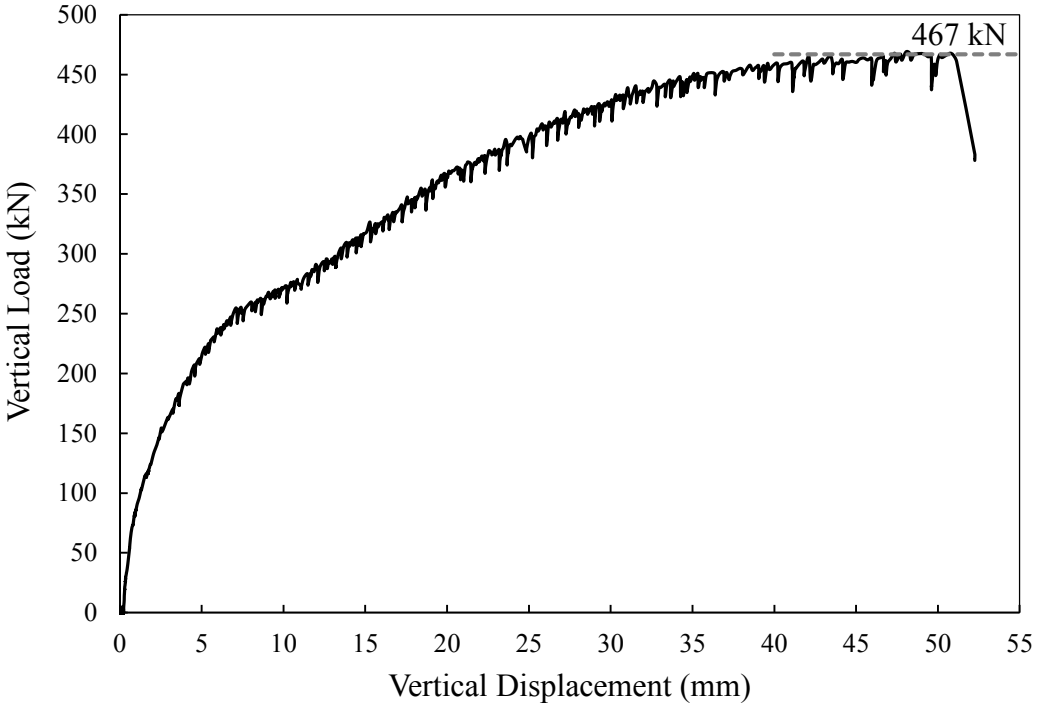

Figure 3-9: Load–displacement curve for 3BR-10-0-L

3.8.2 Limit States

Limit states were considered as the mechanisms contributing to the gradual degradation and failure of the connection. They were identified by close inspection of the connection during the test, as well as monitoring the vertical load–vertical displacement curve and calculation of section forces and moments at critical locations. Several limit states were observed during the tests, each discussed in detail below. The limit state causing the load carried by the connection to drop immediately after the peak load was regarded as the primary failure mode and the limit state causing the significant drop in connection capacity after the occurrence of the primary failure mode was considered the secondary failure mode.

Gross section plasticity was observed in almost all the tests except for some of the 3BM specimens. Gross section plasticity was identified as the extended shear tab reaching its plastic bending moment capacity, as defined by Equation 3-1. The method used to determine the bending moment at the support face is discussed in section 3.8.3. Photographs of typical gradual section plasticity formation at the support face are shown in Figure 3-10.

3-1 $$M_p = Z \times F_y$$

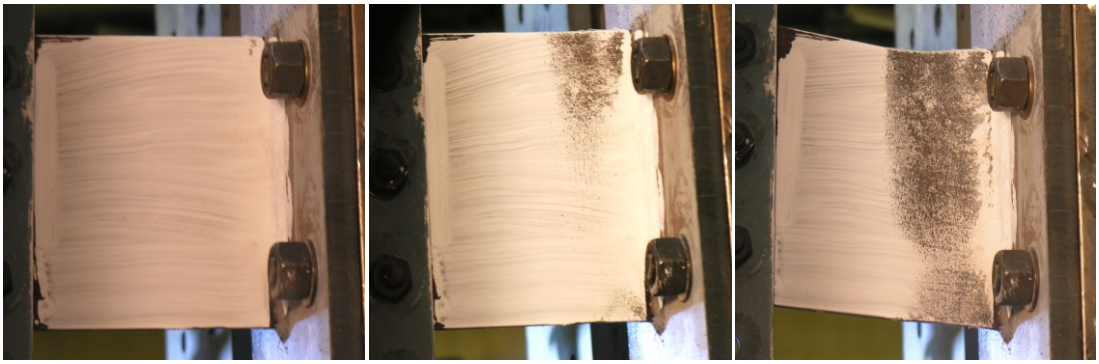

(a) (b) (c)

Figure 3-10: Typical plasticity development at the support face (3BR-10-0): (a) Fully elastic, (b) Partially plastic, and (c) Fully plastic

Net section plasticity at the vertical bolt line closer to the support was identified in many of the tests. Net section plasticity was identified as the extended shear tab reaching its net section bending moment capacity, as defined by Equation 3-1, using the net section plastic modulus instead of that of the gross section. The method used to determine the bending moment at the vertical bolt line is discussed in section 3.8.3.

Out-of-plane deformation was observed in all 3BR tests. The out-of-plane deformation started before the connection reached its capacity and developed as the load increased. In most of the tests, although severe out-of-plane deformation occurred during the test, this phenomenon was not considered a failure mode, i.e., the connection capacity was not limited by out-of-plane deformation.

Photographs of the deformed shape of specimen 3BR-10-0 from different angles are shown in Figure 3-11.

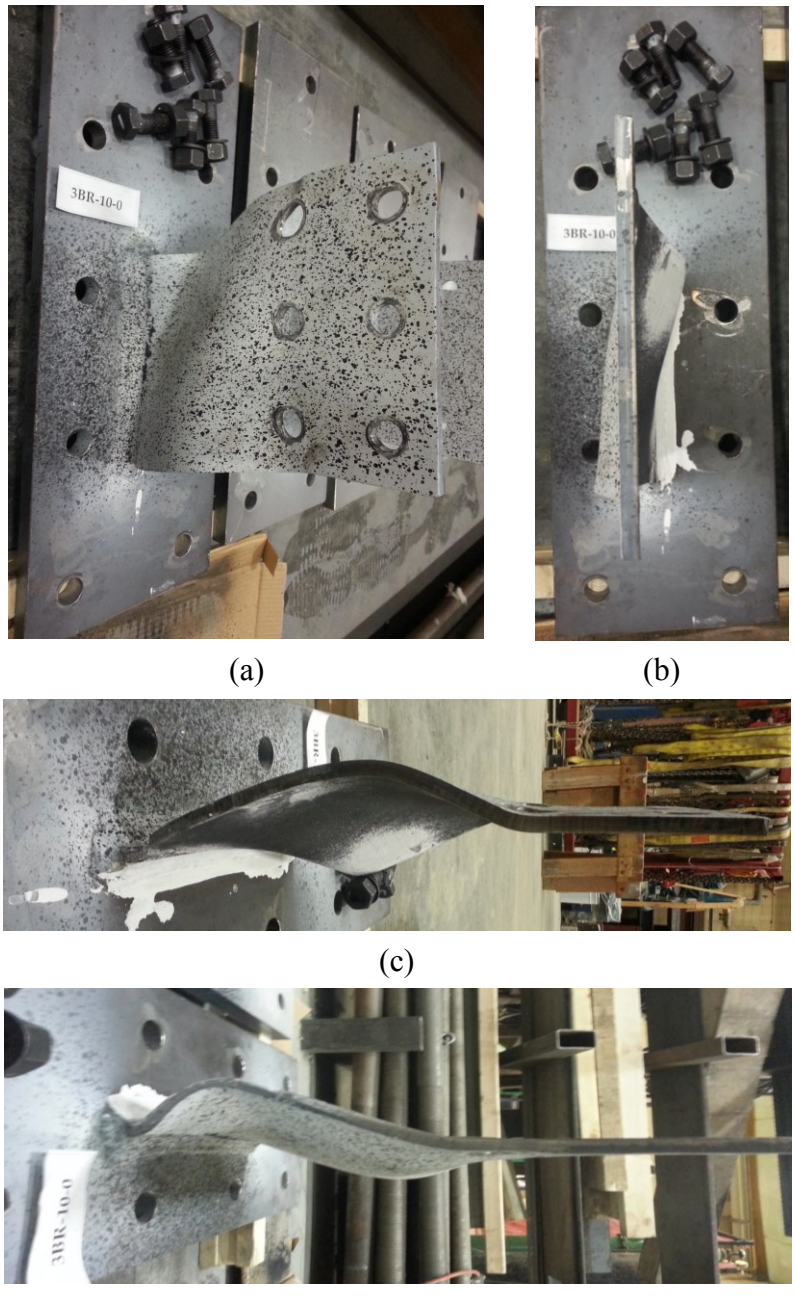

(a) (b)

(c)

(d)

Figure 3-11: Specimen 3BR-10-0 after test, different views:
(a) Overall; (b) Front; (c) Bottom and (d) Top

Bolt fracture was observed in many of the 3BR and some 3BM specimens. Bolt fracture in all cases occurred after the extended shear tab experienced considerable plasticity and out-of-plane deformation. Therefore, bolt fracture was identified as the primary or secondary failure mode in many of the 3BR specimens. It should be noted that since the length of the bolt shanks used in this testing program was specified such that the threads were never intercepted by the shear plane, every bolt fracture occurred in an unthreaded section of the bolt shank. Photographs taken from deformed and fractured bolts are shown in Figure 3-12.

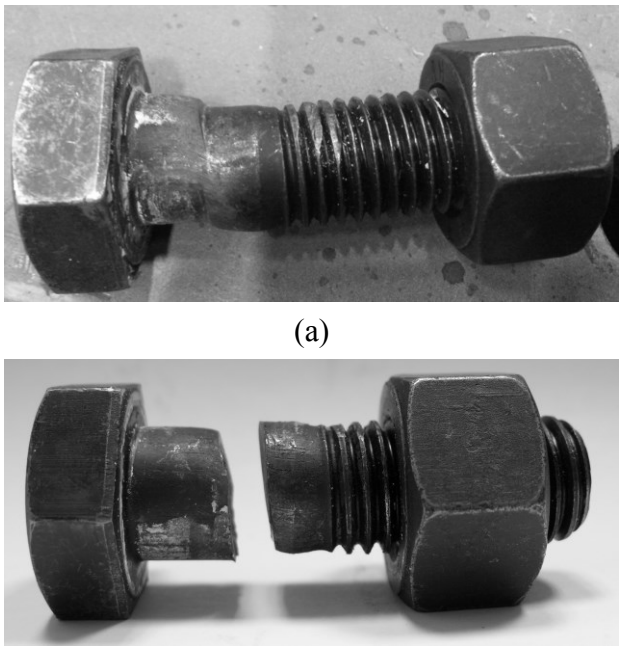

(a)

(b)

Figure 3-12: Bolts after test:
(a) Excessively deformed; (b) Fractured

Weld rupture was observed in all of the 3BM specimens except 3BM-10-200C, but none of the 3BR specimens. (Very small self-limiting tears at the end of a weld were not considered to constitute weld rupture.) It should be noted that when weld rupture occurred, it was before any noticeable out-of-plane deformation happened. Therefore, weld rupture was identified as the primary failure mode in some of the 3BM specimens. This failure mode was also accompanied by a sudden drop in the vertical

load–vertical displacement curve. Photos of weld rupture in specimen 3BM-13-0 are shown in Figure 3-13.

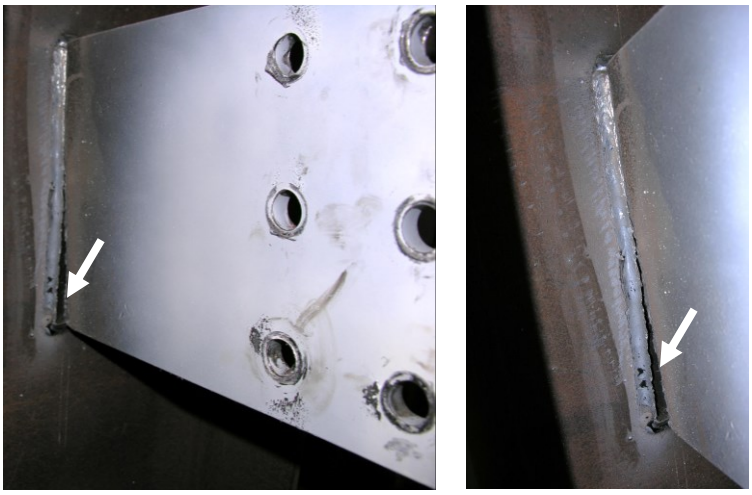

Figure 3-13: Weld rupture in specimen 3BM-13-0

3.8.3 Bending Moment at the Support

In-plane bending moments at the support, M^S, were derived by calculating the summation of the multiplication of the actuator horizontal and vertical load components by their respective moment arms. Load components were calculated by projecting the actuator loads measured by the load cells along the horizontal and vertical directions based on the angle measured by the clinometer mounted on each actuator. Moment arms were calculated geometrically based on the measured elongation and inclination angle of each of the actuators. To get a better understanding of the magnitude of the moments developed at the support, the actual value was divided by the plastic moment capacity of the plate section, M_p, calculated based on the measured material properties achieved from tension coupon tests. The presence of the weld at the support provides extra strength at the support face by increasing the effective section thickness and material strength in this region. To evaluate the influence of this effect, the bending moments on the plate section at both the support face and the weld toe line were calculated for each test, and the associated moment ratio curves for specimen 3BR-10-0-L are presented in Figure 3-14. The

ratio of the moment at the weld toe line to the section plastic moment is presented for all specimens in Table 3-5. Since the ratio is variable during the test, both the maximum moment ratio, and the moment ratio at the maximum shear load are reported in the table.

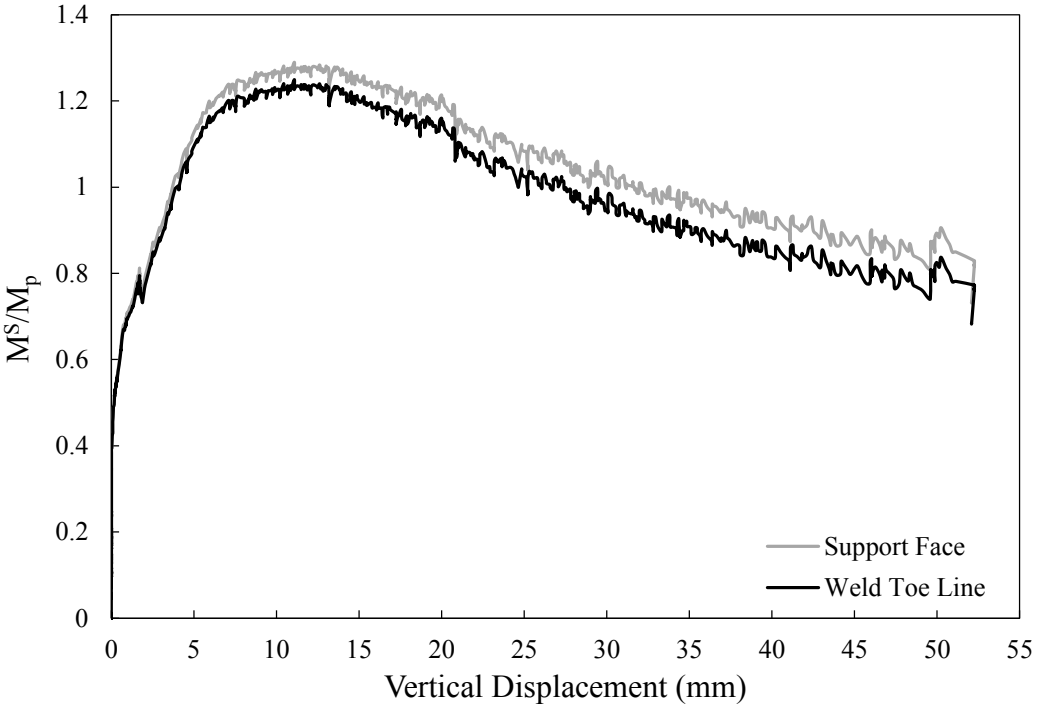

Figure 3-14: Support moment ratios for specimen 3BR-10-0-L

Table 3-5: Weld toe line moment, shear, and eccentricity ratios

Specimen ID	At M^S_{Max}				At V_{Max}	
	M^S/M_p	e_s/e_g	V (kN)	V/V_{Max}	M^S/M_p	e_s/e_g
3BR-10-0	1.22	0.76	354	0.82	1.06	0.48
3BR-13-0	1.35	0.81	353	0.67	1.21	0.48
3BR-10-0-L	1.23	1.00	273	0.58	0.81	0.39
3BR-13-0-L	1.44	0.85	434	0.74	1.39	0.59
3BR-10-0-V1	1.24	1.00	297	0.92	0.87	0.66
3BR-13-0-V1	1.43	0.87	410	0.93	1.37	0.88
3BR-10-100C	1.03	1.00	147	0.42	0.54	0.25
3BR-13-100C	1.22	0.86	292	0.64	0.87	0.41
3BR-10-200C	0.86	1.00	165	0.71	0.20	0.05
3BR-13-200C	1.08	0.80	280	0.67	0.75	0.14
3BR-10-200T	1.41	0.80	347	0.76	1.39	0.59
3BR-13-200T	1.43	0.78	444	0.85	1.42	0.67
3BM-10-0	0.91	0.89	224	0.88	0.30	0.06
3BM-13-0	0.82	0.95	227	0.83	0.24	0.09
3BM-10-200C	0.75	0.89	176	0.64	0.18	0.12
3BM-13-200C	0.84	0.70	287	0.80	0.70	0.50
3BM-10-0-V1	1.07	0.84	318	1.00	1.07	0.84

3.8.4 Bending Moment at the Vertical Bolt Line

In-plane bending moments at the vertical bolt line closer to the support face were derived by calculating the summation of the multiplication of the actuator load components in the horizontal and vertical directions by their respective moment arms. To get a better understanding of the magnitude of the moments developed at the support face the actual value was divided by the nominal plastic moment capacity of the reduced section at the centreline of the bolt holes calculated based on the actual material properties achieved from tension coupon tests. The variation in ratio of the moment developed at the vertical bolt line over the reduced section plastic moment capacity for specimen 3BR-10-0-L is presented in Figure 3-15. To be able to compare

the moment ratio variation at the bolt line to the moment ratio variation at the weld toe line (still normalized by the gross section plastic moment), both variations are shown simultaneously. It should be noted that in the figure, a positive moment ratio indicates that the moment applies compression to the section fibres above the neutral axis of the section. While the moment ratios at the support remained positive throughout each test, it is common for the moment ratio at the bolt line to change its sign. When the weld toe line and bolt line moments have the same sign, the extended shear tab is in single curvature, and when the moment signs are different, it is in double curvature. The moment ratio–vertical displacement curves for all the tested specimens are presented in Appendix B.

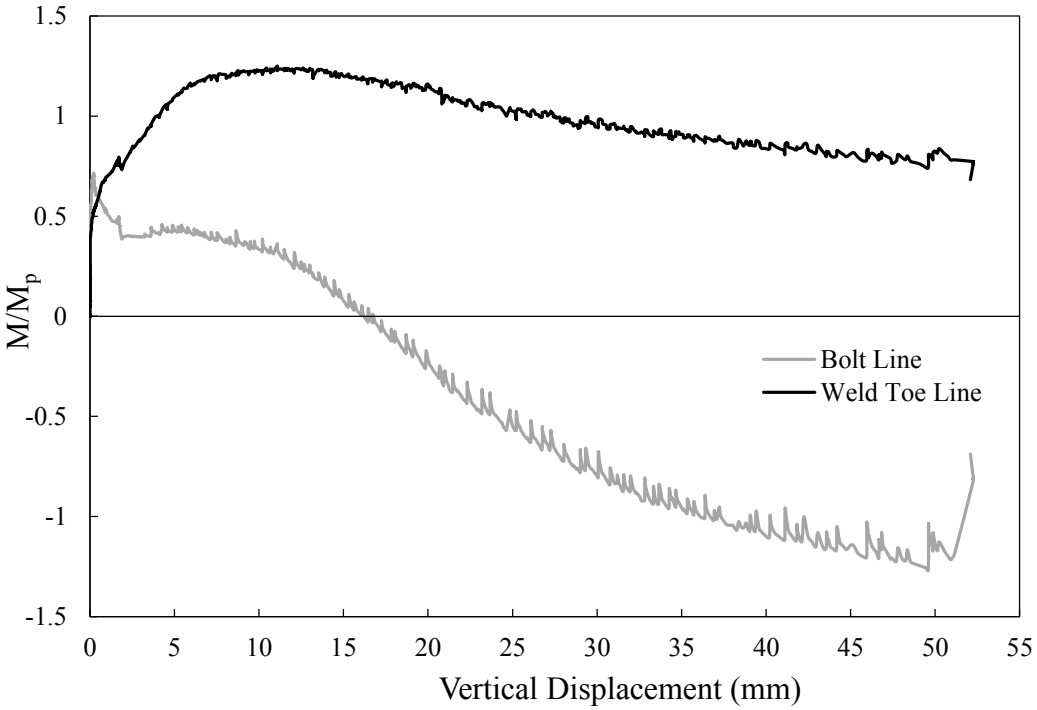

Figure 3-15: Bolt line and weld toe line moment ratios for specimen 3BR-10-0-L

The ratio of the moment at the bolt line, M^B, to the net section plastic moment, M_p, is presented at the maximum moment at both the support (at the weld toe line) and the bolt line for all specimens in Table 3-6.

Table 3-6: Bolt line moment, shear, and eccentricity ratios

Specimen ID	At M^S_{Max}				At M^B_{Max} (V_{Max})	
	M^B/M_p	e_b/e_g	V (kN)	V/V_{Max}	M^B/M_p	e_b/e_g
3BR-10-0	-0.35	0.24	354	0.82	-1.23	0.52
3BR-13-0	-0.13	0.19	353	0.67	-0.99	0.52
3BR-10-0-L	0.35	0.00	273	0.58	-1.22	0.61
3BR-13-0-L	-0.02	0.15	434	0.74	-0.77	0.41
3BR-10-0-V1	-0.04	0.00	297	0.92	-0.73	0.34
3BR-13-0-V1	-0.28	0.13	410	0.93	-0.51	0.22
3BR-10-100C	0.17	0.00	147	0.42	-1.32	0.75
3BR-13-100C	0.07	0.14	292	0.64	-1.26	0.59
3BR-10-200C	0.15	0.00	165	0.71	-1.10	0.95
3BR-13-200C	-0.05	0.20	280	0.67	-1.28	0.66
3BR-10-200T	0.02	0.20	347	0.76	-0.95	0.41
3BR-13-200T	-0.20	0.22	444	0.85	-0.59	0.33
3BM-10-0	0.00	0.11	224	0.88	-1.20	0.94
3BM-13-0	0.09	0.05	227	0.83	-0.99	0.91
3BM-10-200C	0.00	0.11	176	0.64	-1.28	0.88
3BM-13-200C	-0.27	0.30	287	0.80	-0.91	0.50
3BM-10-0-V1	0.00	0.16	318	1.00	0.00	0.16

3.8.5 Shear Load Eccentricity

In the design of shear connections, generally it is assumed that no moment will be transferred to the support and therefore the location of the point of inflection is assumed to be at the support face. The 14th edition of the AISC *Steel Construction Manual* (AISC 2011) states that in the extended shear tab connection, the bolt group should be designed for an eccentricity equal to the distance from the bolt group centre to the support face. This assumption leads to a moment distribution along the extended shear tab length as shown in Figure 3-16(a). However, recent research by the authors and other researchers (Thomas et al. 2014) has revealed that the assumption of zero moment at the support contradicts the actual connection behaviour

in many cases. The actual bending moment distribution along the length of a typical extended shear tab follows the double-curvature pattern, as depicted in Figure 3-16(b).

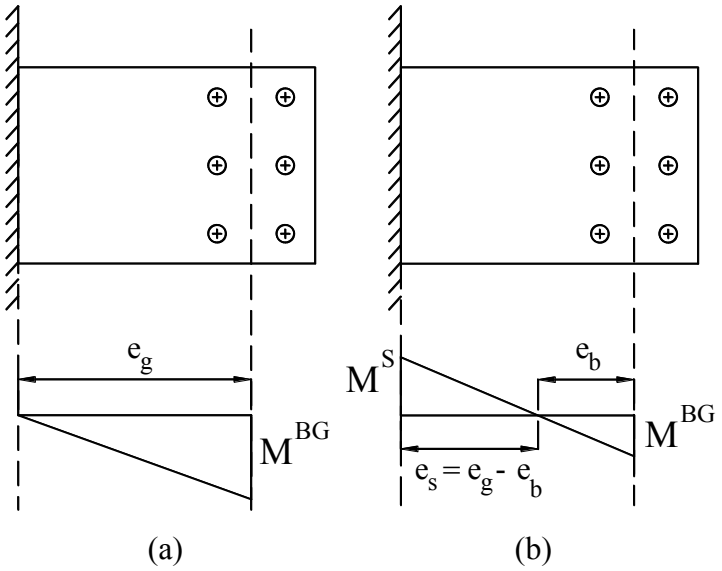

Figure 3-16: Moment distribution along the plate:
(a) Common assumption; (b) Typical

In this study, the shear load eccentricity for the bolt group was measured and recorded during each test. The eccentricity ratio was defined as the ratio of bolt group shear load eccentricity over the geometric eccentricity (e_b/e_g), where the geometric eccentricity for each specimen is defined as the distance from the bolt group centre to the support face. Based on the moment distribution presented in Figure 3-16(b), the bending moment at the bolt group centre, M^{BG}, could be written as a function of the shear force, V, as:

3-2 $$M^{BG} = V \times e_b$$

Moreover, for the whole plate, the static equilibrium equation gives

3-3 $$M^{BG} + M^{S} = V \times e_g$$

Rearranging Equation 3-3:

3-4 $$M^{BG} = V \times e_g - M^S$$

Substituting Equation 3-2 into Equation 3-4, results in Equation 3-5, which was used to calculate the bolt group eccentricity at each loading step.

3-5 $$e_b = e_g - {M^S}/{V}$$

The eccentricity ratio was considerably variable during each test. The variation for specimen 3BR-10-0-L is depicted in Figure 3-17. The eccentricity ratio–vertical displacement curves for all the tested specimens are presented in Appendix B.

As noticed from Figure 3-17, the eccentricity showed a negative value during the initial phases of the loading, implying that the inflection point was located along the beam span and the extended shear tab had a single curvature moment distribution. However, at around 12 mm vertical displacement, due to bolt group slip, the inflection point moved to the bolt group centre and therefore, the eccentricity ratio reached zero. With further increases in the vertical load, as the bolts started to bear on the bolt holes of the extended shear tab, the bolt group started to absorb bending moment and push the inflection point towards the support. The eccentricity ratio increased and the extended shear tab was bent in double curvature until at around 48 mm the maximum vertical displacement was reached and the connection subsequently failed.

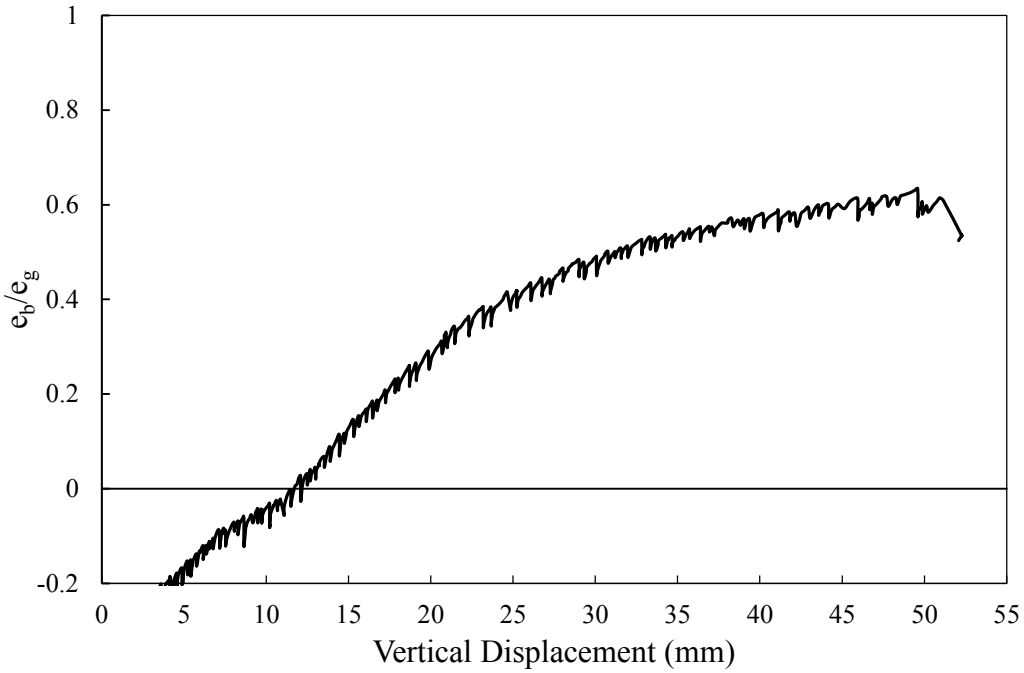

Figure 3-17: Eccentricity ratio variation in specimen 3BR-10-0-L

Considering Figure 3-14, Figure 3-17, and Table 3-6, for specimen 3BR-10-0-L, the eccentricity ratio was around zero when the weld toe line moment reached its maximum value, and the eccentricity ratio was 0.61 when the connection reached its capacity. As noticed from Table 3-6, the eccentricity ratio was quite variable for different specimens; however, for the majority of the specimens, it was small when the weld toe line moment reached its maximum value and it tended to increase quite rapidly as the connection approached its capacity. At V_{max}, the eccentricity ratio ranges from 0.16 to 0.95 over all of the specimens tested. The eccentricity ratio values were quite diverse for the tests with horizontal load, which reveals the need for further research to identify the relationship between horizontal load and shear load eccentricity.

3.8.6 Effects of Key Variables

The 17 specimens could be categorized into two main groups: the 3BR group, which consisted of twelve specimens with extended shear tabs welded to a 25 mm (1 in.)

support plate using either 8 or 10 mm thick welds; and the 3BM group, which consisted of five extended shear tabs welded to the web of a column stub using a 6 mm thick weld. Stiffeners were welded to the back side of the column web to restrain the web against out-of-plane deformation.

In the 3BR group, six specimens had a 9.5 mm (3/8 in.) thick plate and six had a 12.7 mm (1/2 in.) thick plate. For each thickness within the 3BR group, one specimen had a shorter length and one specimen had only one vertical bolt line.

In the 3BM group specimens, three had a 9.5 mm (3/8 in.) thick plate and two had a 12.7 mm (1/2 in.) thick plate. Out of the three 9.5 mm (3/8 in.) thick extended shear tabs, one had only one vertical bolt line.

The specimens were tested under pure vertical load and combinations of different horizontal loads and vertical load.

Several observations are made about the effects of the variables on the behaviour of the extended shear tab connections in the following sections.

3.8.6.1 Plate Length

Comparing specimens 3BR-10-0-L and 3BR-13-0-L with 3BR-10-0 and 3BR-13-0, it is observed that by decreasing the extended shear tab length, the connection capacity was significantly increased. Extended shear tabs with shorter length had an increased resistance to out-of-plane deformation due to their reduced unrestrained length. Moreover, the load eccentricity imposed on the bolt group and the plate section at the vertical bolt line was lower, resulting in increased bolt group capacity and increased vertical load causing the net section plasticity. The ductility of the shorter specimens was only slightly lower. The vertical load–vertical displacement curves for specimens 3BR-13-0 and 3BR-13-0-L are presented in Figure 3-18.

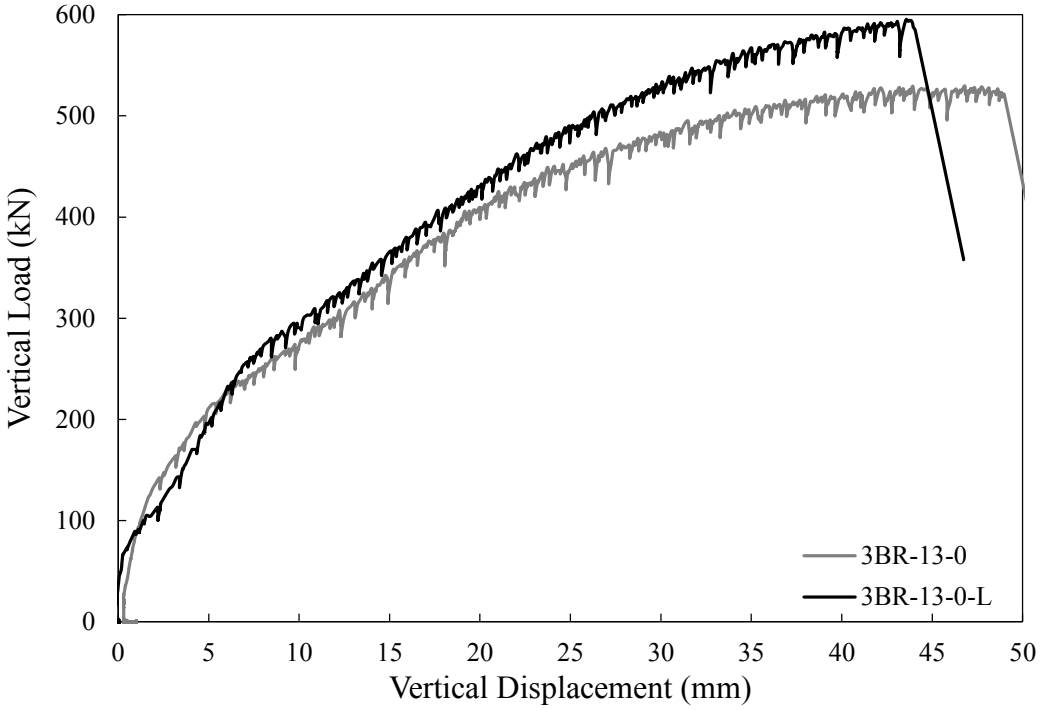

Figure 3-18: Effect of extended shear tab length on connection behaviour

3.8.6.2 Plate Thickness

Using the test matrix, a one-to-one comparison could be made between the 9.5 mm thick and 12.7 mm thick extended shear tabs. Increasing the plate thickness always resulted in an increase in the peak vertical load, as expected. Increasing the plate thickness resulted in an increased section plastic capacity as well as increased connection resistance against failure due to out-of-plane deformation. A comparison between the vertical load–vertical displacement curves of specimens 3BR-10-0-L and 3BR-13-0-L is presented in Figure 3-19. As shown, increasing the thickness by 3 mm resulted in an increase in the connection capacity by almost 21%. The thicker specimens tended to show slightly lower ductility.

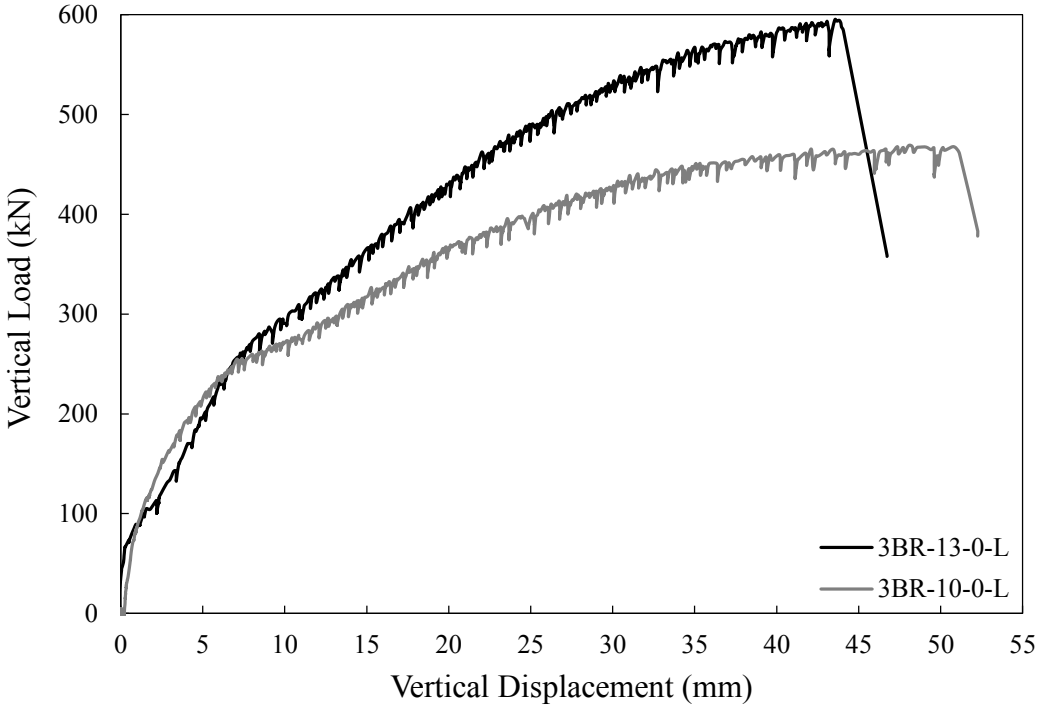

Figure 3-19: Effect of extended shear tab thickness on connection behaviour

3.8.6.3 Number of Vertical Bolt Lines

Using only one vertical bolt line resulted in a reduction in the connection peak vertical load, as expected. Changing the bolt configuration was considered such that the distance between the first bolt line and the support face remained constant (see Figure 3-1). Therefore, the geometric eccentricity applied to the centre of the bolt group with one vertical bolt line was lower than the one for the regular specimens with two vertical bolt lines. Based on this discussion, although the number of bolts in the connection was reduced by one-half, the eccentricity applied to the bolt group was also reduced. Therefore, the two effects acted in contrast to each other, resulting in the fact that the reduction in connection capacity due to using one vertical bolt line was only around 18%. In addition, the ductility was somewhat reduced. A comparison between the vertical load–vertical displacement curves of specimens 3BR-13-0 and 3BR-13-0-V1 is presented in Figure 3-20.

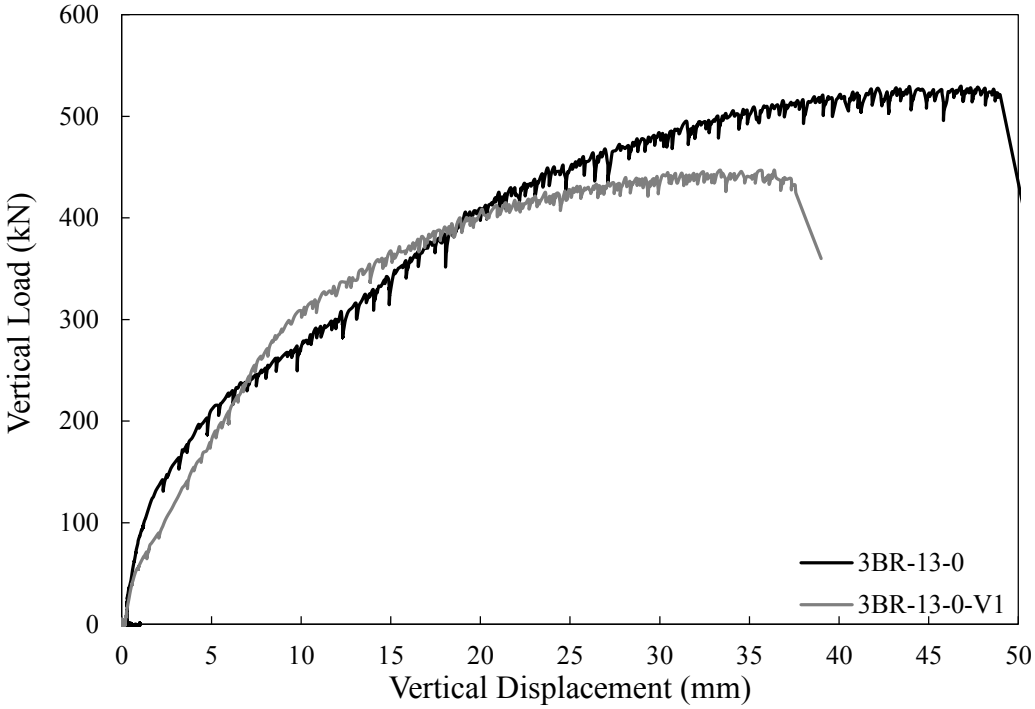

Figure 3-20: Effect of number of vertical bolt lines on connection behaviour

3.8.6.4 Presence of Horizontal Load

The presence of horizontal load had a significant effect on the connection capacity. The behaviour of specimen 3BR-13 under 0, 100 kN and 200 kN compressive horizontal load is depicted in Figure 3-21. As noticed from the figure, application of 100 kN compressive horizontal load reduced the capacity by 13%. Addition of another 100 kN compressive horizontal load resulted in 7% more reduction in the capacity. Application of horizontal load reduced the section plastic flexural capacity, resulting in reduced overall connection capacity. Moreover, adding compressive horizontal load added more demand on the bolt group resulting in earlier bolt fracture, which reduced the connection ductility and bolt group vertical load resistance.

Figure 3-22 shows the capacities of the 3BR and 3BM specimens, with "L" and "V1" specimens removed for geometric consistency, under various horizontal loads. In this figure, negative horizontal forces are compressive and positive values indicate that the horizontal load was tensile. For the 3BR specimens, the application of

compressive horizontal load resulted in reduced connection capacity and application of tensile horizontal load had only a minor effect on the connection capacity. However, for the 3BM specimens the trend was reverse, meaning that by application of compressive horizontal load, the connection capacity improved. This phenomenon could be described based on the failure mode observed in 3BM specimens. Both 3BM-10-0 and 3BM-13-0 specimens failed due to weld rupture. The weld rupture occurred as a result of a combination of tensile normal stresses developed by the moment at the support and shear stresses developed by the vertical load applied to the connection. Application of compressive horizontal load resulted in a considerably reduced tensile stress transferred from the bottom edge of the plate to the support weld. Therefore, the support weld was less susceptible to premature rupture in 3BM-10-200C and 3BM-13-200C specimens. It should be noted that with larger welds, an increase in connection capacity may not be realized through the addition of compressive load.

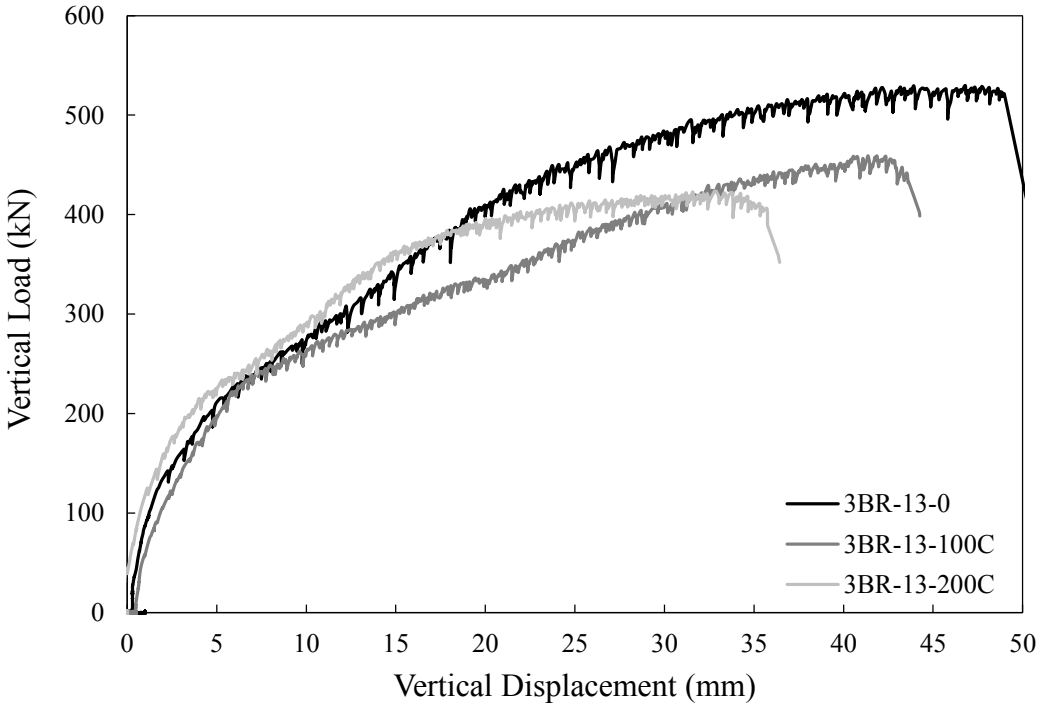

Figure 3-21: Effect of horizontal load on connection behaviour

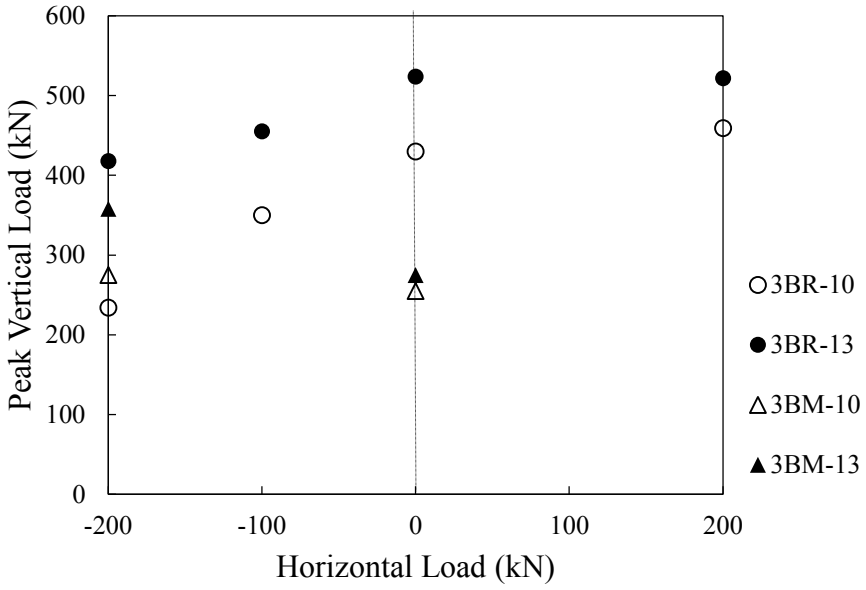

Figure 3-22: Effect of horizontal load on connection capacity

3.8.6.5 Support Condition

As described in Section 3.8.5, the specimens are categorized into two groups based on the support condition. The 3BR group specimens were extended shear tabs welded to a 25 mm (1 in.) support plate using either 8 or 10 mm thick welds, while the 3BM group consisted of extended shear tabs welded to a column web using 6 mm thick welds. Stabilizer plates were welded to the back side of the column to restrain the web against out-of-plane deformation. Results of the tests showed that most of the 3BM specimens failed due to weld rupture and the 6 mm thick weld lacked the required capacity to hinder premature weld rupture. However, in all 3BR specimens, the welds remained intact during the test. It is concluded that a 6 mm thick weld, which was designed based on the assumption of pure shear at the support, was not sufficient and the assumption of pure shear at the support resulted in an overestimation of connection capacity.

3.9 Comparison of Results with Current Design Methods

Two design methods were used to evaluate the connection behaviour and to calculate each connection capacity, including the method presented in 14th edition of the AISC *Steel Construction Manual* (2011) and the method developed by Thomas et al. (2014). In all calculations, the resistance factor is omitted and measured material properties are used to provide a direct comparison with the test results. As discussed in Chapter 2, the AISC method does not account for the application of axial load in the calculation of the connection capacity. Therefore, the capacities calculated based on the AISC method are reported only for the specimens without any axial load. Moreover, in the method developed by Thomas et al. (2014), since the support is almost rigid, the support web yielding failure mode was not considered in evaluating the connection capacity. The capacities achieved from the two methods are presented in Table 3-7.

As can be seen from Table 3-7, the Thomas et al. (2014) method under-predicted the capacities of almost all the 3BR specimens. Specimen 3BR-10-200C, which included the most slender extended shear tab under the highest axial compressive load, produced a test-to-predicted load ratio of less than 1.0. In this special case, the specimen was subjected to significant load amplification from second-order effects that are not taken into account in the design method.

The design method minimum weld size recommendation was not satisfied for the 3BM specimens. Therefore, premature weld rupture was expected to occur during the tests, giving test-to-predicted ratios lower than 1.0.

As discussed earlier, the AISC method is only capable of calculating the connection capacity in the absence of axial load. As noticed from Table 3-7, the AISC method under-predicted the connection capacity by a huge margin.

Table 3-7: Comparison of current design methods and experimental results

Specimen ID	Test Capacity (kN)	Thomas et al. (2014)		AISC (2011)	
		Capacity (kN)	Test/Predicted	Capacity (kN)	Test/Predicted
3BR-10-0	430	328	1.31	119	3.61
3BR-13-0	524	349	1.50	143	3.66
3BR-10-0-L	467	395	1.18	153	3.05
3BR-13-0-L	590	395	1.49	167	3.53
3BR-10-0-V1	323	180	1.79	113	2.86
3BR-13-0-V1	442	180	2.46	113	3.91
3BR-10-100C	350	325	1.08	-	-
3BR-13-100C	455	340	1.34	-	-
3BR-10-200C	234	313	0.75	-	-
3BR-13-200C	418	330	1.27	-	-
3BR-10-200T	459	313	1.46	-	-
3BR-13-200T	522	346	1.51	-	-
3BM-10-0	255	328*	0.78	119	2.14
3BM-13-0	275	349*	0.79	143	1.92
3BM-10-200C	275	313*	0.88	-	-
3BM-13-200C	358	330*	1.08	-	-
3BM-10-0-V1	318	180*	1.77	113	2.81

* Minimum weld size not met

Based on the ratio of the tested peak vertical load to predicted capacity achieved using the two design methods, it could be concluded that both the Thomas et al. (2014) method and the AISC method under-predicted the specimens' capacities. However, the Thomas et al. (2014) method produced results much closer to the actual capacity than the AISC method.

Although the two design methods in most cases under-predicted the peak vertical load, the trends observed from the tests were similar to those observed from the design methods. The peak vertical loads for the thicker plates were higher than those for the thinner plates. Shorter plates had a higher capacity. The specimens with one

vertical bolt line had lower capacities than those with two vertical bolt lines. As the axial load increased, the connection capacity decreased.

The expected failure modes based on both design methods were compared with the failure modes observed during the tests, and the results are reported in Table 3-8. In the table, the limit states observed in each test are reported and the one accountable for vertical load reduction is indicated in bold as the failure mode. Moreover, it should be noted that although out-of-plane deformation was observed in all 3BR specimens, it was identified as the failure mode only in the cases where the vertical load carried by the connection declined due to this phenomenon.

Table 3-8: Comparison of observed and predicted failure modes

Specimen ID	Test	Thomas et al.	AISC
3BR-10-0	GSP, NSP, **OPD**	FY	OPD
3BR-13-0	GSP, NSP, **BF**	BF	PB
3BR-10-0-L	GSP, NSP, **BF**	FY	PB
3BR-13-0-L	GSP, **BF**	BF	PB
3BR-10-0-V1	GSP, **BF**	BF	BF
3BR-13-0-V1	GSP, **BF**	BF	BF
3BR-10-100C	GSP, NSP, **OPD**	FY	-
3BR-13-100C	GSP, NSP, **BF**	BF	-
3BR-10-200C	GSP, NSP, **OPD**	FY	-
3BR-13-200C	GSP, NSP, **OPD**, BF	BF	-
3BR-10-200T	GSP, **BF**	FY	-
3BR-13-200T	GSP, **BF**	FY	-
3BM-10-0	WR, NSP, **OPD**	WR	OPD
3BM-13-0	WR, **NSP**	WR	PB
3BM-10-200C	GSP, NSP, **OPD**	WR	-
3BM-13-200C	GSP, WR, **BF**	WR	-
3BM-10-0-V1	GSP, **WR**	WR	BF

The method of Thomas et al. (2014) predicted flexural yielding as the failure mode for many of 3BR specimens. Based on Table 3-5, all the 3BR specimens reached their section flexural capacities and therefore the predictions were correct for some specimens. However, the peak vertical loads in the tests exceeded the predicted values considerably. Moreover, in most of the 3BM specimens, the Thomas et al. (2014) method identified the failure mode correctly.

In the AISC method, plate buckling and out-of-plane deformation failure modes are distinguished and evaluated using different procedures. Plate buckling is evaluated using the elastic buckling equation developed for coped beams (Cheng et al. 1984) and represents a sudden elastic out-of-plane buckling of the plate. Out-of-plane deformation, however, is judged to be the failure mode when the required stabilizer plates are not present in the connection configuration and is evaluated based on the equation developed by Thornton and Fortney (2011). Based on this discussion, the AISC method predicted the failure mode correctly only for specimens 3BR-10-0, 3BM-10-0, 3BR-10-0-V1, and 3BR-13-0-V1.

Based on the failure mode predictions using the two design methods, it could be concluded that the Thomas et al. (2014) method is capable of predicting the failure mode of the extended shear tab connection quite accurately. However, the AISC method lacks the required accuracy in predicting the failure mode of the extended shear tab connection.

3.10 One-to-one Comparison with Thomas et al. (2014) Tests

As discussed earlier, the specimen dimensions considered in this study were defined such that one-to-one comparisons could be made between the results acquired from this study and those achieved from the study conducted by Thomas et al. (2014). Moreover, the 3BM specimens were fabricated with the Thomas et al. (2014) specimens and were therefore exactly the same as the 3B specimens of Thomas et al. (2014) in terms of material properties and geometry, except for the addition of the stiffeners welded to the other side of the column stub web. The 3BR specimens considered in this study had the same plate geometry as the Thomas et al. (2014)

specimens; however, they had a stiff 25 mm (1 in.) plate as the support. Moreover, since the specimens were fabricated from different plates from the Thomas et al. (2014) plates, the steel yield and ultimate stresses were different in the 3BR and 3B specimens. The specifications of the three categories are provided in Table 3-9.

Table 3-9: Specimen category specifications

Specimen Category	3B		3BM		3BR	
Plate Thickness (mm)	10	13	10	13	10	13
Steel F_y (MPa)	455	418	455	418	427	351
Support Condition	Stub Column Web		Stub Column Web with Stiffeners		Stiff Plate	
Weld Size (mm)	6	6	6	6	8	10

To evaluate the effect of support condition on the behaviour of extended shear tabs, the tested specimens were compared to their corresponding specimens in the Thomas et al. (2014) study, as reported in Table 3-10.

Table 3-10: One-to-one comparison with Thomas et al. (2014) results

Current Study			Thomas et al.		
Specimen ID	Capacity (kN)	Failure Mode	Specimen ID	Capacity (kN)	Failure Mode
3BR-10-0	430	OPD	3B-10-U-0	151	WR
3BM-10-0	255	WR			
3BR-10-200C	234	OPD	3B-10-U-200C	142	WR
3BM-10-200C	275	OPD			
3BR-13-200C	418	OPD	3B-13-U-200C	194	BF
3BM-13-200C	358	WR			
3BR-10-200T	459	OPD	3B-10-U-200T	142	WR

Several conclusions could be made by comparing the three series of specimens. Adding stiffeners resulted in a greatly increased resistance to the stub column web

against rotation and formation of yield line mechanism, resulting in considerably improved connection capacity. Stiffening the connection against rotation reduced the stress concentration at the weld close to the tip of the extended shear tab and therefore resulted in delayed weld rupture. However, since the weld size was under-sized for the 3BM specimens, weld rupture still governed the connection capacity in some of the specimens in this category.

The specimens within the 3BR category could be compared to their counterparts in the 3B group. However, as shown in Table 3-9, the average yield strength of the 3BR specimens was slightly lower than that of their 3B equivalents. Despite this fact, a one-to-one comparison of the specimens reveals that the support rotational stiffness had a significant effect on the overall connection behaviour. In some cases the connection capacity with the stiff support even reached more than three times the capacity of the connection with the flexible support. The primary reason behind the improvement of connection behaviour by using a stiff support is its effect on the location of the inflection point along the plate length and the failure mode. When the extended shear tab is welded to a flexible support, the relatively low rotational stiffness of the support causes the inflection point to move towards the support face, which consequently increases the shear load demand on the bolt group. Moreover, the excessive rotation of the support face results in the formation of a yield line mechanism in the column web, which contributes to the gradual loss of stiffness in the connection. On the other hand, the stiff support condition pushes the inflection point far from the support face and thus the bolt group is subjected to a relatively low shear load eccentricity. As the load is increased, the highly eccentric shear load applied to the support face results in gradual plasticity of the plate section and formation of a plastic hinge at the support face. After this stage, due to the loss of stiffness of the section, the inflection point starts to migrate towards the support face. Based on Equation 3-6, which is derived from the static equilibrium of the extended shear tab, as the support eccentricity, e_s, decreases, the shear load increases and the connection is able to sustain additional load. Due to the excessive distortion in the plate, out-of-plane deformation is initiated in the extended shear tab. Moreover, as the shear load increases in the connection and the inflection point moves towards the

support face, the bolt group experiences higher demand and shear load eccentricity. Moreover, the plate net section at the vertical bolt line closer to the support is subjected to an increasing bending moment which eventually results in section plasticity at this location. Finally, the connection fails due to either excessive out-of-plane deformation or sudden bolt fracture.

3-6 $$V \times e_s = M^S \Rightarrow e_S = {M^S}/{V}$$

Based on this discussion, the load resistance mechanism in the case of an extended shear tab with a stiff support allows for taking advantage of the plate gross section flexural capacity. Moreover, it allows for redistribution of forces and moments along the plate length, which consequently results in the ability of the connection to sustain significant additional shear load even after the formation of a plastic hinge at the support face. On the contrary, in the case of an extended shear tab with a flexible support, the inflection point is located closer to the support face and therefore imposes a high shear load eccentricity on the bolt group. This phenomenon may result in sudden bolt group fracture before the connection reaches its full section plastic capacity and before any force redistribution can occur.

3.11 Summary

A total of 17 extended shear tabs were tested. The connections varied in shear tab length, thickness, bolt configuration, support condition and application of horizontal load.

An existing set-up was modified to meet the specific research needs and several instruments were used in the test set-up to capture and record the desired parameters. Each test was conducted by applying the rotation of 0.03 radians to the specimen, followed by application of horizontal load (if any) and finally failing the connection by application of vertical load.

The peak vertical load was recorded for each test. Several limit states were observed, including gross section plasticity, net section plasticity, out-of-plane deformation, bolt

fracture, and weld rupture. Bending moment variations were recorded at the support and at the vertical bolt line. It was observed that in most cases, the bending moment at the two locations reached or exceeded the plate nominal plastic moment. Bolt group shear load eccentricity variation was also evaluated for each test.

The effects of key variables on the behaviour and capacity of the connections were investigated. The results were compared with the prediction of two design methods and it was concluded that both method provide conservative predictions for the connection capacity.

CHAPTER 4: FINITE ELEMENT INVESTIGATION ON EXTENDED SHEAR TABS

4.1 Introduction

In this chapter, a detailed finite element model for extended shear tabs is developed. The efficiency and accuracy of the model is validated by comparing the analysis results with the available test data obtained by the authors and Thomas et al. (2014). The validated model is then used to conduct a comprehensive parametric study to expand the scope of the research and to get a better understanding of the extended shear tab connection behaviour. The design method developed by Thomas et al. (2014) is then evaluated based on the analysis results, and additional aspects of connection behaviour are identified.

4.2 Model Development

In this section, development of the finite element model for extended shear tabs is discussed as a hierarchy of several steps. The model was developed and analyzed using the Abaqus finite element package (Dassault Systèmes 2012).

4.2.1 Typical Model Overview and components

The members that form an extended shear tab connection include the shear tab plate, supported beam, supporting column, and connection bolts. A typical model assembly is shown in Figure 4-1(a). The components were created individually in Abaqus using customized modelling techniques. In the current section, the procedure used to create each individual part is discussed.

The connection plate was created as a three-dimensional part. The bolt holes were then cut through the plate thickness based on the specific hole pattern for the considered model. A typical extended shear tab is shown in Figure 4-1(b).

A beam was used to apply loads to the connection. In the models considered in this study, only a limited length of the beam close to the connection was modelled. To create the beam part, the I-shape section was drawn and extruded to a certain beam length. The bolt holes were then cut through the web thickness. A typical loading beam is shown in Figure 4-1(c).

The model included a column as the extended shear tab support. To create the column, the same procedure as for creating beam was used except that the column was modelled as a shell member. A typical column is shown in Figure 4-1(d).

All bolts used in this study were ASTM A325 bolts having a 19 mm (3/4 in.) diameter. The dimensions of the bolt head, bolt shank and nut were taken from the CISC Handbook of Steel Construction (CISC 2012). Since in the scope of this study all the shear planes passed through the unthreaded section of the bolt shank, threads were not modelled. A typical bolt is shown in Figure 4-1(c).

A rigid rectangular plate was modelled and attached to the beam end farther from the connection. The main purpose of using this loading plate was to apply load and rotation uniformly to the beam and to avoid any local stress concentration. A reference point was defined for the rigid plate at the centre of the plate.

4.2.2 Meshing

4.2.2.1 Element Type Selection

The complex nature of shear connections dictated the need for three-dimensional elements in this study. Shell elements were used only in structural components in which one dimension was considerably smaller than the other two.

Different solid element types are available in Abaqus, including quadratic and tetrahedral elements. Tetrahedral elements tend to be overly stiff, and extremely fine meshes are required to obtain accurate results (Dassault Systèmes 2012). Quadratic elements offer an improved convergence rate and decrease the analysis cost significantly. Based on this discussion, quadratic elements were used to model most

steel parts in this study, and special care was taken to avoid severe initial distortion in the elements. Moreover, first-order reduced-integration-type shell and solid elements were used in this study. Using these types of elements provided sufficient accuracy, while reducing the analysis time.

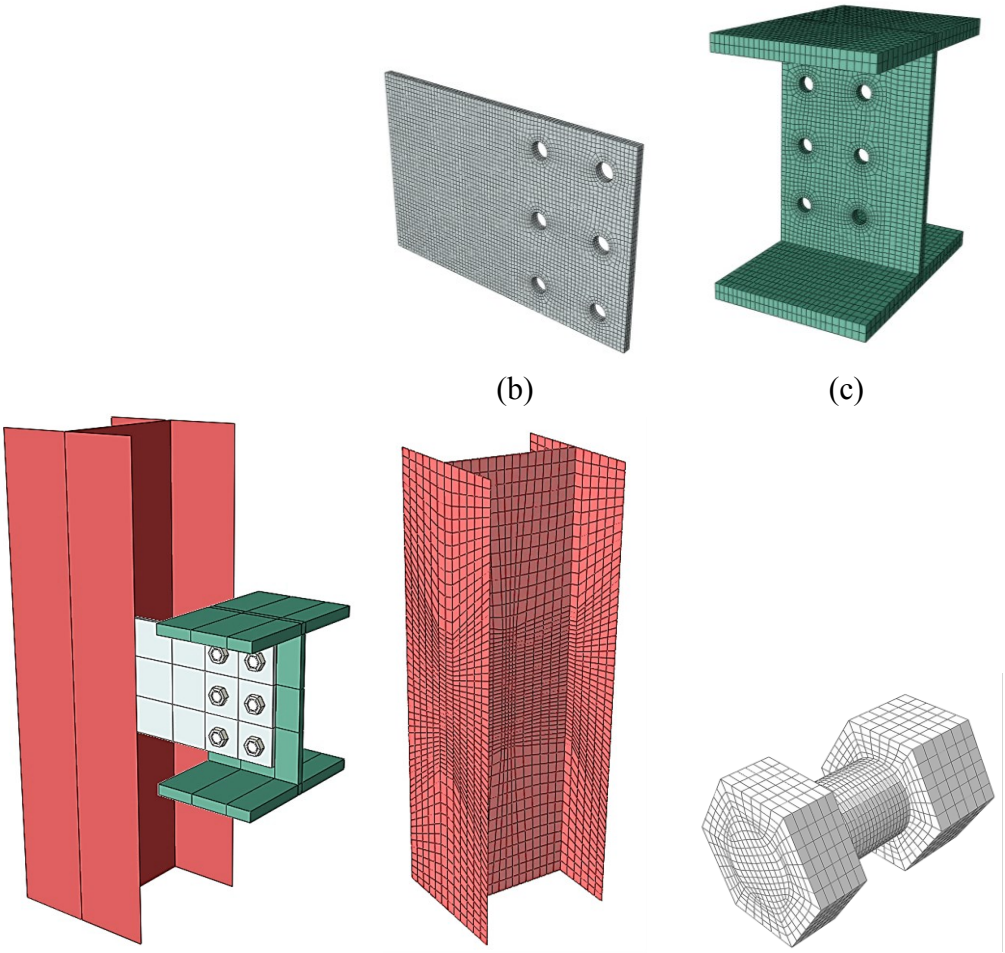

Figure 4-1: Extended shear tab finite element model:
(a) Overall assembly, (b) Extended plate, (c) Loading beam,
(d) Column support, and (e) Bolt

4.2.2.2 Meshing Generation Procedure

Due to the three-dimensional nature of the problem, solid 8-node brick elements were used to mesh the extended shear tab and loading beam. A hex-dominated meshing technique was used to mesh the bolts. 4-node shell elements were used to mesh the column web and flanges as well as the loading plate. Mesh density was increased around certain regions within each part that had steep strain gradients, namely the bolt holes in extended shear tabs and beams' web.

4.2.3 Material Properties

Material data defined in Abaqus should be in terms of the true values (Dassault Systèmes 2012). When defining a typical plastic material, it is necessary to decompose the elastic and plastic portions of the stress–strain curve. In the definition of the elastic section, modulus of elasticity and Poisson's ratio are defined. The plastic behaviour of the material starts from zero plastic strain, which corresponds to the yield stress, followed by more data points characterising the full plastic material response. Abaqus interpolates between the data points provided to capture the overall material behaviour.

4.2.3.1 Plates and Hot-rolled Sections

For model verification, tension coupon test data from Section 3.3.1 were used to develop the steel material curves for different components of the numerical models. To be able to use the stress–strain curves achieved from the tension coupon tests for numerical analysis, the curves should be processed in two steps. First, since the purpose of the numerical investigation is to evaluate the connection behaviour under static load, the static stress–strain curve should be constructed based on the dynamic stress–strain curve achieved from the tension coupon test. Since static points were recorded during the tension coupon tests, a curve parallel to the dynamic stress–strain curve, passing through the static points, was developed. Second, the static curve should be converted to the true stress–strain curve, which is used as input for plate

material properties in Abaqus. Since no tension coupon tests were performed on beam and column members, the same material properties as the plate were used for these members. The two-step process to develop the stress–strain curve as the input for material properties used in Abaqus is depicted in Figure 4-2.

To assure the accuracy of the method used to construct the stress–strain curve for the numerical analysis, the specific coupon associated with the stress–strain curve shown in Figure 4-2 was modelled in Abaqus using the measured section dimensions. The coupon was loaded in uniaxial tension and the load-displacement response was recorded and compared with the load-displacement curve achieved directly from the tension coupon test. Very good agreement was observed in the results derived from numerical modeling and the tension coupon test, as shown in Figure 4-3.

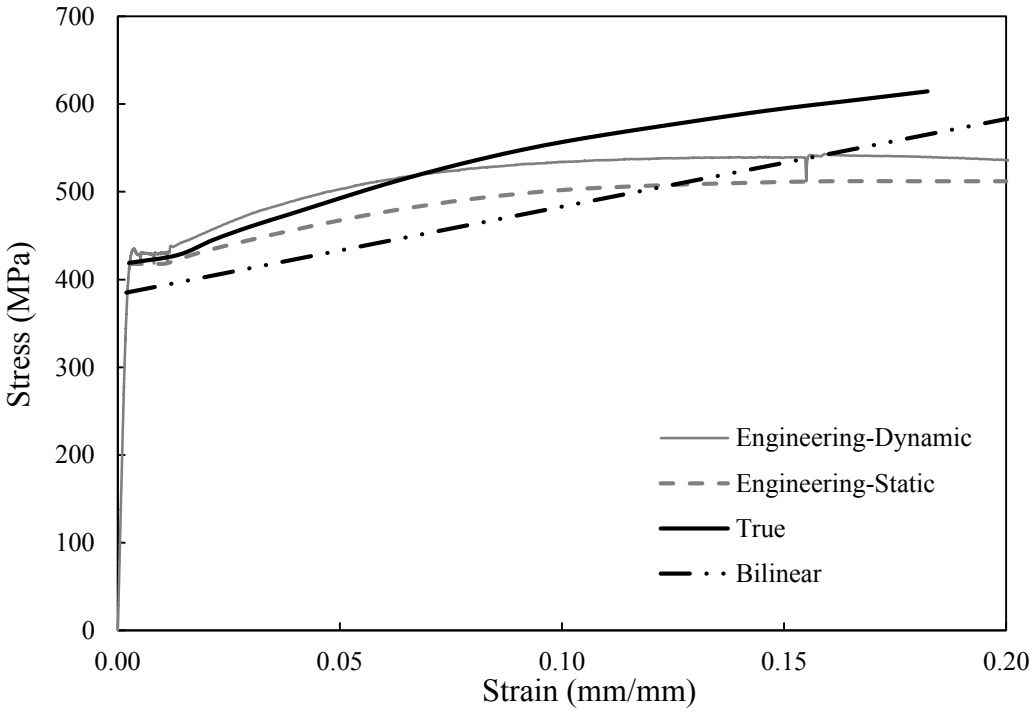

Figure 4-2: Conversion of tested material properties to Abaqus input

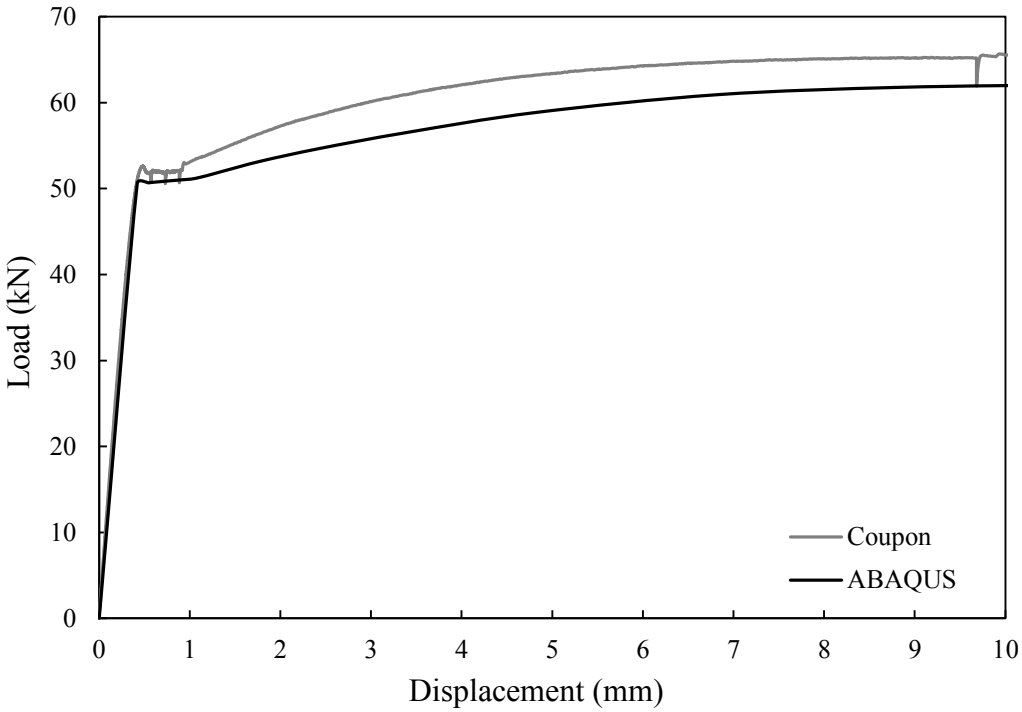

Figure 4-3: Comparison of coupon test and finite element coupon modelling

While the full material curve was used to compare with available test results, for conducting the parametric study the steel stress–strain curve was approximated as a bilinear curve consisting of an elastic portion and a plastic portion. The slope of the line forming the plastic portion was taken as 0.5% of the modulus of elasticity of the steel material. This value is believed to provide a line almost parallel to the true stress–strain curve achieved from a typical tension coupon test. The material yield stress was taken as 385 MPa, which represents 350W steel with an amplification factor of 1.1 to account for the probable yield stress. The bilinear approximation of the stress–strain curve is shown in Figure 4-2.

4.2.3.2 High Strength Bolts

In this study, A325 bolts were used and their stress–strain curve was needed as the material properties for bolt modelling. The bolt test described in Section 3.3.2 was modelled in Abaqus and the load-displacement curve achieved was verified versus the load-displacement curves derived from the three bolt tests. Results of verification,

as depicted in Figure 4-4, show satisfactory correlation between numerical modelling and bolt tests. It should be noted that in all the numerical models described in this chapter, bolt failure was deemed to have occurred when the shear load at the bolt critical section reached 177 kN. The bolt shear load capacity was considered as the average of the three bolt tests described in Section 3.3.2. The bolt test model and the deformed bolt are shown in Figure 4-5.

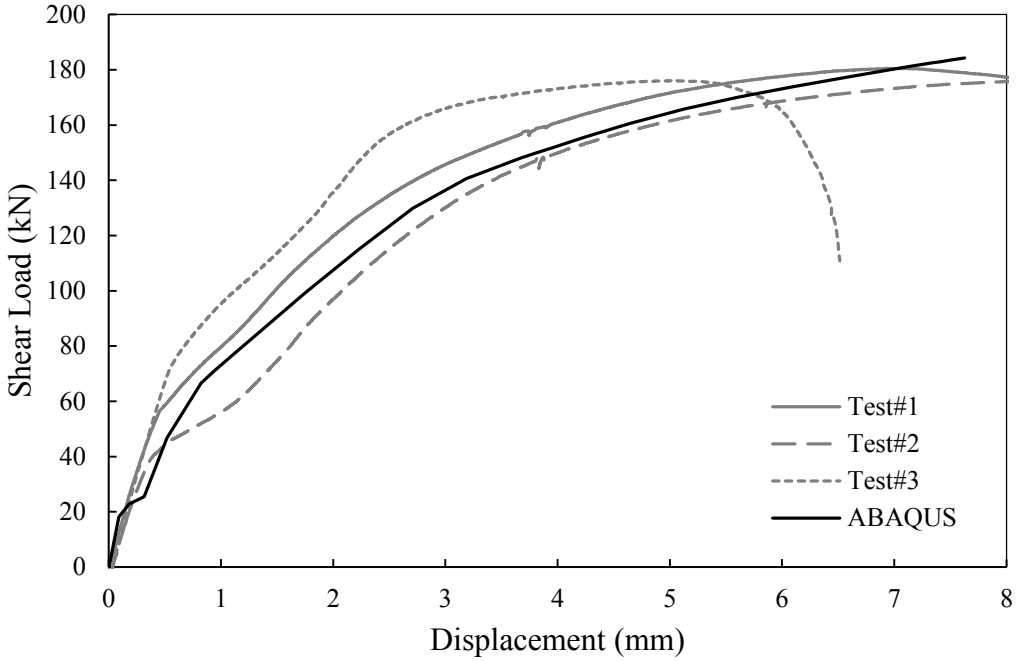

Figure 4-4: Comparison between bolt shear test and bolt finite element modeling

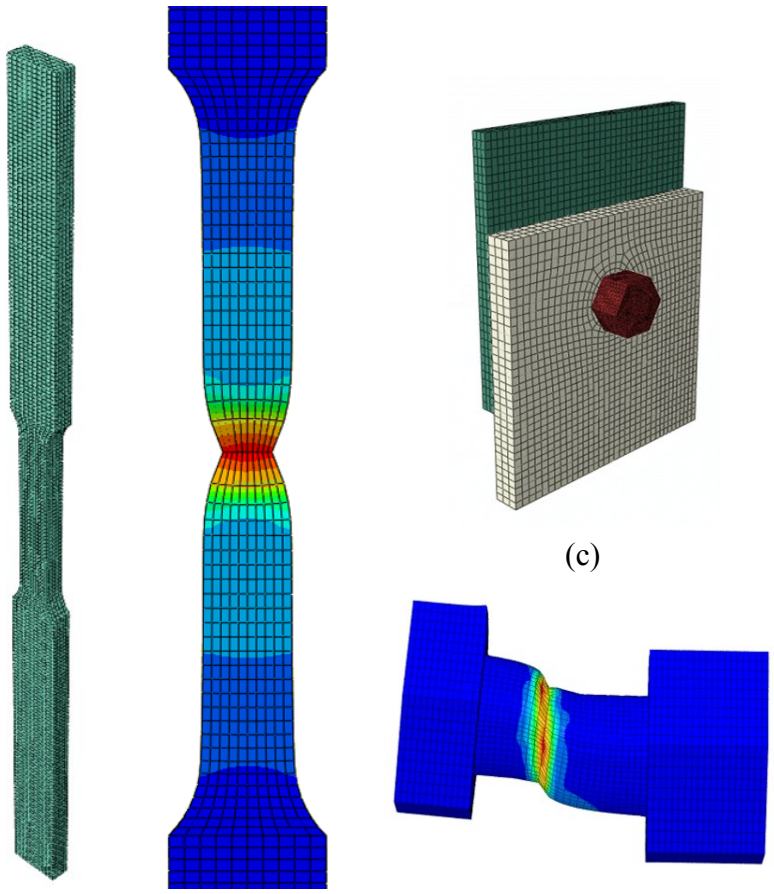

Figure 4-5: Coupon and bolt finite element modeling:
(a) Meshed coupon, (b) Deformed coupon at necking
(c) Bolt shear test model assembly, and (d) Deformed bolt

4.2.4 Parts Interaction

The extended shear tab was attached to the column web using the "tie" constraint in Abaqus. The "tie" constraint attaches two surfaces together such that no relative motion is allowed between the two (Dassault Systèmes 2012). In the models, it was assumed that the connection weld size was sufficient to transfer the loads from the extended shear tab to the column without rupture; therefore, connection welds were not modelled in any of the connection models.

The rigid loading plate was tied to the beam far-end cross-section. This ensured that each condition applied to the rigid plate was directly transferred to the beam section, while eliminating local stress concentration.

The most critical interaction between the model members was the contact between different components. Contact allows force transmission between different members using certain contact properties used to model the structure in the most realistic way possible. Several surfaces were in contact with each other in a typical model, including bolt shank contact with bolt holes in extended shear tab and beam web, bolt head contact with extended shear tab surface, nut contact with beam web surface, and shear tab surface to beam web surface. The general contact feature was used to model the contact among different members.

The normal and shear behaviour of contact was implemented using the penalty method. The coefficient of friction of 0.3 was used for steel material friction.

4.2.5 Loading

Loading is applied to the model in three or four consecutive steps, depending on each specific case. First, the internal tensile load developed in the bolts due to snug-tightening was applied. The load was applied to each bolt individually using the "bolt load" load type in Abaqus. In an actual connection, the magnitude of the bolt load could vary based on the ironworker effort. However, it has been confirmed that the magnitude of the bolt load due to snug-tightening has no effect on the bolt shear capacity. In this study, the load applied to each bolt was 20 kN. The clamping effect of the connection bolts was maintained in the subsequent loading steps by fixing the bolt at the reduced length after snug-tightening.

The next phase of loading was to rotate the beam up to 0.03 radians. The rotation of 0.03 radians is widely used to represent a typical rotation in shear connections at the beam flexural limit state, i.e., when the first plastic hinge is formed in the beam. The rotation was applied as a rotational angle to the rigid plate reference point. During the application of rotation, since the rigid plate was free to translate, no vertical or

horizontal load was developed in the connection. The rotation of 0.03 was maintained during the subsequent loading steps.

After the rotation phase, the horizontal load (if any) was applied to the specimen using a point load applied to the reference point of the rigid plate. As described before, the rigid plate eliminated the effect of stress concentration and ensured almost uniform distribution of normal stresses over the beam cross-section.

Finally, the vertical load was applied to the connection (with no additional rotation) using the vertical displacement of the rigid plate reference point. During this phase, the horizontal load was maintained at the value applied in the previous loading phase. The vertical displacement was increased until the load developed in the connection started to decline or any of the connection bolts reached their shear load capacity.

4.2.6 Boundary Conditions

Several boundary conditions were applied to the model components. The connection support ends were intended to be fixed against translation and rotation. Therefore, both column ends were restrained against all translational and rotational degrees of freedom. Since the focus of this study is to evaluate the behaviour of the extended shear tab, any undesirable condition that could potentially occur in the supported element should be eliminated. For this purpose, the beam flanges were restrained against out-of-plane displacement. Moreover, beam was selected such that the beam web exceeded the plate thickness.

4.2.7 Solution Method

The nature of the applied loads in this study was static. Therefore, it was appropriate to use the implicit method using the static/General algorithm. The general method is capable of including the effect of nonlinearities in the model, which can have different sources including material nonlinearity, geometric nonlinearity and boundary nonlinearity.

In the general method, loading is applied gradually in each step through increments that are fractions of the total applied load. The size of loading increments was set as "automatic", which enables the software to change the increment size to achieve numerical convergence.

4.2.8 Derivation of Results

The most significant result achieved from the numerical studies was the connection peak vertical load or capacity. Moreover, the variation of vertical load versus connection vertical deformation represents the nonlinear behaviour of the connection. To derive the vertical load–deformation curve of the connection during the desired loading step, the reaction force developed at the rigid plate reference point was plotted against the vertical deformation of the beam at a point located on the beam flange aligned with the vertical bolt line closer to the support. The bending moment at different locations along the shear tab plate was also derived and investigated.

Visual inspection of the model was an important tool in defining the failure mode and development of plasticity in the model. To track the plasticity development in the model, development of strains needed to be monitored closely. In this study, the equivalent plastic strain (PEEQ in Abaqus) was selected as an appropriate indication of the yielded areas of the connection. The von Mises plasticity criterion was used to investigate the plasticity development in the connection.

4.3 Model Verification

The model verification was done using the available data from two recent experimental studies on extended shear tabs conducted by Thomas et al. (2014) and the authors (see Chapter 3). The internal loads diagrams, deformed shapes and failure modes achieved from the analysis of the model were compared with the experimental results.

4.3.1 Thomas et al. (2014)

Six specimens were selected from the study by Thomas et al. (2014), including specimens 3B-10-U-0, 3B-10-U-100C, 3B-10-U-200C, 3B-10-S-0, 3B-10-S-100C, and 3B-10-S-200C. These cases all represent connections with three horizontal bolt lines and a 9.5 mm thick shear tab plate, with a variety of axial forces as well as with (stiffened) or without (unstiffened) stabilizer plates. The material properties reported by the researchers were assigned to the steel members. The specimens' drawings were used to create the different components of the models.

The comparison of the three stiffened models with the three corresponding specimens tested by Thomas et al. (2014) is depicted in Figure 4-6 in terms of vertical load–vertical displacement curves. The comparisons for the three unstiffened models are presented in Figure 4-7 to Figure 4-9. As can be observed from the figures, very good correlation was achieved between numerical and experimental results. It should be noted that in specimen 3B-10-U-0 the specimen failed due to weld rupture. However, since the weld was not simulated in the finite element models, the failure mode was not captured in this case and therefore the connection capacity, which was based on weld rupture, was not achieved.

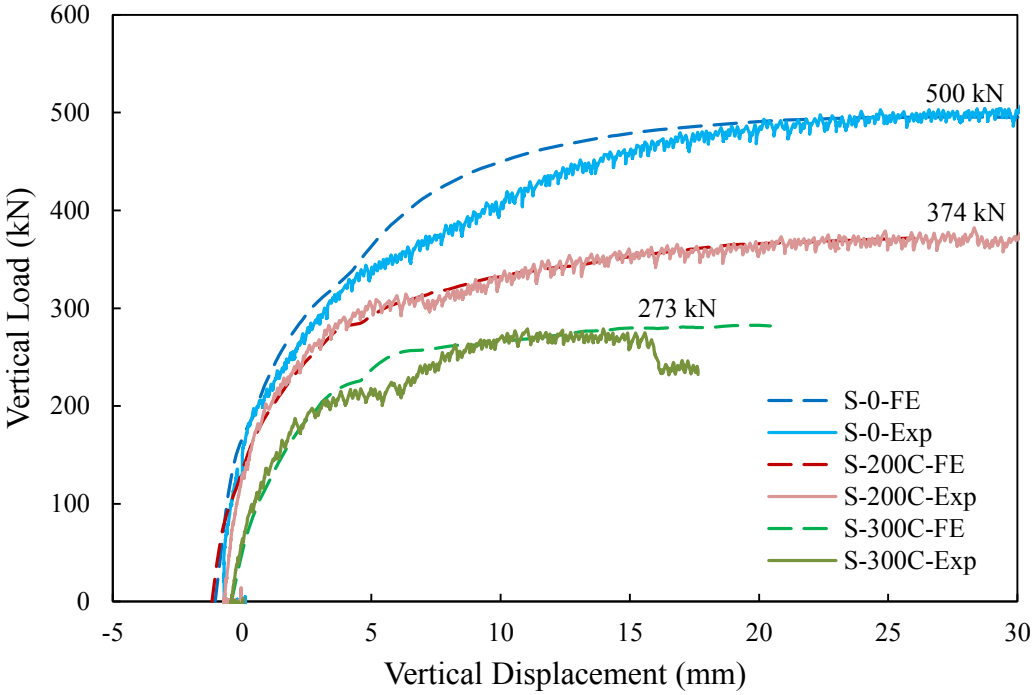

Figure 4-6: Comparison of finite element and test results for stiffened specimens

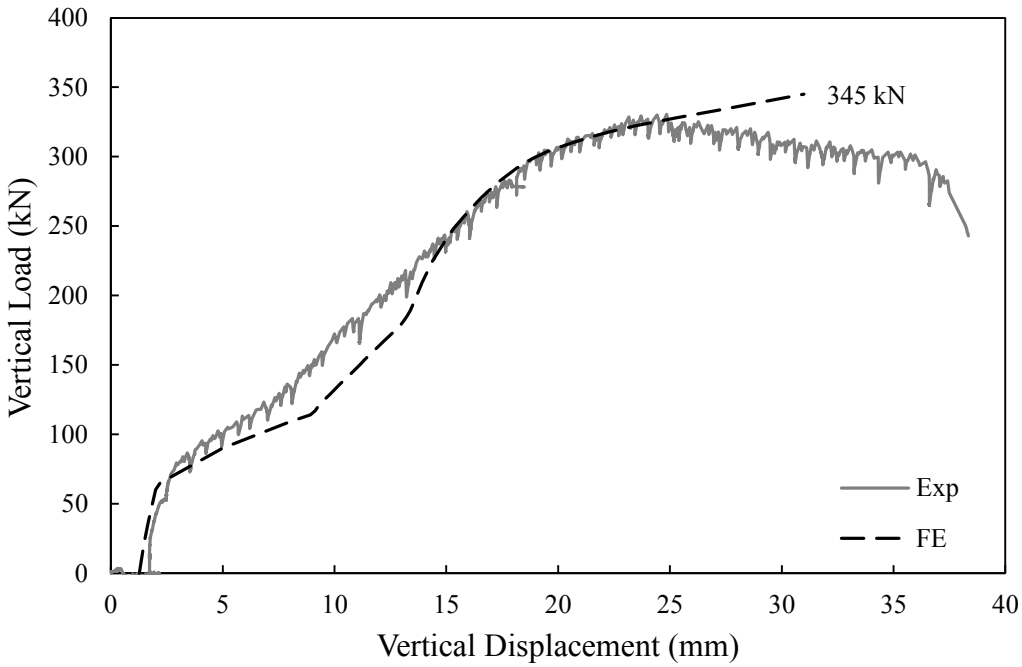

Figure 4-7: Comparison of finite element and test results
for specimen 3B-10-U-0

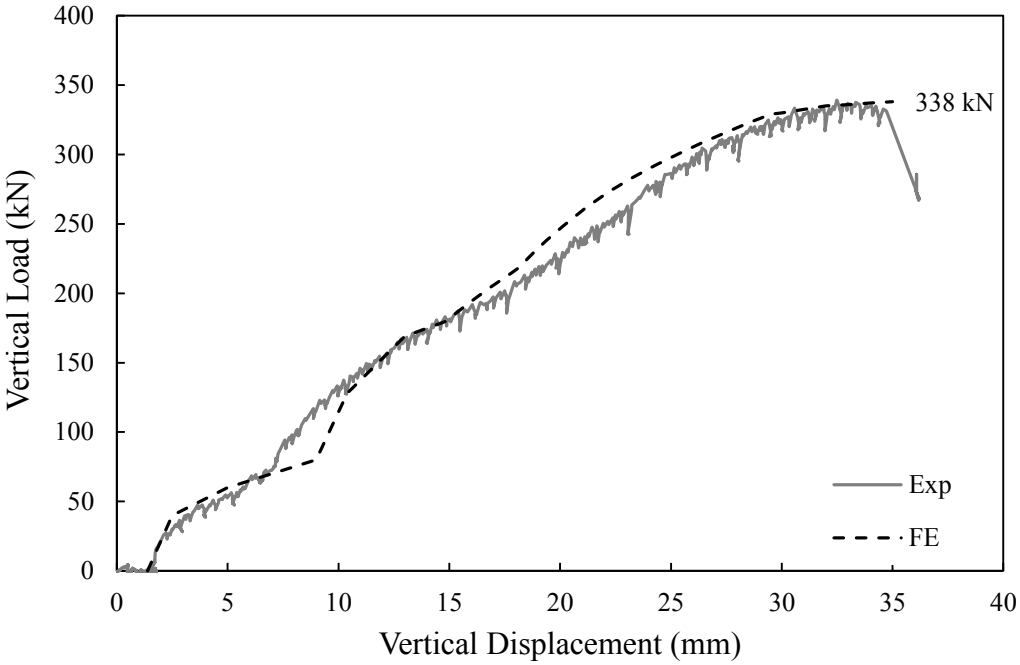

Figure 4-8: Comparison of finite element and test results
for specimen 3B-10-U-100C

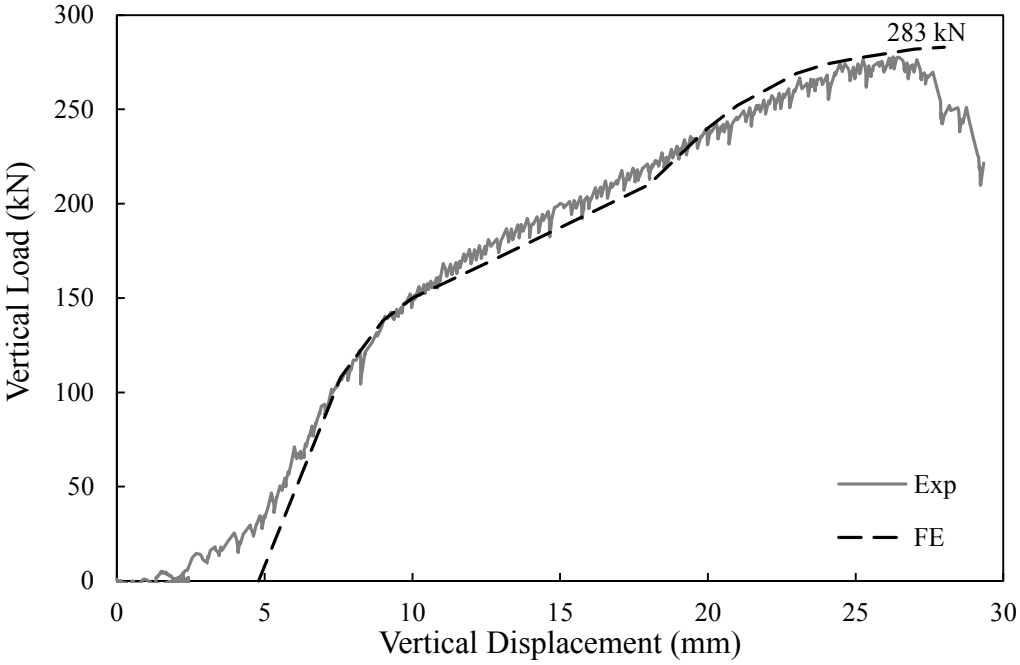

Figure 4-9: Comparison of finite element and test results
for specimen 3B-10-U-200C

Other than the quantitative verification of the model, a qualitative verification is necessary. In this regard, the failure modes and deformed shapes of the models and test specimens were compared. Figure 4-10 shows comparisons between numerical results and tested specimens. As observed from the figures, the deformed shapes resulting from finite element analysis closely mimic the actual observed deformations in the testing program. It could be concluded that the simulation was capable of modelling the actual deformation in the real structure quite accurately.

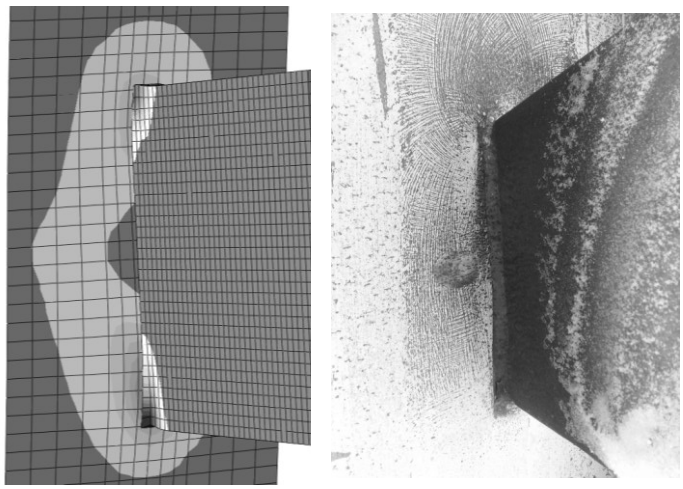

(a)

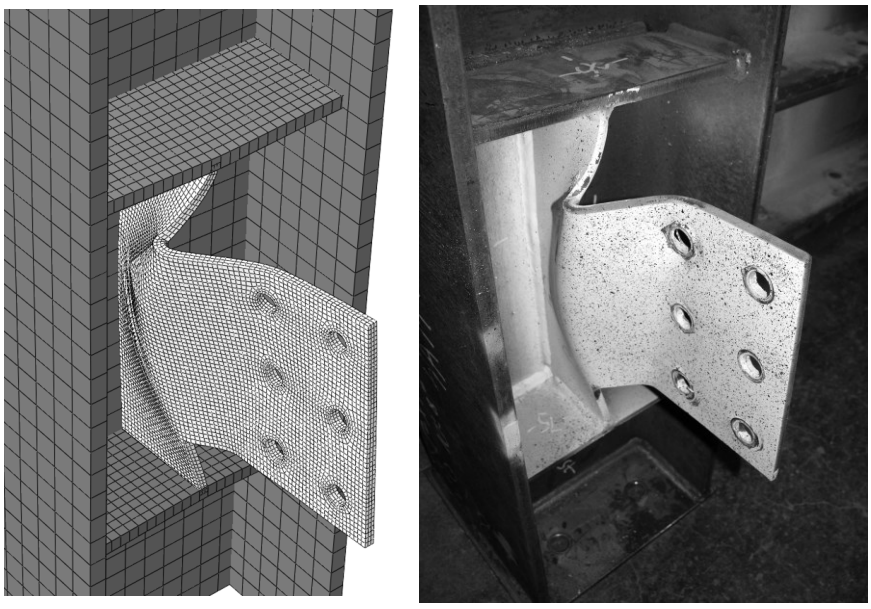

(b)

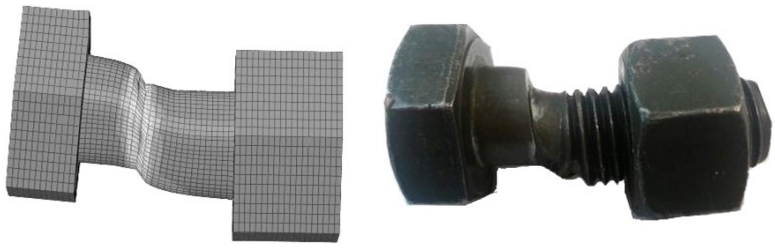

(c)

Figure 4-10: Qualitative verification of model for tests by Thomas et al. (2014):
(a) Column web yielding in specimen 3B-10-U-200C,
(b) Out-of-plane deformation in specimen 3B-10-S-200C, and
(c) Bolt fracture in specimen 3B-10-U-200C

4.3.2 Tests in Current Research

The test results presented in Chapter 3 were used to further validate the modelling procedure developed in this chapter. As discussed in Chapter 3, 17 full-scale tests were conducted on unstiffened extended shear tabs with a stiff support. The specimens vary in extended shear tab length, thickness, bolt configuration, support condition and application of horizontal load. Three tests, including 3BR-10-0, 3BR-10-0-L, and 3BR-10-100C, were selected to be compared with their corresponding finite element models. The material properties obtained from the coupon tests were assigned to the steel members. The loading procedure was as described in Section 4.2.5, and results were derived using the procedure described in Section 4.2.8.

The comparisons of the three models with the three corresponding specimens tested by the authors are depicted in Figure 4-11 to Figure 4-13 in terms of vertical load–vertical displacement curves. Very good correlation was observed between numerical and experimental results.

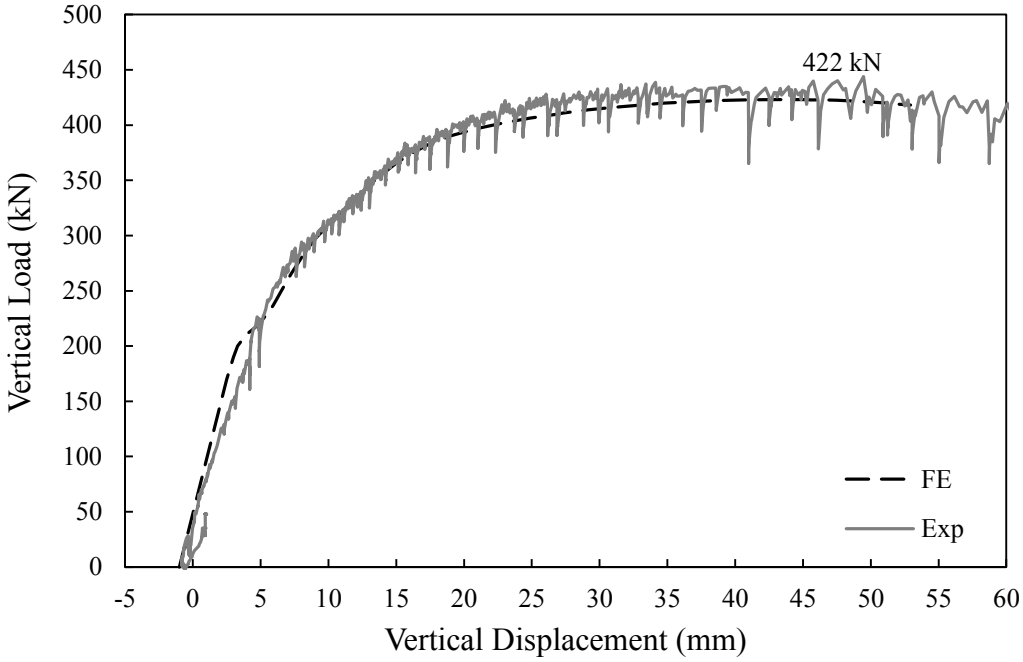

Figure 4-11: Comparison of finite element and test results for specimen 3BR-10-0

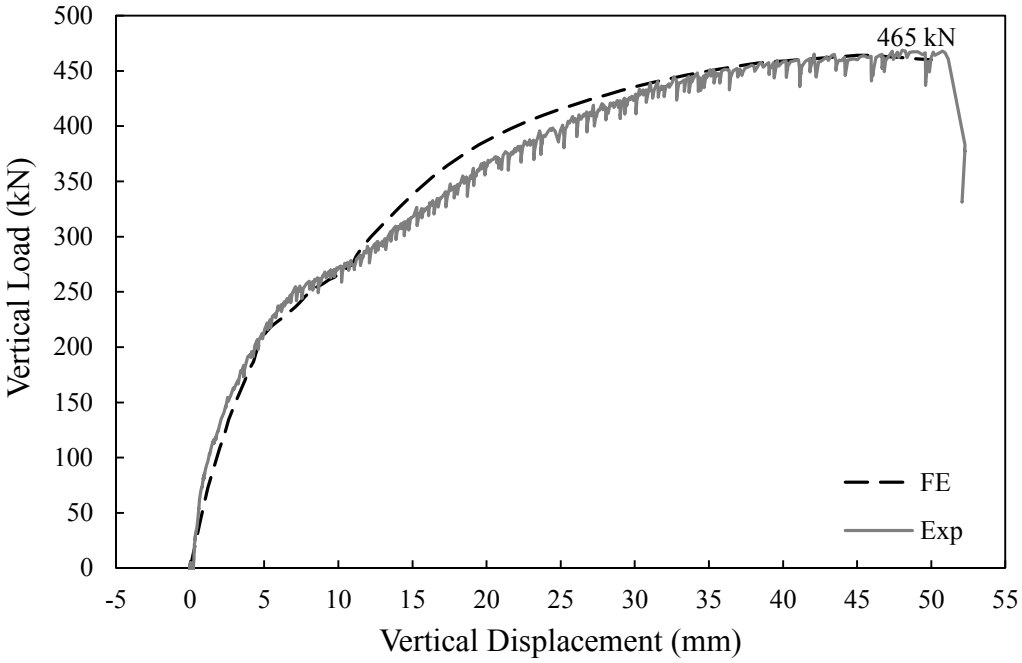

Figure 4-12: Comparison of finite element and test results
for specimen 3BR-10-0-L

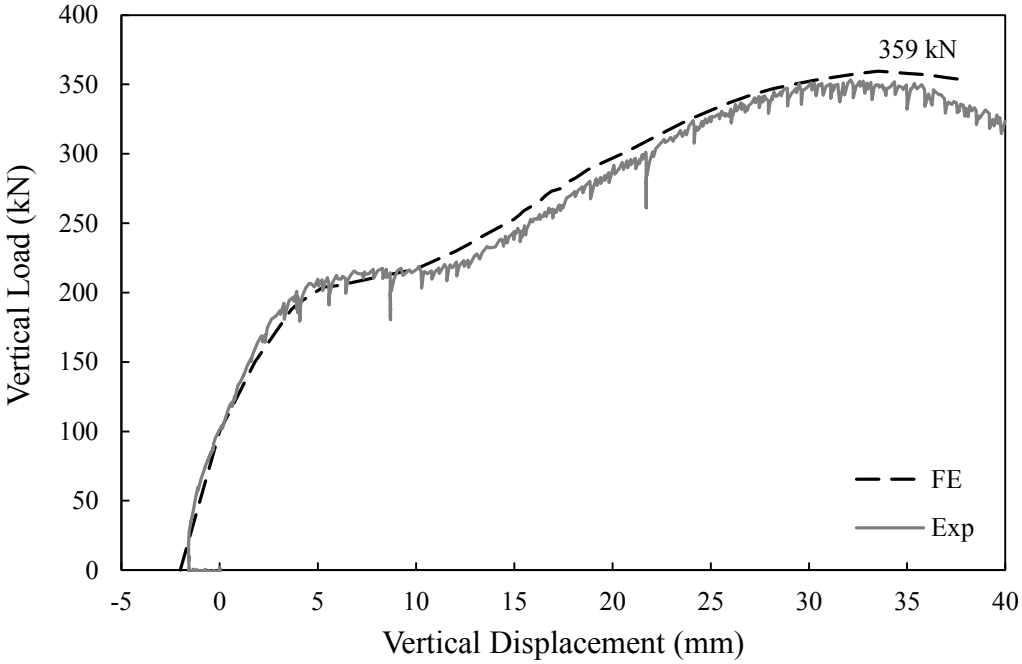

Figure 4-13: Comparison of finite element and test results
for specimen 3BR-10-100C

The results achieved from finite element analysis were also compared to those achieved from the tests qualitatively. Figure 4-14 shows the comparison between the finite element modelling results and the observations in the testing program. Based on the comparison, the model was able to predict the plasticity development and the deformed shape of the connection quite reasonably.

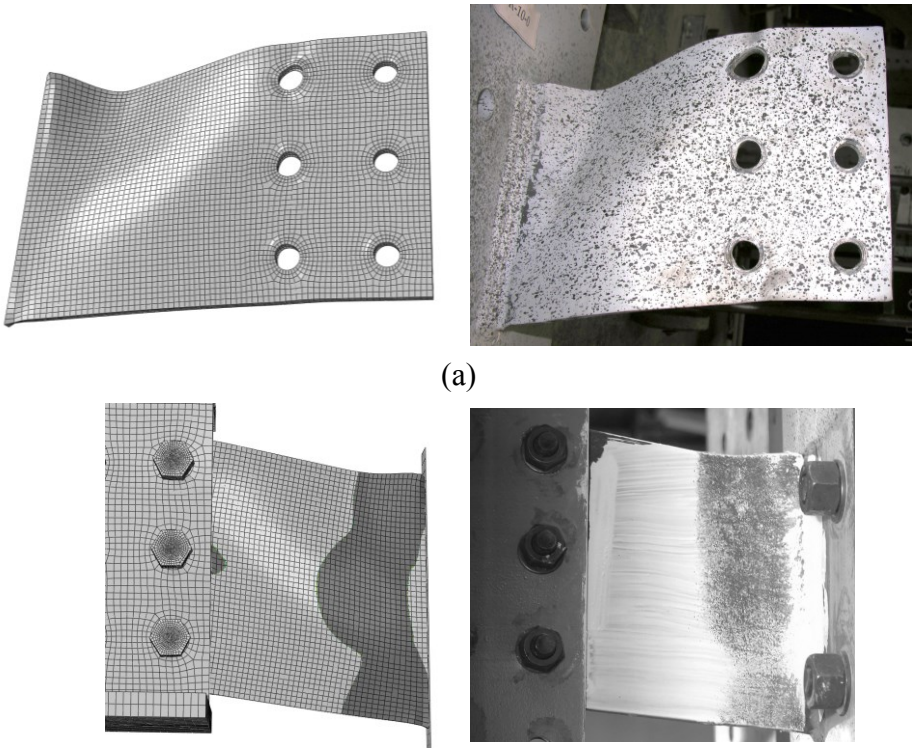

Figure 4-14: Qualitative verification of model for current study tests:
(a) Out-of-plane deformation in specimen 3BR-10-200C, and
(b) Gross section plasticity in specimen 3BR-10-0

A mesh sensitivity analysis was performed on the models to determine the optimum mesh size for further studies. To achieve this, the extended shear tab in the finite element model was meshed using a range of mesh sizes and the behaviour and capacity of the models were compared. Figure 4-15 shows results of the mesh sensitivity analysis conducted for model 3BR-10-0. The horizontal axis depicts the total number of elements in the extended shear tab, which is a function of the mesh

size. The vertical axis depicts the ratio of the capacity predicted by each model to the capacity predicted by the model with the finest mesh size. As observed from the figure, changing the total number of elements from 12000 to 28000 did not have any effect on the model capacity prediction. However, as the mesh density started to decrease to 10000 elements, the model capacity prediction started to show evidence of inaccuracy. Based on the mesh sensitivity analysis, the mesh size corresponding to the mesh density of 12000 elements in the plate was selected for the parametric study.

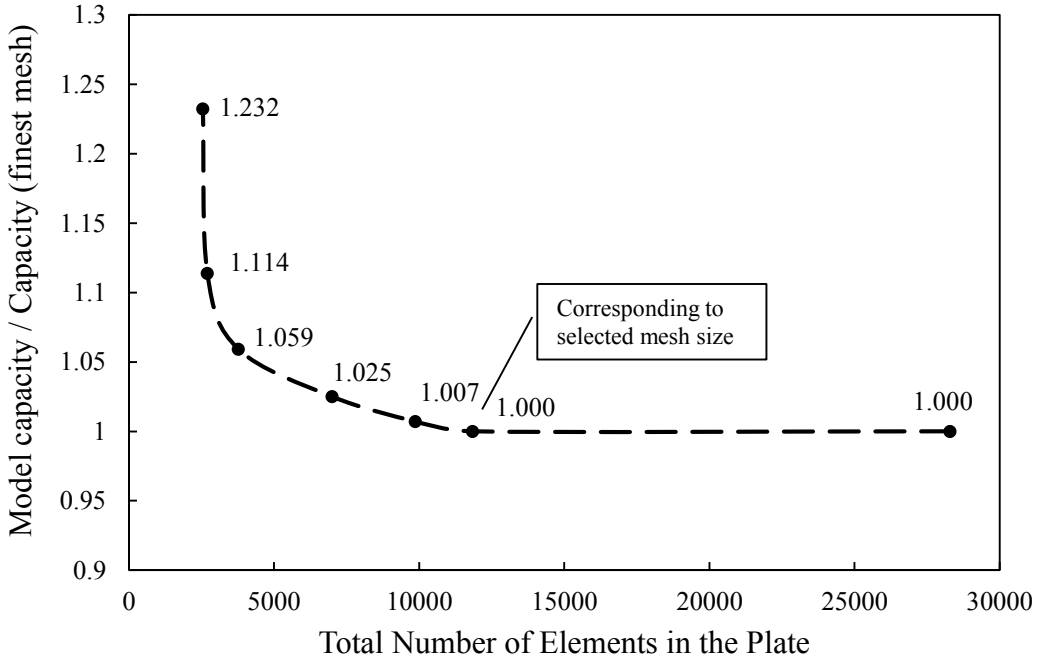

Figure 4-15: Mesh sensitivity analysis results for model 3BR-10-0

4.4 Parametric Study

A well-detailed and robust model was developed to capture the behaviour of extended shear tabs. Available test data by other researchers (Thomas et al. 2014) and the authors were used to verify and validate the accuracy of the model. The validated model is used to investigate the behaviour further through a comprehensive parametric study that considers various geometric configurations and boundary

conditions. The purpose of the parametric study is to expand the scope of the previous research and to identify new aspects of extended shear tab behaviour patterns.

The study consisted of 36 models varying in extended shear tab length, thickness, number of horizontal bolt lines (plate depth), number of vertical bolt lines, and support condition. The naming scheme of the specimens is alphanumeric. The first number and letter depict the number of horizontal bolt lines, varying among 2B, 3B and 4B. The letter next to the horizontal bolt line definition implies whether the specimen support was a stiff plate (S) or a flexible plate (F). The flexible plate dimensions were 700×180×11 mm. It should be noted that the plate flexibility would be altered if other arbitrary dimensions were selected; however, the objective was only to provide a support that would be considered relatively flexible on the spectrum of potential connection designs. The next number indicates the extended shear tab thickness rounded up to the closest millimeter. Each combination of the preceding parameters is considered a "reference" case and had two vertical bolt lines and a complete plate length equal to 348 mm. The term just after the thickness depicts the variation in specimen geometry, if any, from the associated reference case. Specimens with the shorter length (298 mm) are identified by "LS" and specimens with longer length (398 mm) are identified by "LL". Moreover, specimens with one vertical bolt line are identified by "VBL". As an example, model 3BF-10-LL is a 9.5 mm thick extended shear tab with three horizontal bolt lines and two vertical bolt lines, attached to a flexible support, with an extended shear tab longer than that of the reference model. As another example, model 2BS-10-VBL is a 9.5 mm thick extended shear tab with two horizontal bolt lines and one vertical bolt line, attached to a stiff support, with an extended shear tab of the reference length. The geometrical specifications for the considered models are reported in Table 4-1.

Table 4-1: Model specifications

No. of Horizontal Bolt Lines /Plate Depth	Plate Thickness (mm)	Plate Length (mm)	No. of Vertical Bolt Lines	Support Condition and Identifier	
				Flexible	Stiff
2 / 150 mm	6.35	348	2	2BF-7	2BS-7
	9.5	348	2	2BF-10	2BS-10
	9.5	298	2	2BF-10-LS	2BS-10-LS
	9.5	398	2	2BF-10-LL	2BS-10-LL
	9.5	348	1	2BF-10-VBL	2BS-10-VBL
	12.7	348	2	2BF-13	2BS-13
3 / 230 mm	6.35	348	2	3BF-7	3BS-7
	9.5	348	2	3BF-10	3BS-10
	9.5	298	2	3BF-10-LS	3BS-10-LS
	9.5	398	2	3BF-10-LL	3BS-10-LL
	9.5	348	1	3BF-10-VBL	3BS-10-VBL
	12.7	348	2	3BF-13	3BS-13
4 / 310 mm	6.35	348	2	4BF-7	4BS-7
	9.5	348	2	4BF-10	4BS-10
	9.5	298	2	4BF-10-LS	4BS-10-LS
	9.5	398	2	4BF-10-LL	4BS-10-LL
	9.5	348	1	4BF-10-VBL	4BS-10-VBL
	12.7	348	2	4BF-13	4BS-13

4.5 Results and Discussion

Connection capacity, as the most significant result of the study, was investigated for each model. Several limit states observed in the models are also discussed. Bending moment at the support face, as well as the vertical bolt line closer to the support, were derived and are discussed as a measure of plasticity development in the extended shear tab. Shear load eccentricities applied to the bolt group and to the support are

examined and, finally, the effect of various geometric configurations on the behaviour and capacity of the connection is investigated.

4.5.1 Connection Capacity

The vertical load–vertical displacement curve was derived for every model and was used to evaluate the connection capacity. The capacity of the connection was taken at the point right before the vertical load started to decline or when bolt fracture was observed. The curve for model 3BF-10 is presented in Figure 4-16, where the capacity was evaluated as 346 kN and was reached due to bolt fracture. Vertical load–vertical displacement curves for other select models are presented in Appendix C. All model capacities are reported in Table 4-2.

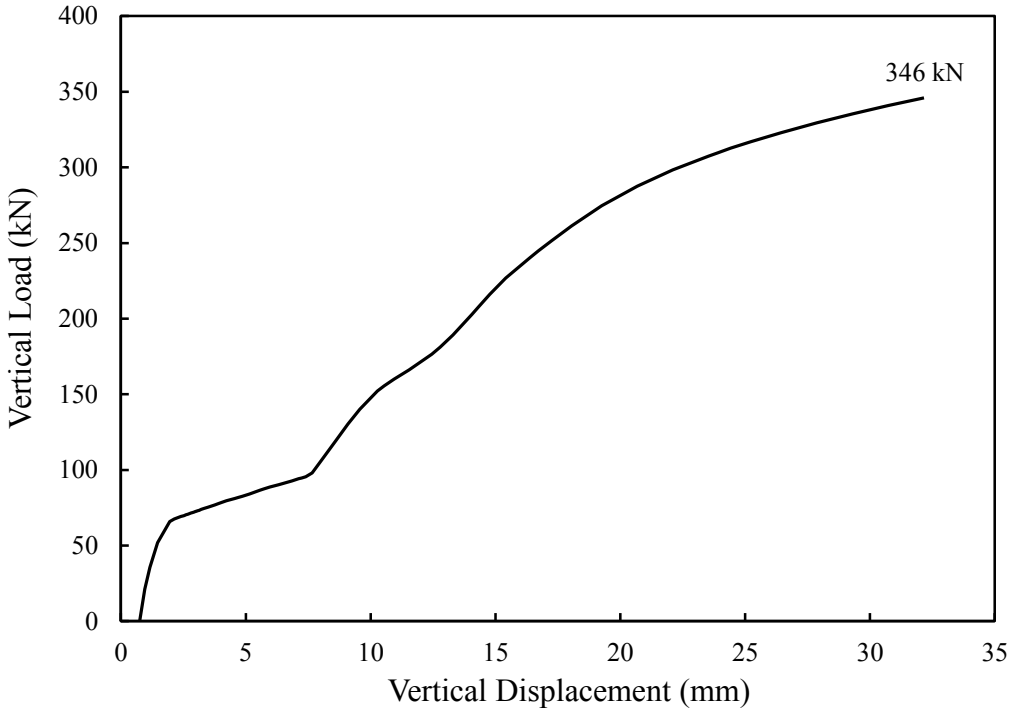

Figure 4-16: Load–displacement curve for model 3BF-10

Table 4-2: Model capacities and limit states

Model ID	Connection Capacity (kN)	Limit States
2BF-7	141	NSP, **OPD**
2BF-10	187	NSP, **BF**
2BF-10-LS	220	NSP, **BF**
2BF-10-LL	155	NSP, **BF**
2BF-10-VBL	156	**BF**
2BF-13	191	**BF**
2BS-7	104	GSP, **OPD**
2BS-10	222	GSP, NSP, **BF**
2BS-10-LS	269	GSP, NSP, **BF**
2BS-10-LL	193	GSP, NSP, OPD, **BF**
2BS-10-VBL	186	GSP, OPD, **BF**
2BS-13	254	GSP, **BF**
3BF-7	262	NSP, **OPD**
3BF-10	346	NSP, **BF**
3BF-10-LS	407	NSP, **BF**
3BF-10-LL	296	NSP, **BF**
3BF-10-VBL	273	**BF**
3BF-13	352	**BF**
3BS-7	199	GSP, **OPD**
3BS-10	421	GSP, NSP, **BF**
3BS-10-LS	496	GSP, NSP, **BF**
3BS-10-LL	323	GSP, NSP, OPD, **BF**
3BS-10-VBL	344	GSP, OPD, **BF**
3BS-13	510	GSP, **BF**
4BF-7	371	NSP, **OPD**
4BF-10	543	NSP, **BF**
4BF-10-LS	655	NSP, **BF**
4BF-10-LL	463	NSP, **BF**
4BF-10-VBL	399	**BF**
4BF-13	535	**BF**
4BS-7	294	**OPD**
4BS-10	546	GSP, NSP, OPD, **BF**
4BS-10-LS	688	GSP, NSP, **BF**
4BS-10-LL	455	GSP, NSP, OPD, **BF**
4BS-10-VBL	538	GSP, OPD, **BF**
4BS-13	810	GSP, NSP, **BF**

4.5.2 Limit States

Limit states are considered to be the mechanisms contributing to the gradual degradation and failure of the connection. These were identified by close inspection of the connection during the model analysis, as well as monitoring the vertical load–vertical displacement curve and calculation of section forces and moments at critical locations. Several limit states were observed in the analyzed models, each discussed in detail below. The limit state causing the load carried by the connection to drop immediately after the peak load is regarded as the "failure mode". The observed limit states for each model are reported in Table 4-2 in order of occurrence, using the abbreviations specified in the following paragraphs, and the limit state responsible for failure of each connection is highlighted as the failure mode using bold font. It should be noted that the failure mode always happened after all other limit states.

Gross section plasticity (GSP) was observed in almost all the models with the stiff support. Gross section plasticity was identified as plasticity that developed throughout the whole depth of the extended shear tab, as defined by Equation 2-9. Images of development of section plasticity at the support face in model 3BS-10 are shown in Figure 4-17. The dark regions in the figure depict the plastic regions. Gross section plasticity was not the failure mode for any of the models.

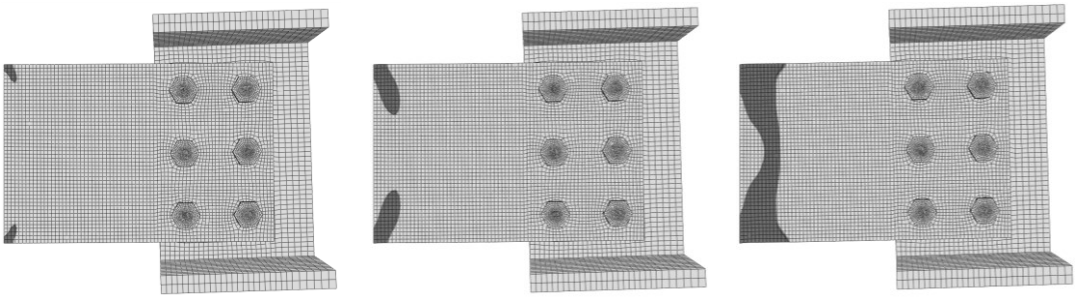

Figure 4-17: Plasticity development at gross section

Net section plasticity (NSP) at the vertical bolt line closer to the support was identified in a number of models. Net section plasticity was identified as plasticity that developed throughout the whole depth of the extended shear tab net section at the

bolt line, as defined by Equation 2-9, using the net section properties instead of the gross section. Images of gradual net section plasticity in model 3BF-10 at the bolt line are shown in Figure 4-18. Net section plasticity was not the failure mode for any of the models.

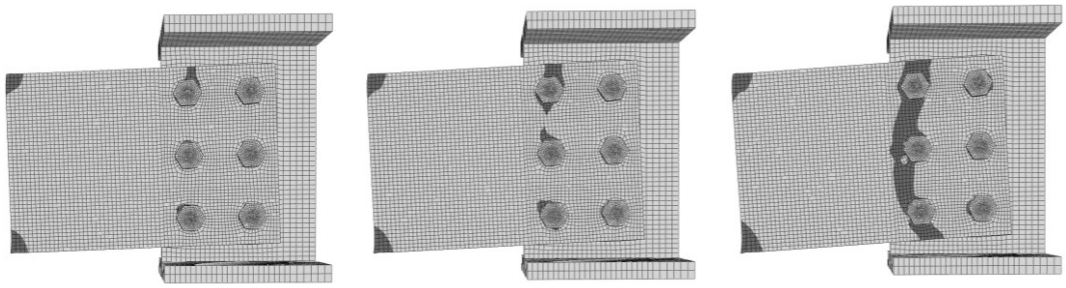

Figure 4-18: Plasticity development at net section

Out-of-plane deformation (OPD) was observed in all the models with stiff support. In most cases, the out-of-plane deformation started before the connection reached its capacity and developed gradually as the load increased. In most of the models, although severe out-of-plane deformation occurred during the analysis, this phenomenon was not the failure mode; i.e., the connection capacity was not limited by out-of-plane deformation. Images of the deformed shape of model 3BS-10-LL from different angles are shown in Figure 4-19.

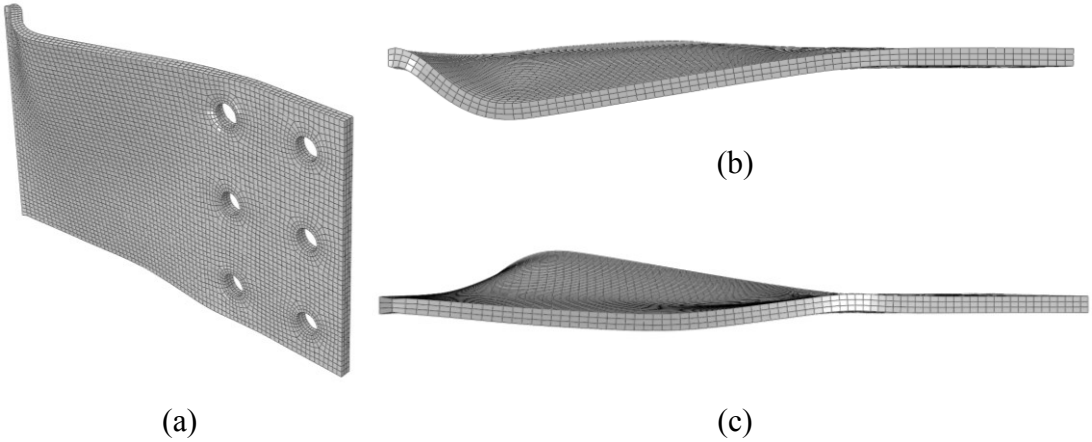

Figure 4-19: Out-of-plane deformation:
(a) Three-dimensional view, (b) Top view, and (c) Bottom view

Bolt fracture (BF) was observed in many of the models as the failure mode. In most cases bolt fracture occurred after the extended shear tab had experienced considerable plasticity and out-of-plane deformation.

4.5.3 Development of Plasticity through the Plate Section

In-plane bending moments at the support face and the bolt line closer to the support were derived by cutting a plane through the extended shear tab cross-section at the support face and at the bolt line and recording the in-plane bending moment at each loading step. The locations of the cuts are shown in Figure 4-20.

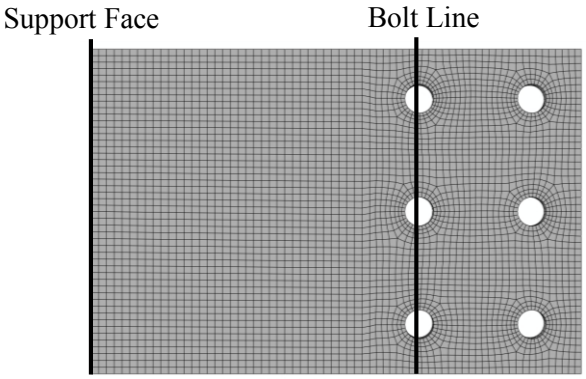

Figure 4-20: Locations of section cuts at the support face and at the bolt line

To get a better understanding of the magnitude of the moments developed at the specified locations, the actual values were divided by the nominal plastic moment capacity of the same section calculated using the material properties selected for the parametric study. The variations of the ratios of moment developed at the support face and the bolt line to the gross and net section plastic moment capacities, respectively, for model 4BS-10 are presented in Figure 4-21. These ratios are presented for all specimens in Table 4-3 to Table 4-5, separated into three groups according to section depth. Since the moment ratios are extremely variable during the analysis, the ratios at each individual limit state specified in Table 4-1 are reported.

Shear load, which can be approximated as the vertical load at each loading step, was also derived and divided by the plastic shear capacity of the associated section. The ratio was again derived at the two critical locations: support face and net section at bolt line. It should be noted that the section cut at the net section passed only through the plate and did not include the bolts. Therefore, the shear load carried by the net section was only a fraction of the total shear load applied to the plate.

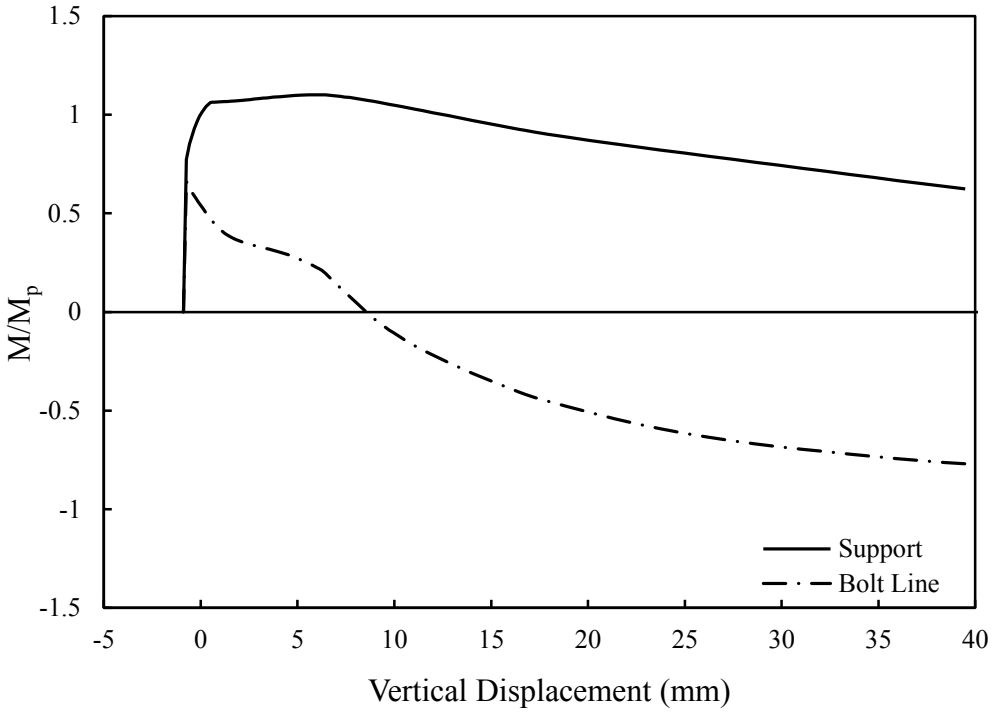

Figure 4-21: Bending moment ratio variation for model 4BS-10

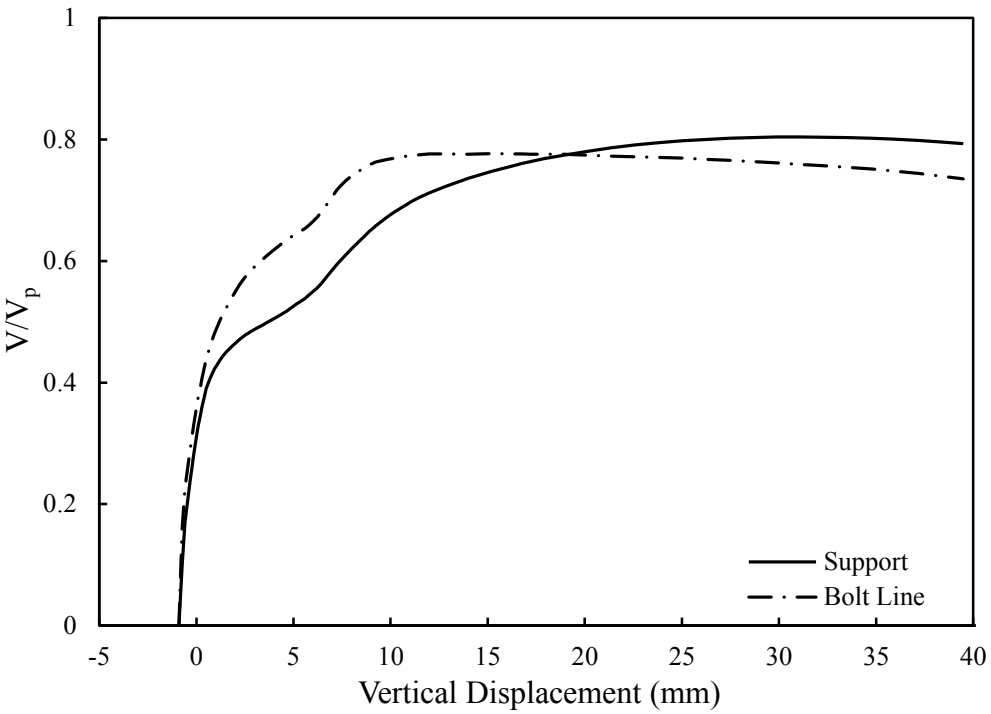

Figure 4-22: Shear load ratio variation for model 4BS-10

Table 4-3: 2B Model section demands and eccentricity ratios

Model ID	Limit State	V (kN)	Support		Bolt Line		e_b/e_g
			V/V_p	M/M_p	V/V_p	M/M_p	
2BF-7	NSP	116	0.52	0.80	0.40	0.98	0.54
	OPD	141	0.59	0.84	0.56	1.26	0.57
2BF-10	NSP	157	0.45	0.82	0.36	1.03	0.58
	BF	187	0.48	0.94	0.49	1.18	0.55
2BF-10-LS	NSP	190	0.55	0.82	0.36	0.94	0.58
	BF	220	0.59	0.92	0.48	1.09	0.57
2BF-10-LL	NSP	136	0.37	0.83	0.18	1.08	0.56
	BF	155	0.38	0.94	0.28	1.21	0.53
2BF-10-VBL	**BF**	156	0.36	0.95	0.45	0.46	0.24
2BF-13	**BF**	191	0.37	0.67	0.34	1.00	0.58
2BS-7	GSP	53	0.25	1.06	0.37	0.27	0.33
	OPD	104	0.47	0.84	0.33	0.92	0.59
2BS-10	GSP	75	0.24	1.07	0.29	0.32	0.03
	NSP	198	0.62	1.38	0.52	0.90	0.49
	BF	222	0.70	1.46	0.60	1.06	0.52
2BS-10-LS	GSP	90	0.29	1.08	0.36	0.41	-0.06
	NSP	230	0.72	1.31	0.64	0.73	0.49
	BF	269	0.84	1.41	0.77	0.97	0.53
2BS-10-LL	GSP	68	0.21	1.08	0.25	0.26	0.00
	NSP	169	0.53	1.40	0.41	0.99	0.49
	OPD	193	0.60	1.46	0.52	1.19	0.53
	BF	193	0.60	1.45	0.52	1.20	0.53
2BS-10-VBL	GSP	97	0.30	1.09	0.30	0.02	0.04
	OPD	186	0.58	1.43	0.54	0.42	0.33
	BF	185	0.58	1.39	0.53	0.43	0.35
2BS-13	GSP	98	0.23	1.06	0.29	0.34	0.05
	BF	254	0.59	1.40	0.53	0.76	0.45

Table 4-4: 3B Model section demands and eccentricity ratios

Model ID	Limit State	V (kN)	Support		Bolt Line		e_b/e_g
			V/V_p	M/M_p	V/V_p	M/M_p	
3BF-7	NSP	221	0.66	0.82	0.60	0.83	0.57
	OPD	262	0.76	0.88	0.70	0.99	0.59
3BF-10	NSP	317	0.60	0.64	0.56	0.90	0.63
	BF	346	0.64	0.70	0.63	0.96	0.62
3BF-10-LS	NSP	373	0.73	0.62	0.69	0.77	0.63
	BF	407	0.78	0.68	0.77	0.83	0.62
3BF-10-LL	NSP	286	0.52	0.68	0.49	1.01	0.61
	BF	296	0.53	0.71	0.51	1.03	0.61
3BF-10-VBL	**BF**	273	0.48	0.73	0.51	0.36	0.38
3BF-13	**BF**	352	0.48	0.50	0.48	0.76	0.64
3BS-7	GSP	118	0.35	1.01	0.41	0.28	-0.02
	OPD	199	0.58	0.56	0.48	0.80	0.66
3BS-10	GSP	163	0.33	1.08	0.40	0.40	-0.14
	NSP	400	0.81	1.21	0.75	0.68	0.47
	BF	421	0.85	1.14	0.78	0.86	0.53
3BS-10-LS	GSP	191	0.39	1.07	0.46	0.48	-0.19
	NSP	437	0.88	1.10	0.84	0.51	0.47
	BF	496	1.00	1.17	0.95	0.64	0.50
3BS-10-LL	GSP	143	0.29	1.08	0.34	0.34	-0.11
	NSP	320	0.64	0.99	0.56	0.86	0.54
	OPD	323	0.64	0.88	0.55	0.98	0.59
	BF	322	0.64	0.84	0.54	1.01	0.61
3BS-10-VBL	GSP	220	0.45	1.06	0.39	0.02	0.03
	OPD	344	0.68	1.14	0.63	0.31	0.31
	BF	343	0.68	1.13	0.63	0.68	0.32
3BS-13	GSP	225	0.34	1.08	0.43	0.39	-0.12
	BF	510	0.77	1.27	0.76	0.51	0.42

Table 4-5: 4B Model section demands and eccentricity ratios

Model ID	Limit State	V (kN)	Support		Bolt Line		e_b/e_g
			V/V_p	M/M_p	V/V_p	M/M_p	
4BF-7	NSP	356	0.78	0.42	0.72	0.69	0.57
	OPD	371	0.81	0.48	0.75	0.77	0.59
4BF-10	NSP	490	0.71	0.55	0.69	0.77	0.64
	BF	543	0.78	0.62	0.77	0.84	0.62
4BF-10-LS	NSP	542	0.80	0.52	0.78	0.60	0.63
	BF	655	0.95	0.63	0.96	0.75	0.61
4BF-10-LL	NSP	434	0.63	0.57	0.60	0.87	0.64
	BF	463	0.66	0.61	0.64	0.92	0.63
4BF-10-VBL	**BF**	399	0.58	0.57	0.56	0.34	0.45
4BF-13	**BF**	535	0.58	0.43	0.60	0.64	0.65
4BS-7	**OPD**	294	0.63	0.46	0.57	0.67	0.66
4BS-10	GSP	366	0.45	1.07	0.52	0.38	-0.12
	NSP	541	0.80	0.81	0.78	0.61	0.52
	OPD	546	0.80	0.73	0.76	0.70	0.57
	BF	536	0.79	0.62	0.74	0.77	0.63
4BS-10-LS	GSP	340	0.51	1.03	0.59	0.45	-0.17
	NSP	587	0.88	0.90	0.91	0.34	0.43
	BF	688	1.01	0.81	0.98	0.60	0.53
4BS-10-LL	GSP	276	0.41	1.09	0.49	0.31	-0.06
	NSP	455	0.66	0.64	0.62	0.80	0.61
	OPD	455	0.66	0.64	0.62	0.80	0.61
4BS-10-VBL	GSP	357	0.53	1.00	0.44	0.06	-0.03
	BF	537	0.79	1.03	0.71	0.27	0.28
4BS-13	GSP	403	0.45	1.07	0.43	0.39	-0.13
	NSP	754	0.84	1.08	0.87	0.38	0.39
	BF	810	0.91	1.12	0.92	0.45	0.41

Plasticity in the connection is developed under the combined effect of bending moment and shear. Therefore, both effects need to be considered when section plasticity is evaluated. Plasticity was evaluated at the support face and at the bolt line

by monitoring the vertical load–vertical displacement curve and plastic strain contour over the extended shear tab. Neal's (1961) interaction equation (Equation 2-9) was then evaluated for comparison at the loading step when section plasticity became complete. The ratio of bending moment to the section plastic moment and the ratio of shear force to the section plastic shear for the models that experienced plasticity are presented in Table 4-6 and Table 4-7.

Table 4-6: Neal interaction equation value for plasticity at gross section (support face)

Model ID	V/V_p	M/M_p	Neal
2BS-7	0.25	1.06	1.06
2BS-10	0.24	1.07	1.07
2BS-10-LS	0.29	1.08	1.09
2BS-10-LL	0.21	1.08	1.08
2BS-10-VBL	0.30	1.09	1.10
2BS-13	0.23	1.06	1.06
3BS-7	0.35	1.01	1.03
3BS-10	0.33	1.08	1.09
3BS-10-LS	0.39	1.07	1.09
3BS-10-LL	0.29	1.08	1.09
3BS-10-VBL	0.45	1.06	1.10
3BS-13	0.34	1.08	1.09
4BS-10	0.45	1.07	1.11
4BS-10-LS	0.51	1.03	1.10
4BS-10-LL	0.41	1.09	1.12
4BS-10-VBL	0.53	1.00	1.08
4BS-13	0.45	1.07	1.11
		Mean	**1.09**
		Std. Dev.	**0.02**

Table 4-7: Neal interaction equation value for plasticity at net section (bolt line)

Model ID	V/V_p	M/M_p	Neal
2BF-7	0.40	0.98	1.01
2BF-10	0.36	1.03	1.05
2BF-10-LS	0.36	0.94	0.96
2BF-10-LL	0.18	1.08	1.08
2BS-10	0.52	0.90	0.97
2BS-10-LS	0.64	0.73	0.90
2BS-10-LL	0.41	0.99	1.02
3BF-7	0.60	0.83	0.96
3BF-10	0.56	0.90	1.00
3BF-10-LS	0.69	0.77	1.00
3BF-10-LL	0.49	1.01	1.07
3BS-10	0.75	0.68	1.00
3BS-10-LS	0.84	0.51	1.01
3BS-10-LL	0.56	0.86	0.96
4BF-7	0.72	0.69	0.96
4BF-10	0.69	0.77	1.00
4BF-10-LS	0.78	0.60	0.97
4BF-10-LL	0.60	0.87	1.00
4BS-10	0.78	0.61	0.98
4BS-10-LS	0.91	0.34	1.03
4BS-10-LL	0.62	0.80	0.95
4BS-13	0.87	0.38	0.95
		Mean	**0.99**
		Std. Dev.	**0.04**

Based on the values calculated using Neal's interaction equation, it is observed that the equation is quite capable of predicting the development of section plasticity. Moreover, the contributions of shear load and bending moment in the formation of plasticity is quite variable for different models. However, as a general trend, as the depth of the connection was increased the contribution of shear load in plasticity was

amplified. In other words, the section plasticity was dominated by shear in the extended shear tabs that had a lower length-to-depth ratio.

Over a constant extended shear tab depth and length, the relative contributions of shear load and bending moment in plasticity development were not altered appreciably with thickness variation.

When models with the same extended shear tab dimensions and different boundary conditions are compared, it is concluded that in models with the stiff support the role of shear load in section plasticity is higher than in the models with the flexible support.

It should be noted that the gross section plasticity that occurred in the models with the stiff support developed in very early load levels; therefore, the shear load contribution to gross section plasticity was relatively low.

4.5.4 Shear Load Eccentricity

The shear load eccentricity applied to the support face and the bolt group centre is a crucial parameter in the design of the bolt group as well as the support. In this study, the shear load eccentricity applied to the bolt group centre was calculated and recorded during the application of vertical load to the models. The eccentricity ratios for the bolt group centre are defined as the ratio of the bolt group shear load eccentricity over the geometric eccentricity (e_b/e_g). It should be noted that the geometric eccentricity for each specimen is defined as the distance from the bolt group centre to the support face.

The eccentricity ratios were quite variable during loading of models. The variation of the bolt group eccentricity ratio for model 4BF-10 is depicted in Figure 4-23. As noticed from the figure, the eccentricity ratio showed a negative value during the initial phases of the loading, implying that the inflection point was located along the beam span and the extended shear tab had a single-curvature moment distribution. However, at around 1 mm vertical displacement the eccentricity ratio reached zero, which indicates that the inflection point had moved towards the support and was

located at the centre of bolt group. With further increases in the vertical load, the eccentricity ratio increased and the extended shear tab was bent in double curvature. At around 10 mm vertical displacement, the eccentricity ratio reached a stable value and remained almost constant through the connection failure at around 40 mm. The extended shear tab was in double-curvature when the capacity was reached.

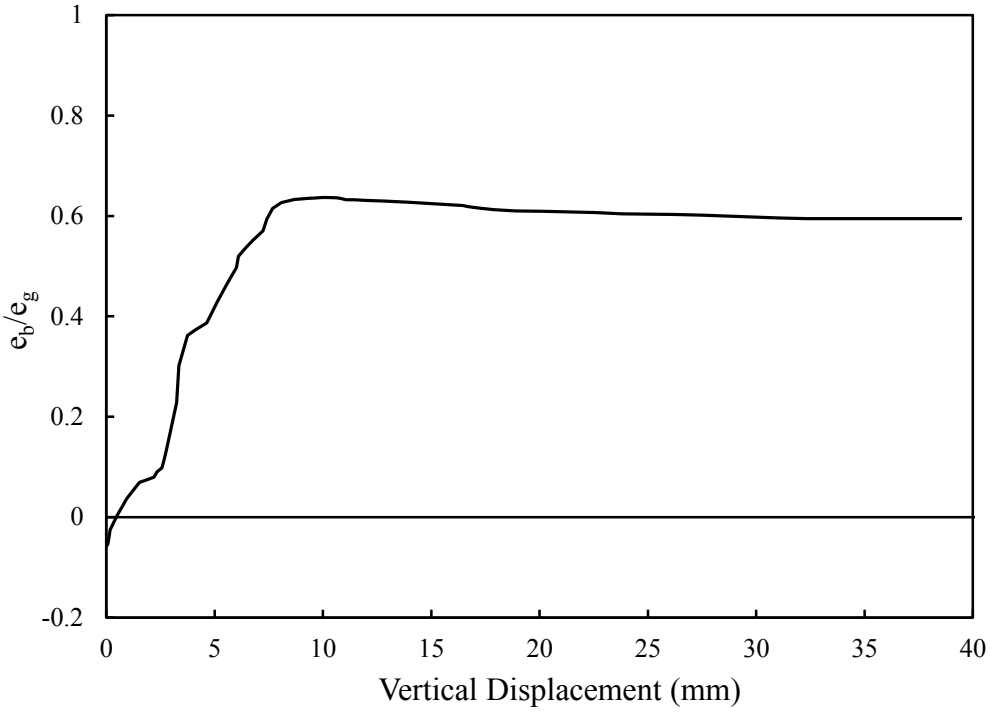

Figure 4-23: Bolt group eccentricity ratio variation for model 4BF-10

The bolt group eccentricity ratio values were derived at instances when a significant phenomenon occurred in the connection. The three major points of concern are gross section plasticity, net section plasticity, and bolt fracture. The values are presented for applicable models in Table 4-8.

Table 4-8: Bolt group eccentricity ratios

At GSP		At NSP		At BF	
Model ID	e_b/e_g	Model ID	e_b/e_g	Model ID	e_b/e_g
2BS-7	0.01	2BF-7	0.54	2BF-10	0.55
2BS-10	0.03	2BF-10	0.58	2BF-10-LS	0.57
2BS-10-LS	-0.06	2BF-10-LS	0.58	2BF-10-LL	0.53
2BS-10-LL	0.00	2BF-10-LL	0.56	2BF-10-VBL	0.24
2BS-10-VBL	0.04	2BS-10	0.49	2BF-13	0.58
2BS-13	0.05	2BS-10-LS	0.49	2BS-10	0.52
3BS-7	-0.02	2BS-10-LL	0.49	2BS-10-LS	0.53
3BS-10	-0.14	3BF-7	0.57	2BS-10-LL	0.53
3BS-10-LS	-0.19	3BF-10	0.63	2BS-10-VBL	0.35
3BS-10-LL	-0.11	3BF-10-LS	0.63	2BS-13	0.45
3BS-10-VBL	0.03	3BF-10-LL	0.61	3BF-10	0.62
3BS-13	-0.12	3BS-10	0.47	3BF-10-LS	0.62
4BS-10	-0.12	3BS-10-LS	0.47	3BF-10-LL	0.61
4BS-10-LS	-0.17	3BS-10-LL	0.54	3BF-10-VBL	0.38
4BS-10-LL	-0.06	4BF-7	0.57	3BF-13	0.64
4BS-10-VBL	-0.03	4BF-10	0.64	3BS-10	0.53
4BS-13	-0.13	4BF-10-LS	0.63	3BS-10-LS	0.50
		4BF-10-LL	0.64	3BS-10-LL	0.61
		4BS-10	0.52	3BS-10-VBL	0.32
		4BS-10-LS	0.43	3BS-13	0.42
		4BS-10-LL	0.61	4BF-10	0.62
		4BS-13	0.39	4BF-10-LS	0.61
				4BF-10-LL	0.63
				4BF-10-VBL	0.45
				4BF-13	0.65
				4BS-10	0.63
				4BS-10-LS	0.53
				4BS-10-VBL	0.28
				4BS-13	0.41

Eccentricity ratios are categorized into different groups in Table 4-9 based on the limit state and the support condition. Since the gross section plasticity limit state was only observed for models with the stiff support, this is the only category for gross section plasticity. The standard deviations (Std. Dev.) indicate that the results are fairly consistent within each group. It should be noted that for consistency, models with single vertical bolt line were not included in calculating the ratios reported in the table.

Table 4-9: Mean bolt group eccentricity ratio for different model groups at different limit states

Limit State	Support Condition	Mean e_b/e_g	Std. Dev.
GSP	S	-0.06	0.08
NSP	F	0.60	0.04
	S	0.49	0.06
	All	0.55	0.07
BF	F	0.60	0.04
	S	0.51	0.07
	All	0.56	0.06

Although the net section plasticity and bolt fracture limit states were observed in models with both flexible and stiff supports, the eccentricity ratios were slightly lower for the models with stiff support. The reason behind this could be described by considering the effect of support stiffness on the moment distribution along the extended shear tab length. Qualitatively, increasing the support stiffness tends to increase the bending moment carried by the support and therefore pushes the inflection point farther from the support face, resulting in a reduced shear load eccentricity applied to the bolt group. Other than treating models with different support conditions separately, the average eccentricity ratio was also calculated considering all models regardless of their support condition.

Based on the information summarized in Table 4-9, the following conclusions are made:

- At gross section plasticity, the average bolt group shear load eccentricity ratio was -0.06. This value indicates that the point of inflection was located almost at the centre of bolt group when the plate gross section at the support face experienced plasticity through the full plate depth.
- If all the models are considered together, it could be concluded that net section plasticity occurred when the eccentricity ratio of the bolt group was 0.55.
- Considering all the models, the eccentricity ratio applied to the bolt group causing all or part of the bolt group to fracture was 0.56.

As described in Chapter 2, Neal's interaction equation (Equation 2-9) proposes a relationship between bending moment and shear load to predict section plasticity. The correlation between bending moment and shear load is defined using the shear load eccentricity. If the bending moment in the equation is substituted by the multiplication of shear load and eccentricity, the interaction equation can be rewritten as Equation 2-13. The equation is considered for a connection without axial load.

4-1
$$\frac{V \cdot e}{M_p} + \left(\frac{V}{V_p}\right)^4 \leq 1.0$$

In the equation, if the proper eccentricity applied to the gross section at the gross section plasticity limit state and the eccentricity applied to the net section at the net section plasticity limit state are used, the shear load causing these two limit states could be predicted. It should be noted that when evaluating the plasticity development at the gross and net sections, the plastic moment and shear capacities of the associated section must be considered in the equation. Moreover, the shear load, V, causing net section plasticity predicted using Equation 2-13 is the shear load acting on the net section of the plate. To evaluate the total shear load causing this limit state, a reasonable estimate is to multiply the shear load achieved from the equation by the ratio of gross section area to net section area of the plate. This estimate is based on evaluation of the ratio of the shear load acting on the net section to the total shear load and its correlation with the ratio of net to gross sectional area of the plate.

As presented in Table 4-9, gross section plasticity occurred when the inflection point was located very close to the bolt group centre. Therefore, using the full geometric eccentricity as the eccentricity value in Equation 2-13 is appropriate to predict the shear load associated with the gross section plasticity limit state. To evaluate net section plasticity, the shear load eccentricity is found by subtracting the distance from the bolt group centre to the first vertical bolt line (net section) from the eccentricity ratios at net section plasticity given in Table 4-9.

Based on the aforementioned discussion, Equation 2-13 can be used to evaluate section plasticity at the gross and net sections using the following eccentricities:

For gross section plasticity:

4-2 $$e = e_g$$

For net section plasticity with flexible support:

4-3 $$e = 0.6\, e_g - 0.5\, s$$

For net section plasticity with stiff support:

4-4 $$e = 0.5\, e_g - 0.5\, s$$

It should be noted that the eccentricity value for net section plasticity evaluation of extended shear tabs with flexible supports is specifically based on the flexibility of the support considered in this study and may not be valid for supports with different flexibilities. As an example, if the support is extremely flexible (e.g., a very slender girder) the eccentricity applied to the net section could be close to Equation 4-5, which implies no rotational stiffness at the support and no moment reaction.

4-5 $$e = e_g - 0.5\, s$$

4.5.5 Effects of Key Variables

The 36 models could be categorized into two main groups: 18 models with stiff support and 18 models with flexible support. In each category, six models included 150 mm deep extended shear tabs with two horizontal bolt lines, six models included 230 mm deep extended shear tabs with three horizontal bolt lines, and six models included 310 mm deep extended shear tabs with four horizontal bolt lines.

Within each group of six models, four extended shear tabs were 9.5 mm (3/8 in.) thick, one extended shear tab was 12.7 mm (1/2 in.) thick and one extended shear tab was 6.4 mm (1/4 in.) thick. Among the 9.5 mm thick extended shear tabs, three otherwise identical models included lengths of 298 mm, 348 mm, and 398 mm. Moreover, out of the 9.5 mm thick extended shear tab models, one model had only one vertical bolt line.

Several observations can be made on the effect of the variables on the behaviour of the extended shear tab connection. For this purpose, Table 4-2 was considered together with the vertical load–vertical displacement curves derived from the analysis.

4.5.5.1 Plate Length

Comparing models 3BF-10, 3BF-10-LS and 3BF-10-LL, it is observed that by decreasing the extended shear tab length, the connection capacity was significantly increased. This trend was observed in models both with flexible support and stiff support. Extended shear tabs having the stiff support with shorter length had an increased resistance to out-of-plane deformation due to their reduced unrestrained length. Moreover, in shorter plates, the load eccentricities associated with the bolt group and the plate section at the vertical bolt line were lower than those in longer plates, resulting in increased bolt group capacity and vertical load causing the net section plasticity. The ductility of the shorter extended shear tabs was only slightly lower. The vertical load–vertical displacement curves for models having the flexible

support with various lengths are presented in Figure 4-24 and the curves for models having the rigid support with various lengths are presented in Figure 4-25.

4.5.5.2 Plate Thickness

Using the study matrix, direct comparisons can be made among the 9.5 mm thick, 6.4 mm thick and 12.7 mm thick extended shear tabs. Increasing the plate thickness always resulted in an increase in the peak vertical load, as expected. That is, increasing the plate thickness resulted in an increased plastic section capacity as well as increased resistance against failure due to out-of-plane deformation. However, the influence of the thickness on the connection capacity was greater in the case of the stiff support. The vertical load–vertical displacement curves for models having the flexible support with various thicknesses are presented in Figure 4-26 and the curves for models having the rigid support with various thicknesses are presented in Figure 4-27. It should be noted that in the two figures, increasing the extended shear tab thickness from 6.35 mm to 9.5 mm resulted in alteration of failure mode from out-of-plane deformation to bolt fracture, which resulted in a significant increase in capacity.

4.5.5.3 Plate Depth

Using the study matrix, direct comparisons can be made among the extended shear tabs with depths of 150 mm, 230 mm and 310 mm. Increasing the plate depth always resulted in an increase in the peak vertical load, as expected. Increasing the plate depth resulted in an increased plastic section capacity as well as increased resistance against failure due to out-of-plane deformation. The vertical load–vertical displacement curves for models having the flexible support with various depths are presented in Figure 4-28 and the curves for models having the rigid support with various depths are presented in Figure 4-29.

4.5.5.4 Number of Vertical Bolt Lines

Using only one vertical bolt line instead of two resulted in a reduction in the connection peak vertical load, as expected. Changing the bolt configuration was considered such that the distance between the first bolt line and the support face remained constant. Therefore, the geometric eccentricity applied to the centre of the bolt group with one vertical bolt line was lower than the one for the regular models with two vertical bolt lines. Moreover, the rotational stiffness of the bolt group was significantly reduced. The net result of the various effects is that the reduction in connection capacity due to using one vertical bolt line instead of two was on average only around 22%. It should be noted that this capacity reduction could be greater if the decrease to one vertical bolt line from two changed the failure mode to bolt fracture from some other limit state. A comparison of the vertical load–vertical displacement curves of models 3BF-10 and 3BF-10-VBL is presented in Figure 4-30. The comparison for 3BS models is presented in Figure 4-31.

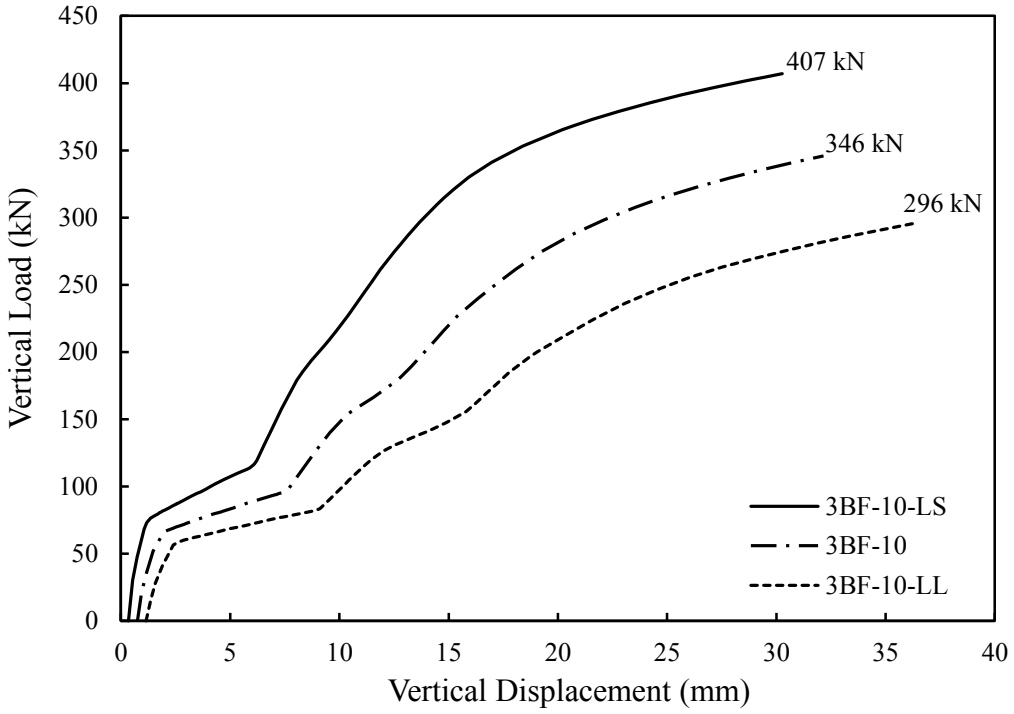

Figure 4-24: Effect of plate length on the response of models with flexible support

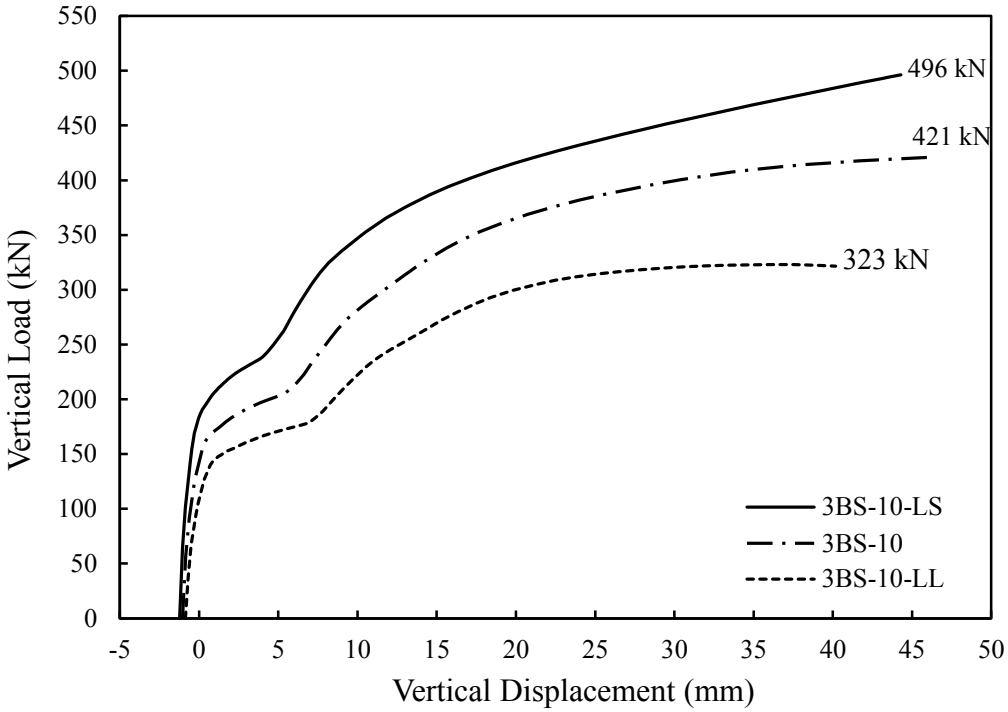

Figure 4-25: Effect of plate length on the response of models with stiff support

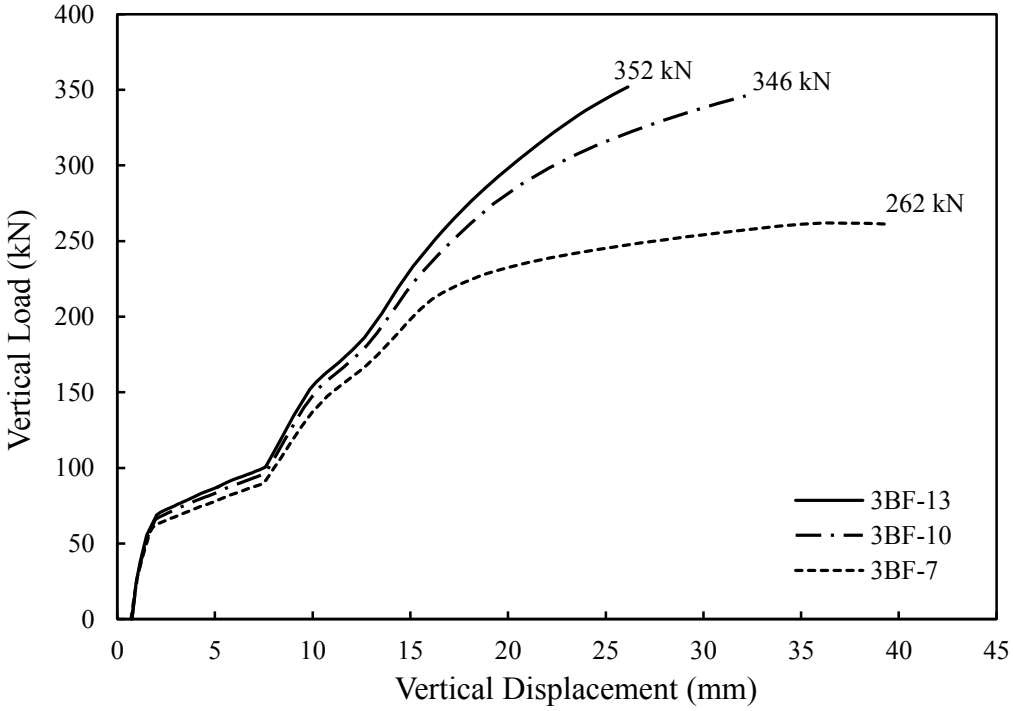

Figure 4-26: Effect of plate thickness on the response of models with flexible support

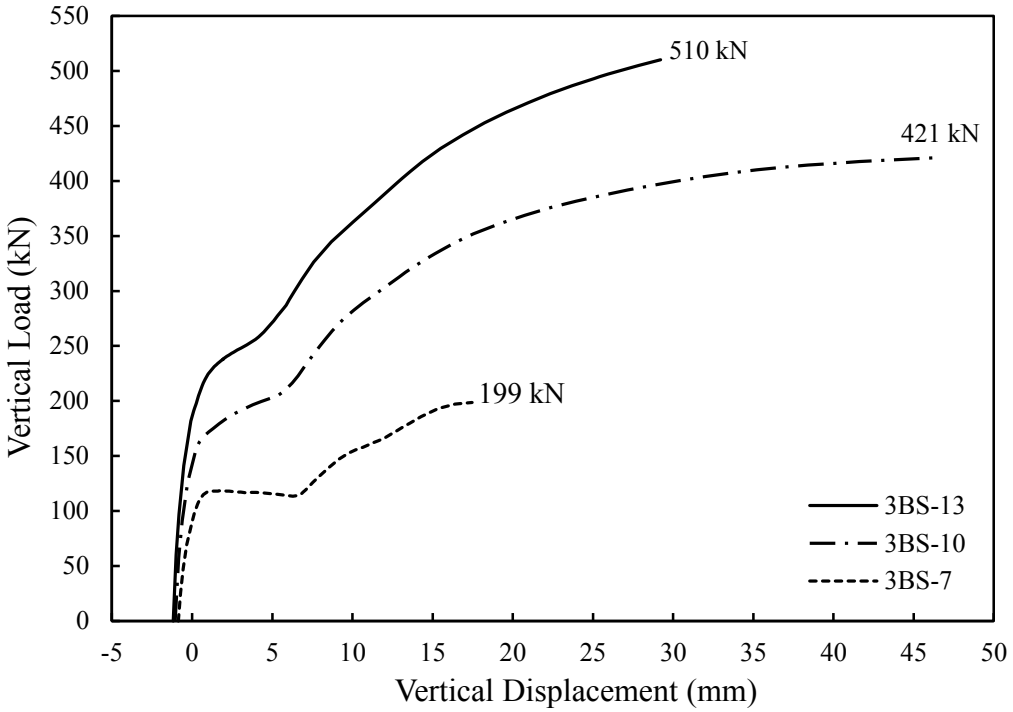

Figure 4-27: Effect of plate thickness on the response of models with stiff support

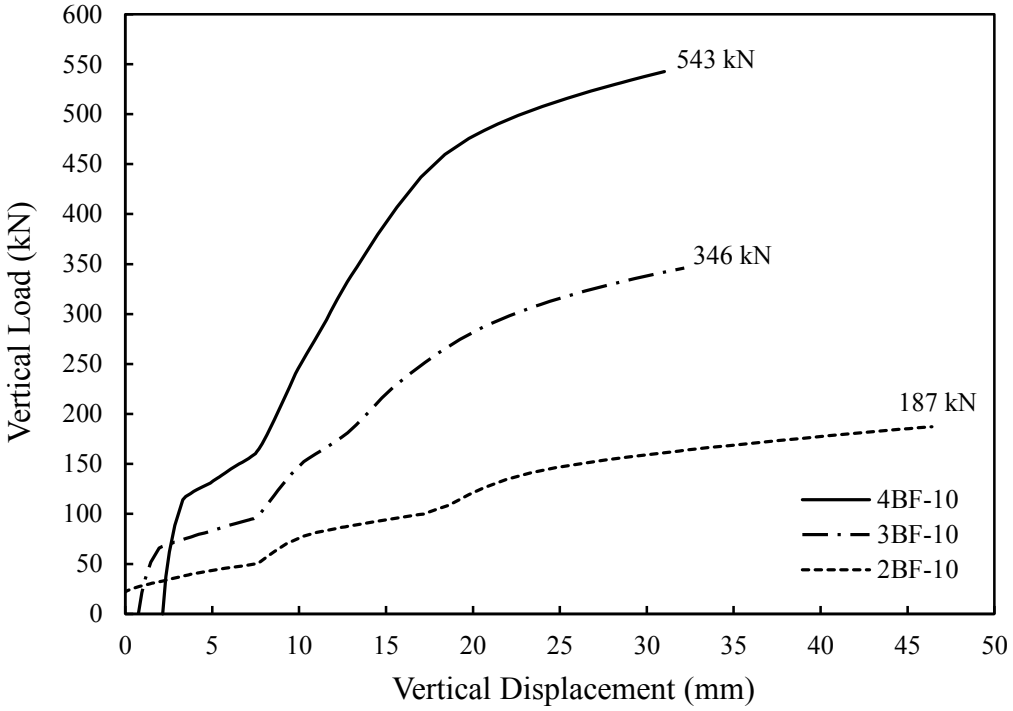

Figure 4-28: Effect of plate depth on the response of models with flexible support

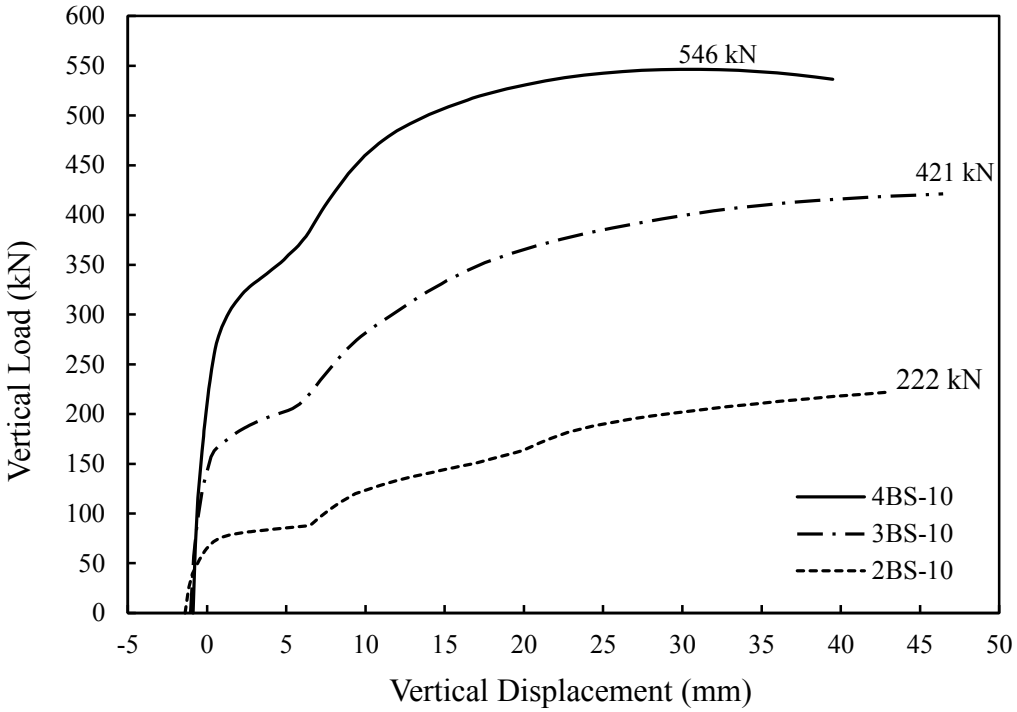

Figure 4-29: Effect of plate depth on the response of models with stiff support

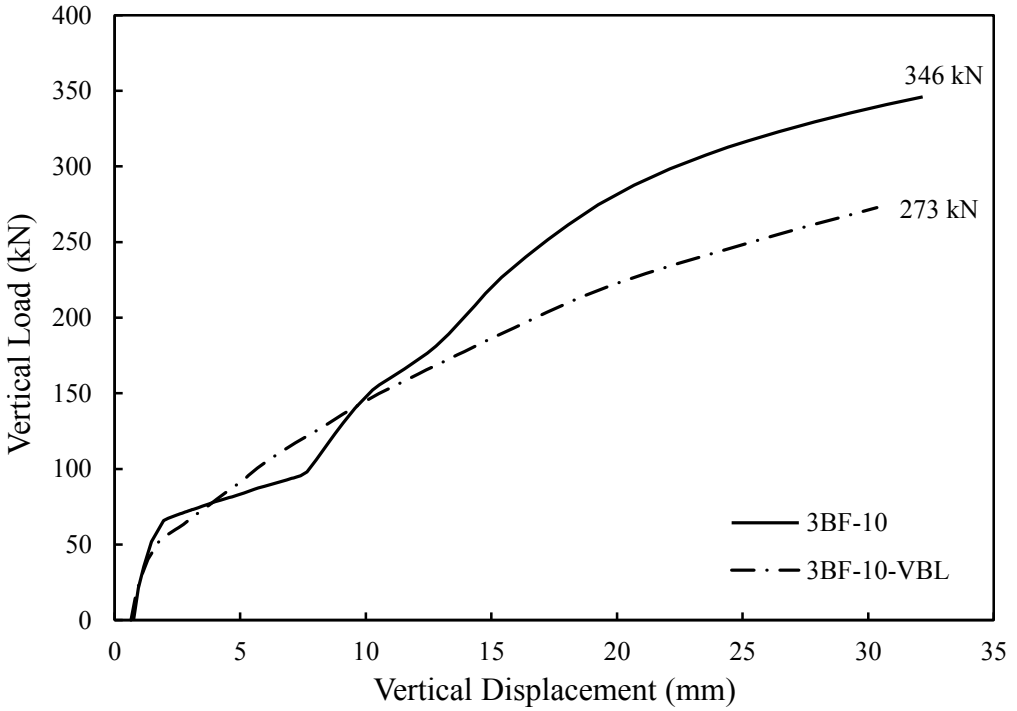

Figure 4-30: Effect of bolt configuration on the response of models with flexible support

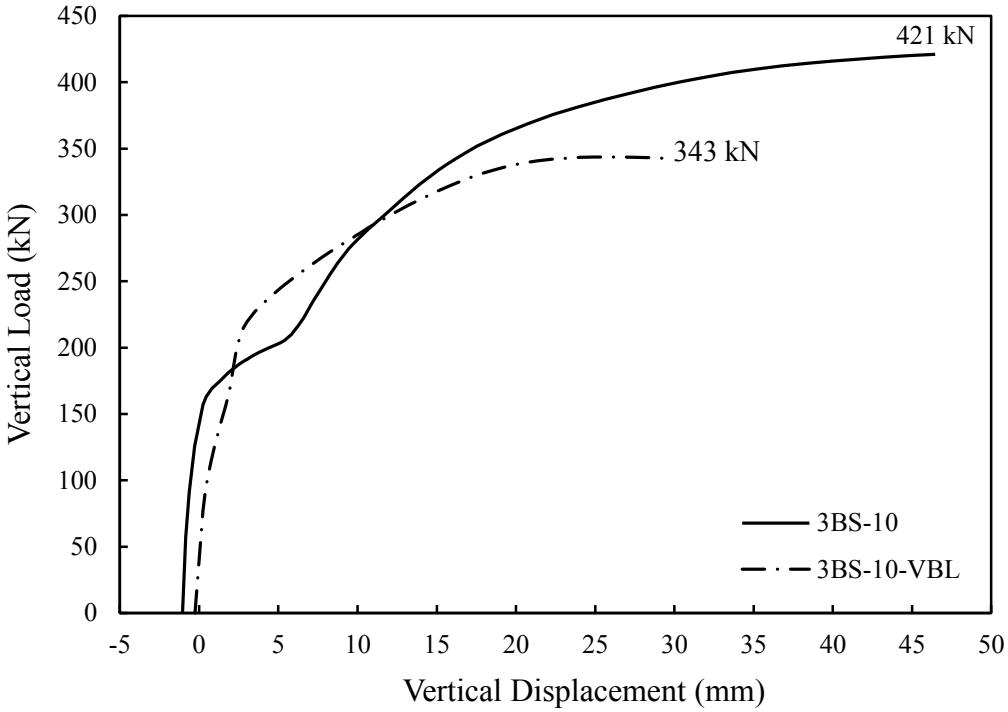

Figure 4-31: Effect of bolt configuration on the response of models with stiff support

4.5.5.5 Support Condition

Results of the parametric study showed a fundamental difference in the behaviour of extended shear tabs due to the rotational flexibility of the support. The behaviour is described according to Figure 4-32, where the plasticity sequence is indicated schematically for two extreme support conditions: completely flexible and totally fixed.

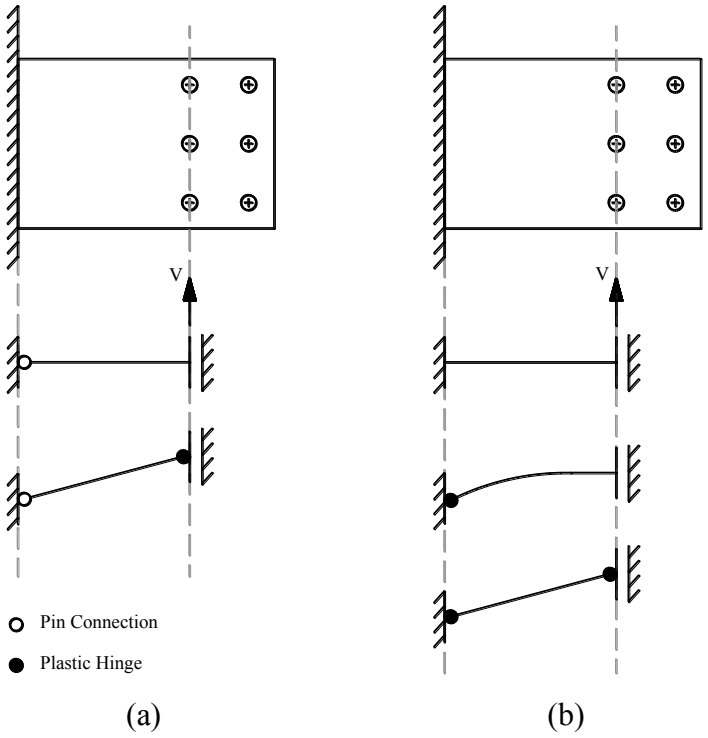

Figure 4-32: Typical plasticity sequence in extended shear tabs with (a) Flexible support and (b) Fixed support

In the case of the connection models with the flexible support, the connection could be simplified by a beam supported by a pin at one end and a roller-fixed support at the other end, as shown in Figure 4-32(a). Due to the flexibility of the support, a relatively low bending moment was induced there. Therefore, the inflection point was located closer to the support. This created a significant shear load eccentricity on the bolt group, which eventually led to bolt group rupture in most cases. Moreover, the net section at the first vertical line of bolts was prone to a high shear load eccentricity, resulting in a high bending moment demand applied to the section. The simultaneous effect of vertical load and bending moment resulted in the development of plasticity at the plate net section at lower vertical load values compared to the models with stiff support. After the formation of a plastic hinge at the net section, the connection reached a stability mechanism resulting in a considerable stiffness loss.

In the case of connections with the stiff support, the connection could be simplified by a beam with a fixed support at one end and a roller-fixed support at the other end,

as shown in Figure 4-32(b). Due to the significant rotational stiffness of the support, a considerable bending moment was developed there. In this case, the inflection point was pushed towards the beam span. As the shear load was increased, the bending moment at the support face was increased until plasticity was developed at the plate gross section. At this point, the inflection point was located very close to the bolt group centre. The connection was able to sustain considerable additional shear load, since only one plastic hinge was formed along the plate and, based on Figure 4-32, two plastic hinges are needed to form a mechanism in the connection. The reduction of section stiffness at the support resulted in the migration of the inflection point towards the support face. Moreover, out-of-plane deformation started to occur in the plate. With the increased shear load eccentricity applied to the bolt group, the bolt group eventually ruptured in most cases resulting in the connection reaching its peak vertical load. In some models, the simultaneous effect of shear and bending moment at the net section resulted in the development of plasticity at this location before bolt rupture was observed. After the formation of the second plastic hinge at the net section, the connection reached a stability mechanism resulting in a considerable stiffness loss.

A comparison between the vertical load–vertical displacement curves of models 2BS-10 and 2BF-10 is presented in Figure 4-33. The comparison for 3B models is presented in Figure 4-34.

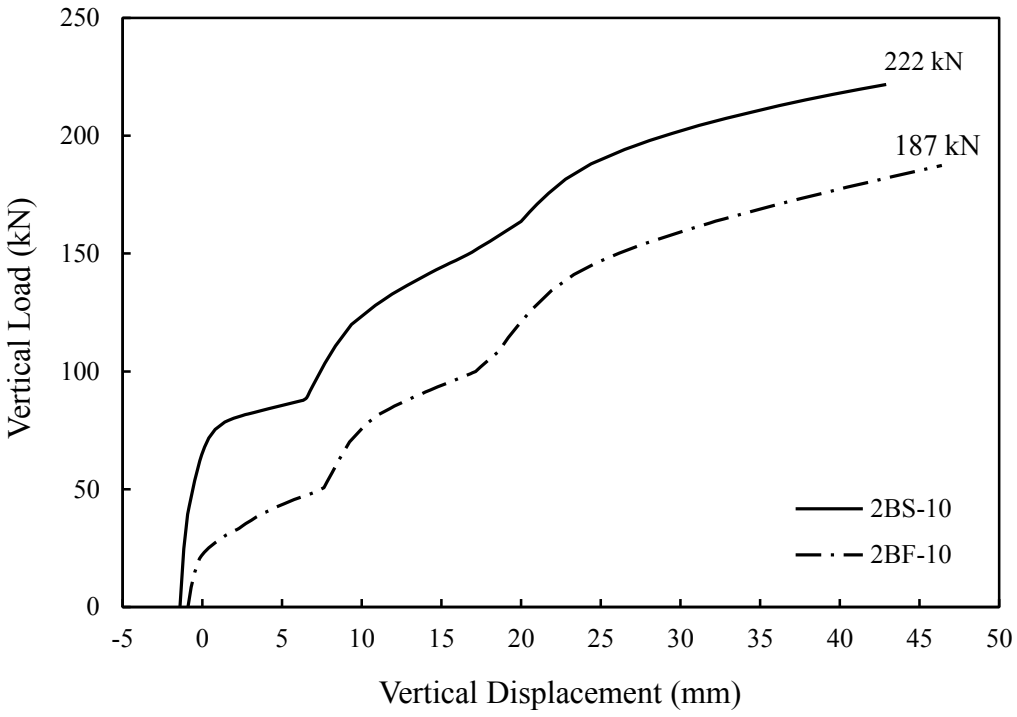

Figure 4-33: Effect of support condition on the response of 2B models

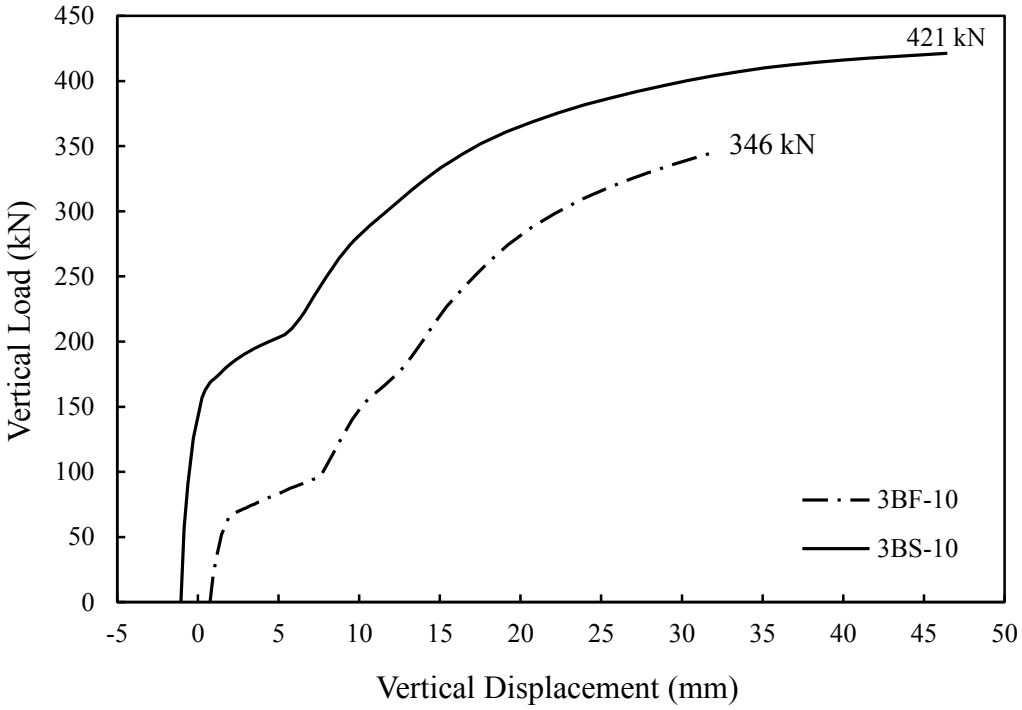

Figure 4-34: Effect of support condition on the response of 3B models

4.6 Comparison of Results with Thomas et al. (2014) Method

The design method proposed by Thomas et al. (2014) was used to evaluate the model failure modes and to calculate each connection capacity. In all calculations, the resistance factor was ignored to produce a direct comparison with the numerical analysis results. Moreover, the material properties used in the parametric study were also used in the design method. The support web yielding failure mode calculation from the method by Thomas et al. (2014) is to assess the yield line capacity of an unstiffened flexible column web support, so it was not considered in evaluating the connection capacity in this study. Also, the weld failure mode was not considered, as the weld was implemented as a tie in Abaqus and therefore this mode was not captured in the models. The capacities from the finite element analyses and the design method are presented for comparison in Table 4-10. The symbol FY in Table 4-10 indicates the flexural yielding limit state (termed Flexural Capacity by Thomas et al. (2014)), which constitutes the formation of a fully plastic moment on the gross section.

Table 4-10: Model capacities and limit states

Model ID	Finite Element		Thomas et al. (2014)		Analysis-to-Predicted Ratio
	Capacity (kN)	Failure Mode	Capacity (kN)	Failure Mode	
2BF-7	141	OPD	83	FY	1.70
2BF-10	187	BF	125	FY	1.50
2BF-10-LS	220	BF	162	FY	1.36
2BF-10-LL	155	BF	102	FY	1.51
2BF-13	191	BF	167	FY	1.14
2BS-7	104	OPD	83	FY	1.25
2BS-10	222	BF	125	FY	1.77
2BS-10-LS	269	BF	162	FY	1.66
2BS-10-LL	193	BF	102	FY	1.89
2BS-13	254	BF	167	FY	1.52
3BF-7	262	OPD	196	FY	1.34
3BF-10	346	BF	294	FY	1.18
3BF-10-LS	407	BF	380	FY	1.07
3BF-10-LL	296	BF	239	FY	1.24
3BF-13	352	BF	326	BF	1.08
3BS-7	199	OPD	196	FY	1.01
3BS-10	421	BF	294	FY	1.43
3BS-10-LS	496	BF	380	FY	1.31
3BS-10-LL	323	BF	239	FY	1.35
3BS-13	510	BF	326	FY	1.56
4BF-7	371	OPD	357	FY	1.04
4BF-10	543	BF	533	FY	1.02
4BF-10-LS	655	BF	670	BF	0.98
4BF-10-LL	463	BF	434	FY	1.07
4BF-13	535	BF	568	BF	0.94
4BS-7	294	OPD	357	FY	0.82
4BS-10	546	BF	533	FY	1.03
4BS-10-LS	688	BF	670	FY	1.03
4BS-10-LL	455	BF	434	FY	1.05
4BS-13	810	BF	568	FY	1.43
				Mean	**1.28**
				Std. Dev.	**0.27**

As observed in Table 4-10, the Thomas et al. (2014) method under-predicts the capacities of the majority of the models. However, the trends observed from the model analyses are similar to those observed from the design method. The peak vertical loads for the thicker plates were higher than those for the thinner plates. Shorter and deeper plates had a higher capacity.

As discussed in Chapter 2, the Thomas et al. (2014) method does not incorporate the effect of support stiffness in predicting the connection behaviour and capacity. Therefore, for the models with stiff support, the method under-prediction was more noticeable.

The expected failure mode based on the design method was compared with the failure mode observed from the numerical study and the results are reported in Table 4-10.

4.7 Summary and Conclusion

A high-fidelity finite element model was developed that is capable of accurately predicting the behaviour of extended shear tabs. The model was verified and validated using the available test data. It was then used to conduct a comprehensive parametric study on extended shear tabs having a variety of geometries and boundary conditions. The geometric parameters varied in the study included extended shear tab thickness, depth, and length. Two boundary conditions were considered: rotationally flexible and fixed.

Several limit states were observed in this study. In-plane bending moment was evaluated at the extended shear tab plate gross section at the support and at the plate net section at the first vertical line of bolts. The bending moment and shear force were used to evaluate plasticity of the extended shear tab at the two locations. Plasticity was also monitored by tracking the equivalent plastic strain contour over the extended shear tab area. Variation in shear load eccentricity applied to the bolt group was recorded for each model. The effect of key variables on the behaviour and capacity of the connection was investigated. Finally, the results were compared with the predictions of the design method proposed by Thomas et al. (2014).

The following are conclusions drawn from the parametric study:

- Extended shear tabs can experience several limit states, including: out-of-plane deformation, bolt fracture, net section plasticity, and gross section plasticity. Weld behaviour was not modelled.
- Out-of-plane deformation occurs after significant yielding has happened in the plate. In most cases, extended shear tabs reach the fully plastic state either at one or two locations along the plate length. Therefore, stability is not an issue limiting the performance of extended shear tabs within the considered dimensions in this study.
- The capacity of extended shear tabs is higher for deeper and thicker connections due to the increased cross-sectional area.
- Increasing the length of extended shear tabs results in connection capacity reduction. The shear load eccentricity imposed on the bolt group and the plate section at the vertical bolt line is higher for longer plates, resulting in decreased bolt group capacity and lower vertical load causing the net section plasticity.
- Plasticity is developed in extended shear tabs due to the combined effect of shear load and bending moment. Therefore, both effects need to be considered in plasticity evaluation in the plate.
- Plasticity development in extended shear tabs having higher depth-to-length ratios is more dominated by the effect of shear load, whereas plasticity development in extended shear tabs with lower depth-to-length ratios is more dominated by bending moment.
- The equation proposed by Neal (1961) provides an accurate evaluation of the loads that cause section plasticity.
- When Neal's interaction equation is used to evaluate plasticity development in extended shear tabs, the correlation between bending moment and shear load is defined using the shear load eccentricity. If the bending moment in the equation is substituted by the multiplication of shear load and a proper value for eccentricity, the shear load causing the plasticity of each section could be predicted by solving the equation for shear load.

- The eccentricity varies based on the considered limit state and support condition. Therefore, no unified eccentricity could be proposed for plasticity evaluation along extended shear tabs.
- The support condition has a significant effect on connection behaviour and capacity. In general, increasing the support rotational stiffness results in higher connection capacity.
- The shear load eccentricity varies quite considerably during the application of shear load. The point of inflection is located close to the centre of bolt group during the early stages of loading. However, with increase in shear load, the point of inflection moves towards the support resulting in an increase in the bolt group eccentricity. The extended shear tab was in double curvature when the capacity was reached.
- The eccentricity ratio was defined as the ratio of the shear load eccentricity to the geometric eccentricity. This ratio is a crucial parameter for determining when significant phenomena occur in the connection during loading.
- In connections with a flexible support, the inflection point is located closer to the support resulting in significant shear load eccentricity applied to the bolt group. Moreover, the net section at the first vertical line of bolts is prone to a high shear load eccentricity, resulting in a high bending moment demand applied to the section. The simultaneous effect of vertical load and bending moment results in the development of plasticity at the plate net section at lower vertical load values compared to the models with the stiff support.
- In the case of connections with a stiff support, a considerable bending moment is developed at the support and the inflection point is pushed back towards the beam span. As the shear load is increased, plasticity is developed at the plate gross section at early stages of loading. At this point, the inflection point is located very close to the bolt group centre. With a further increase in the shear load, the rotational stiffness of the plate is gradually reduced due to section plasticity resulting in the migration of the inflection point towards the support face. Concurrently, out-of-plane deformation started to occur in the plate. With the increased shear load eccentricity applied to the bolt group, the bolt

group eventually ruptures. Moreover, the simultaneous effect of vertical load and bending moment at the net section could result in the development of plasticity at this location before bolt rupture is observed.

- The design method of Thomas et al. (2014) under-predicted the capacity of most of the models considered in this study. The method recommends the effective eccentricity applied to the bolt group be taken as $0.75e_g$. However, in many of the models the observed effective eccentricity was lower than this value, resulting in conservative predictions of capacity.

CHAPTER 5: FINITE ELEMENT INVESTIGATION ON DOUBLE-COPED BEAMS

5.1 Introduction

In this chapter, a detailed finite element model for double-coped beams is developed. The efficiency and accuracy of the model was validated by comparing the analysis results with the available test data obtained by Johnston et al. (2015). The validated model is then used to conduct a comprehensive parametric study to expand the scope of the research and to get a better understanding of the double-coped beam connection behaviour.

5.2 Model Development

In this section, development of the finite element model for double-coped beam is discussed as a hierarchy of several steps. The model was developed and analyzed using the Abaqus finite element package (Dassault Systèmes 2012).

5.2.1 Typical Model Overview and Components

The members that form a double-coped beam joint model include the double-coped beam, supporting column or girder, connection bolts (if any), end plate (if any), loading plate, and rigid plate support (if any). It should be noted that not all of these members were used in a single model. Each component was used in the assembly based on the specific purpose of developing the model. As an example, a column was used for model verification, but was not used for the parametric study conducted in this research. A model assembly consisting of a double-coped beam bolted to a column flange using an end plate is shown in Figure 5-1(a). Another typical model consisting of a double-coped beam welded directly to a girder web is shown in Figure 5-1(b).

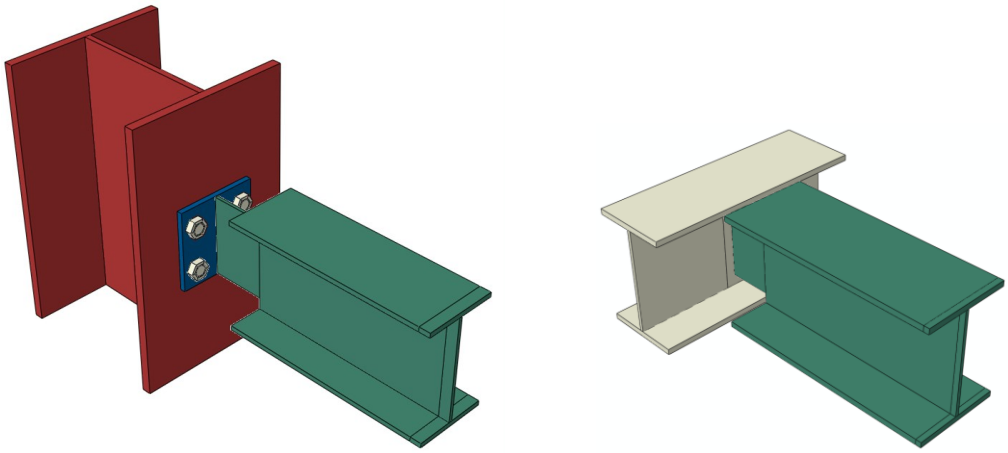

(a) (b)

Figure 5-1: Double-coped beam finite element model assembly:
(a) Beam bolted to a column flange and (b) Beam welded to a girder web

The components are created individually in Abaqus using customized modelling techniques. In the current section, the procedure used to create each individual part is discussed.

The double-coped beam was created as a three-dimensional part generated by sketching an I-shaped section and extruding it by a certain length. The coped region was then created using two rectangles in-plane with the double-coped beam web, cut through the whole beam flange. A typical double-coped beam is shown in Figure 5-2(a).

A typical girder model was created using the same procedure used to create the double-coped beam, except no coped region was cut through the girder section. A typical girder is shown in Figure 5-2(b).

To create a column, the same procedure used for creating the girder was used. A typical column is shown in Figure 5-2(c). The bolt holes were created by sketching the hole pattern on the column flange surface and extruding the pattern as a cut section through the column flange thickness.

The end plate was generated by sketching a rectangle using the specified length and depth dimensions and extruding the rectangle by the thickness of the end plate. The

bolt holes were then cut through the plate thickness based on the specific bolt hole pattern for the considered model. A typical end plate is shown in Figure 5-2(d).

All bolts used in this study were grade ASTM A325 having a 19 mm (3/4 in.) diameter. The dimensions of the bolt head, bolt shank and nut were taken from the CISC Handbook of Steel Construction (CISC 2012). Since in the scope of this study all the shear planes passed through unthreaded sections of the bolt shanks, threads were not modelled.

A rigid rectangular plate was modelled and attached to the beam end farther from the connection. The main purpose of using this loading plate was to apply load and rotation uniformly to the beam and to avoid any local stress concentration. Another rigid plate was attached to the coped end to replicate a fully restrained support (if needed). A reference point was defined for each rigid plate at the centre of the plate.

5.2.2 Meshing

5.2.2.1 Element Type Selection

Based on the discussion in Section 4.2.2.1, for this study first-order reduced-integration solid elements were used for all parts except for the rigid plates. Rigid shell elements were used to mesh these plates.

5.2.2.2 Meshing Generation Procedure

Due to the three-dimensional nature of the problem, solid 8-node brick elements were used to mesh the double-coped beam, girder, column and end plate. A hex-dominated meshing technique was used to mesh the bolts. 4-node shell elements were used to mesh the loading plate as well as the rigid support plate. Mesh density was increased around certain regions within each part, namely the coped region and bolt holes in the end plate and column flange.

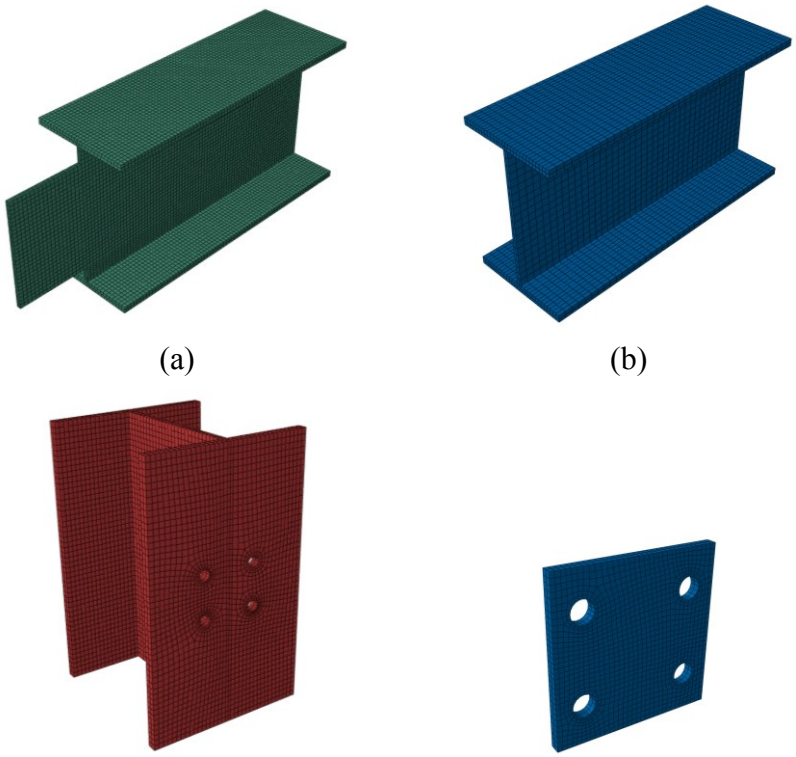

Figure 5-2: Double-coped beam finite element model components:
(a) Double-coped beam, (b) Girder, (c) Column and (d) End plate

5.2.3 Material Properties

When defining a typical plastic material, it is necessary to decompose the elastic and plastic portions of the stress–strain curve. In the definition of the elastic domain, the modulus of elasticity and Poisson's ratio are defined. The plastic behaviour of the material starts from the point of zero plastic strain, which corresponds to the yield stress, followed by data points characterising the full plastic material response. Abaqus interpolates between the data points provided to capture the overall material behaviour.

5.2.3.1 Plates and Hot-rolled Sections

For model verification purposes, tension coupon test data from Johnston et al. (2015) were used to develop the steel material curves for different components of the

numerical models. To be able to use the stress–strain curve from the tension coupon test for numerical analysis, the curve is processed in two steps, as discussed in Section 4.2.3.1.

For parametric study purposes, a bilinear stress–strain relationship was used. More details on the material properties used for the parametric study can be found in Section 5.4.

5.2.3.2 High Strength Bolts

Bolts were modelled based on the discussion in Section 4.2.3.2.

5.2.4 Parts Interaction

In the models with an end plate component, the double-coped beam was attached to the end plate using the "tie" constraint in Abaqus, which attaches two surfaces together such that no relative motion is allowed (Dassault Systèmes 2012). It was assumed that the connection weld size was sufficient to transfer the loads from the double-coped beam to the end plate without rupture; therefore, welds were not simulated in any of the models.

The rigid loading plate was tied to the double-coped beam far-end cross-section. This ensured that each condition applied to the rigid plate was directly transferred to the double-coped beam section, while eliminating local stress concentrations.

The double-coped beam and end plate sub-assembly was then connected to the column flange using high strength bolts. The interactions between the end plate, bolts, and column flange were established using contact. Contact allows force transmission between different members with certain contact properties used to model the structure in the most realistic way possible. Several surfaces were in contact with each other in the typical model, including bolt shank contact with bolt holes in the end plate and column flange, bolt head contact with the end plate surface and nut contact with the column flange surface, and end plate surface contact with the column flange surface. The general contact feature was used to model the contact among different members.

The normal and shear behaviour of contact was implemented using the penalty method. The coefficient of friction of 0.3 was used for steel material friction.

In the models consisting of a double-coped beam attached directly to the web of a girder, the coped section was tied to the girder web and no other contact was considered in the models.

5.2.5 Loading

Loading is applied to the model in two, three or four consecutive steps, depending on the specific case. In the models that incorporate bolts, the internal load developed in the bolts due to snug-tightening was applied as the first step of loading. The load was applied to each bolt individually using the "bolt load" load type in Abaqus. More details on the procedure for the application of bolt load are discussed in Section 4.2.5.

The next phase of loading was to rotate the double-coped beam to 0.03 radians. The rotation of 0.03 radians is widely used to represent a typical rotation in shear connections at the beam flexural limit state, i.e., when the first plastic hinge is formed in the beam. The rotation was applied as a rotational angle to the rigid plate reference point. During the application of rotation, since the rigid plate was free to translate in the vertical and horizontal directions, no vertical or horizontal load was developed in the connection. The rotation of 0.03 was maintained during the subsequent loading steps.

After the rotation phase, the horizontal load (if any) was applied to the specimen using a point load applied to the reference point of the rigid plate.

Finally, the vertical load was applied to the connection (with no additional rotation) using the vertical displacement of the rigid plate reference point. The vertical displacement was increased until the load developed in the connection started to decline or the connection reached its full coped section capacity.

5.2.6 Boundary Conditions

Several boundary conditions were applied to the model components. The two ends of the connection supporting member were intended to be fixed against translation and rotation. Therefore, both column ends were restrained against all translational and rotational degrees of freedom. In the case of a double-coped beam welded to a girder, both girder ends were restrained against all translational and rotational degrees of freedom. Since the focus of this study is to evaluate the behaviour of the coped region of the double-coped beam, the beam flanges were restrained against lateral displacement adjacent to the copes.

5.2.7 Solution Method

The nature of the applied loads in this study was static. Therefore, it was appropriate to use the implicit solution method using the Static/General algorithm in Abaqus. The general method is capable of including the effects of nonlinearities in the model, which can have different sources including material nonlinearity, geometric nonlinearity and boundary nonlinearity.

In the general method, loading is applied gradually in each step through increments that are fractions of the total applied load. The size of loading increments was set as "automatic", which enables the software to change the increment size as needed to achieve numerical convergence.

5.2.8 Derivation of Results

The most significant result achieved from the numerical studies was the connection peak vertical load or capacity. Moreover, the variation of vertical load versus connection vertical deformation represents the nonlinear behaviour of the connection. To derive the vertical load–deformation curve of the connection during the desired loading step, the reaction force developed at the rigid plate reference point was plotted against the vertical deformation of the beam at a point located on the double-coped beam flange at the end of the cope.

The bending moments at specific locations along the coped region needed to be investigated, and were derived directly from Abaqus using the "free body cut" feature. This feature creates a section cut at a user-defined location and calculates the internal forces and moments acting on the section using the nodal forces.

Visual inspection of the model was an important tool in defining the failure mode and development of plasticity in the model. To track the plasticity development, strains needed to be monitored closely. In this study, the equivalent plastic strain (PEEQ in Abaqus) was selected as an appropriate indication of the yielded areas of the connection. The von Mises yield criterion was used to investigate the plasticity development in the connection.

5.3 Model Verification

The model verification was carried out using the available data from a recent experimental study on double-coped beams conducted by Johnston et al. (2015) at the University of Alberta. Finite element models of five specimens were constructed based on the measured dimensions and tested material properties, and the results achieved from the numerical analyses were compared to the results achieved from the tests. In this regard, load–displacement curves, deformed shapes, and failure modes obtained from the analysis and the tests were the basis of comparison.

As discussed in Section 2.3.3, Johnston et al. (2015) evaluated the performance of double-coped beams through a comprehensive testing program. The study consisted of 29 full-scale tests on double-coped beams with equally coped top and bottom flanges. The cope length and beam section (which accounted for both uncoped depth and thickness) were considered as test variables. End-supports with different rotational stiffnesses were tested in the research. The specimens were tested under various combinations of axial and shear loads, with the axial load being either compressive, tensile or zero.

Five tested specimens were selected to verify the double-coped beam modelling technique used in this study. The selected specimens included: 2A-1-0, 2B-3-0, 3D-2-0-NR, 4B-3-300C and 4A-3-100T (Johnston et al. 2015). The models were

selected such that they include various boundary conditions, reduced beam depths, cope lengths, and applied horizontal loads. The material properties reported by the researchers were assigned to the steel members.

The comparisons of the five finite element models with their corresponding specimens tested by Johnston et al. (2015) are presented in Figure 5-3 to Figure 5-7 in terms of vertical load–vertical displacement curves. As indicated by the figures, good correlation was observed between numerical and experimental results.

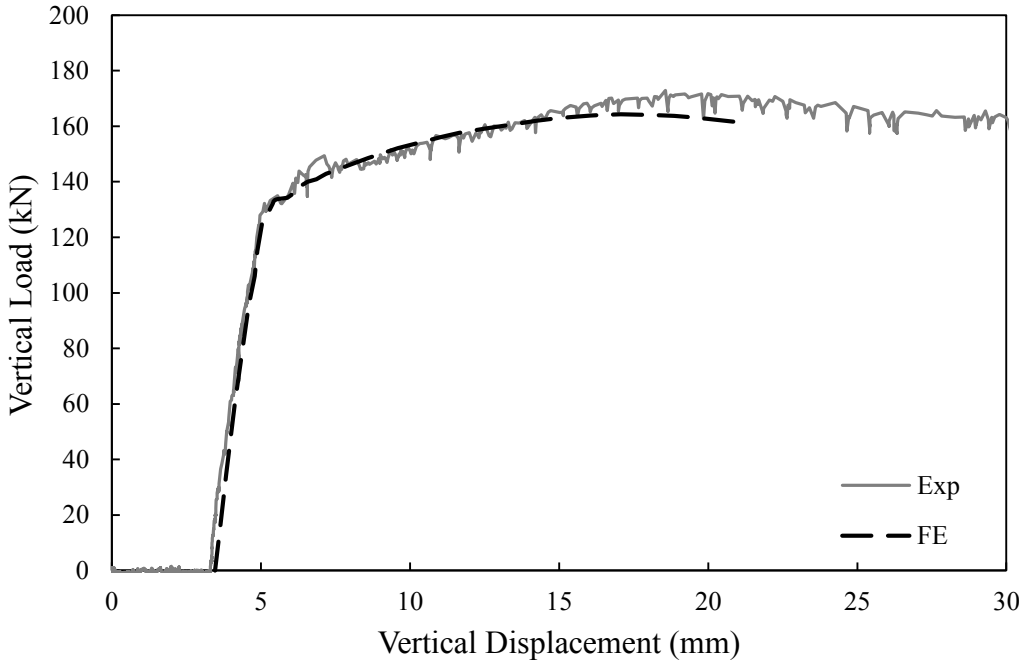

Figure 5-3: Comparison of finite element and test results for specimen 2A-1-0

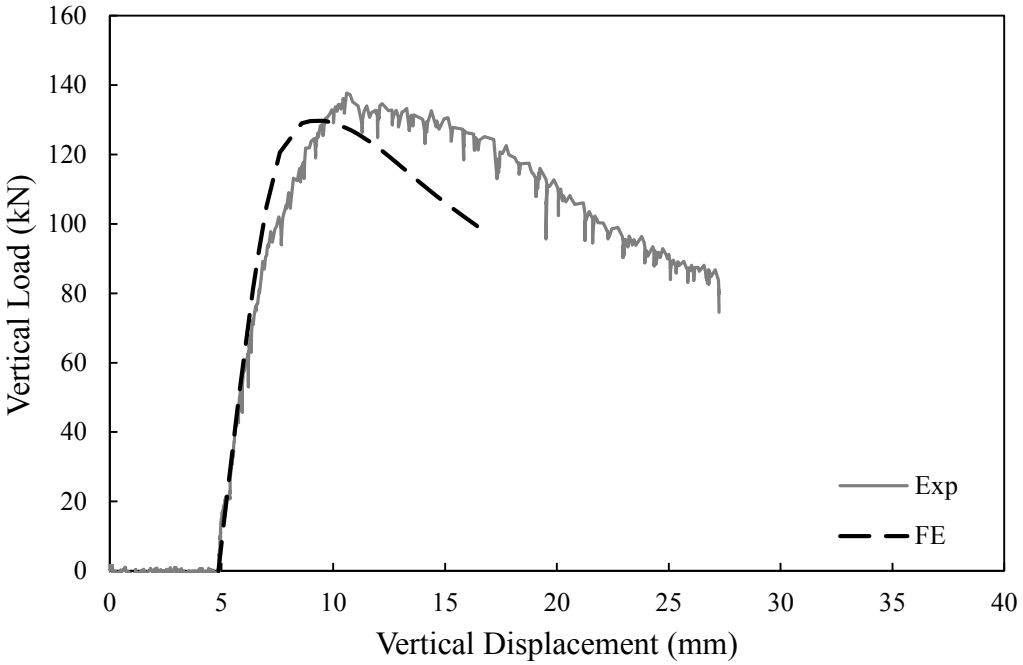

Figure 5-4: Comparison of finite element and test results for specimen 2B-3-0

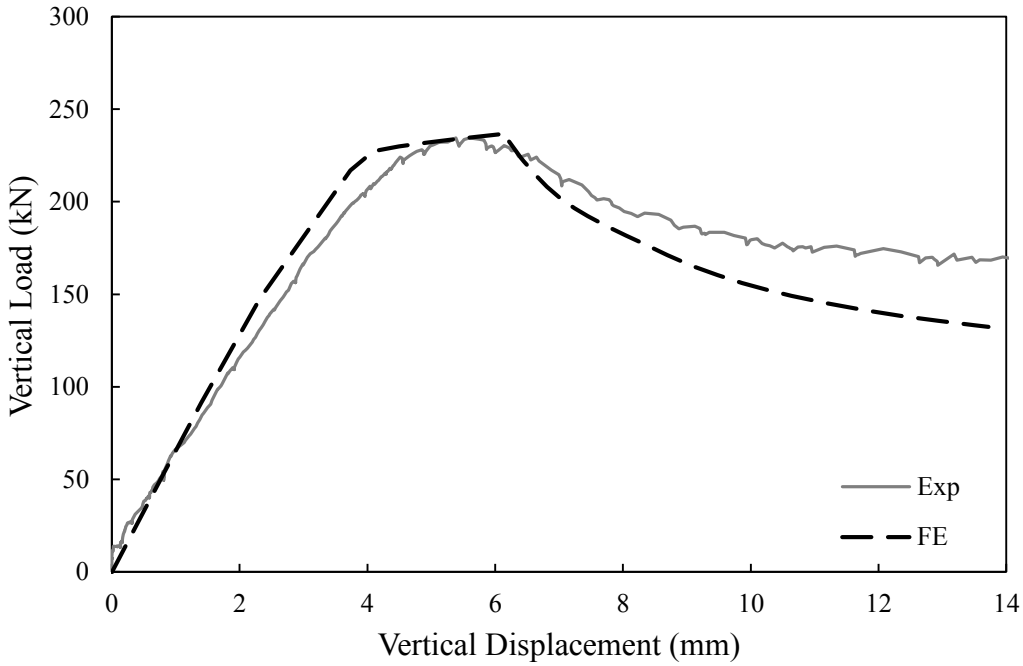

Figure 5-5: Comparison of finite element and test results for specimen 3D-2-0-NR

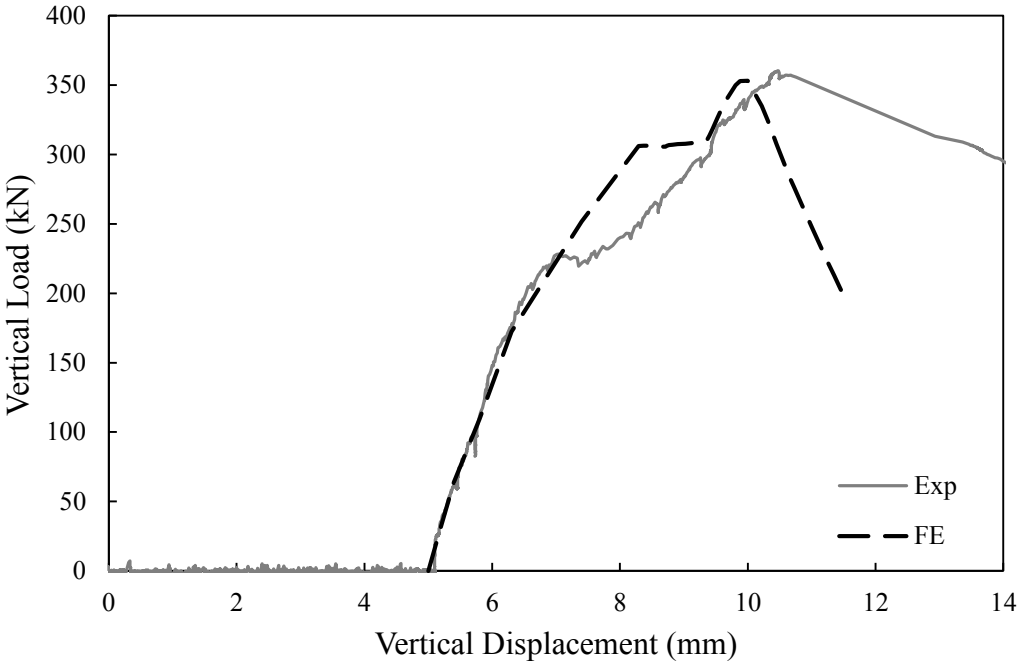

Figure 5-6: Comparison of finite element and test results for specimen 4B-3-300C

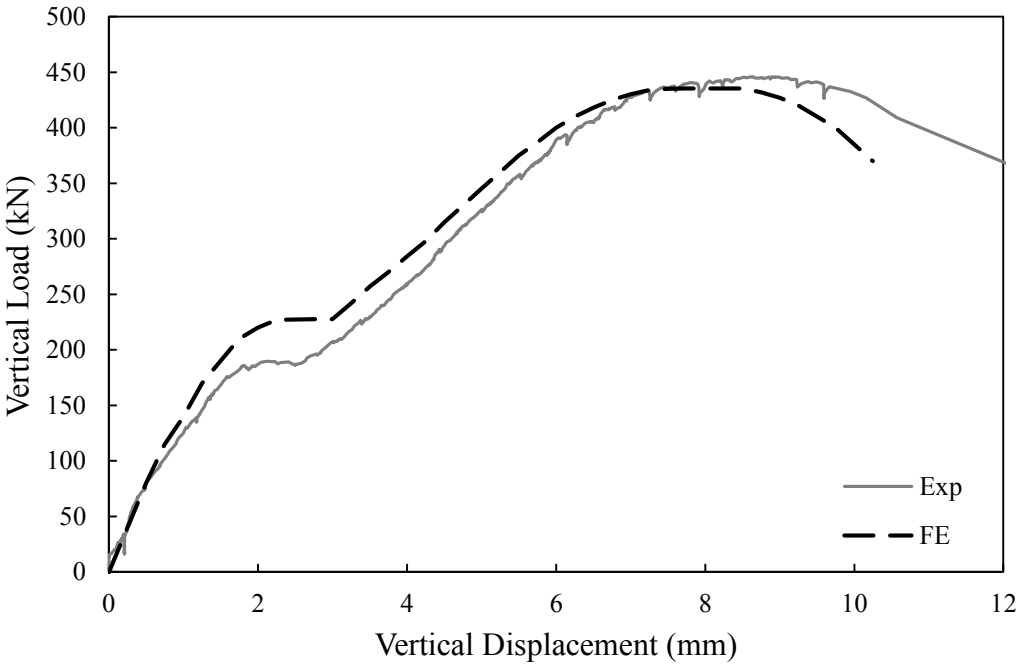

Figure 5-7: Comparison of finite element and test results for specimen 4A-3-100T

Other than the quantitative verification of the model, a qualitative verification is also necessary. In this regard, the failure modes and deformed shapes of the models and test specimens were compared. Figure 5-8 and Figure 5-9 show comparisons between numerical results and tested specimens. As observed from the figures, the deformed shapes resulting from finite element analysis closely mimic the actual observed deformations in the test program. The simulation was capable of modelling the actual deformation in the real structure quite accurately.

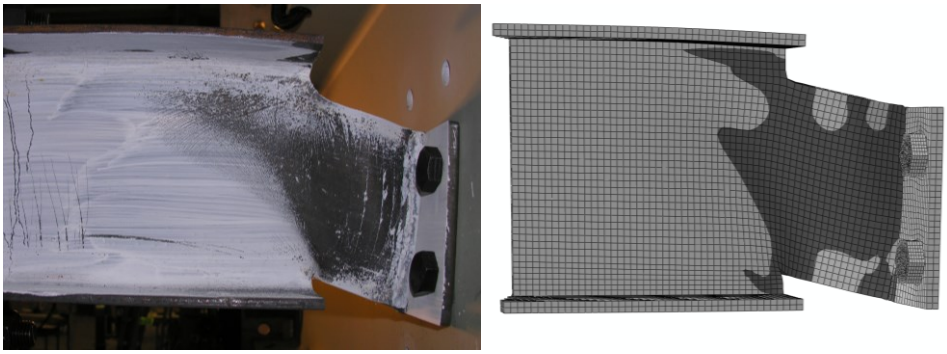

(a)

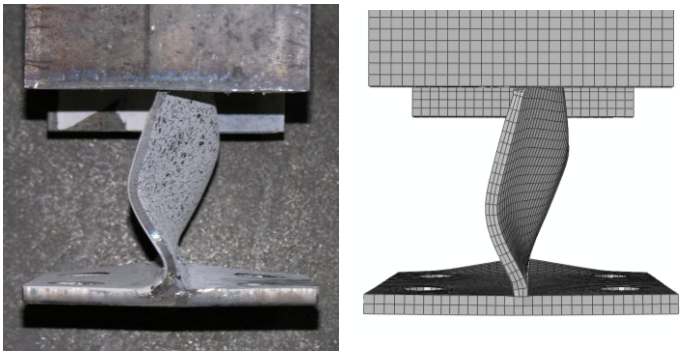

(b)

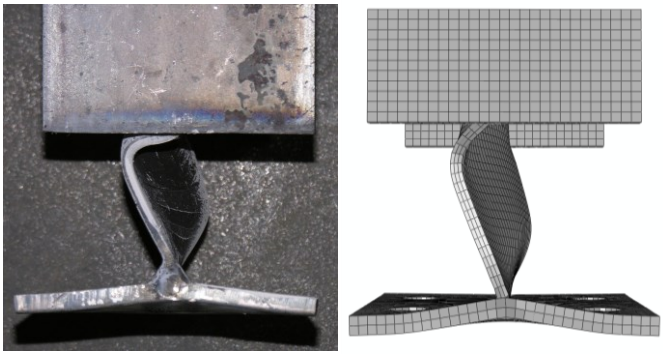

(c)

Figure 5-8: Test and finite element deformed shape comparisons for specimen 2A-1-0: (a) Side view (b) Top view and (c) Bottom view

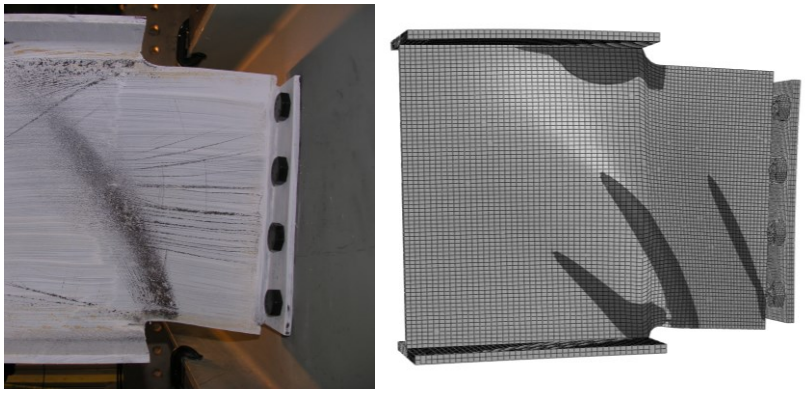

(a)

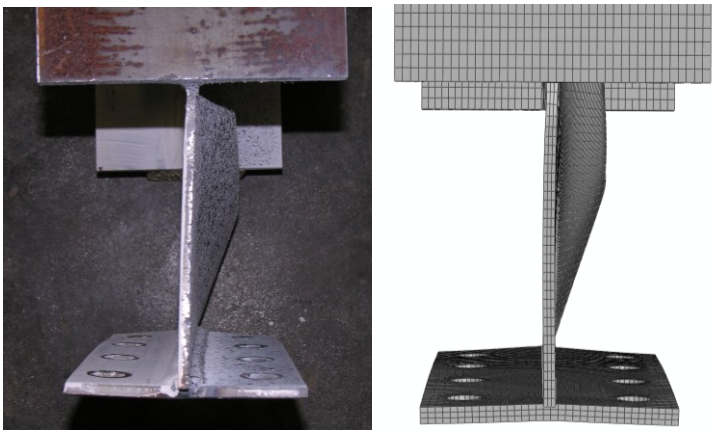

(b)

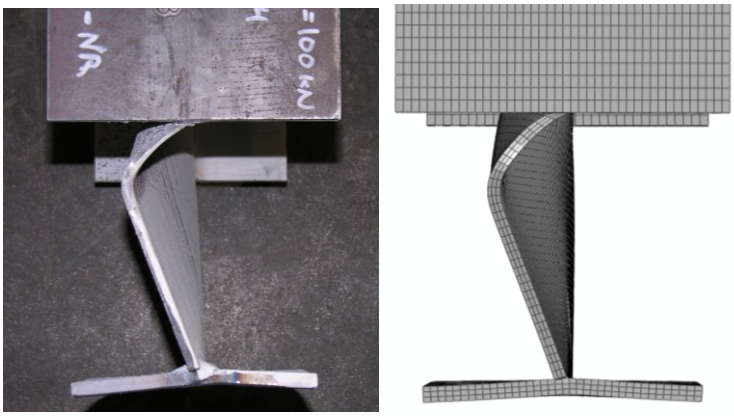

(c)

Figure 5-9: Test and finite element deformed shape comparisons for specimen 4A-3-100t-NR: (a) Side view (b) Top view and (c) Bottom view

5.4 Parametric Study

A well-detailed and robust model was developed to capture the behaviour of double-coped beams. Available test data by other researchers (Johnston et al. 2015) were used to verify and validate the accuracy of the model. The validated model is used to investigate the behaviour further through a comprehensive parametric study that considers various geometric configurations and boundary conditions. The purpose of the parametric study is to expand the scope of the previous research and to identify new aspects of double-coped beams behaviour patterns.

The study consisted of 54 models varying in cope length, web thickness, reduced beam depth in the coped region, and support condition. In all cases, the material stress–strain curve was bilinear, with a slope of 200,000 MPa in the elastic region and 0.5% of that value after reaching the yield stress of 385 MPa. Further discussion about the origin of this curve can be found in Section 4.2.3.1. The naming scheme of the specimens is alphanumeric. The first letter and number represent the reduced beam depth, varying among h1, h2 and h3. The next letter and number imply cope length, varying among c1, c2 and c3. The third letter and number imply beam web thickness, varying among t1, t2 and t3. The final letter indicates whether the support condition was stiff (S) or flexible (F). In this study, the stiff support was modelled as a rigid plate attached directly to the end of the coped section of the double-coped beam. The flexible support in each case was a girder having the same cross-section as the double-coped beam and unbraced between its ends, with the length-to-section-depth ratio of 20. This ratio was believed to represent an extremely flexible, but plausible, support for the double-coped beam. It should be noted that in the models considered in the parametric study, since reasonable limits of the range of possible web support rotational stiffnesses were targeted the connection between the double-coped beam and the support was simplified using the tie constraint and therefore no end plate and bolts were used as connection components. The modelling scheme and the variable ranges considered are presented in Figure 5-10.

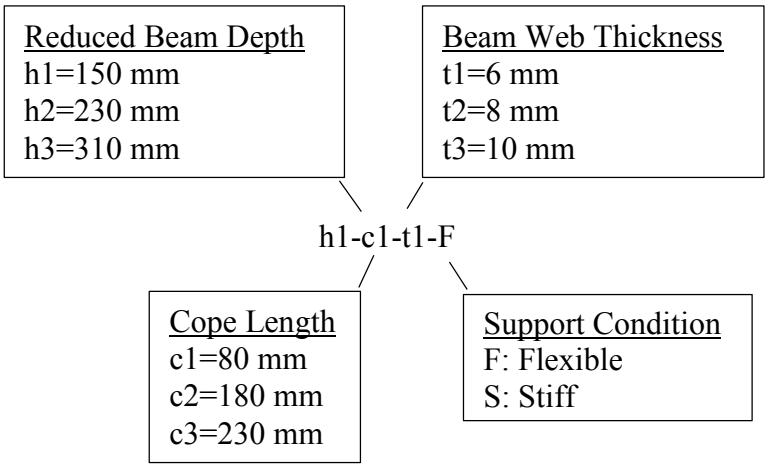

Figure 5-10: Model ID convention

5.5 Results and Discussion

Connection capacity, as the most significant result of the study, was investigated for each model. Several limit states observed in the models are also discussed. Bending moments at the support face, as well as the cope face, were derived and discussed as a measure of plasticity development in the coped region. Shear load eccentricities applied to the cope face are examined and, finally, the effects of various geometric configurations on the behaviour and capacity of the connection are investigated.

5.5.1 Connection Capacity

The vertical load–vertical displacement curve was derived for every model and was used to evaluate the connection capacity, taken at the point right before the vertical load started to decline or when the reduced section reached its theoretical fully plastic shear capacity, defined by Equation 5-1. The equation represents the von-Mises yield criterion rounded to one significant digit.

5-1 $$V_p = 0.6F_y h_0 t_w$$

Imposing the latter limit was necessitated by the fact that the post-yield material curve was not designed to capture material-level deterioration. The curve for model h2-c2-t1-S is presented in Figure 5-11, where the capacity was evaluated as 313 kN and was reached due to severe out-of-plane deformation of the coped region. Vertical load–vertical displacement curves for other select models are presented in Appendix D. All model capacities are reported in Table 5-1.

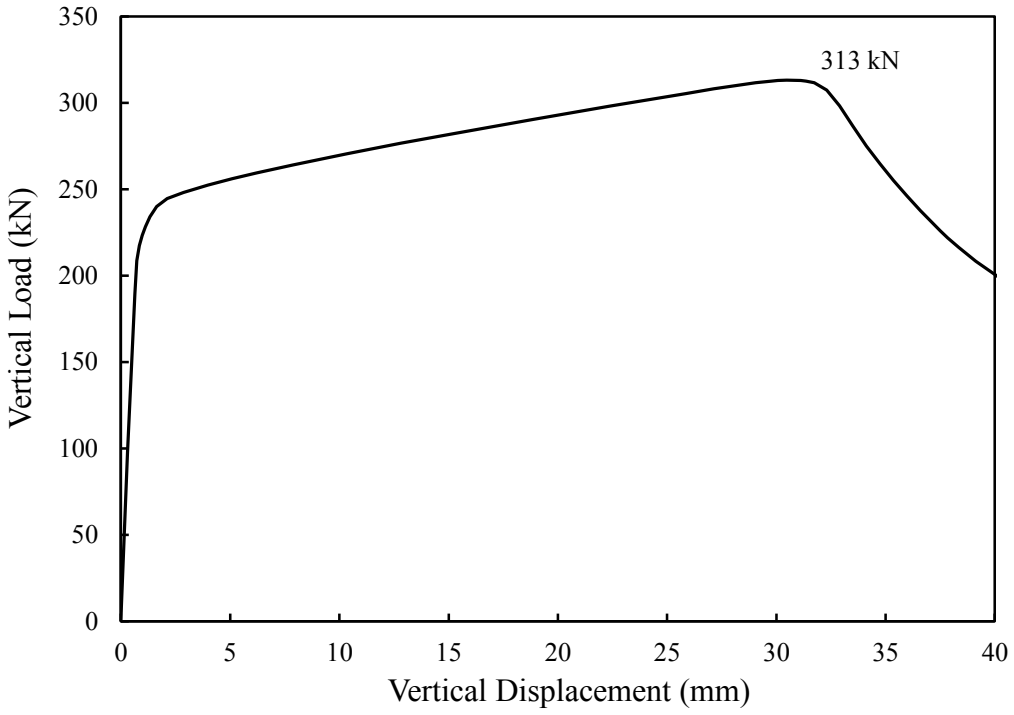

Figure 5-11: Load–displacement curve for model h2-c2-t1-S

Table 5-1: Model capacities and limit states

Models with flexible support			Models with stiff support		
Model ID	Connection Capacity (kN)	Limit States	Model ID	Connection Capacity (kN)	Limit States
h1-c1-t1-F	208	CFP, **SC**	h1-c1-t1-S	208	SFP, CFP, **SC**
h1-c1-t2-F	277	CFP, **SC**	h1-c1-t2-S	277	SFP, CFP, **SC**
h1-c1-t3-F	347	CFP, **SC**	h1-c1-t3-S	347	SFP, CFP, **SC**
h1-c2-t1-F	162	CFP, **OPD**	h1-c2-t1-S	195	SFP, CFP, **OPD**
h1-c2-t2-F	171	CFP, **OPD**	h1-c2-t2-S	256	SFP, CFP, **OPD**
h1-c2-t3-F	255	CFP, **OPD**	h1-c2-t3-S	347	SFP, CFP, **SC**
h1-c3-t1-F	115	CFP, **OPD**	h1-c3-t1-S	150	SFP, CFP, **OPD**
h1-c3-t2-F	142	CFP, **OPD**	h1-c3-t2-S	209	SFP, CFP, **OPD**
h1-c3-t3-F	172	CFP, **OPD**	h1-c3-t3-S	347	SFP, CFP, **SC**
h2-c1-t1-F	319	CFP, **SC**	h2-c1-t1-S	319	SFP, CFP, **SC**
h2-c1-t2-F	425	CFP, **SC**	h2-c1-t2-S	425	SFP, CFP, **SC**
h2-c1-t3-F	531	CFP, **SC**	h2-c1-t3-S	531	SFP, CFP, **SC**
h2-c2-t1-F	222	CFP, **OPD**	h2-c2-t1-S	313	SFP, CFP, **OPD**
h2-c2-t2-F	309	CFP, **OPD**	h2-c2-t2-S	409	SFP, CFP, **OPD**
h2-c2-t3-F	363	CFP, **OPD**	h2-c2-t3-S	531	SFP, CFP, **SC**
h2-c3-t1-F	172	CFP, **OPD**	h2-c3-t1-S	282	SFP, CFP, **OPD**
h2-c3-t2-F	249	CFP, **OPD**	h2-c3-t2-S	341	SFP, CFP, **OPD**
h2-c3-t3-F	282	CFP, **OPD**	h2-c3-t3-S	482	SFP, CFP, **OPD**
h3-c1-t1-F	430	CFP, **SC**	h3-c1-t1-S	430	SFP, CFP, **SC**
h3-c1-t2-F	573	CFP, **SC**	h3-c1-t2-S	573	SFP, CFP, **SC**
h3-c1-t3-F	716	CFP, **SC**	h3-c1-t3-S	716	SFP, CFP, **SC**
h3-c2-t1-F	315	CFP, **OPD**	h3-c2-t1-S	430	SFP, CFP, **SC**
h3-c2-t2-F	433	CFP, **OPD**	h3-c2-t2-S	573	SFP, CFP, **SC**
h3-c2-t3-F	552	CFP, **OPD**	h3-c2-t3-S	716	SFP, CFP, **SC**
h3-c3-t1-F	271	CFP, **OPD**	h3-c3-t1-S	387	SFP, CFP, **OPD**
h3-c3-t2-F	362	CFP, **OPD**	h3-c3-t2-S	542	SFP, CFP, **OPD**
h3-c3-t3-F	456	CFP, **OPD**	h3-c3-t3-S	710	SFP, CFP, **OPD**

5.5.2 Limit States

"Limit states" were considered as the mechanisms contributing to the gradual degradation and eventual failure of the connection. These were identified by close inspection of the connection during the model analysis, as well as monitoring the

vertical load–vertical displacement curve and calculation of section forces and moments at critical locations. Several limit states were observed in the analyzed models, each discussed in detail below. The limit state predominantly responsible for the load carried by the connection dropping immediately after the peak load is regarded as the "failure mode". The observed limit states for each model are reported in Table 5-1, in order of occurrence, using the abbreviations specified in the following paragraphs, and the limit state responsible for failure of each connection is highlighted as the failure mode using bold font. It should be noted that the failure mode always happened after all other limit states listed.

Support face plasticity (SFP) was observed in all the models with the stiff support. Support face plasticity was identified as plasticity that developed throughout the whole depth of the coped region at the support face, as identified by the equivalent plastic strain parameter PEEQ. This phenomenon was accompanied by a drop in the slope of the connection vertical load–displacement curve, which was an indication of stiffness loss due to plasticity. Images of the development of section plasticity at the support face in model h3-c2-t1-S are shown in Figure 5-12. The dark regions in the figure depict the plastic regions. Support face plasticity was not the failure mode for any of the models.

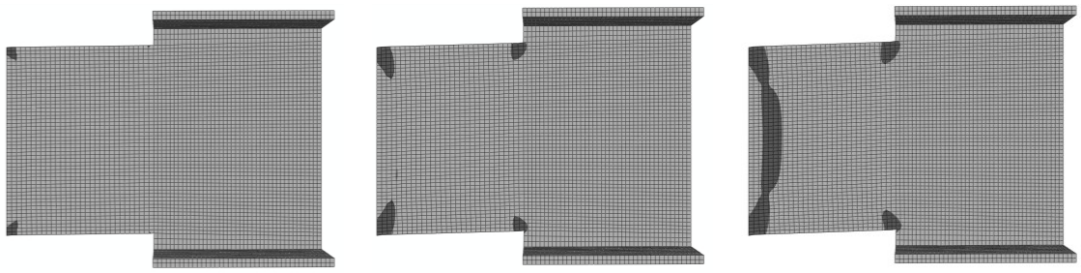

Figure 5-12: Plasticity development at support face section

Cope face plasticity (CFP) was observed in all models. Cope face plasticity was identified as plasticity that developed throughout the whole depth of the coped region at the cope face, as identified by the equivalent plastic strain parameter PEEQ.

Images of gradual cope face plasticity development in model h3-c2-t1-F are shown in Figure 5-13. Cope face plasticity was not the failure mode for any of the models.

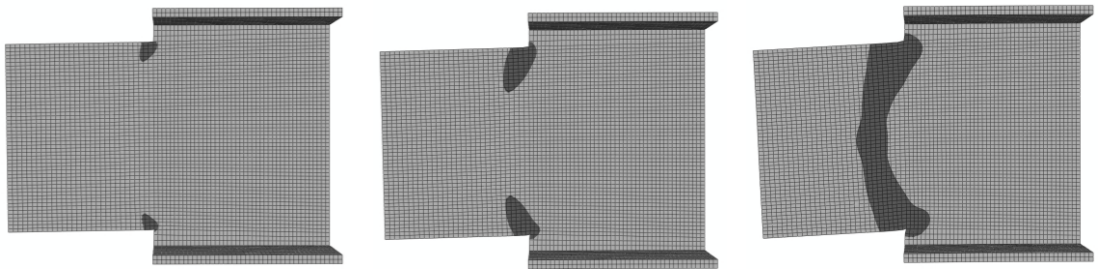

Figure 5-13: Plasticity development at cope face section

Out-of-plane deformation (OPD) was observed in many of the models. Images of the deformed shape of model h2-c2-t1-S from different angles are shown in Figure 5-14. In many cases, out-of-plane deformation, as it became severe, was identified as the failure mode for the connection.

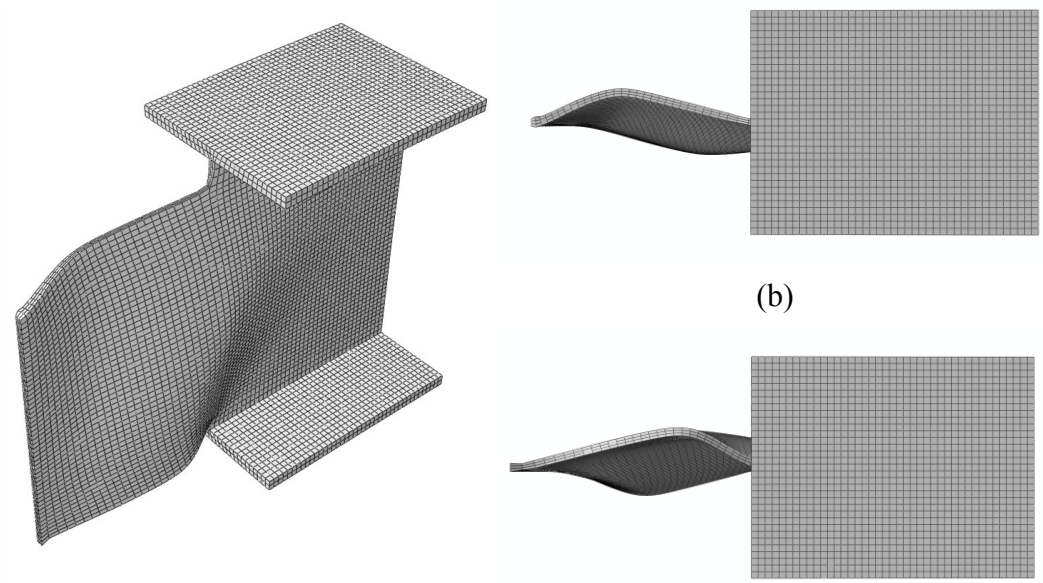

(a) (b) (c)

Figure 5-14: Out-of-plane deformation in model h2-c2-t1-S:
(b) Three-dimensional view, (b) Top view and (c) Bottom view

Shear capacity (SC) was considered a limit state when the shear load applied to the connection reached the theoretical plastic shear capacity of the reduced beam depth, defined by Equation 5-1. This was the failure mode for several models. This limit state defined the highest shear load the connection was able to sustain without any other limit state limiting its performance.

5.5.3 Development of Plasticity Through the Reduced Beam Depth

In-plane bending moments at the support face and the cope face were derived by cutting planes through the coped region cross-sections at the support face and at the cope face, and recording the in-plane bending moment at each loading step. The locations of the cuts are shown in Figure 5-15.

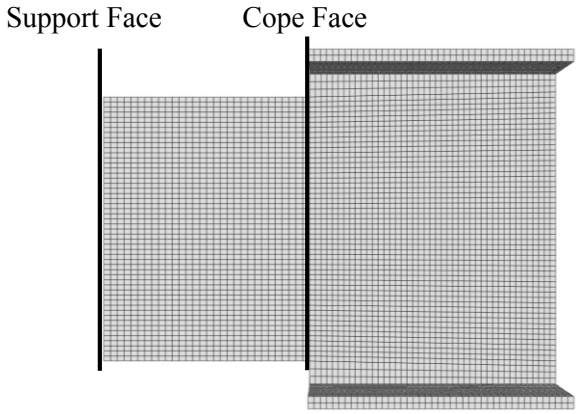

Figure 5-15: Locations of section cuts at support face and at cope face

To get a better understanding of the magnitude of the moments developed at the specified locations, the actual values were divided by the nominal plastic moment capacity of the section, M_p, calculated using the material and geometric properties selected for the parametric study. The variations of the ratios of moment developed at the support face and the cope face to the section nominal plastic moment capacity for model h2-c2-t1-S are presented in Figure 5-16. These ratios are presented for all specimens in Table 4-6 and Table 5-3. Since the moment ratios are extremely variable

during the analysis, only the ratios at the cope face plasticity and support face plasticity limit states are reported.

Shear load, which can be approximated as the vertical load at each loading step, was also derived and divided by the plastic shear capacity of the section, V_p. The variation of this ratio is shown for model h2-c2-t1-S in Figure 5-17. These ratios are presented for all specimens in Table 5-2 and Table 5-3 at the cope and support face limit states, respectively.

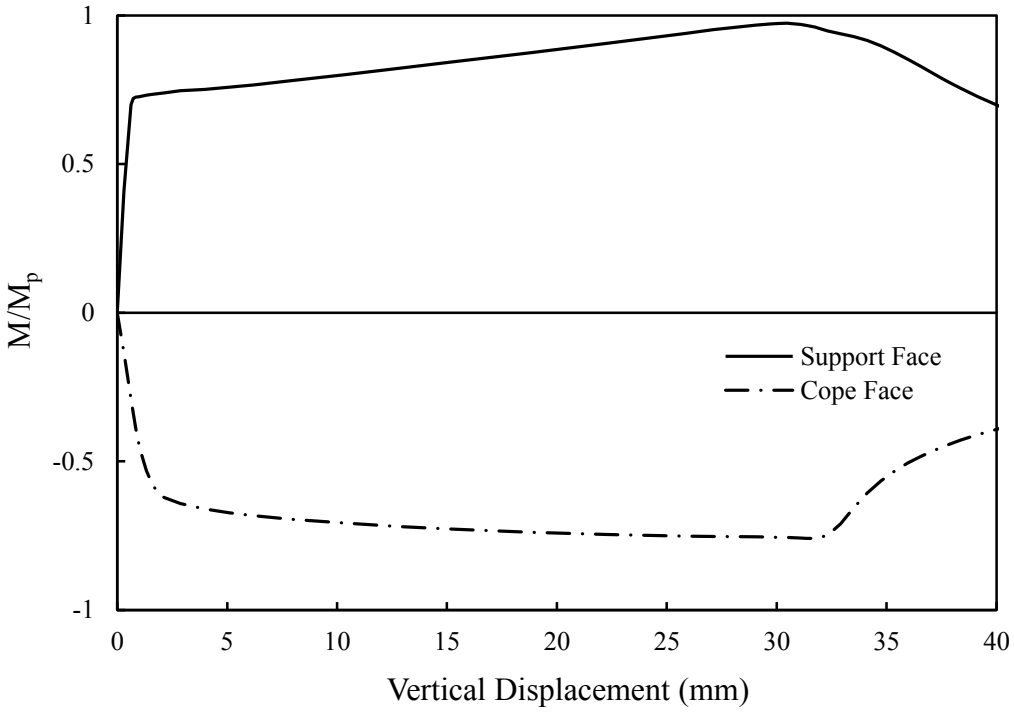

Figure 5-16: Bending moment ratio variation for model h2-c2-t1-S

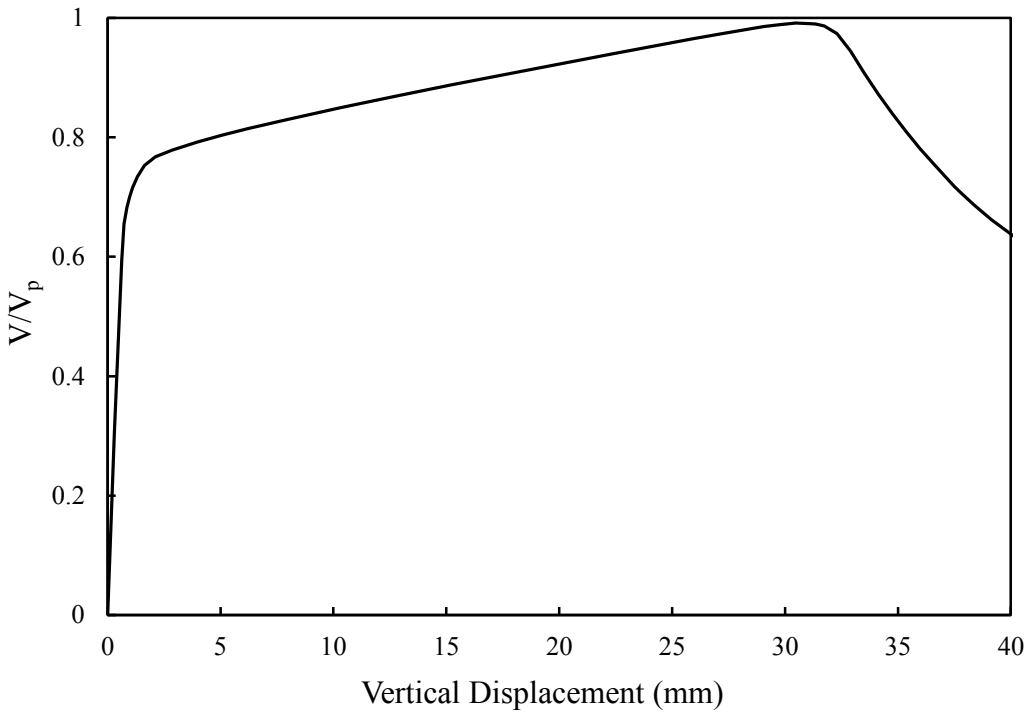

Figure 5-17: Shear load ratio variation for model h2-c2-t1-S

Plasticity in the connection is developed under the combined effect of bending moment and shear. Therefore, both effects need to be considered when section plasticity is evaluated. Plasticity was evaluated at both the support face and the cope face by monitoring the vertical load–vertical displacement curve and plastic strain contour over the reduced beam depth. Neal's (1961) interaction equation (Equation 2-9) was then evaluated for comparison at the loading step when section plasticity became complete at that section. The ratio of bending moment to the section plastic moment and the ratio of shear load to the section plastic shear for all models are presented in Table 5-2 and Table 5-3 for the cope and support face plasticity limit states, respectively. The result from Neal's interaction equation is also given, where a value of 1.0 would indicate a fully plastic cross-section.

Table 5-2: Neal interaction equation values at CFP

Model ID	V/V_p	M/M_p	Neal	Model ID	V/V_p	M/M_p	Neal
h1-c1-t1-F	0.67	0.85	1.05	h1-c1-t1-S	0.86	0.45	1.00
h1-c1-t2-F	0.66	0.85	1.04	h1-c1-t2-S	0.84	0.41	0.92
h1-c1-t3-F	0.68	0.88	1.09	h1-c1-t3-S	0.84	0.40	0.91
h1-c2-t1-F	0.35	1.02	1.04	h1-c2-t1-S	0.63	0.83	0.98
h1-c2-t2-F	0.36	1.05	1.07	h1-c2-t2-S	0.62	0.82	0.97
h1-c2-t3-F	0.33	0.97	0.98	h1-c2-t3-S	0.63	0.84	1.00
h1-c3-t1-F	0.28	1.05	1.05	h1-c3-t1-S	0.53	0.93	1.01
h1-c3-t2-F	0.29	1.08	1.09	h1-c3-t2-S	0.54	0.95	1.04
h1-c3-t3-F	0.26	1.00	1.01	h1-c3-t3-S	0.51	0.92	0.99
h2-c1-t1-F	0.76	0.64	0.98	h2-c1-t1-S	0.91	0.29	0.98
h2-c1-t2-F	0.77	0.66	1.01	h2-c1-t2-S	0.92	0.29	1.01
h2-c1-t3-F	0.77	0.66	1.01	h2-c1-t3-S	0.91	0.27	0.97
h2-c2-t1-F	0.49	0.92	0.97	h2-c2-t1-S	0.75	0.62	0.94
h2-c2-t2-F	0.52	0.99	1.06	h2-c2-t2-S	0.76	0.62	0.95
h2-c2-t3-F	0.52	0.99	1.06	h2-c2-t3-S	0.75	0.61	0.93
h2-c3-t1-F	0.40	0.97	1.00	h2-c3-t1-S	0.69	0.76	0.98
h2-c3-t2-F	0.43	1.05	1.09	h2-c3-t2-S	0.69	0.75	0.97
h2-c3-t3-F	0.41	1.00	1.03	h2-c3-t3-S	0.70	0.77	1.01
h3-c1-t1-F	0.82	0.52	0.98	h3-c1-t1-S	0.94	0.22	1.00
h3-c1-t2-F	0.83	0.54	1.00	h3-c1-t2-S	0.94	0.22	1.00
h3-c1-t3-F	0.82	0.53	0.98	h3-c1-t3-S	0.94	0.20	0.98
h3-c2-t1-F	0.63	0.88	1.04	h3-c2-t1-S	0.82	0.49	0.95
h3-c2-t2-F	0.60	0.86	0.99	h3-c2-t2-S	0.83	0.50	0.96
h3-c2-t3-F	0.61	0.83	0.97	h3-c2-t3-S	0.81	0.47	0.91
h3-c3-t1-F	0.53	0.95	1.03	h3-c3-t1-S	0.77	0.61	0.96
h3-c3-t2-F	0.54	0.98	1.07	h3-c3-t2-S	0.77	0.60	0.95
h3-c3-t3-F	0.52	0.96	1.03	h3-c3-t3-S	0.77	0.60	0.95
Mean			**1.03**	**Mean**			**0.97**
Std. Dev.			**0.04**	**Std. Dev.**			**0.03**

Table 5-3: Neal interaction equation values at SFP

Model ID	V/V_p	M/M_p	Neal
h1-c1-t1-S	0.78	0.71	1.08
h1-c1-t2-S	0.69	0.83	1.05
h1-c1-t3-S	0.64	0.88	1.05
h1-c2-t1-S	0.55	0.96	1.05
h1-c2-t2-S	0.54	0.97	1.05
h1-c2-t3-S	0.51	0.95	1.02
h1-c3-t1-S	0.47	1.00	1.05
h1-c3-t2-S	0.49	1.02	1.08
h1-c3-t3-S	0.48	1.01	1.06
h2-c1-t1-S	0.76	0.70	1.03
h2-c1-t2-S	0.72	0.75	1.02
h2-c1-t3-S	0.76	0.73	1.07
h2-c2-t1-S	0.68	0.83	1.04
h2-c2-t2-S	0.67	0.85	1.05
h2-c2-t3-S	0.69	0.84	1.06
h2-c3-t1-S	0.61	0.90	1.03
h2-c3-t2-S	0.59	0.90	1.02
h2-c3-t3-S	0.62	0.92	1.06
h3-c1-t1-S	0.80	0.61	1.02
h3-c1-t2-S	0.77	0.66	1.02
h3-c1-t3-S	0.75	0.69	1.00
h3-c2-t1-S	0.76	0.70	1.04
h3-c2-t2-S	0.72	0.75	1.02
h3-c2-t3-S	0.71	0.76	1.01
h3-c3-t1-S	0.70	0.79	1.03
h3-c3-t2-S	0.69	0.80	1.03
h3-c3-t3-S	0.68	0.81	1.03
Mean			**1.04**
Std. Dev.			**0.02**

As can be deduced from Tables 5-2 and 5-3, Neal's interaction equation predicts the development of section plasticity quite accurately, even though the contribution of shear load and bending moment in the formation of plasticity is quite variable for different models. In each case, the mean ratio is close to 1.0 and the standard deviation is small.

Some general trends are observed from the results. As the depth of the coped region increased, the contribution of shear load in developing section plasticity was amplified. In other words, the plasticity was dominated by shear in the beams that had a lower length-to-depth ratio of the coped region. Conversely, with an increase in cope length, the contribution of shear load decreased, while the bending moment contribution increased. Beams with higher length-to-depth ratios of the coped region were dominated by bending moment rather than shear load. When the reduced beam depth and length are held constant, the relative contributions of shear load and bending moment in plasticity development were not altered appreciably with thickness variation. When models with the same dimensions but different boundary conditions are compared, it is concluded that in models with the stiff support the role of shear load in developing section plasticity is higher than in the models with the flexible support.

5.5.4 Shear Load Eccentricity

The shear load eccentricities applied to the support face and cope face are crucial parameters in defining the development of plasticity at the extreme points of the coped region. In this study, the shear load eccentricity applied to the cope face was calculated and recorded during the application of vertical load to the models. The eccentricity ratios for the cope face are defined as the ratio of cope face shear load eccentricity to the cope length (e/c). The shear load eccentricity at the cope face was calculated by dividing the bending moment at the cope face by the vertical load at each loading step.

The eccentricity ratios were quite variable during loading of the models. The variation of the eccentricity ratios for models h2-c2-t1-S and h2-c2-t1-F are depicted

in Figure 5-18. In the model with the stiff support, the eccentricity ratio showed a very low value during the initial phases of loading, implying that the inflection point was located close to the cope face. However, the inflection point tended to move rapidly towards the support, reaching a stable value near the mid-point of the coped region and remaining almost constant up to the connection failure at around 33 mm of vertical displacement. In the model with the flexible support, the eccentricity ratio showed an almost constant value throughout the loading. The eccentricity ratio value was close to 1.0, implying that the inflection point was located close to the support face.

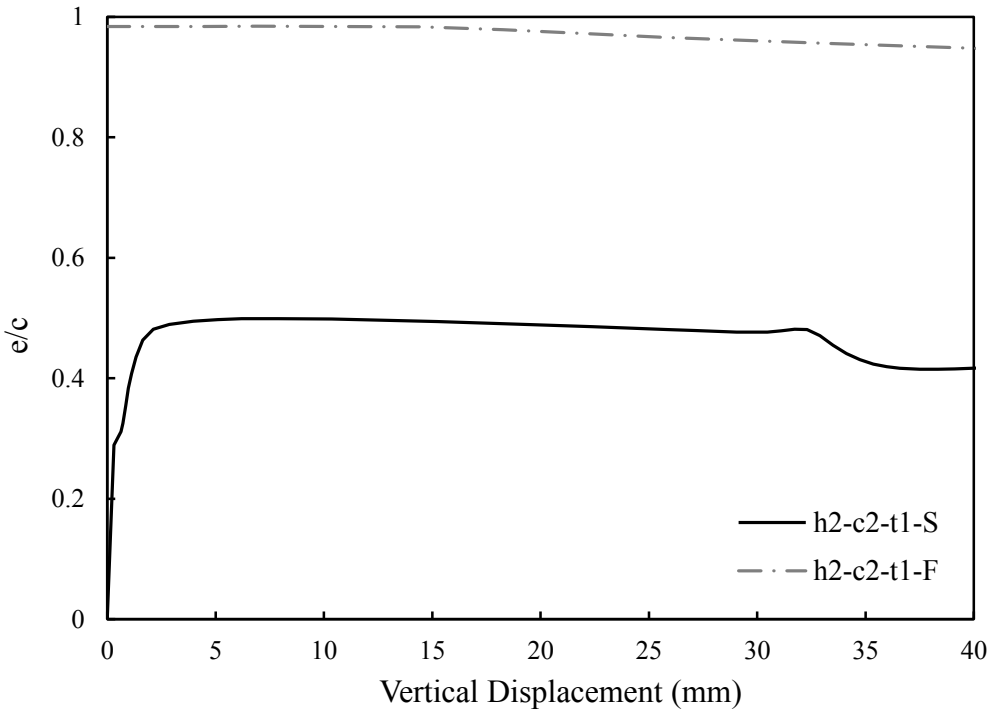

Figure 5-18: Eccentricity ratio variation for sample models with different boundary conditions

The cope face eccentricity ratios were derived at instances when a significant phenomenon occurred in the connection. The two major points of interest are CFP and SFP. The values are presented for applicable models in Table 5-4.

Table 5-4: Cope face eccentricity ratio, e/c

At CFP				At SFP	
Model ID	e/c	Model ID	e/c	Model ID	e/c
h1-c1-t1-F	1.00	h1-c1-t1-S	0.49	h1-c1-t1-S	0.29
h1-c1-t2-F	1.00	h1-c1-t2-S	0.47	h1-c1-t2-S	0.20
h1-c1-t3-F	1.00	h1-c1-t3-S	0.45	h1-c1-t3-S	0.16
h1-c2-t1-F	0.96	h1-c2-t1-S	0.50	h1-c2-t1-S	0.40
h1-c2-t2-F	0.97	h1-c2-t2-S	0.49	h1-c2-t2-S	0.37
h1-c2-t3-F	0.98	h1-c2-t3-S	0.50	h1-c2-t3-S	0.36
h1-c3-t1-F	0.95	h1-c3-t1-S	0.50	h1-c3-t1-S	0.43
h1-c3-t2-F	0.95	h1-c3-t2-S	0.50	h1-c3-t2-S	0.43
h1-c3-t3-F	0.97	h1-c3-t3-S	0.49	h1-c3-t3-S	0.42
h2-c1-t1-F	1.00	h2-c1-t1-S	0.46	h2-c1-t1-S	0.15
h2-c1-t2-F	1.00	h2-c1-t2-S	0.47	h2-c1-t2-S	0.15
h2-c1-t3-F	1.00	h2-c1-t3-S	0.45	h2-c1-t3-S	0.18
h2-c2-t1-F	0.98	h2-c2-t1-S	0.48	h2-c2-t1-S	0.36
h2-c2-t2-F	0.98	h2-c2-t2-S	0.47	h2-c2-t2-S	0.32
h2-c2-t3-F	0.99	h2-c2-t3-S	0.47	h2-c2-t3-S	0.35
h2-c3-t1-F	0.97	h2-c3-t1-S	0.48	h2-c3-t1-S	0.38
h2-c3-t2-F	0.97	h2-c3-t2-S	0.48	h2-c3-t2-S	0.37
h2-c3-t3-F	0.98	h2-c3-t3-S	0.49	h2-c3-t3-S	0.38
h3-c1-t1-F	1.00	h3-c1-t1-S	0.45	h3-c1-t1-S	0.17
h3-c1-t2-F	1.00	h3-c1-t2-S	0.45	h3-c1-t2-S	0.15
h3-c1-t3-F	1.00	h3-c1-t3-S	0.43	h3-c1-t3-S	0.13
h3-c2-t1-F	0.98	h3-c2-t1-S	0.47	h3-c2-t1-S	0.34
h3-c2-t2-F	0.99	h3-c2-t2-S	0.47	h3-c2-t2-S	0.25
h3-c2-t3-F	1.00	h3-c2-t3-S	0.45	h3-c2-t3-S	0.23
h3-c3-t1-F	0.98	h3-c3-t1-S	0.47	h3-c3-t1-S	0.36
h3-c3-t2-F	0.98	h3-c3-t2-S	0.47	h3-c3-t2-S	0.35
h3-c3-t3-F	0.99	h3-c3-t3-S	0.47	h3-c3-t3-S	0.33

Eccentricity ratios are categorized into groups in Table 5-5 based on the limit state and the support condition. Since the support face plasticity limit state was only

observed for models with the stiff support, this is the only support condition category for support face plasticity.

Table 5-5: Mean cope face eccentricity ratio for different model groups at different limit states

Limit State	Support Condition	Mean e/c	Std. Dev.
SFP	S	0.30	0.10
CFP	F	0.98	0.02
	S	0.47	0.02
	All	0.73	0.26

Although the cope face plasticity limit state was observed in all models with both flexible and stiff supports, the eccentricity ratios were considerably lower for the models with the stiff support. The reason behind this is evident by considering the effect of support stiffness on the moment distribution along the cope length. Qualitatively, increasing the support rotational stiffness tends to increase the bending moment carried by the support and therefore pushes the inflection point farther from the support face, resulting in a reduced shear load eccentricity applied to the cope face. Besides treating models with different support conditions separately, the average eccentricity ratio was also calculated considering all models reaching the cope face plasticity limit state, regardless of their support condition.

Based on the information summarized in Table 5-5, the following conclusions are made:

- At the support face plasticity limit state, the average cope face shear load eccentricity ratio was 0.30. This value indicates that the point of inflection was located closer to the cope face when the support face experienced plasticity through the full plate depth, as would be expected due to the beam rotation. The variability of this ratio was somewhat higher for this limit state than for the cope face plasticity limit state when the two support conditions are treated separately.

- If only the models with the flexible support are considered, cope face plasticity occurred when the eccentricity ratio was close to 1.0. This implies that the inflection point was located very close to the support face.
- If only the models with the stiff support are considered, cope face plasticity occurred when the eccentricity ratio was close to 0.5. This implies that the inflection point was located very close to the mid-length of coped region. This category showed the least variability of all those considered.

As described in Chapter 2, Neal's interaction equation (Equation 2-9) proposes a relationship between bending moment and shear load to predict section plasticity. The correlation between bending moment and shear load is defined by the shear load eccentricity. If the bending moment in the equation is substituted by the product of shear load and the appropriate shear eccentricity, Neal's interaction equation can be rewritten as Equation 4-1. Accordingly, the shear loads causing the support face and cope face plasticity limit states can be predicted.

As presented in Table 5-5, support face plasticity occurred in connections with the stiff support when the inflection point was located closer to cope face. Therefore, using 0.7 times the geometric eccentricity (cope length) as the eccentricity value in Equation 4-1 is appropriate to predict the shear load associated with the support face plasticity limit state. To evaluate cope face plasticity, the shear load eccentricity applied to the cope face at that limit state should be considered. As presented in Table 5-5, the values were quite different for the two support conditions and therefore the eccentricity for the two support conditions need to be different to achieve accurate results.

Based on the aforementioned discussion, Equation 4-1 can be used to evaluate section plasticity at the support face and the cope face using the following eccentricities:

For support face plasticity:

5-2 $$e = 0.7\,c$$

For cope face plasticity with flexible support:

5-3 $$e = c$$

For cope face plasticity with stiff support:

5-4 $$e = 0.5\,c$$

It should be noted that the eccentricity value for cope face plasticity evaluation of double-coped beams with flexible support is specifically based on the flexibility of the supports considered in this study and may not be valid for other flexible supports with different flexibilities. As an example, if the support is less flexible (e.g., a short or torsionally braced girder) the eccentricity applied to the net section could be any fraction of the cope length between the two values recommended by Equation 5-3 and Equation 5-4. It must also be observed that in no case considered in the parametric study did reaching the full plasticity of the net section in the coped region constitute "failure" of the connection. That is, there was always some margin of capacity beyond this limit state being reached.

5.5.5 Effects of Key Variables

The 54 models can be categorized into two main groups: 27 models with stiff support and 27 models with flexible support. In each category, nine models included each of a 150 mm deep, 230 mm deep, and 310 mm deep net section in the coped region. Within each group of nine models, cope lengths of 80, 180 and 230 mm were combined with web thicknesses of 6, 8 and 10 mm.

Several observations are made on the effects of the variables on the behaviour of the double-coped beam connection. For this purpose, Table 5-1 was considered together with the vertical load–vertical displacement curves derived from the analysis.

5.5.5.1 Cope Length

Three cope lengths were modelled: 80 mm, 180 mm, and 230 mm. The cope length defines the distance between the support face and cope face. Longer copes tend to apply higher moment to the cope face and therefore decrease the vertical load causing plasticity to develop at the cope face or causing the coped region to fail due to out-of-plane deformation.

The vertical load–vertical displacement curves for sample models having the flexible support with various cope lengths are presented in Figure 5-19 and the curves for sample models having the rigid support with various cope lengths are presented in Figure 5-20.

It is noted from Figure 5-19 and Figure 5-20 that by decreasing the cope length, the connection capacity was significantly increased, as expected, particularly for the cases with the flexible support. This is a consequence of both the increased resistance to out-of-plane deformation due to the reduced unrestrained length and the fact that the load eccentricities for the cope and support faces are shorter, resulting in increased vertical load required to cause the cope face plasticity. For both support conditions, the strength of the shortest coped region was limited by the shear capacity of the cross-section.

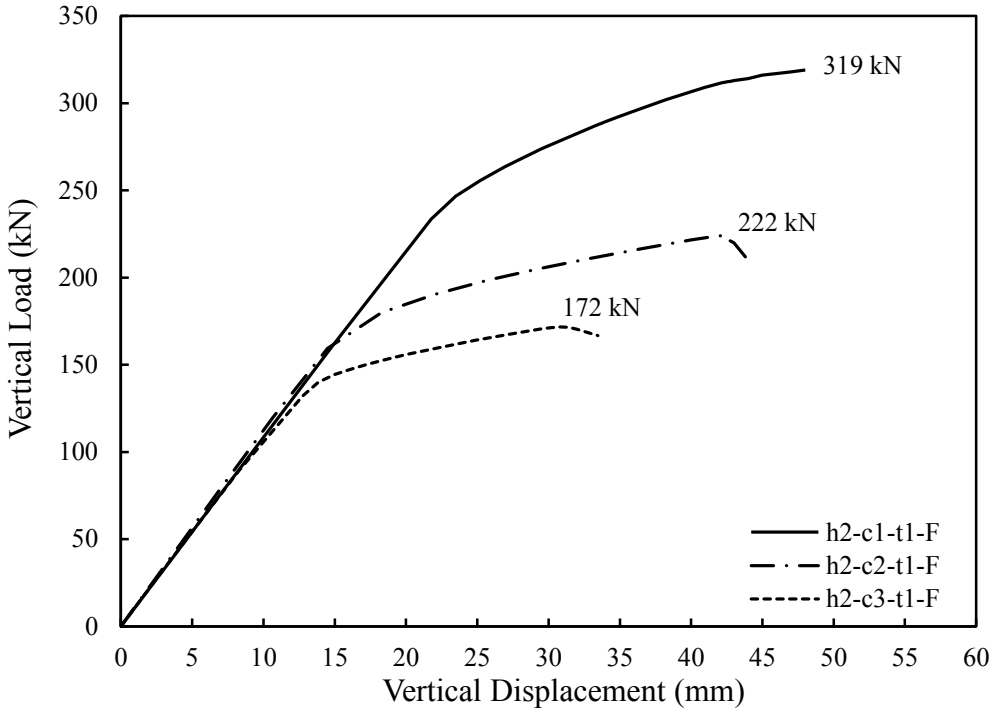

Figure 5-19: Effect of cope length on the response of models with flexible support

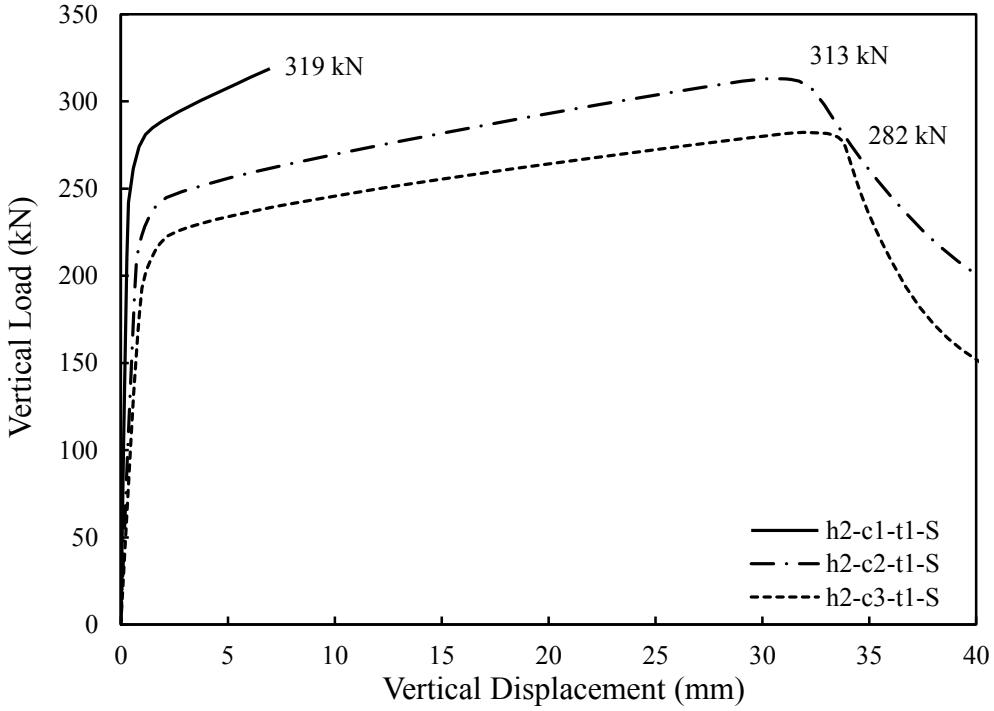

Figure 5-20: Effect of cope length on the response of models with stiff support

5.5.5.2 Beam Web Thickness

Using the test matrix, a direct comparison can be made among the 6 mm thick, 8 mm thick and 10 mm thick double-coped beam webs. Increasing the beam web thickness always resulted in an increase in the peak vertical load, as expected, since it resulted in an increased plastic section capacity as well as increased resistance to out-of-plane deformation. The vertical load–vertical displacement curves for models having the flexible support with various thicknesses are presented in Figure 5-21 and the curves for models having the rigid support with various thicknesses are presented in Figure 5-22.

5.5.5.3 Reduced Beam Depth

Using the test matrix, a direct comparison can be made among the double-coped beams with reduced beam depths of 150 mm, 230 mm and 310 mm. Increasing the section depth always resulted in an increase in the peak vertical load, as expected, since it increased the plastic section capacity. In general, the connection displacement ductilities were higher for the shallower sections. The vertical load–vertical displacement curves for models having the flexible support with various depths are presented in Figure 5-23 and the curves for models having the stiff support with various depths are presented in Figure 5-24.

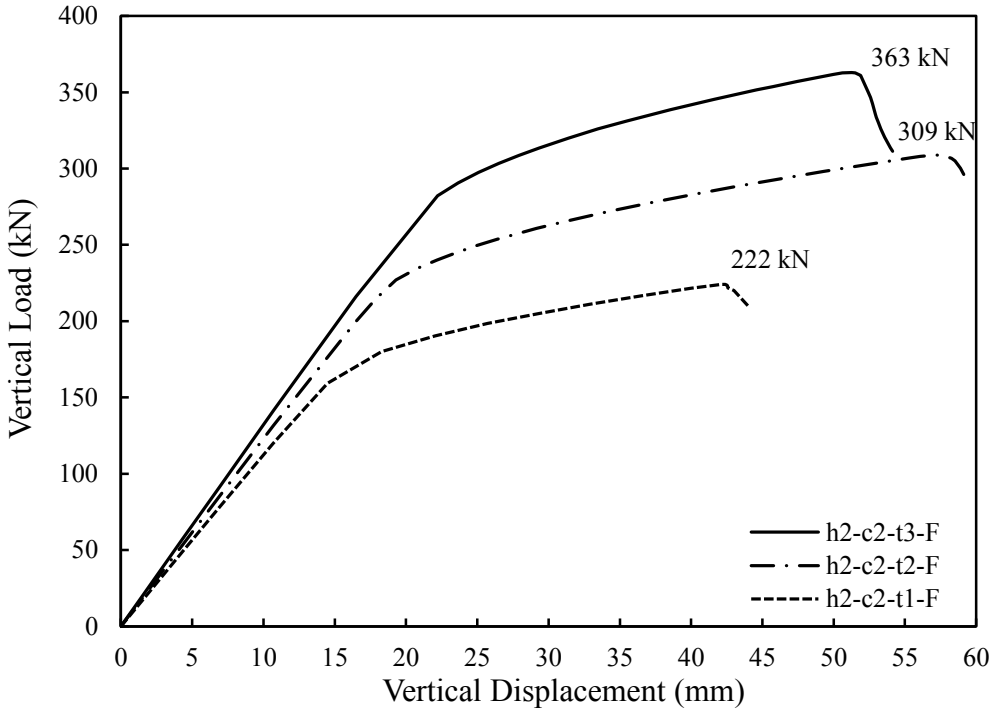

Figure 5-21: Effect of web thickness on the response of models with flexible support

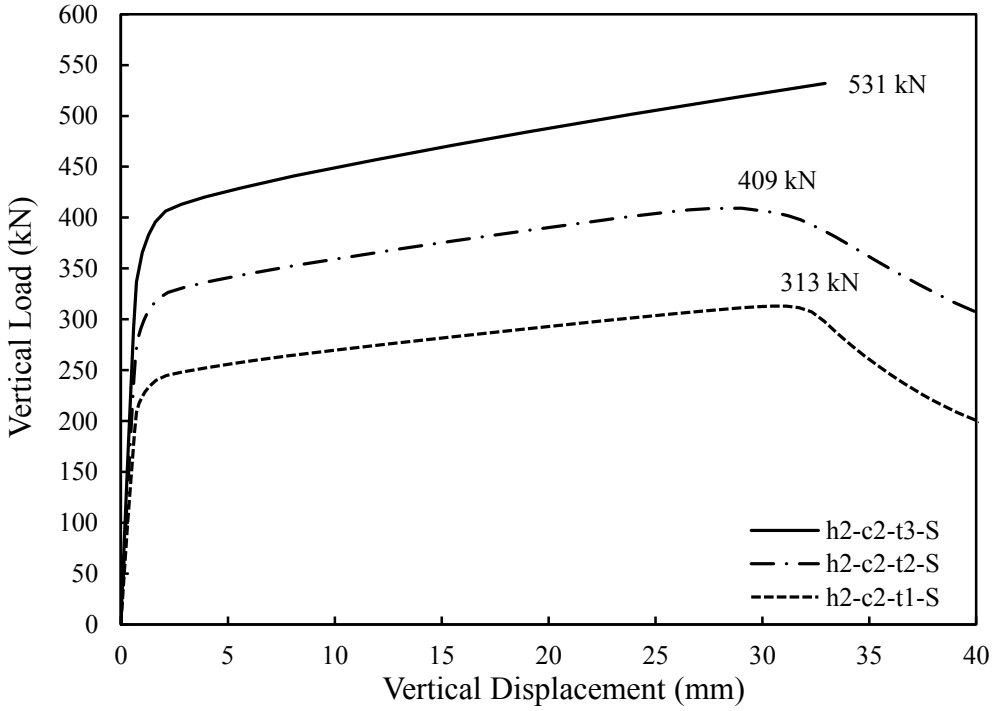

Figure 5-22: Effect of web thickness on the response of models with stiff support

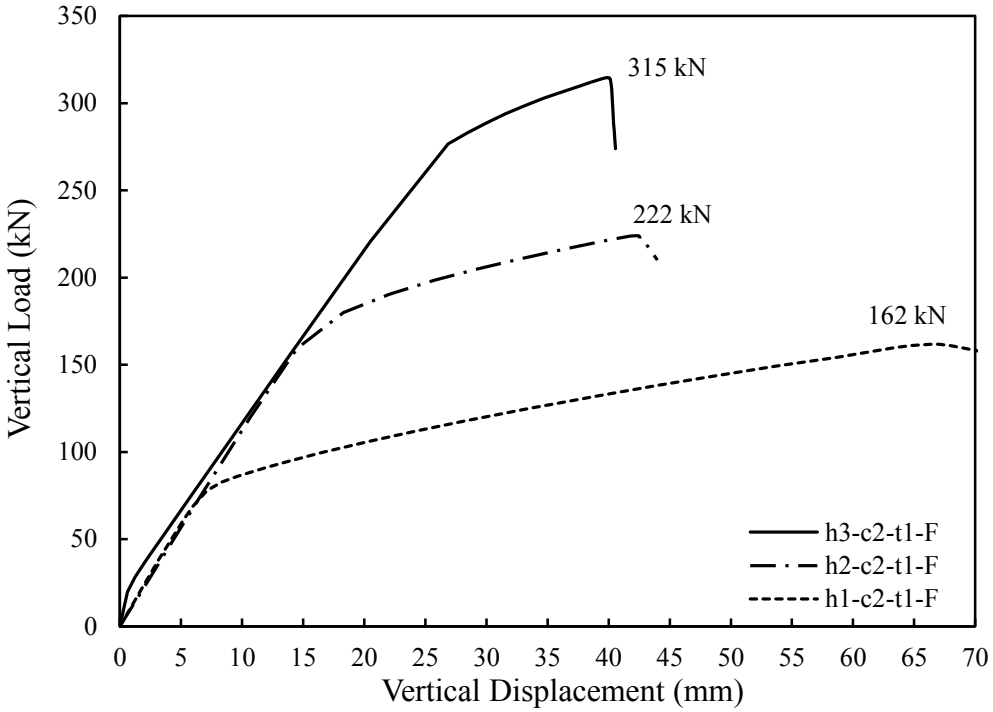

Figure 5-23: Effect of reduced beam depth on the response of models with flexible support

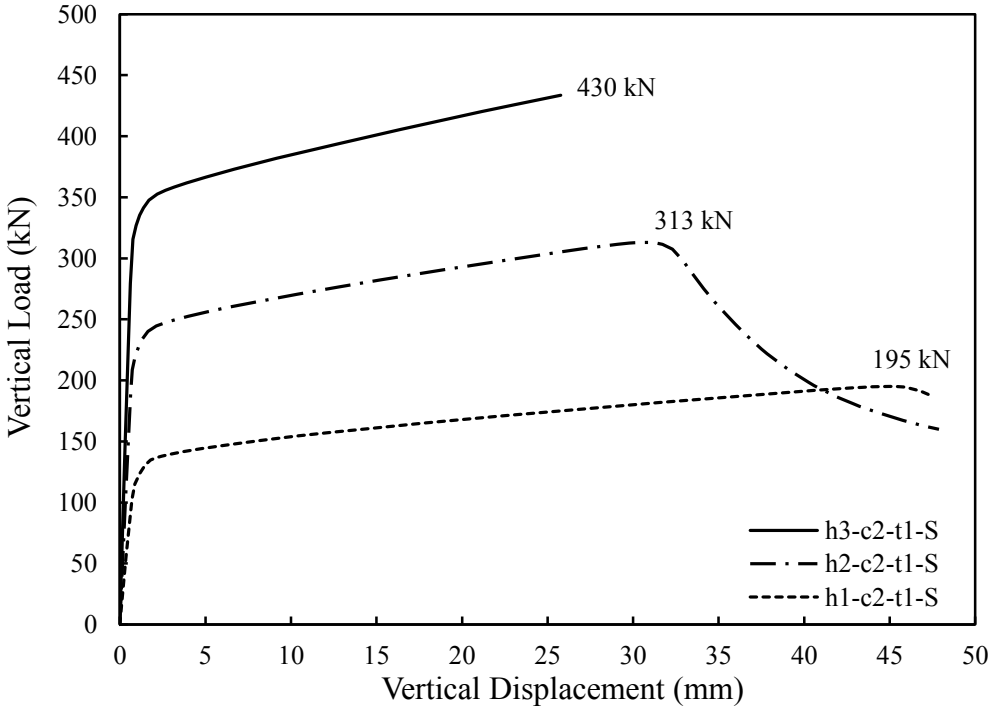

Figure 5-24: Effect of reduced beam depth on the response of models with stiff support

5.5.5.4 Support Condition

As described in Section 5.4, the specimens can be categorized into two main groups based on the support condition: models with stiff support and models with flexible support. Results of this parametric study showed a fundamental difference in the behaviour of double-coped beams due to the rotational flexibility of the support.

In the case of connections with the flexible support, a relatively low bending moment is formed at the support and the inflection point is therefore located closer to the support. In fact, in most models with the flexible support the shear load eccentricity relative to the cope face either was equal to or slightly exceeded the cope length. This created a significant shear load eccentricity on the cope face, which led to cope face plasticity. After the formation of a plastic hinge at the cope face, the connection reached a stability mechanism resulting in a considerable stiffness loss. Eventually, the connection failed due to out-of-plane deformation or reaching the plastic shear capacity of the coped section.

In connections with the stiff support, a considerable bending moment is formed at the support. In this case, the inflection point was pushed back towards the beam span. As the shear load is increased, the bending moment at the support face increased until the coped region at the support face became fully plastic due to the simultaneous effect of shear load and bending moment. At this point, the inflection point was located closer to the cope face. With a further increase in the shear load, the inflection point migrates towards the support face due to the increased bending moment at the cope face. With the increased shear load eccentricity applied to the cope face, the cope face eventually plasticized under the simultaneous effects of shear load and bending moment. After the formation of the second plastic hinge at the cope face, the connection reached a stability mechanism resulting in a considerable stiffness loss. Eventually, the connection failed due to out-of-plane deformation or reaching the plastic shear capacity of the coped section.

A comparison between the vertical load–vertical displacement curves of models h2-c2-t1-S and h2-c2-t1-F (h2 models) is presented in Figure 5-25. The comparison for models h3-c2-t1-S and h3-c2-t1-F (h3 models) is presented in Figure 5-26.

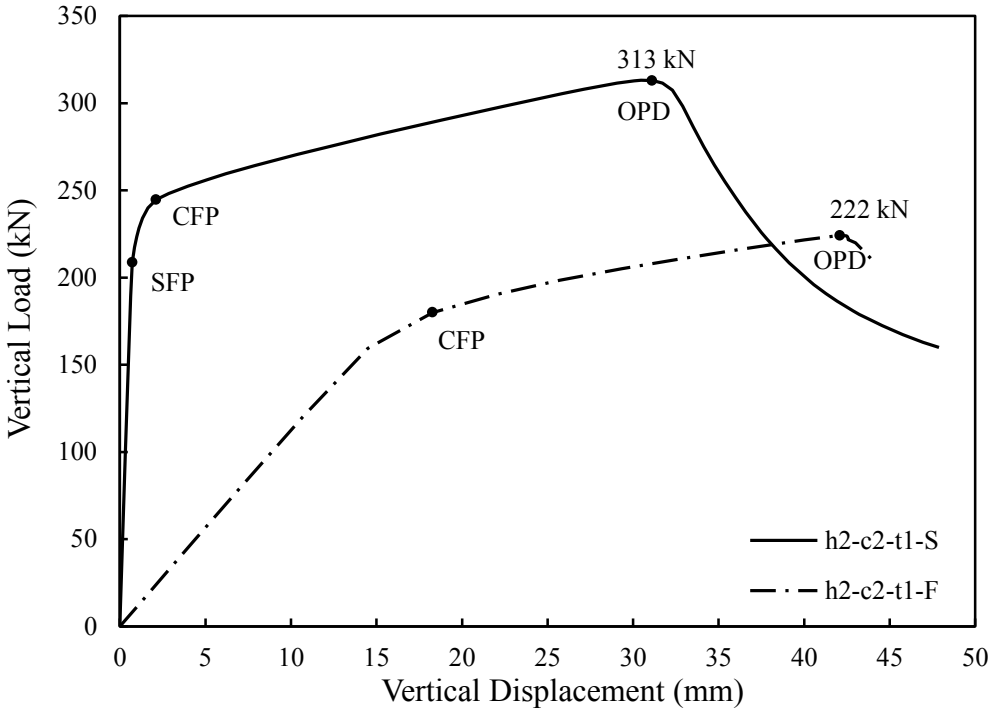

Figure 5-25: Effect of support condition on the response of h2 models

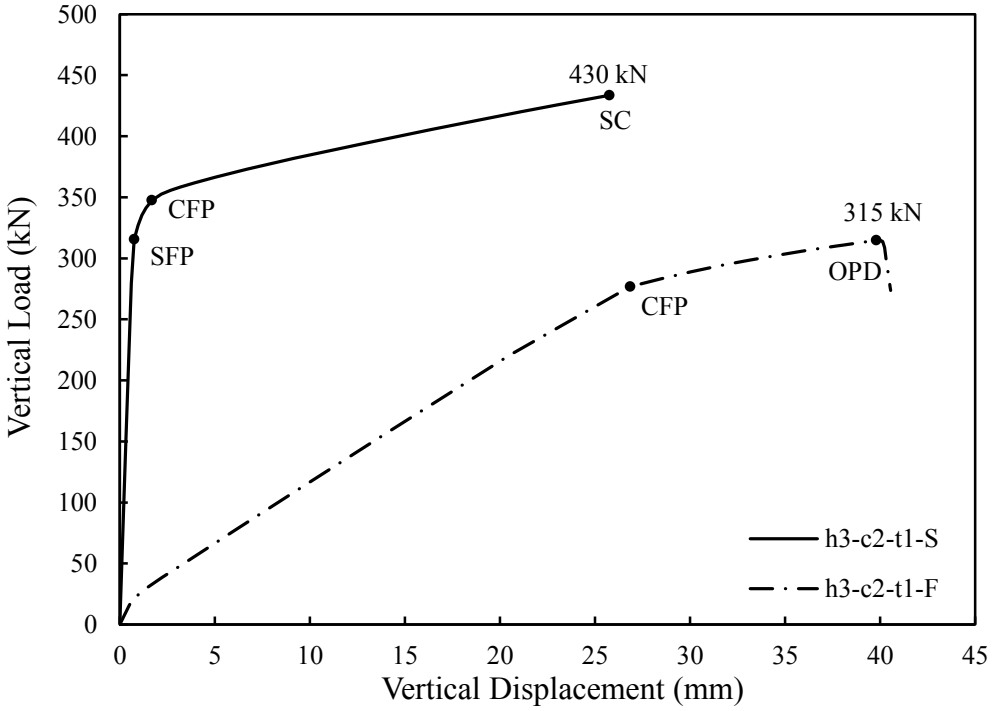

Figure 5-26: Effect of support condition on the response of h3 models

5.6 Summary and Conclusion

A high-fidelity finite element model was developed that is capable of accurately predicting the local behaviour of double-coped beams. The model was verified and validated using the available test data. It was then used to conduct a comprehensive parametric study on double-coped beams having a variety of geometries and boundary conditions. The geometric parameters varied in the study included double-coped beam web thickness, reduced section depth in the coped region, and cope length. Two boundary conditions were considered: rotationally flexible and fixed.

Several limit states were observed in this study. In-plane bending moment was evaluated at the double-coped beam section at the support and cope faces. The bending moment and shear load were used to evaluate plasticity of the double-coped beam at the two locations. Plasticity was also monitored by tracking the equivalent plastic strain contour over the coped region. Variation in shear load eccentricity applied to the cope face was recorded for each model. The effect of key variables on the behaviour and capacity of the connection was investigated.

The following are conclusions drawn from the parametric study:

- Double-coped beams can experience several limit states, including: cope face plasticity, support face plasticity, out-of-plane deformation, and section plastic shear capacity.
- Significant out-of-plane deformation occurs after significant yielding has happened in the coped region. In most cases, double-coped beams reach the fully plastic state either at one or two locations along the cope length. Therefore, stability is not an issue limiting the capacity of double-coped beams within the considered dimensions in this study.
- The capacity of double-coped beams is higher for deeper and thicker net sections due to the increased cross-sectional area.
- Increasing the length of the copes results in connection capacity reduction. The shear load eccentricity imposed on the cope face is higher for longer plates, resulting in decreased vertical load causing the cope face plasticity.

- Plasticity is developed in double-coped beams due to the combined effect of shear load and bending moment. Therefore, both effects need to be considered in plasticity evaluation in the web.
- Plasticity development in double-coped beams having higher depth-to-length ratios in the coped region is dominated by the effect of shear load, whereas with lower depth-to-length ratios it is dominated by bending moment.
- The equation proposed by Neal (1961) provides an accurate evaluation of the loads that cause section plasticity.
- When Neal's interaction equation is used to evaluate plasticity development in double-coped beams, the correlation between bending moment and shear load is defined using the shear load eccentricity. If the bending moment in the equation is substituted by the product of shear load and a proper value for eccentricity, the shear load causing the plasticity of each section can be predicted by solving the equation for shear load.
- The support condition has a significant effect on connection behaviour and capacity. In general, increasing the support rotational stiffness results in higher connection capacity.
- The shear load eccentricity varies quite considerably during the application of shear load. The point of inflection is located closer to the cope face than the support during the early stages of loading. However, with the increase in shear load, the point of inflection moves towards the support face. The coped region was in double curvature when the capacity was reached.
- The eccentricity ratio was defined as the ratio of the shear load eccentricity with respect to the cope face to the geometric eccentricity. This ratio is a crucial parameter for determining when significant phenomena occur in the connection during loading.
- In connections with a flexible support, the cope face is prone to a high shear load eccentricity, resulting in a high bending moment demand applied to the section. The simultaneous effect of vertical load and bending moment results in the development of plasticity at the cope face at lower vertical load values compared to the models with the stiff support.

- In the case of connections with a stiff support, a considerable bending moment is developed at the support face and the inflection point is pushed back towards the beam span, as compared to the flexible-support case. As the shear load is increased, plasticity is developed at the support face and the inflection point is located closer to the cope face than the support. With a further increase in the shear load, the inflection point migrates towards the support face due to the increased bending moment at the cope face. The simultaneous effect of vertical load and bending moment at the cope face results in the development of plasticity at this location, followed by a considerable loss of connection stiffness.

CHAPTER 6: UNIFIED DESIGN RECOMMENDATIONS FOR CANTILEVER PLATE CONNECTION ELEMENTS

6.1 Overview

In Chapters 4 and 5, comprehensive finite element studies were described on extended shear tabs and double-coped beams. The connections varied in geometry and boundary conditions. Connection behaviour was investigated in terms of connection capacity, limit states, plasticity development, and shear load eccentricity. The effects of key variables on the connection response were also studied. In this chapter, the similarities of the behaviours of the two connection configurations are identified and unified recommendations are proposed for the design of the connections. The capacities of the tested extended shear tabs and double-coped beams are then evaluated based on the proposed recommendations.

6.2 Discussion on Common Behaviour of Cantilever Plate Connection Elements

The extended shear tab and double-coped beam connections can be simplified into a representative beam, as shown in Figure 6-1(a). In this chapter, the left support of the beam is defined as the support located at the actual connection support and the right support of the beam is defined as the section of the extended shear tab at the first vertical bolt line of the bolt group or at the cope face of the double-coped beam. The beam span can therefore be regarded as the distance between the support and the first vertical bolt line or the cope length, for extended shear tabs and double-coped beams, respectively.

The right-side support of the beam can be considered a rotationally fixed roller support through which the loading is applied to the connection. That is, the support can move vertically as load is applied, but rotation is prevented. The left side support of the beam can be fixed, partially fixed, or pin-supported, depending on the rotational stiffness of the support condition, and in this section the two extreme cases

of fixed and pinned are discussed. Connections having partially fixed support are bounded by the fully fixed and pinned conditions.

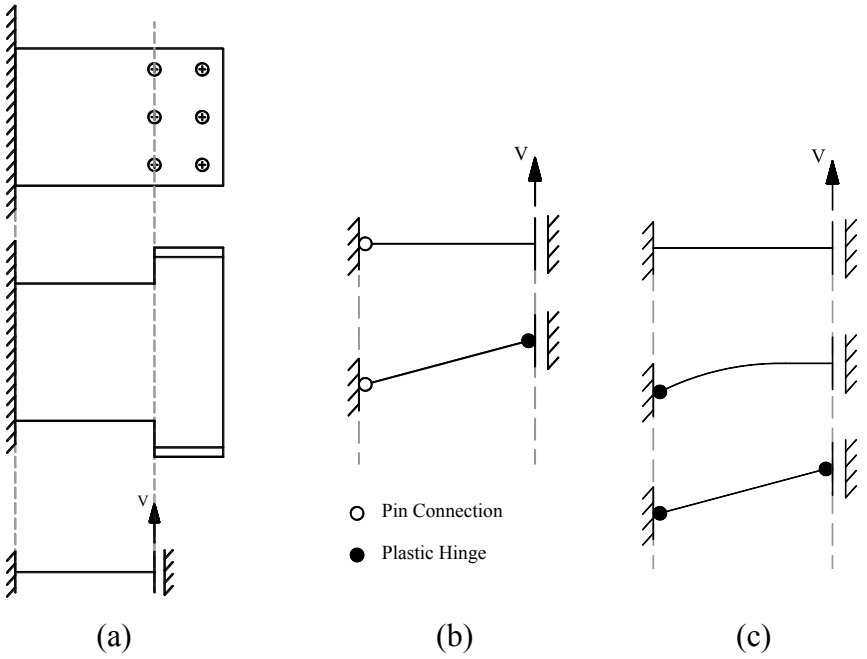

Figure 6-1: (a) Beam analogy for extended shear tabs and double-coped beams, (b) Plasticity sequence for connection with flexible support, and (c) Plasticity sequence for connection with fixed support

In the case of a connection having a support with relatively low rotational stiffness, such as a connection to a long rotationally-unbraced girder, the support can be approximated as a pin, as shown in Figure 6-1(b). A schematic response curve for this case is depicted in Figure 6-2. As the connection is loaded in shear, due to the low rotational stiffness of the left support, the inflection point tends to move towards the left support, resulting in an increased eccentricity applied to the right support. The section located at the right support is gradually yielded under the combined effect of shear force and bending moment. Finally, a plastic hinge is developed at this location, which results in a considerable loss in the connection stiffness (point F1 in Figure 6-2). However, after this phenomenon, the connection can still carry additional load due to material hardening, until it is "physically" failed due to excessive out-of-plane

deformation, bolt fracture or reaching the section plastic shear capacity (point F2 in Figure 6-2).

In the case of a connection having a support with relatively high rotational stiffness, such as a connection to a short stiff girder or when two similar connections exist on the two opposite sides of the support, the support can be approximated as a fixed support, as shown in Figure 6-1(c). A schematic response curve for this case is also depicted in Figure 6-2. As the connection is loaded in shear, due to the high stiffness of the left support, a considerable eccentricity is applied to the left support. The section located at the left support is gradually yielded under the combined effect of shear load and bending moment. Finally, a plastic hinge is developed at this location (point S1 in Figure 6-2), resulting in a slight loss of stiffness. However, the connection can still withstand considerable additional load until it reaches a shear–flexure mechanism. Due to the stiffness loss at the left support, the inflection point tends to move towards the left support, resulting in an increased eccentricity applied to the right support. The section located at the right support is then gradually yielded under the combined effect of shear force and bending moment. Finally, a plastic hinge is developed at this location, which results in a considerable loss in the connection stiffness (point S2 in Figure 6-2). However, after this phenomenon, the connection can still carry additional load due to material hardening, until it is "physically" failed due to out-of-plane deformation, bolt fracture, or reaching the section plastic shear capacity (point S3 in Figure 6-2).

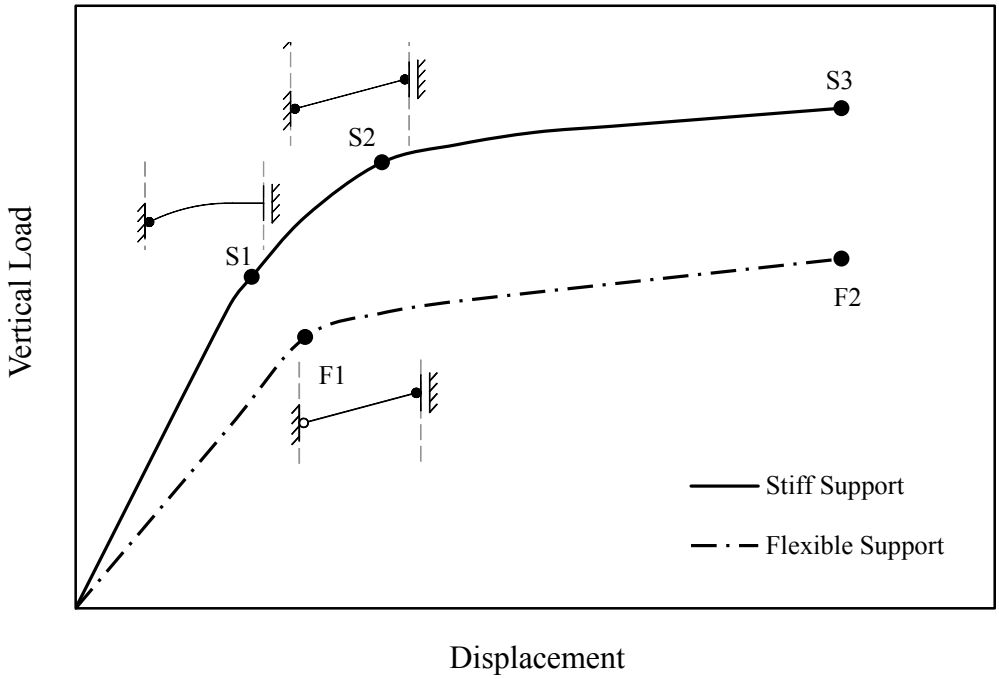

Figure 6-2: Schematic response curves for extended shear tab and double-coped beam with stiff and flexible supports

Based on this discussion, the limit state associated with formation of a plastic hinge at the right support of the beam model, which implies the formation of a complete shear–flexure mechanism in both scenarios, can be considered as a practical design limit state. The design limit state corresponds to net section plasticity for extended shear tabs and cope face plasticity for double-coped beams.

6.3 Design Recommendations

It is recommended that Neal's interaction equation (Equation 4-1) be used to determine the shear load causing net section plasticity at the first line of bolts and gross section plasticity at the cope face for extended shear tabs and double-coped beams, respectively. Based on the discussion in Section 4.5.4, the total shear load causing the net section plasticity can be estimated by multiplying the shear load achieved from Neal's interaction equation by the ratio of the gross section area to the net section area.

For extended shear tabs and double-coped beams with rotationally flexible supports, the eccentricity corresponding to net section/cope face plasticity can be considered as the geometric eccentricity (Refer to Equations 4-5 and 5-3). Similarly, for extended shear tabs and double-coped beams with rotationally stiff supports, the eccentricity corresponding to net section/cope face plasticity can be considered as one-half of the geometric eccentricity (Refer to Equations 4-4 and 5-4). The geometric eccentricity is equal to the distance from the support face to the bolt group centre and the cope length, for extended shear tabs and double-coped beams, respectively. For extended shear tabs with two vertical bolt lines, the effective clear span between the first vertical line of bolts and the support should be considered when using the recommended eccentricities to evaluate net section plasticity; in other words, one-half of the horizontal bolt spacing, 0.5s, is deducted from the recommended values to evaluate net section plasticity in this case.

As indicated in Chapters 3, 4, and 5, the connection support is subjected to bending moment, which must be considered in the design of any components on the support side of the connection. In this regard, it is recommended that the support elements be designed for the shear reaction force applied at an eccentricity of one-half of the geometric eccentricity of the cantilever plate, unless a greater level of rotational flexibility and ductility at the support can be demonstrated to justify a reduced eccentricity.

6.4 Evaluation of Proposed Design Recommendations

The design recommendations are used to evaluate the capacities of the specimens tested by Thomas et al. (2014) and Johnston et al. (2015), as well as those of the current study. Results are shown in Table 6-1and Table 6-2.

For extended shear tabs, the design recommendations represent the consideration of the flexural capacity limit state only, so the recommendations by Thomas et al. (2014) are used for other applicable limit states. The specimens tested by Thomas et al. (2014) are regarded as having flexible supports and the specimens tested in the current study are regarded as having stiff supports. It should be noted that since the

unified eccentricity recommended in Section 6.3 for flexible supports is greater than the eccentricity recommended by Thomas et al. (2014), the results produced by the recommended method are more conservative. In the study conducted by Thomas et al. (2014), the specimens' supports were partially flexible and therefore some bending moment is developed in the extended shear tab close to the support. However, since evaluating the flexibility of the support depends on the properties, details, and boundary conditions of the support and it varies case by case, the partially flexible supports are conservatively regarded as flexible supports. It should also be noted that in addition to the current research recommendations, all other limit states including bolt group capacity, gross shear capacity, and net shear capacity are evaluated and the minimum shear load derived from the limit states evaluation is reported as the design shear load.

Table 6-1: Extended shear tab capacities using design recommendations

Researchers	Specimen ID	Test		Predicted		Test/Predicted Capacity
		Capacity (kN)	Failure Mode	Capacity (kN)	Design Limit State	
Thomas et al. (2014)	2B-10-U-0	188	BF[1]	102	NSP[5]	1.84
	2B-10-U-00	197	BF	101	NSP	1.96
	3B-10-U-0	330	WR[2]	245	NSP	1.35
	5B-10-U-0	762	CWT[3]	634	BF	1.20
Current study	3BR-10-0	430	OPD[4]	434	NSP	0.99
	3BR-13-0	524	BF	473	NSP	1.11
	3BR-10-0-L	467	BF	473	NSP	0.99
	3BR-13-0-L	590	BF	512	NSP	1.15
	3BR-10-0-V1	323	BF	234	BF	1.38
	3BR-13-0-V1	442	BF	234	BF	1.89
					Mean	1.39
					Std. Dev.	0.37

[1]Bolt Fracture, [2]Weld Rupture, [3]Column Web Tearing,
[4]Out-of-plane Deformation, [5]Net Section Plasticity

For double-coped beams, the design limit state recommended in this chapter is evaluated in addition to gross shear capacity of the section. In the specimens tested by Johnston et al. (2015), four end-supports were considered. End-support type A was a one-sided double-coped beam with end plate bolted to a girder. End-support type B represented a double-sided double-coped beam with end plate bolted to a girder. End-support types C and D were similar to types B and A, respectively, except that instead of being bolted to the support, the beams were welded to the support. Based on these configurations, type A and D end-support conditions are regarded as flexible, and type B and C end-support conditions are considered as stiff supports.

Table 6-2: Double-coped beam capacities using design recommendations

Specimen ID	Test		Predicted		Test/Predicted Capacity
	Capacity (kN)	Failure Mode	Capacity (kN)	Design Limit State	
2A-1-0-R	173	OPD[1]	105	CFP[3]	1.65
2A-1-0-NR	149	OPD	107	CFP	1.39
2A-2-0-R	111	OPD	74	CFP	1.50
2A-2-0-NR	110	OPD	75	CFP	1.47
2A-3-0-R	89	OPD	64	CFP	1.39
2A-3-0-NR	99	OPD	67	CFP	1.49
2B-3-0-R	138	OPD	124	CFP	1.11
2D-2-0-NR	105	OPD	77	CFP	1.37
3A-2-0-NR	207	OPD	213	CFP	0.97
3A-3-0-NR	199	OPD	189	CFP	1.05
3D-2-0-NR	235	OPD	225	CFP	1.04
4A-3-0-NR	443	BCK[2]	384	CFP	1.15
				Mean	1.30
				Std. Dev.	0.22

[1]Out-of-plane Deformation, [2]Buckling,
[3]Cope Face Plasticity

The test/predicted ratios in Tables 6-1 and 6-2 indicate that the design procedure overall is quite conservative. However, they don't allow for a direct comparison of the design limit state based on the proposal developed herein and the test results, due to variations in the failure modes observed in the tests. As such, it is beneficial to identify the NSP and CFP limit states in the extended shear tab and double-coped beam tests, respectively, and compare the loads causing these limit states with the associated design predictions. In other words, the accuracy of the predictions is evaluated by comparing them to the loads causing the design limit state in the tests. To identify the load at the design limit state, the vertical load–vertical displacement curves for the test specimens from the studies by Thomas et al. (2014) and Johnston et al. (2015) are considered, and in each case the approximate vertical load at which a significant stiffness loss occurred in the test is identified as the design limit state (i.e., point F1 or S2 in Figure 6-2). To achieve this, a straight line was fit to each of the segments of the vertical load–vertical displacement curve of each specimen before and after stiffness loss, and the vertical load associated with the intersection of the two lines was regarded as the design limit state. It should be noted that to make the comparison, only the test specimens in which NSP/CFP is observed are considered. Results are shown in Table 6-3 and Table 6-4. In both cases, the mean test/predicted ratio is significantly closer to 1.0 and the standard deviation is smaller than those values presented in Tables 6-1 and 6-2.

Table 6-3: Extended shear tab load at NSP

Researchers	Specimen ID	Load at NSP (kN)		Test/Predicted Load
		Test	Predicted	
Thomas et al. (2014)	2B-10-U-0	165	102	1.62
	2B-10-U-00	170	101	1.68
	3B-10-U-0	300	245	1.22
Current study	3BR-10-0	430	434	0.99
	3BR-13-0	480	473	1.01
	3BR-10-0-L	475	473	1.00
	3BR-13-0-L	530	512	1.04
			Mean	1.26
			Std. Dev.	0.30

Table 6-4: Double-coped beam load at CFP

Specimen ID	Load at CFP (kN)		Test/Predicted Load
	Test	Predicted	
2A-1-0-R	135	105	1.29
2A-1-0-NR	95	107	0.89
2A-2-0-R	75	74	1.01
2A-2-0-NR	75	75	1.00
2A-3-0-R	70	64	1.09
2A-3-0-NR	65	67	0.98
2B-3-0-R	130	124	1.05
2D-2-0-NR	90	77	1.17
3A-2-0-NR	207	213	0.97
3A-3-0-NR	195	189	1.03
3D-2-0-NR	230	225	1.02
4A-3-0-NR	425	384	1.11
		Mean	1.05
		Std. Dev.	0.10

6.4.1 Discussion on Extended Shear Tabs

As noticed from Table 6-1, the test-to-predicted ratio is rather high for the specimens tested by Thomas et al. (2014). As discussed before, the reason is the difference between the actual and recommended shear load eccentricities applied to the net section and the bolt group. In these specimens, support conditions were such that the maximum shear load eccentricity applied to the bolt group was about 75% of the geometric eccentricity. However, as long as the flexibility of the support is not evaluated explicitly, it is recommended that the geometric eccentricity be used for design at the NSP limit state (subtracting one-half of the horizontal bold spacing when there are two vertical lines of bolts). The test-to-predicted ratios for the specimens tested in the current research are all close to 1.0. In these specimens, the support conditions were representative of stiff supports and therefore the accuracy of the predictions is higher for these cases. By comparing the results in Tables 6-1 and 6-3, it is concluded that since the development of NSP is considered as the design limit state, the connection is able to carry additional loads due to strain hardening and movement of the inflection point.

Specimens 3BR-10-0-V1 and 3BR-13-0-V1 are the only cases where the failure modes are consistent in Table 6-1; bolt fracture was the test failure mode and the governing design limit state. Bolt group shear load capacity predictions were evaluated using an eccentricity equal to one-half the geometric eccentricity, but the shear load eccentricities applied to the bolt groups, as evaluated from the two tests, were 34% and 22% of the geometric eccentricities, respectively. Since the recommended unified bolt group eccentricity is higher than the two values, the recommendations produce conservative results.

6.4.2 Discussion on Double-coped Beams

As indicated in Table 6-2, the test-to-predicted ratios for almost all specimens are greater than 1.0, implying that the design recommendations provide generally conservative results in predicting the capacity of double-coped beams. Moreover, as was the case for the extended shear tabs tested by Thomas et al. (2014), the specimens tested by Johnston et al. (2015) included partially-restrained supports. Therefore, considering them as having flexible supports, results in conservatism in predicting design capacity. As discussed previously, another source of conservatism is that the development of plasticity at the cope face is considered as the design limit state, whereas in most cases the connection is able to carry additional loads due to strain hardening and movement of the inflection point.

As indicated in Table 6-4, the mean test-to-predicted ratio for the specimens tested by Johnston et al. (2015) is close to 1.0, implying that the design recommendations are accurate in predicting the design limit state in the tests. The higher accuracy of the predictions for the tests by Johnston et al. (2015) compared with the tests by Thomas et al. (2014) occurs because the flexible support conditions of the former (long girder or flexible end-plate) were closer than those of the latter (stub column web) to the fully flexible support considered in the recommendations.

CHAPTER 7: CONCLUSIONS AND RECOMMENDATIONS

7.1 Summary

Shear tab connections are amongst the most popular shear connections in design and construction. Low fabrication expenses and ease of assembly are the two key factors contributing to the desirability of this type of connection. In spite of the benefits, some problems appear in the construction of special cases. When the shear tab is intended to be framed into the web of a supporting column or girder, the flanges of the supporting element form an obstacle in field construction. To overcome this issue, either the shear tab must be extended or the beam should be coped to move the supported member clear of the support and simplify the framing. The modified configurations are called “extended shear tab” and “double-coped beam”, respectively.

The two configurations are examples of steel connections where cantilever plate connection elements are being used. Cantilever plate connection elements are steel plates, which are distinguished from other connection plates by their two opposite unrestrained edges. The increased length of cantilever plate connection elements in some connection configurations raises concern regarding the potential of instability of the plate.

In this study, the behaviour of steel cantilever plate connection elements was investigated. Two major configurations were considered, including extended shear tabs and double-coped beams, in both of which cantilever plate connection elements act as the principal connection element. In all cases, the connected beam was considered laterally braced to isolate the local behaviour of the connection.

In the first phase of study, an experimental program was conducted on the behaviour of extended shear tabs with a stiff support and the behaviour of the connection was evaluated in terms of capacity, limit states, development of plasticity and shear load eccentricity. Results were compared to the predictions by two design methods.

The second phase of study included a comprehensive finite element investigation on the behaviour of extended shear tabs. A total of 36 models were considered in the study that differed in extended shear tab thickness, depth, and length. Two boundary conditions were considered: rotationally flexible and fixed. The behaviour of the models was evaluated in terms of capacity, limit states, development of plasticity and shear load eccentricity.

In the third phase of study, a comprehensive finite element investigation was performed on double-coped beams. A total of 54 models were considered in the study varying in double-coped beam web thickness, depth, length, and support condition.

Using the results and observations achieved from the three phases of study, recommendations are proposed to consider new aspects of the design of cantilever steel connection elements with wide applicability.

7.2 Conclusions

The following conclusions from the study can be made:

- Extended shear tabs can experience several limit states, including: out-of-plane deformation, bolt fracture, net section plasticity, gross section plasticity, and weld fracture.
- Double-coped beams can experience several limit states, including: cope face plasticity, support face plasticity, out-of-plane deformation, and section plastic shear capacity.
- The behaviour of extended shear tabs and double-coped beams is similar. They can be generalized into steel cantilever plate connection elements, the behaviour of which can be unified.
- The capacity of a cantilever plate connection element is higher for deeper and thicker connections due to the increased cross-sectional area.
- Increasing the length of the plate results in connection capacity reduction. The shear load eccentricity imposed on the cope face/net section is higher for

longer plates, resulting in decreased vertical load causing the section plasticity.

- In both connection configurations, out-of-plane deformation occurs after significant yielding has happened in the cantilever plate element. In most cases, cantilever plate elements reach the fully plastic state either at one or two locations along the plate. Therefore, stability is not an issue limiting the performance of cantilever plate elements within the considered dimensions in this study. More slender configurations outside the range of this study need to be investigated further.
- Plasticity is developed in cantilever plate connection elements due to the combined effect of shear load and bending moment. Therefore, both effects need to be considered in plasticity evaluation in the plate.
- The equation proposed by Neal (1961) provides an accurate and reliable evaluation of the load that causes section plasticity at different locations along the plate.
- When Neal's interaction equation is used to evaluate plasticity development in cantilever plate connection elements, the correlation between bending moment and shear load is defined using the shear load eccentricity. If the bending moment in the equation is substituted by the product of shear load and a proper value for eccentricity, the shear load causing the plasticity of each section can be predicted by solving the equation for shear load.
- The support condition has a significant effect on connection behaviour and capacity. In general, increasing the support rotational stiffness results in higher connection capacity.
- In connections with a flexible support, the net section/cope face is prone to a high shear load eccentricity, resulting in a high bending moment demand applied to the section. The simultaneous effect of vertical load and bending moment results in the development of plasticity at this location at lower vertical load values compared to the models with the stiff support.
- In the case of connections with a stiff support, a considerable bending moment is developed at the support face and the inflection point is pushed back

towards the beam span, as compared to the flexible-support case. As the shear load is increased, plasticity is developed at the support. With a further increase in the shear load, the inflection point migrates towards the support face due to the increased bending moment at the net section/cope face. The simultaneous effect of vertical load and bending moment at the net section/cope face results in the development of plasticity at this location, followed by a considerable loss of connection stiffness.

- Based on the unified behaviour, it is recommended that for cases of both stiff and flexible support, formation of plasticity at the net section/cope face be regarded as the design limit state.
- The proposed design limit state permits the utilization of the reliable elements of the connection behaviour and in most cases the connection is able to sustain some additional load. However, excessive vertical deformation occurs in the plate after the limit state is reached, which is an undesirable behaviour due to large deformations imposed on the connection and potential increased sensitivity to out-of-plane stability effects.
- To evaluate the design limit state using Neal's interaction equation, it is recommended that the full geometric eccentricity be used unless sufficient rotational stiffness and ductility at the support can be demonstrated to justify a reduction. The lower bound eccentricity for the design of connections with fixed supports is one-half of the geometric eccentricity.
- It is recommended that the support be designed considering the bending moment that can develop at this location. It is recommended that the support elements be designed for the shear reaction force applied at an eccentricity of one-half of the geometric eccentricity of the cantilever plate, unless a greater level of rotational flexibility and ductility at the support can be demonstrated to justify a reduced eccentricity.

7.3 Recommendations for Further Research

Although this study has included a variety of geometries and boundary conditions for two common connection configurations, and it has contributed significantly to the understanding of the behaviour of cantilever plate connection elements, areas where further research is required are identified as follows:

- Although some of the test specimens were tested under combined axial and shear load, the effect of axial load was only studied qualitatively and for the sake of comparison to the previous tests. It is recommended that further research be conducted to evaluate the accuracy of Neal's interaction equation in predicting plasticity development in cantilever plate connection elements in the presence of axial load.
- Some support conditions used in the finite element investigation were extremely flexible (e.g., long unbraced girders). The high flexibility of these support conditions imposes some extent of conservatism in recommending the design eccentricity for flexible supports. However, this support condition may or may not be used in practical applications. Further research is needed to identify practical flexible support conditions and evaluate the possibility of recommending a lower eccentricity for connections with flexible supports, thus making the designs more efficient.

REFERENCES

AISC. (1994). "Steel Construction Manual LRFD, 2nd Edition." Chicago, IL, USA.

AISC. (2005). "Steel Construction Manual, 13th Edition." *AISC 325-05,* Chicago, IL, USA.

AISC. (2010). "Specification for Structural Steel Buildings." *ANSI/AISC 360-10,* Chicago, Illinois, USA.

AISC. (2011). "Steel Construction Manual, 14th Edition." *AISC 325-11,* Chicago, IL, USA.

ASTM. (2014). *A370-14: Standard Test Methods and Definitions for Mechanical Testing of Steel Products.* ASTM International, West Conshohocken, PA, USA.

Cheng, J. J. R., Yura, J. A., and Johnson, C. P. (1984). "Design and behavior of coped beam." University of Texas, Austin, TX.

CISC. (2010). "Handbook of Steel Construction, 10th Edition." *CISC,* Markham, ON, Canada.

CISC. (2012). *Handbook of Steel Construction, 10th Edition, Fourth Revised Printing 2012.* Canadian Institute of Steel Construction, Markham, ON.

Dassault Systèmes Simulia Corp. (2012). "Abaqus Analysis User's Guide." *Version 6.12,* Providence, RI, USA.

Dowswell, B., and Whyte, R. (2014). "Local stability of double-coped beams." *Engineering Journal, AISC,* 43-52.

Goodrich, W. (2005). "Behavior of extended shear tabs in stiffened beam-to-column web connections". M.Sc. thesis. Vanderbilt Univ., Nashville, TN.

Johnston, G., Driver, R. G., and Callele, L. (2015). "Strength and Behaviour of Double-Coped Steel Beams under Combined Loads." *Rep. No. 306,* University of Alberta, Edmonton, Alberta, Canada.

Mahamid, M., Rahman, A., and Ghorbanpoor, A. (2007). "The Analyses of Extended Shear Tab Steel Connections Part II: Stiffened Connections." *Engineering Journal, AISC,* 44(2), 133-145.

Marosi, M., Tremblay, R., and Rogers, C. A. (2011). "Behaviour of single and double row bolted shear tab connections and weld retrofits". Research Report. Department of Civil Engineering & Applied Mechanics, McGill University, Montreal, QC.

Metzger, K. A. B. (2006). "Experimental verification of a new single plate shear connection design model". M.Sc. thesis. Virginia Polytechnic Institute and State Univ., Blacksburg, VA.

Mirzaei, A., Rogers, C. A., and Tremblay, R. (2013). "Full-Scale Testing of Shear Tab Connections Subjected to Combined Axial and Shear Forces." *3rd Specialty Conference on Material Engineering & Applied Mechanics,* Canadian Society for Civil Engineering, Montréal, QC, Canada.MEC086-1-10.

Muir, L. S., and Hewitt, C. M. (2009). "Design of unstiffened extended single-plate shear connections." *Engineering Journal, AISC,* 46(2), 67-79.

Muir, L. S., and Thornton, W. A. (2011). "The development of a new design procedure for conventional single-plate shear connections." *Engineering Journal, AISC,* 48(2), 141-152.

Muir, L., and Thornton, W. (2004). "A Technical Note: A Direct Method for Obtaining the Plate Buckling Coefficient for Double-Coped Beams." *Engineering Journal, AISC,* 41(3), 133-134.

Neal, B. G. (1961). "The effect of shear and normal forces on the fully plastic moment of a beam of rectangular cross section." *J. App. Mech.,* 28(2), 269-274.

Rahman, A., Mahamid, M., Amro, A., and Ghorbanpoor, A. (2007). "The Analyses of Extended Shear Tab Steel Connections Part I: The Unstiffened Connections." *Engineering Journal, AISC,* 44(2), 117-132.

Sarkar, D., and Wallace, B. (1992). "Design of Single Plate Framing Connections." *Rep. No. FSEL/AISC 92-01,* University of Oklahoma, Norman, OK.

Sherman, D. R., and Ghorbanpoor, A. (2002). "Final report: design of extended shear tabs." American Institute of Steel Construction, University of Wisconsin-Milwaukee.

Suleiman, M. F., Shahrooz, B. M., Bill, H. L., and Rassati, G. A. (2013). "An Evaluation of Expected Mode of Failure in Extended Single-Plate Connections." *CSCE 2013 General Conference,* Canadian Society for Civil Engineering, Montréal, QC, Canada.GEN229-1-8.

Thomas, K., Driver, R. G., Callele, L., and Oosterhof, S. (2014). "Design and Behaviour of Extended Shear Tabs under Combined Loads." *Rep. No. 305,* University of Alberta, Edmonton, Alberta, Canada.

Thornton, W. A., and Fortney, P. J. (2011). "On the Need for Stiffeners for and the Effect of Lap Eccentricity on Extended Single-Plate Connections." *Engineering Journal, AISC,* 48(2), 117-125.

Appendix A: Material Test Results

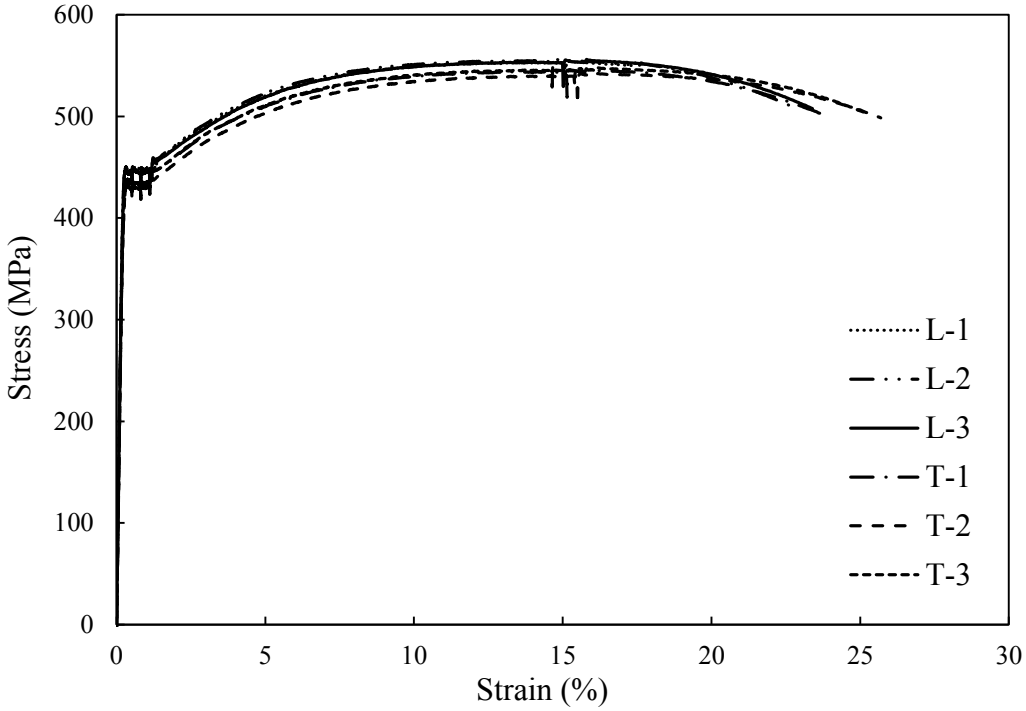

Figure A-1: Stress–strain curves for 10 mm thick extended shear tab

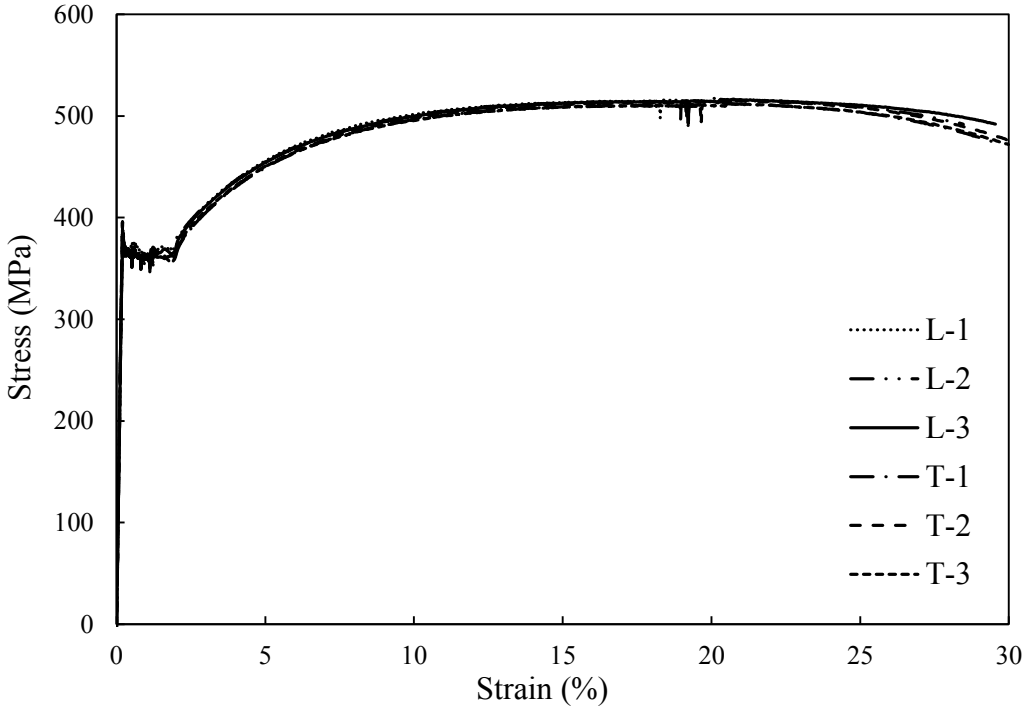

Figure A-2: Stress–strain curves for 13 mm thick extended shear tab

Appendix B: Specimen Response Curves

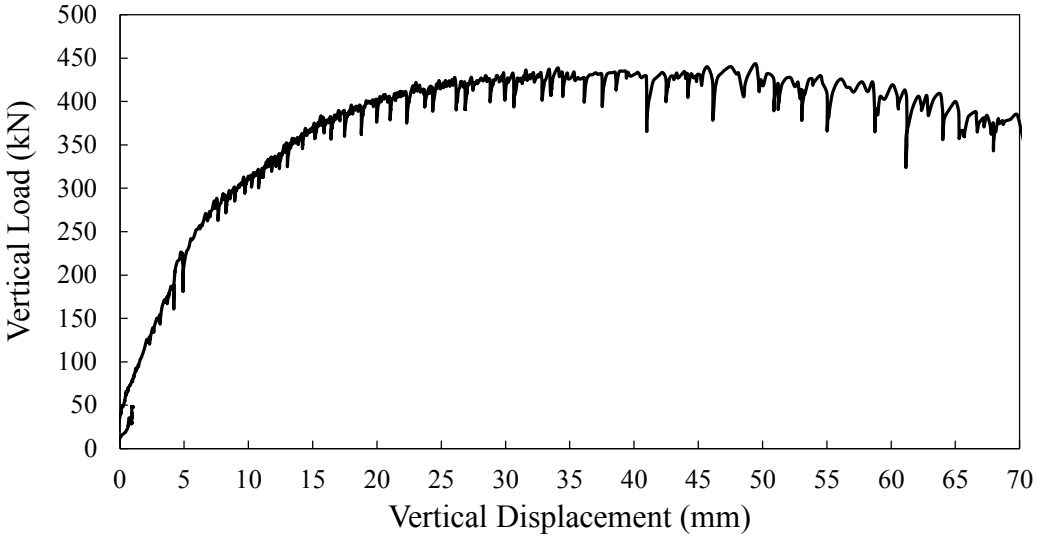

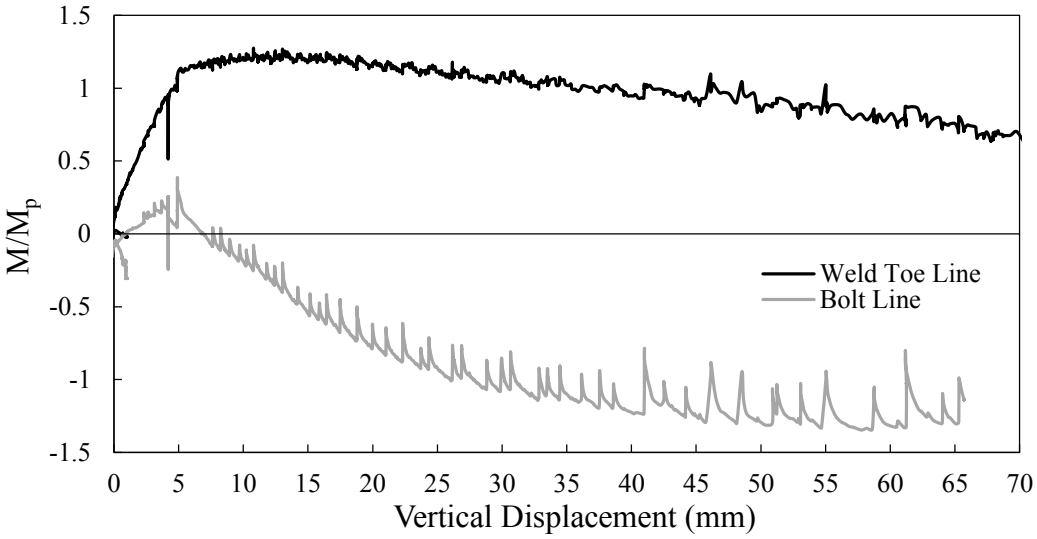

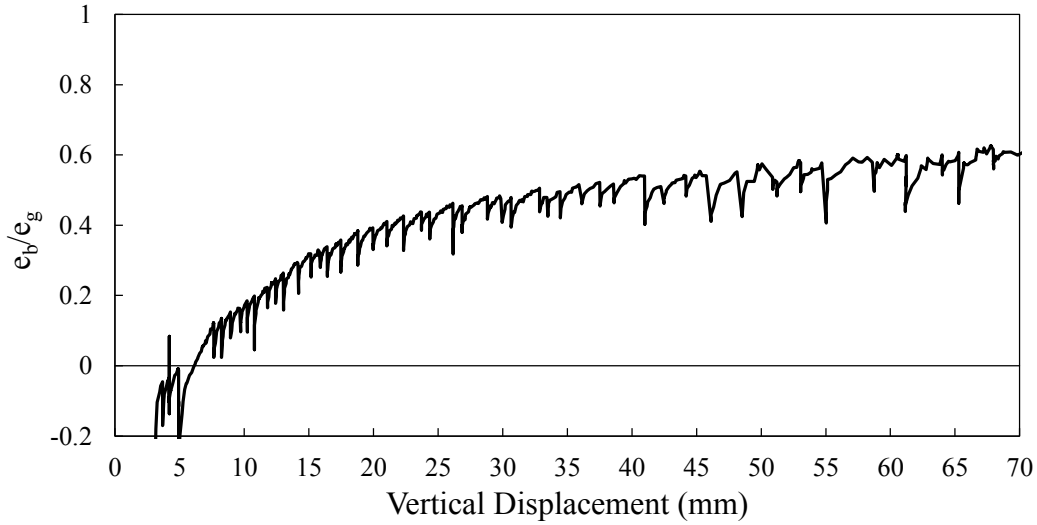

Figure B-1: Specimen 3BR-10-0

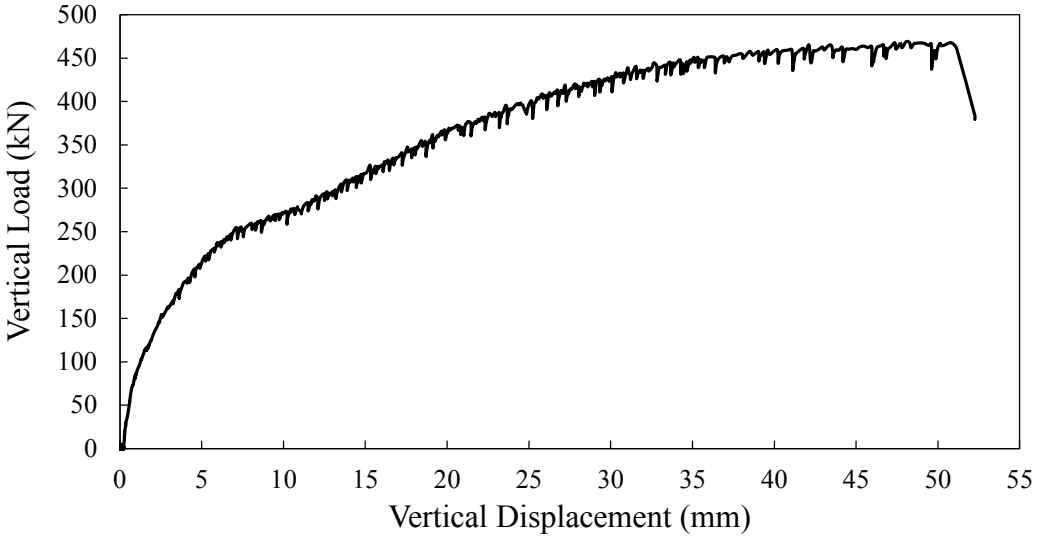

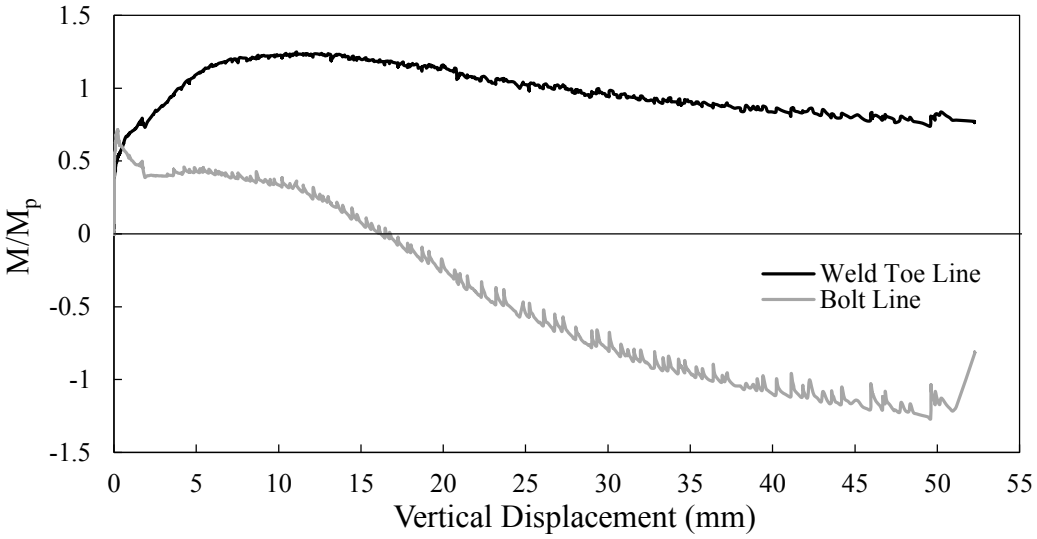

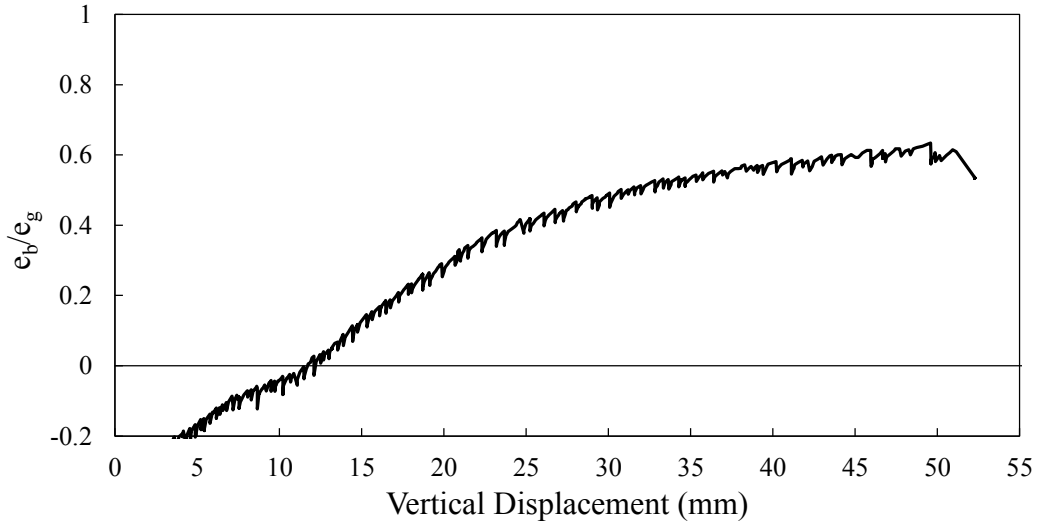

Figure B-2: Specimen 3BR-10-0-L

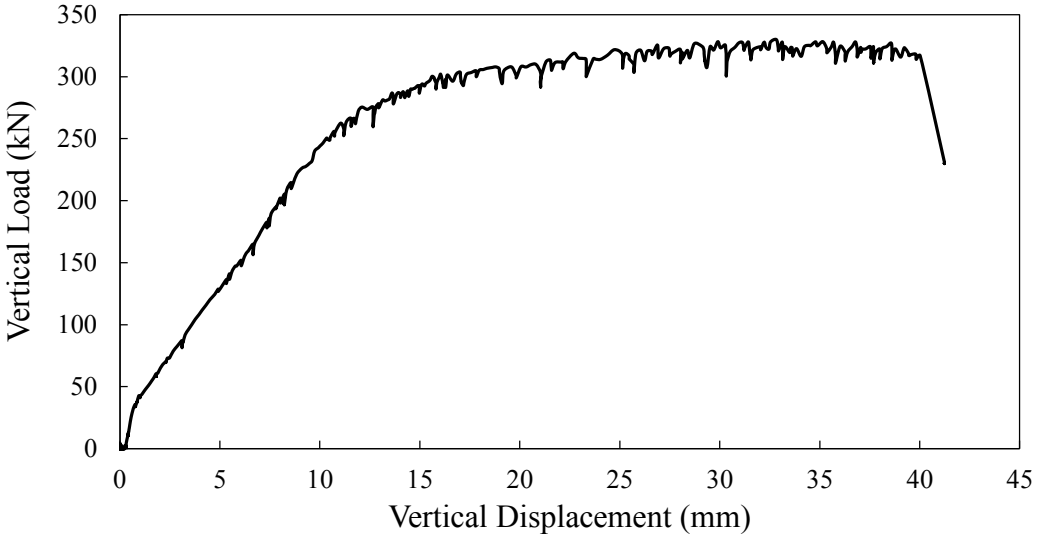

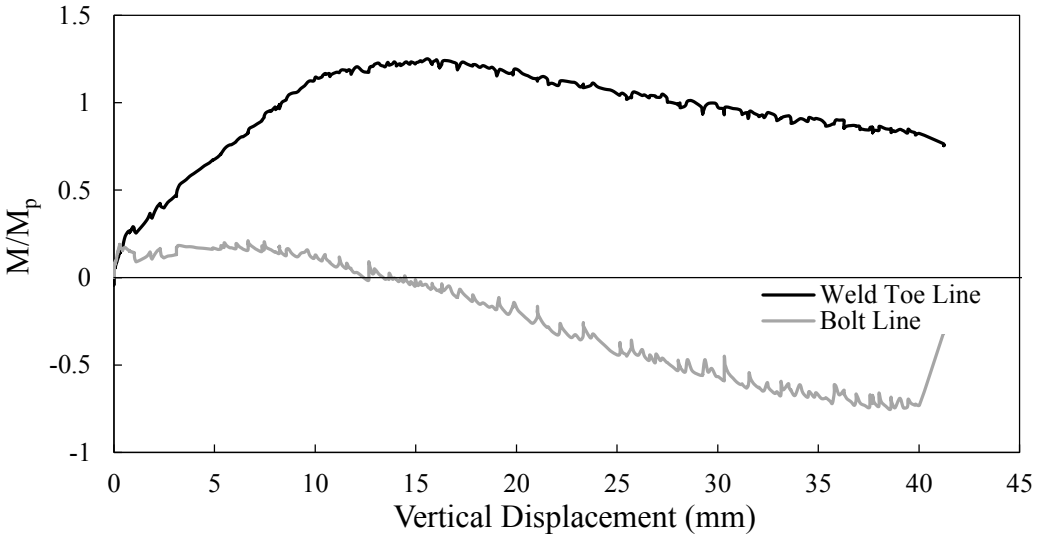

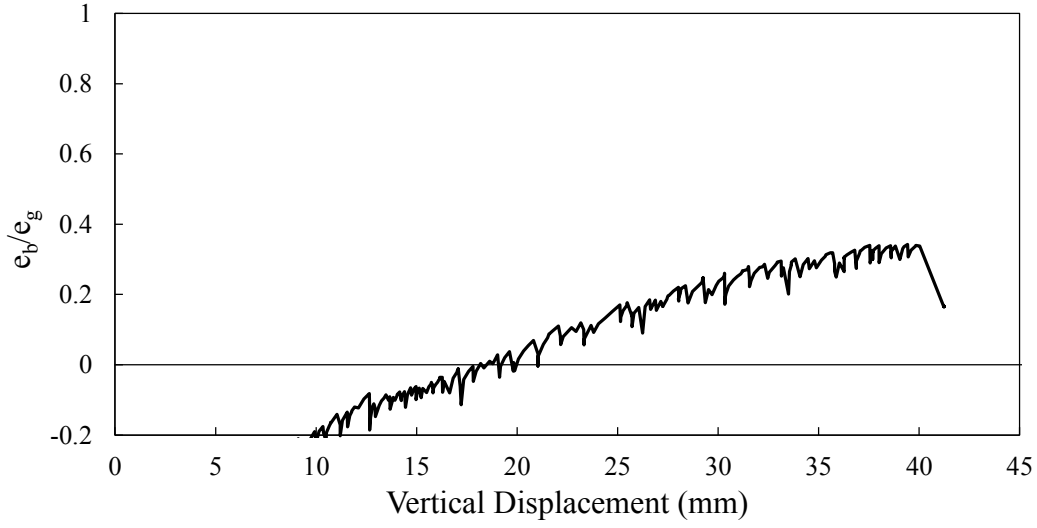

Figure B-3: Specimen 3BR-10-0-V1

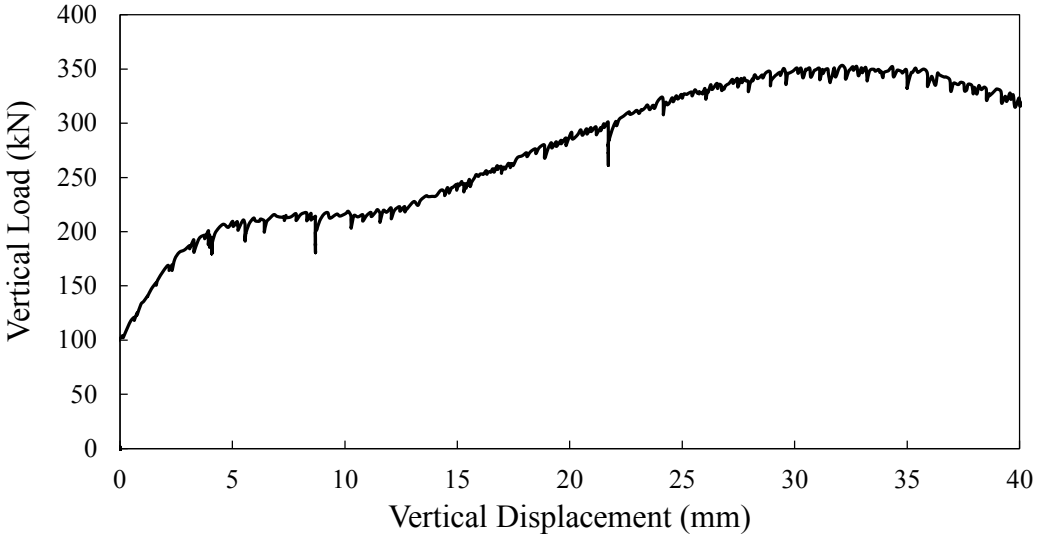

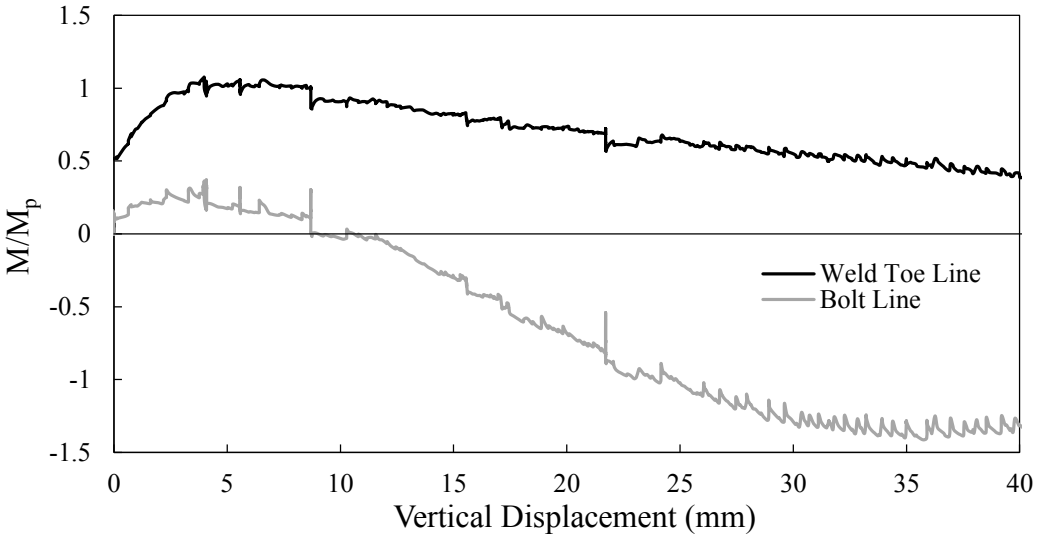

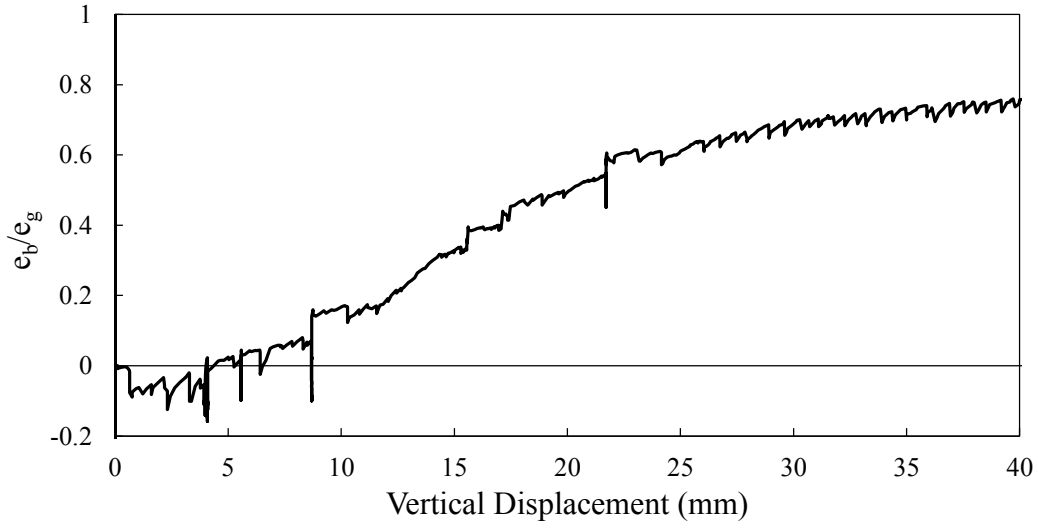

Figure B-4: Specimen 3BR-10-100C

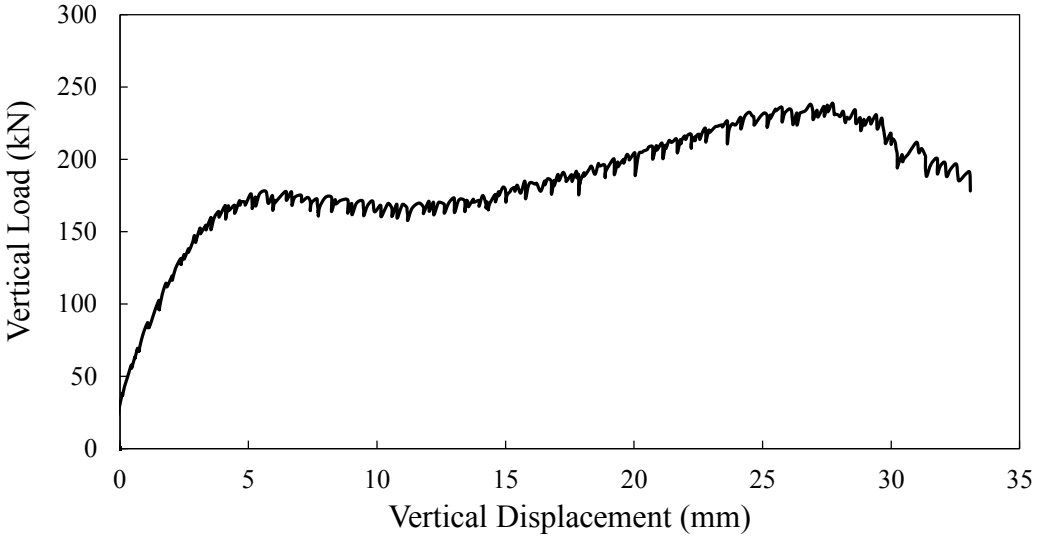

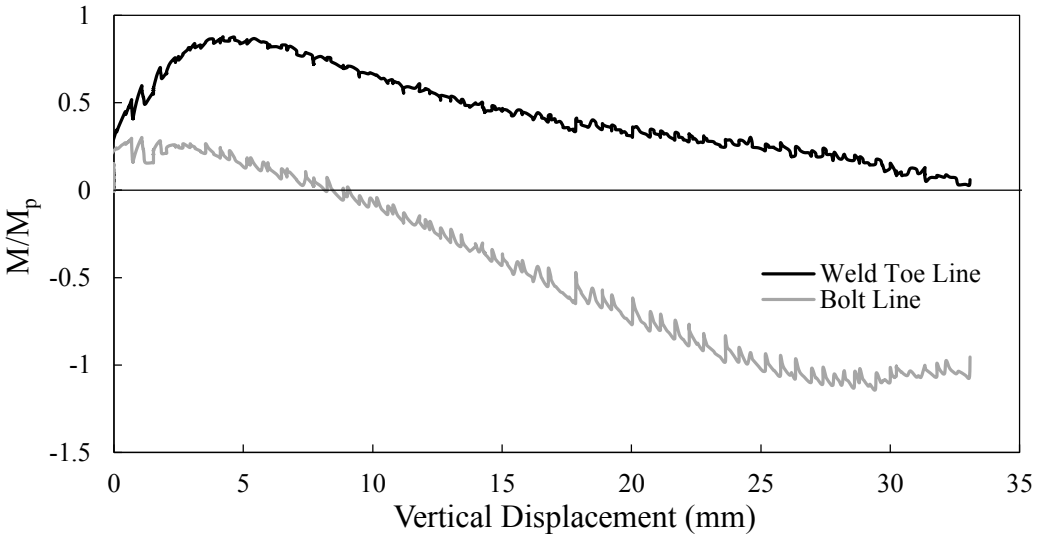

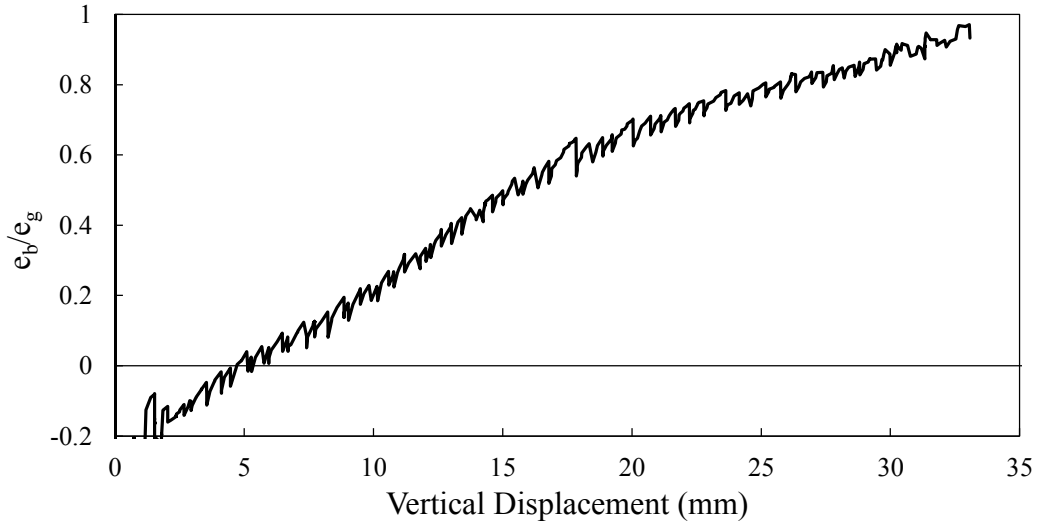

Figure B-5: Specimen 3BR-10-200C

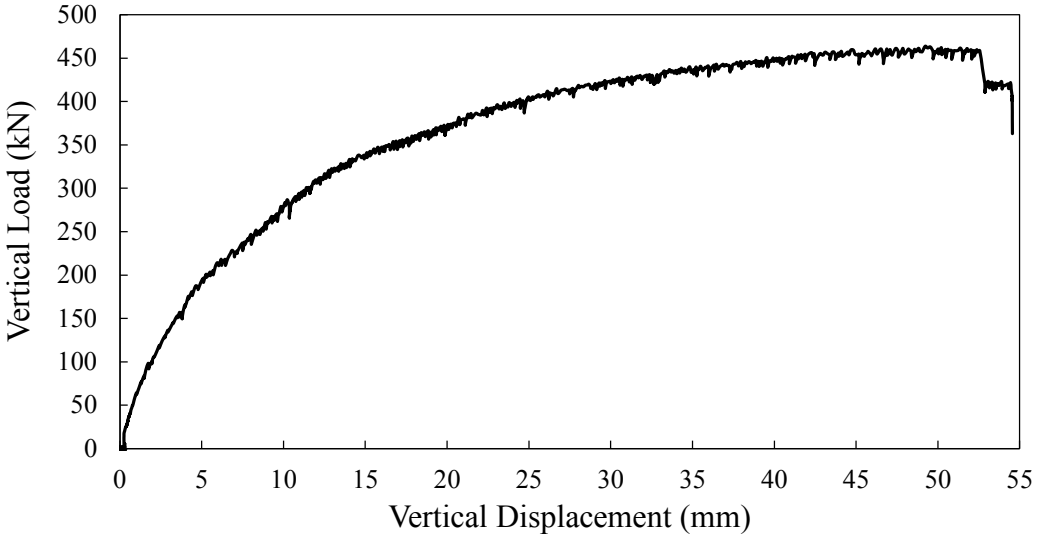

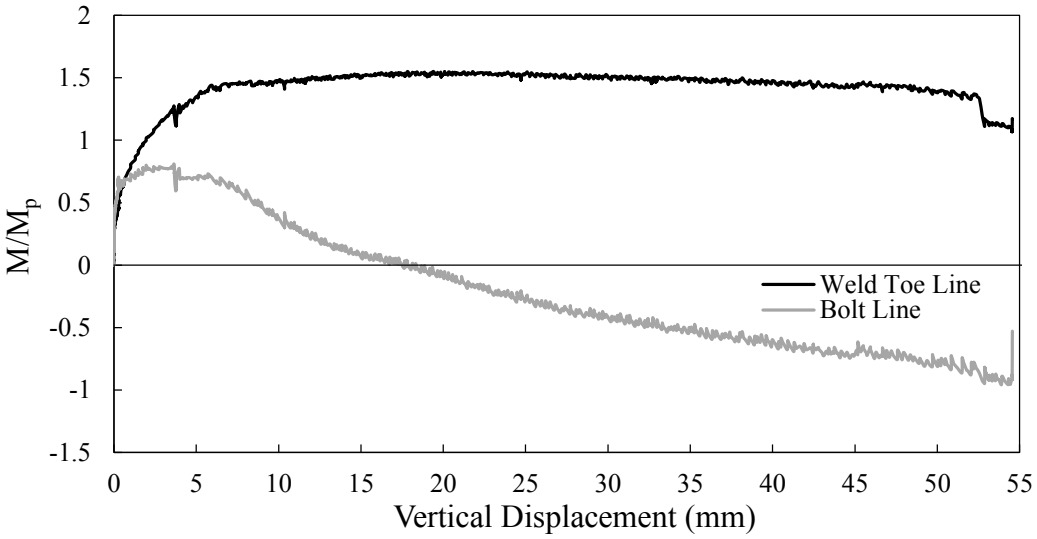

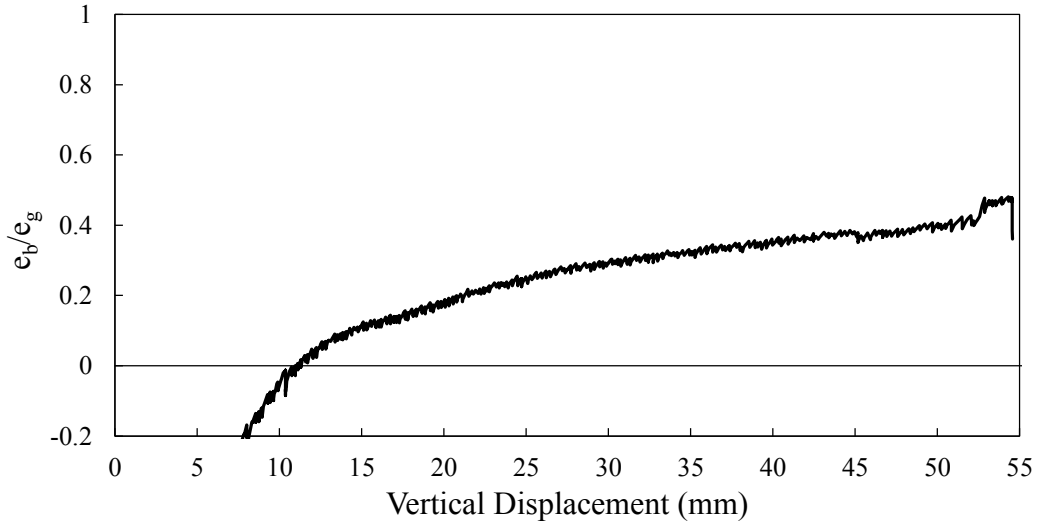

Figure B-6: Specimen 3BR-10-200T

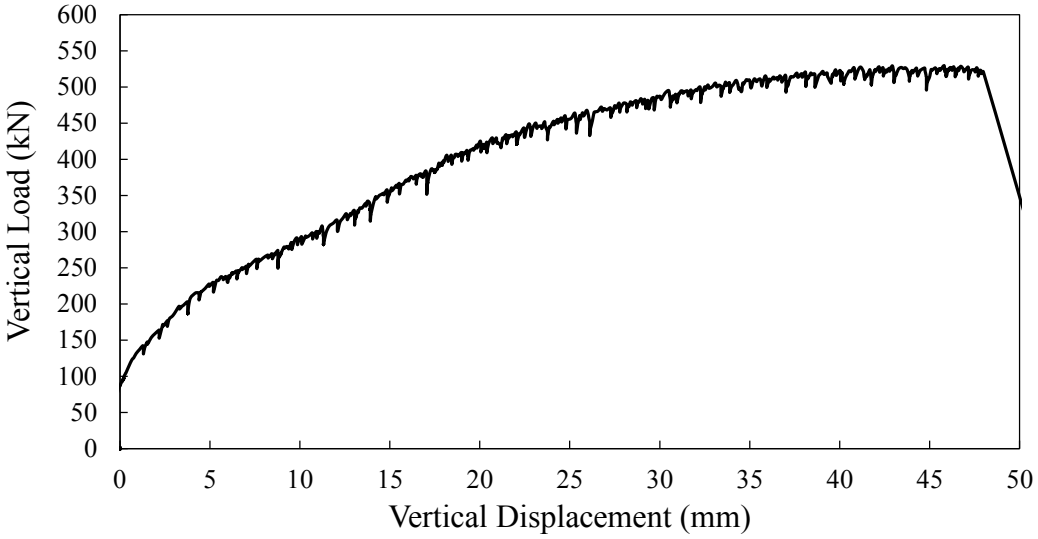

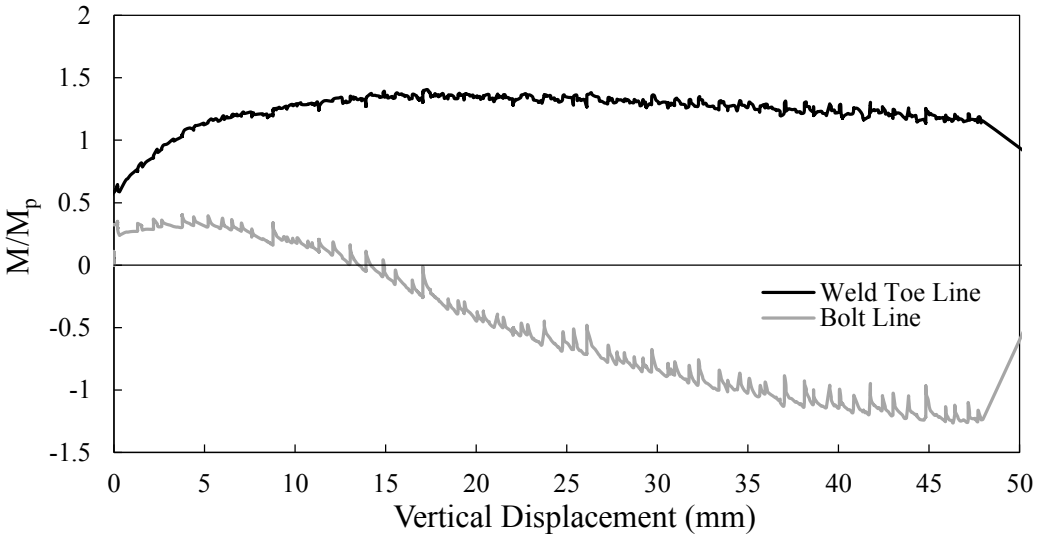

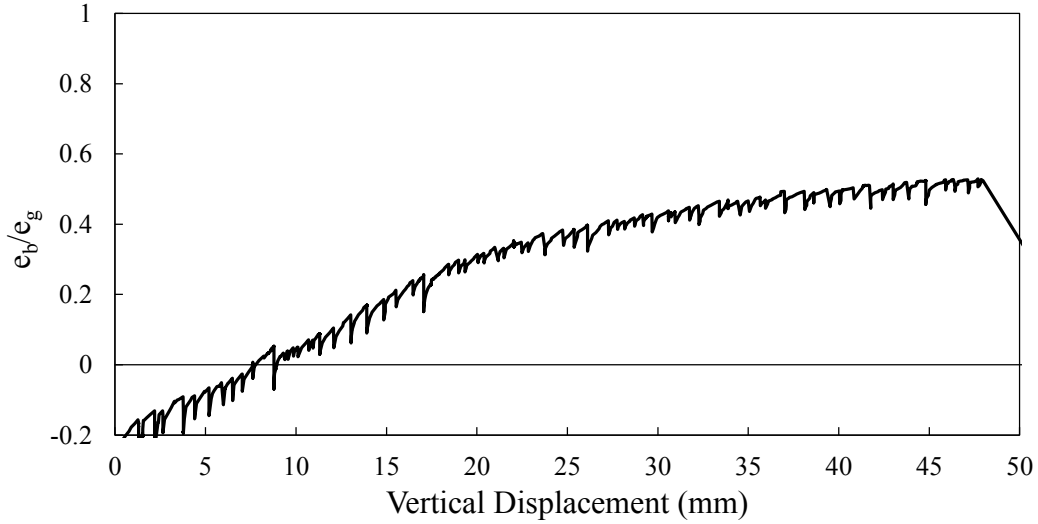

Figure B-7: Specimen 3BR-13-0

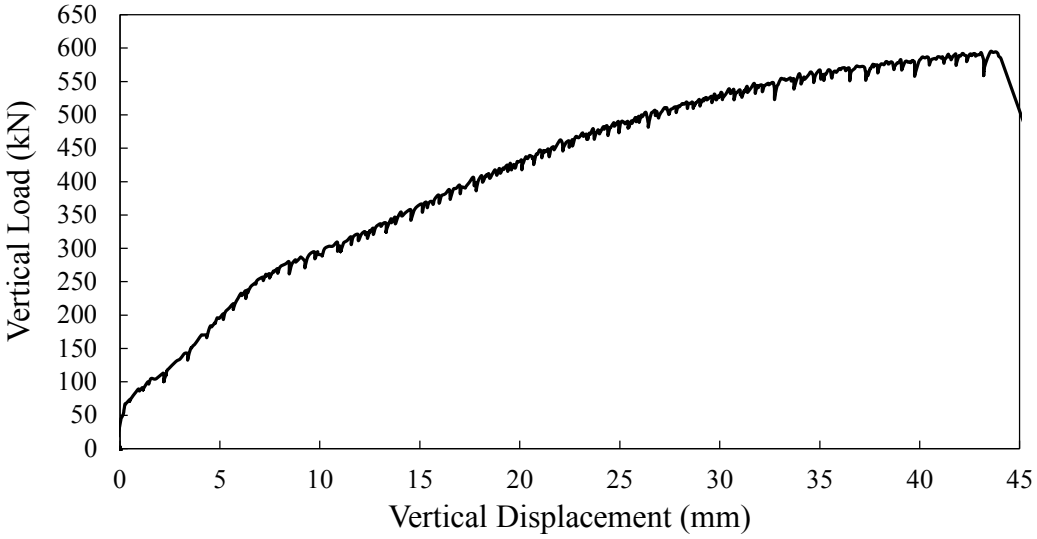

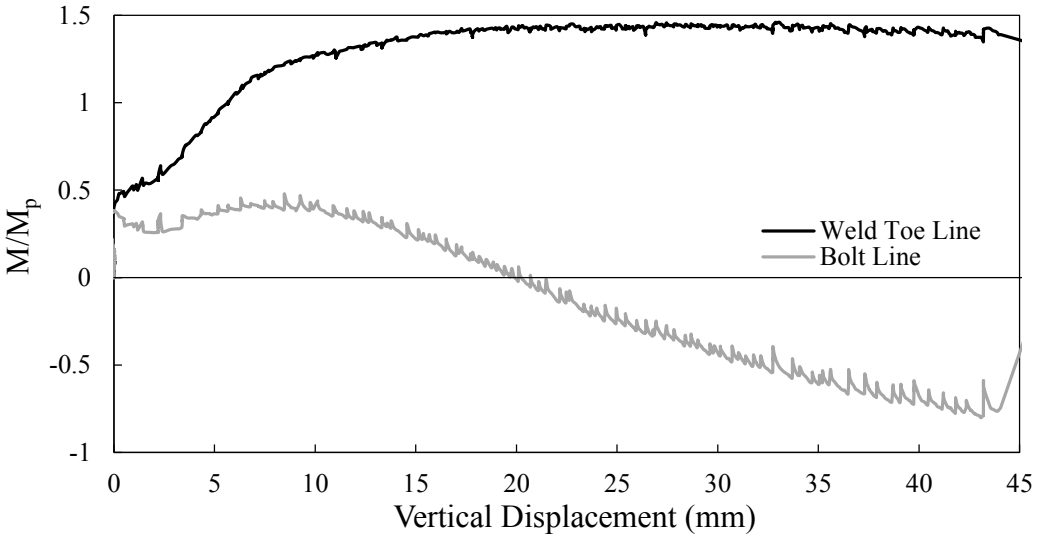

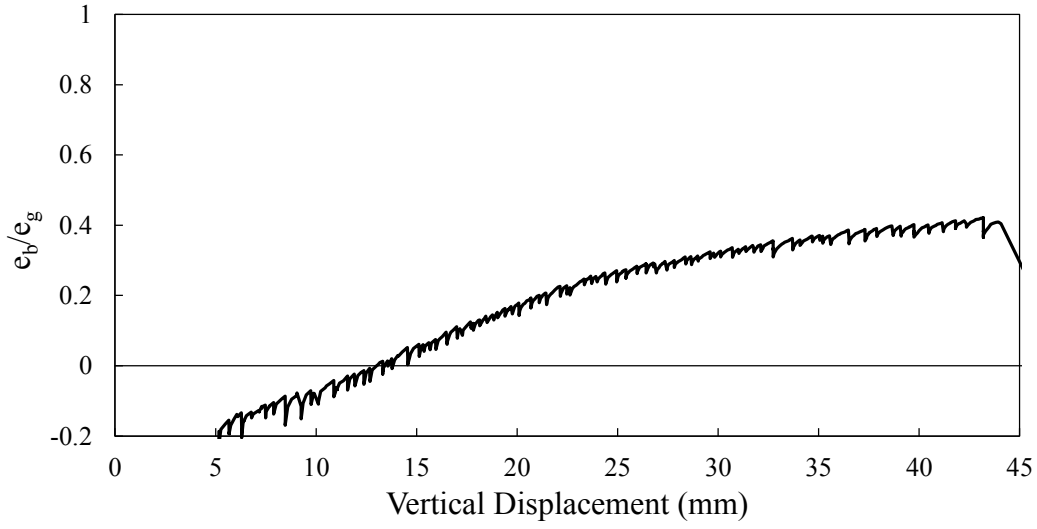

Figure B-8: Specimen 3BR-13-0-L

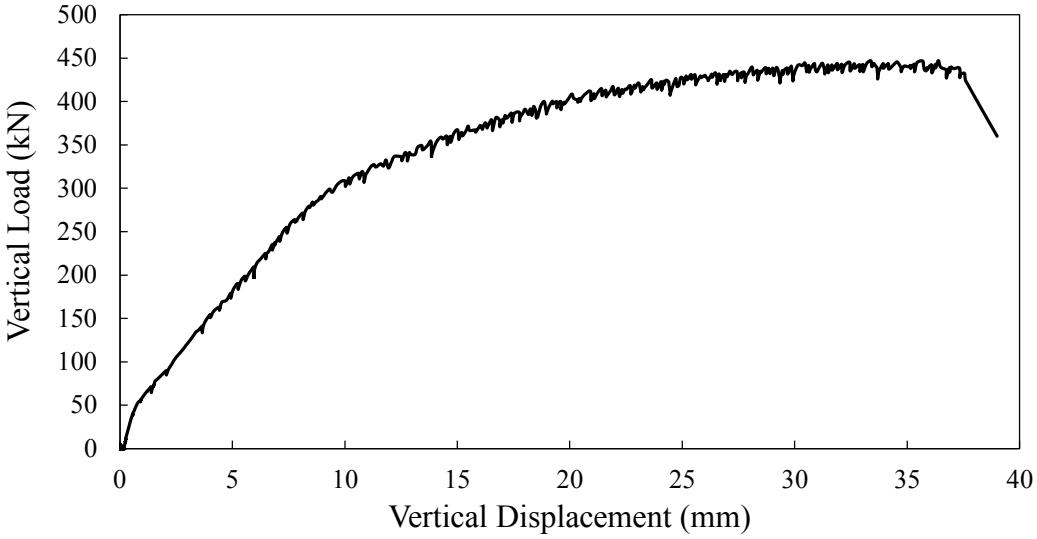

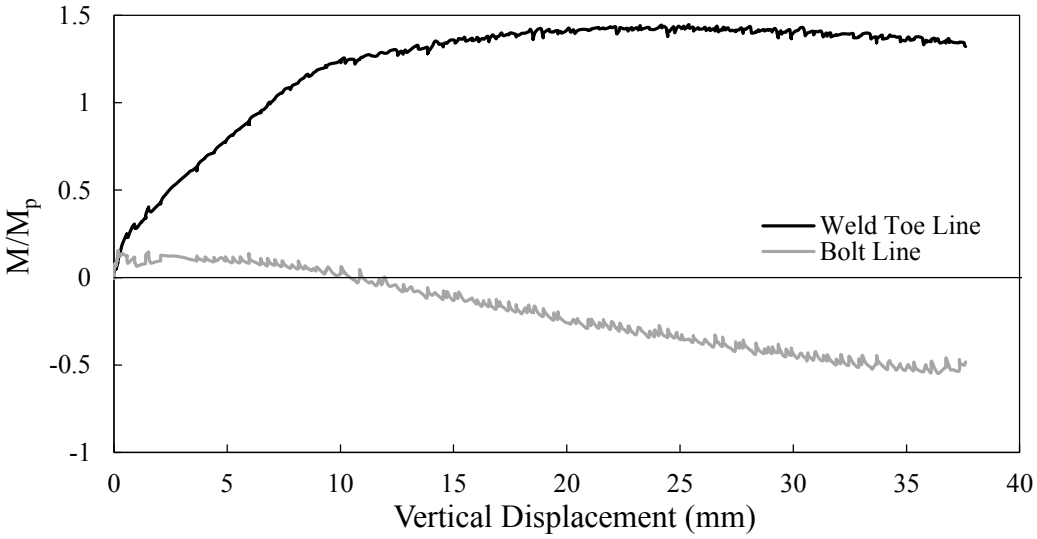

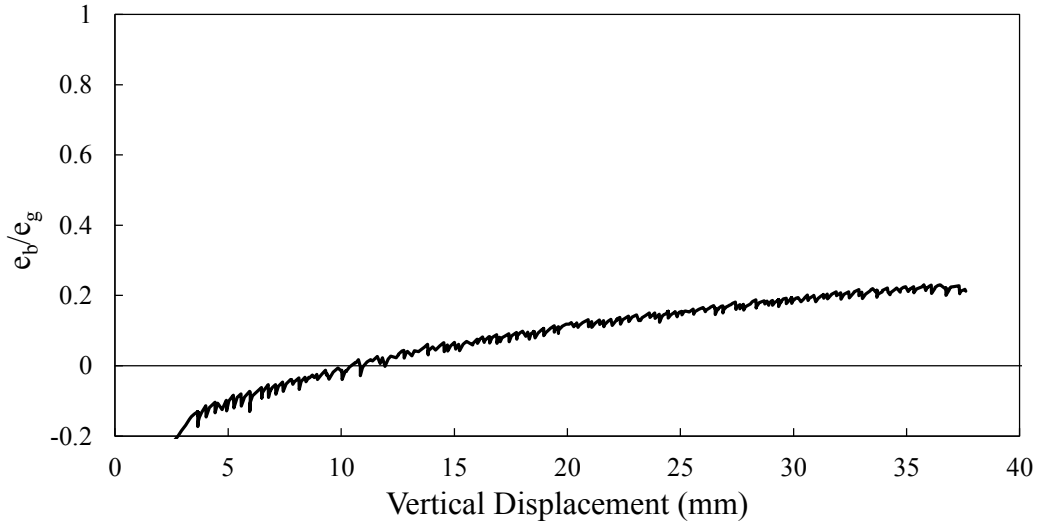

Figure B-9: Specimen 3BR-13-0-V1

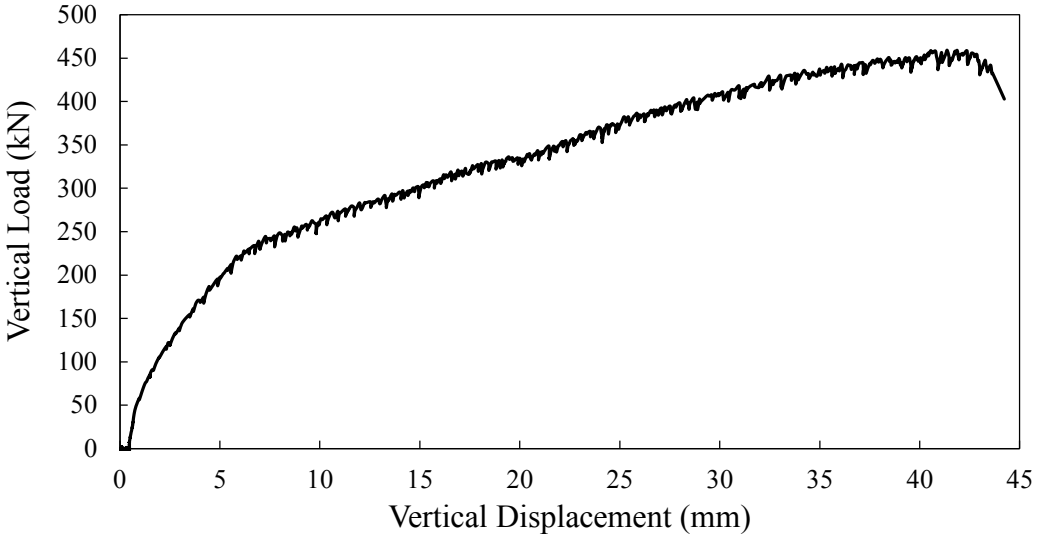

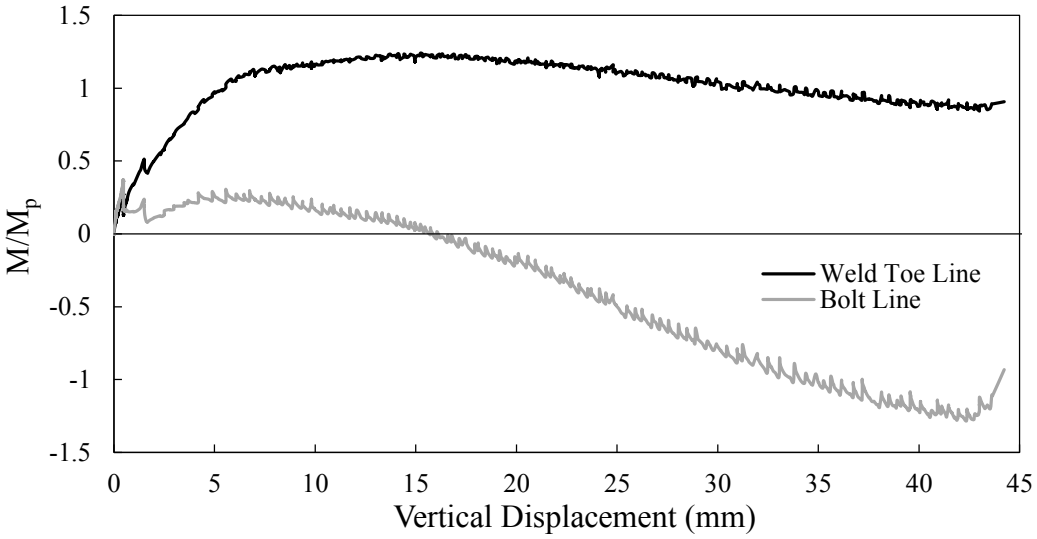

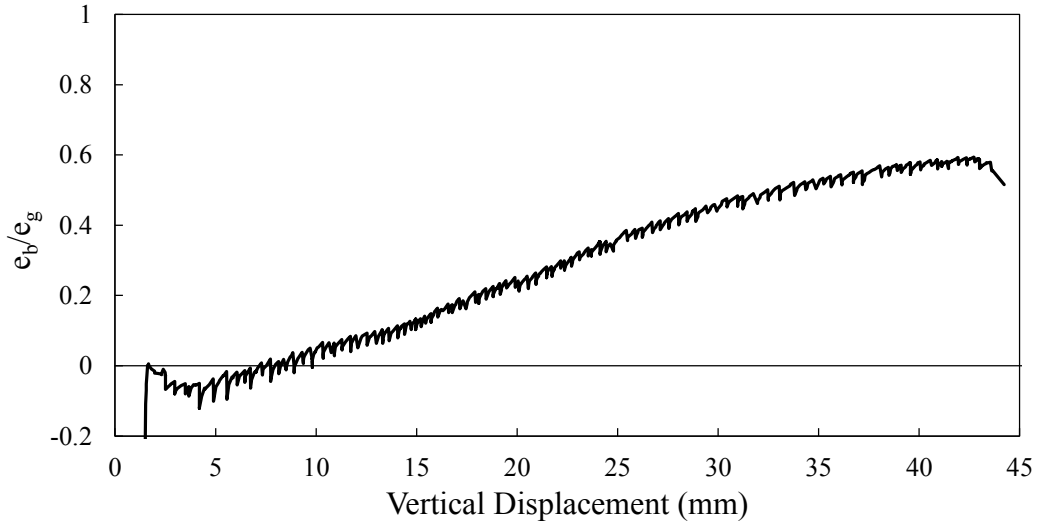

Figure B-10: Specimen 3BR-13-100C

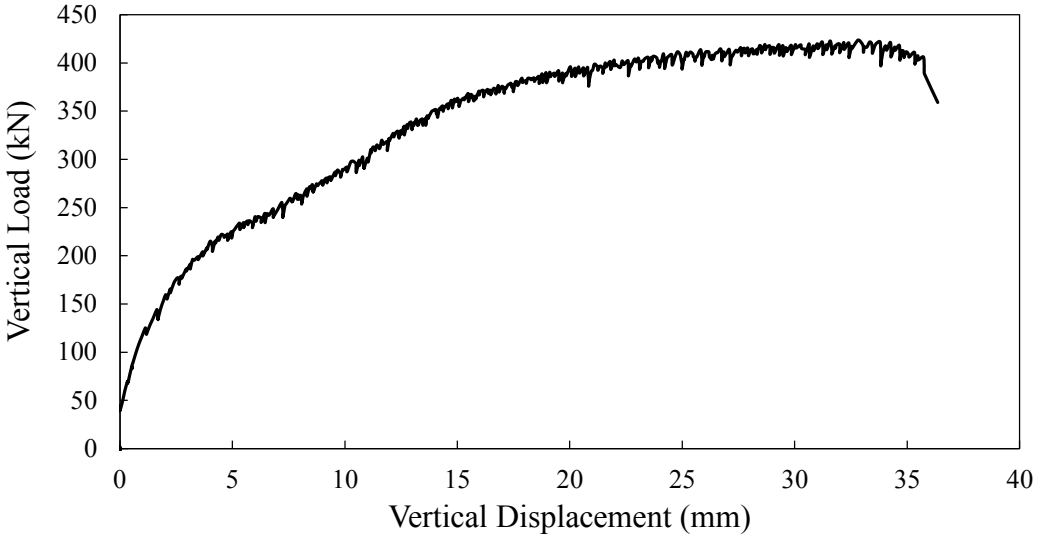

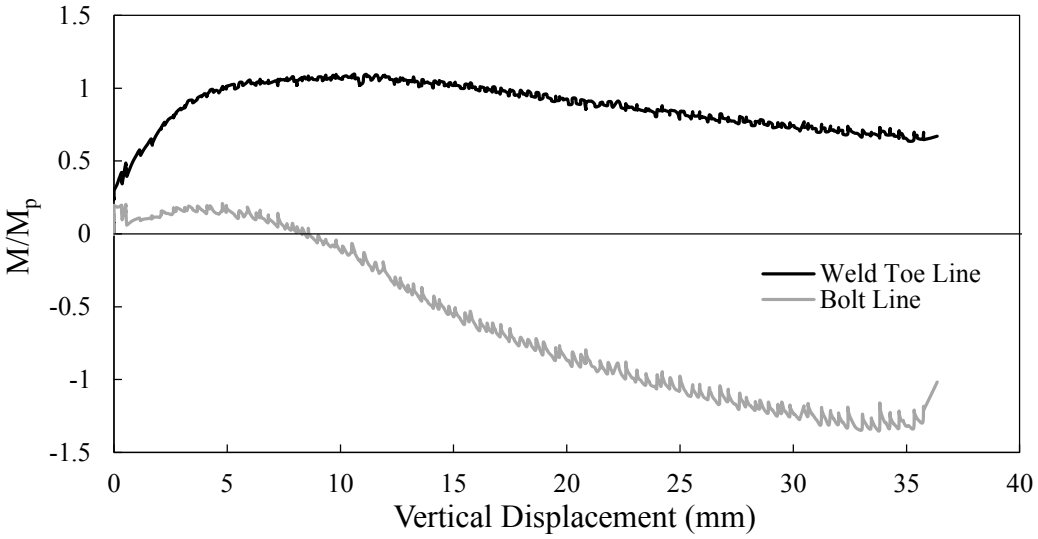

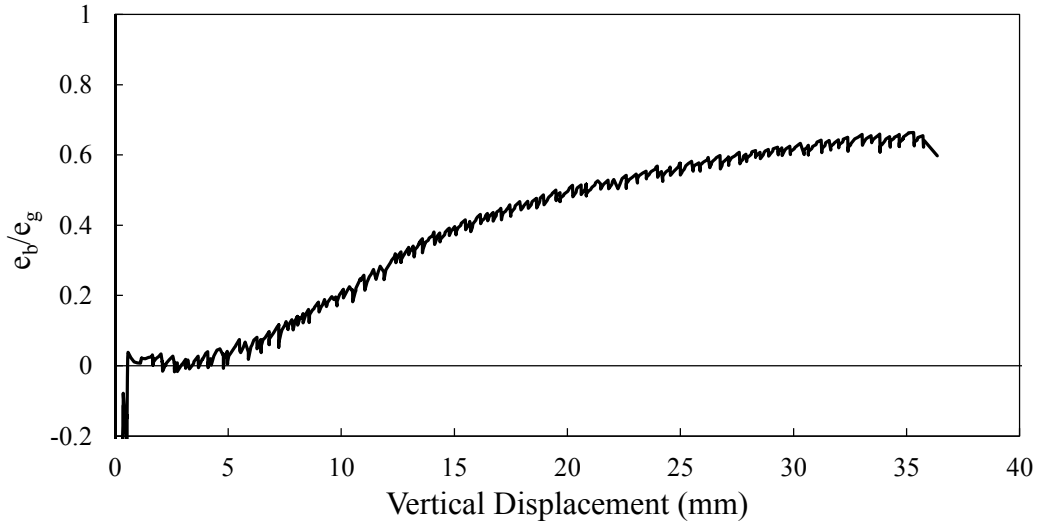

Figure B-11: Specimen 3BR-13-200C

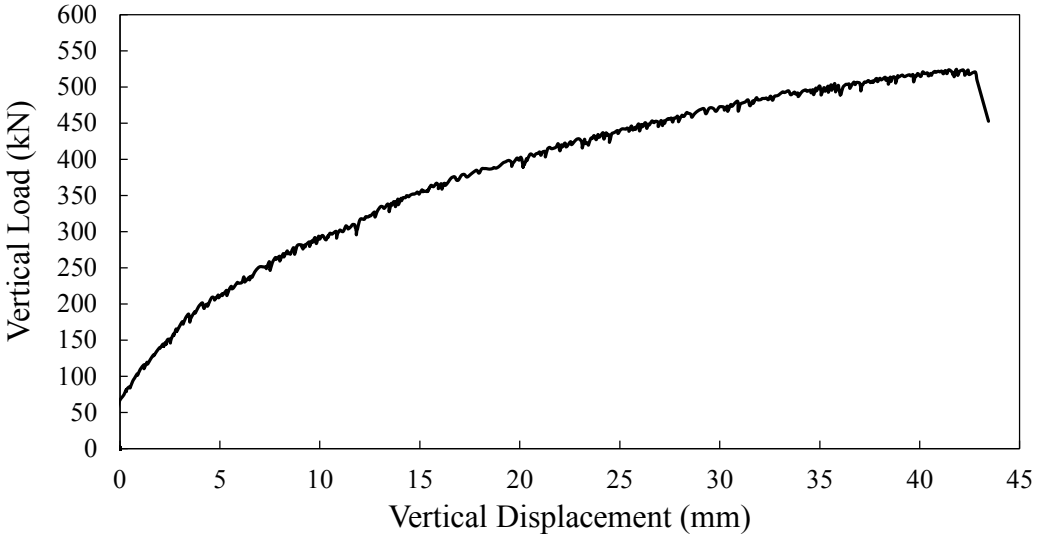

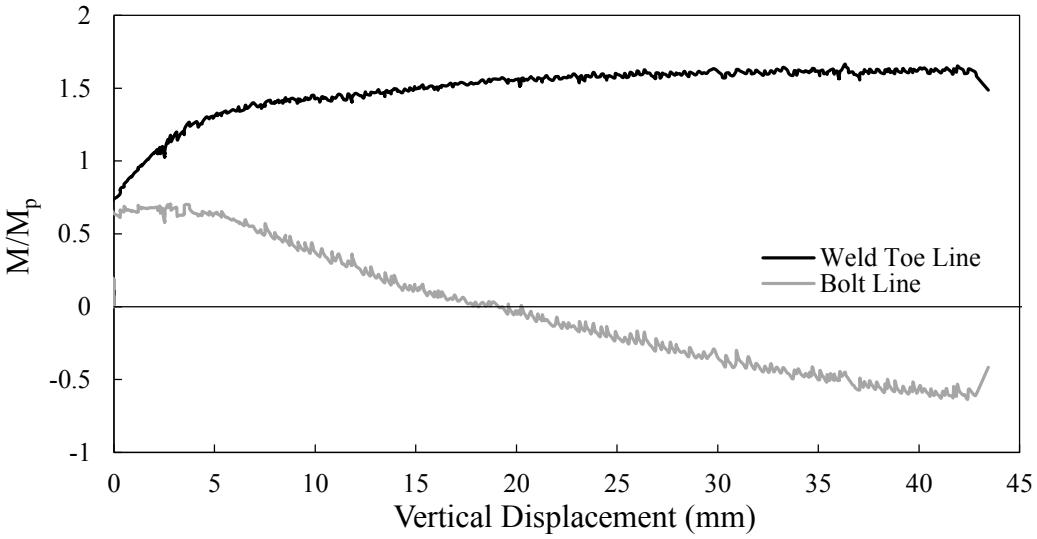

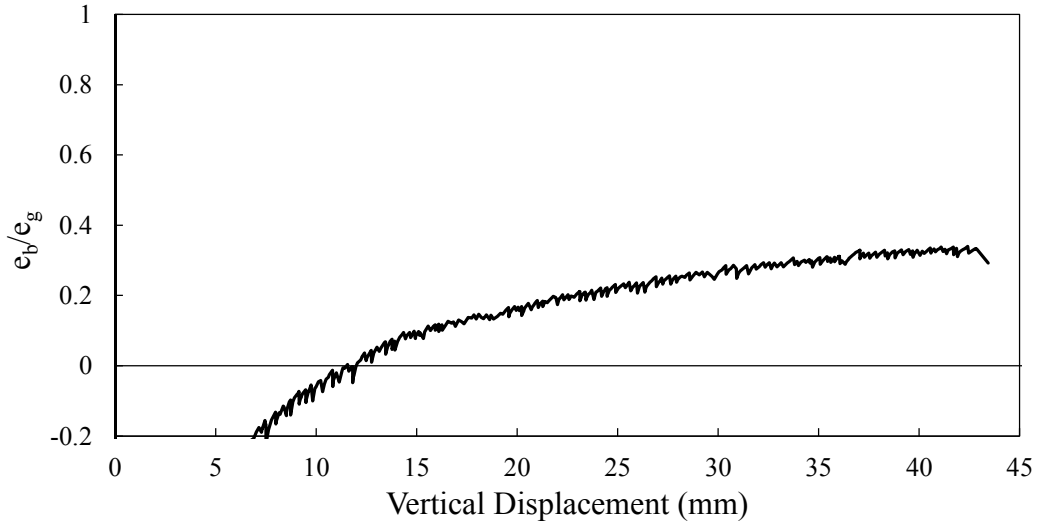

Figure B-12: Specimen 3BR-13-200T

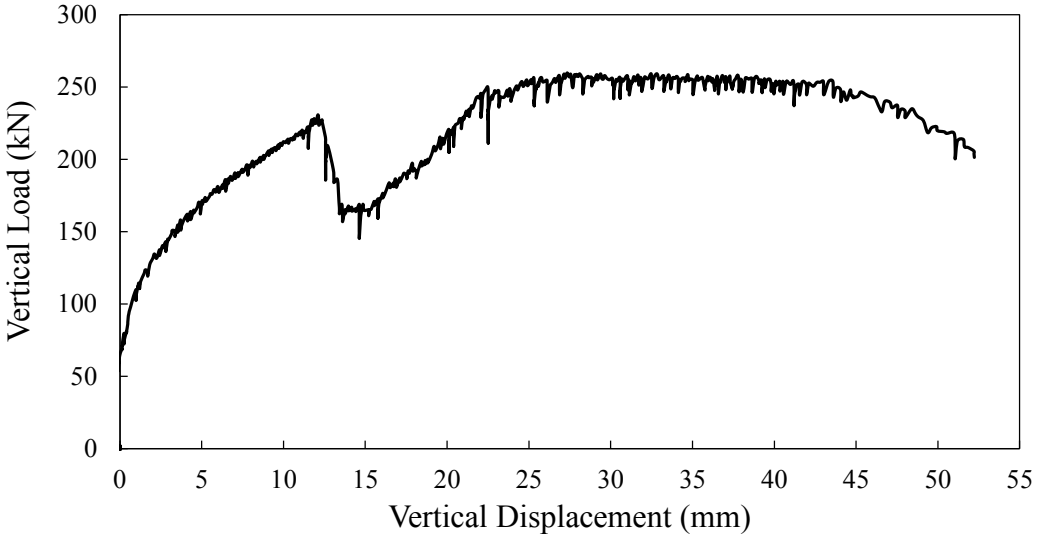

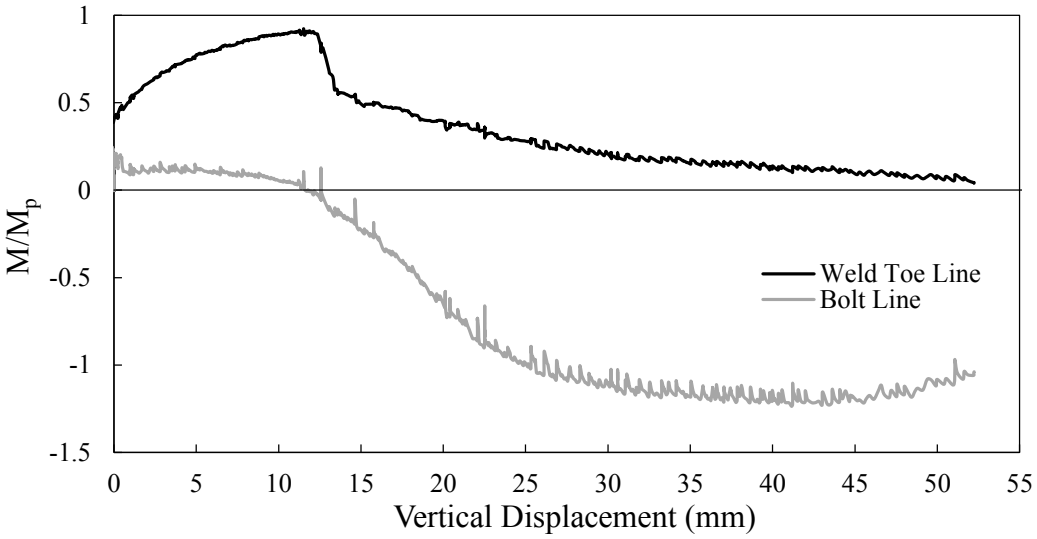

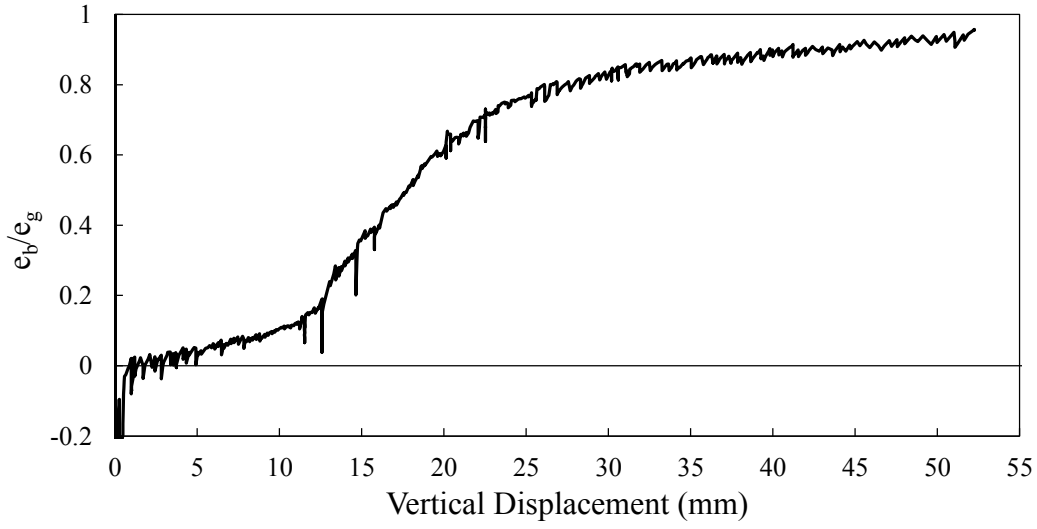

Figure B-13: Specimen 3BM-10-0

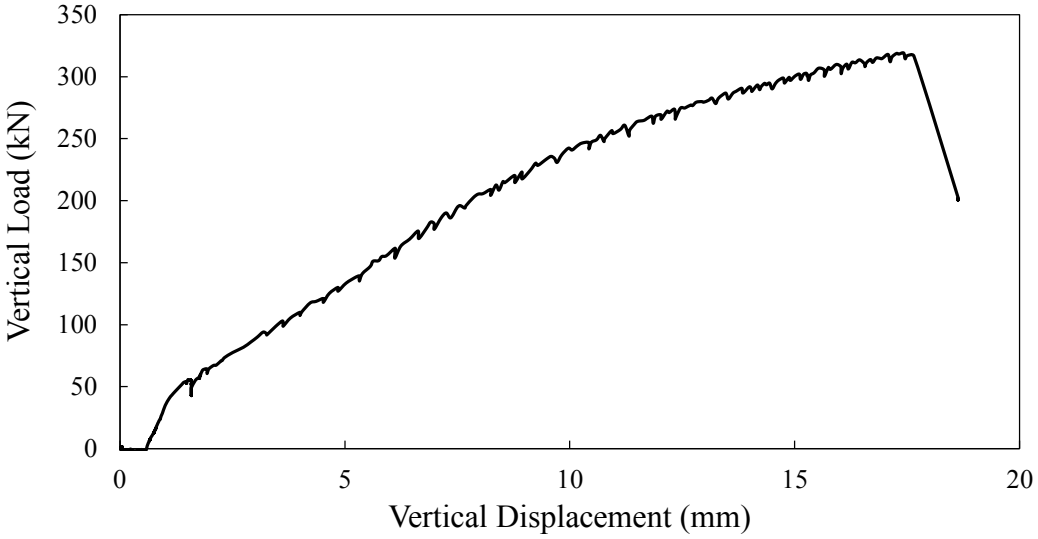

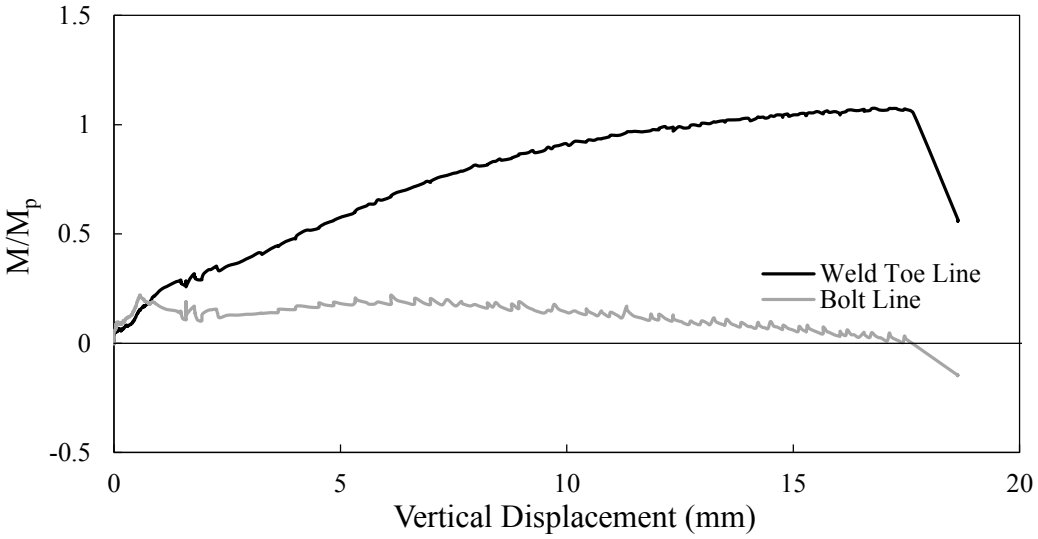

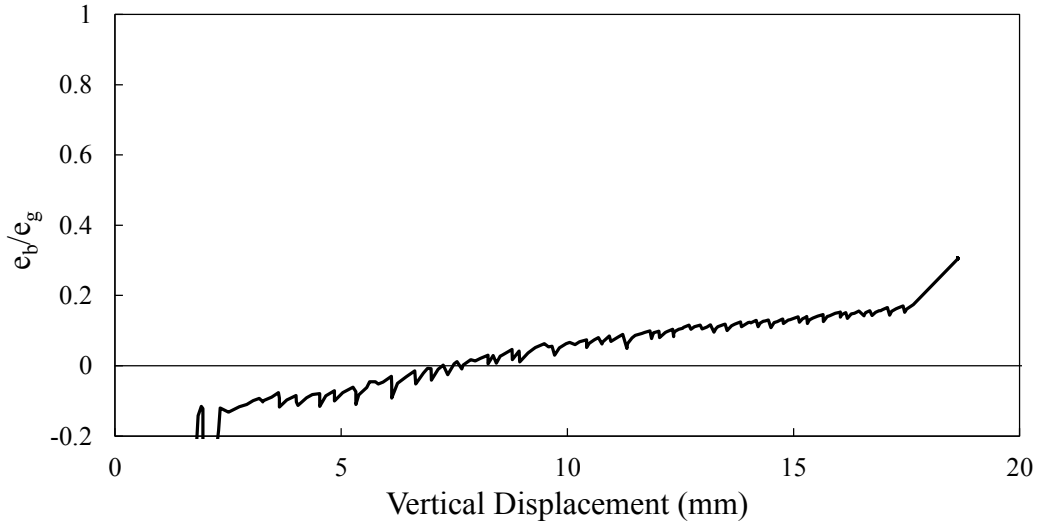

Figure B-14: Specimen 3BM-10-0-V1

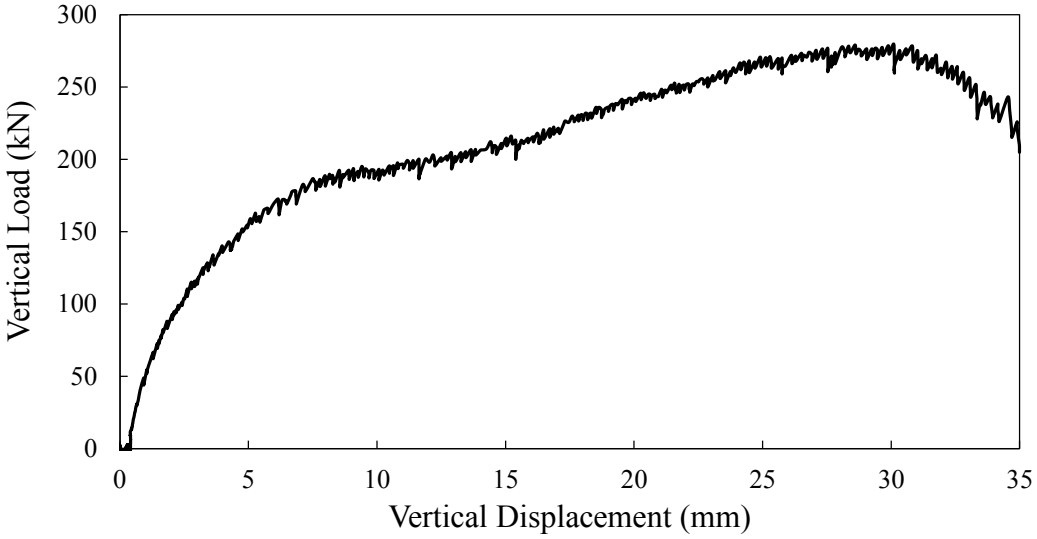

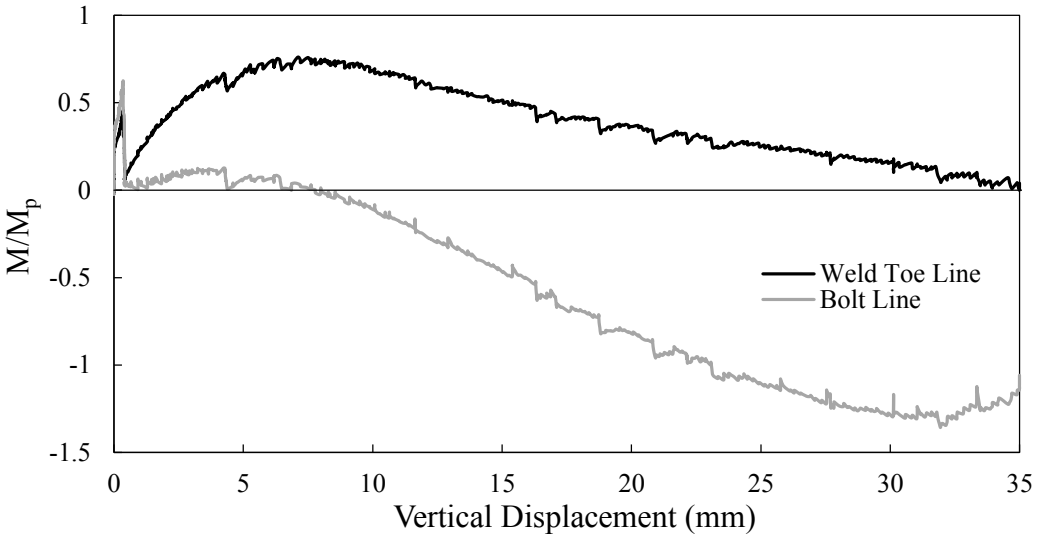

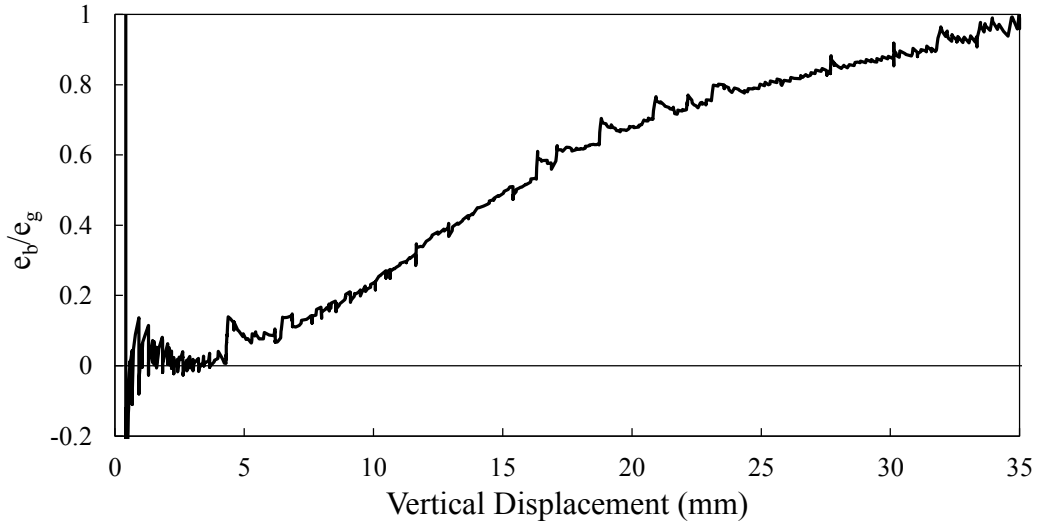

Figure B-15: Specimen 3BM-10-200C

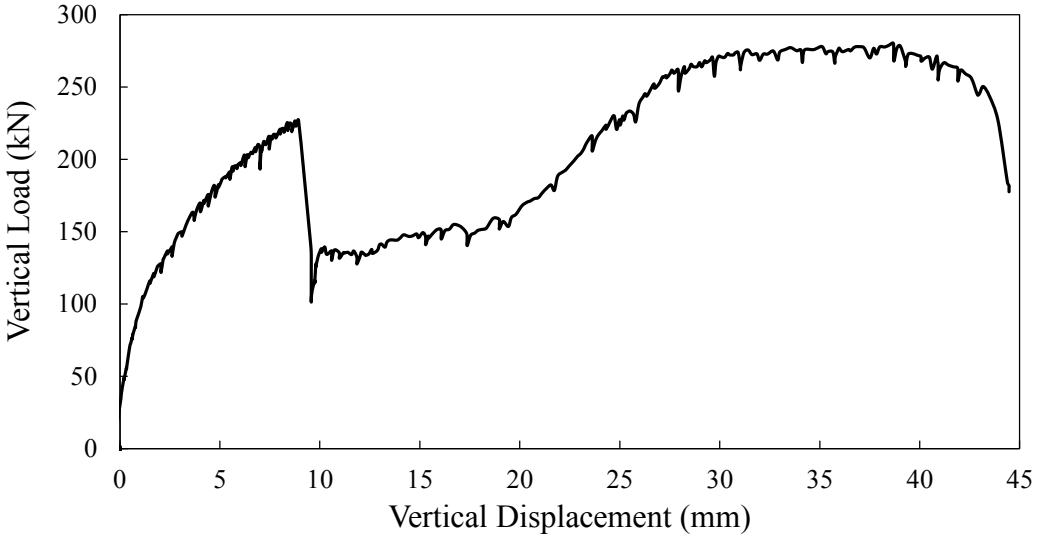

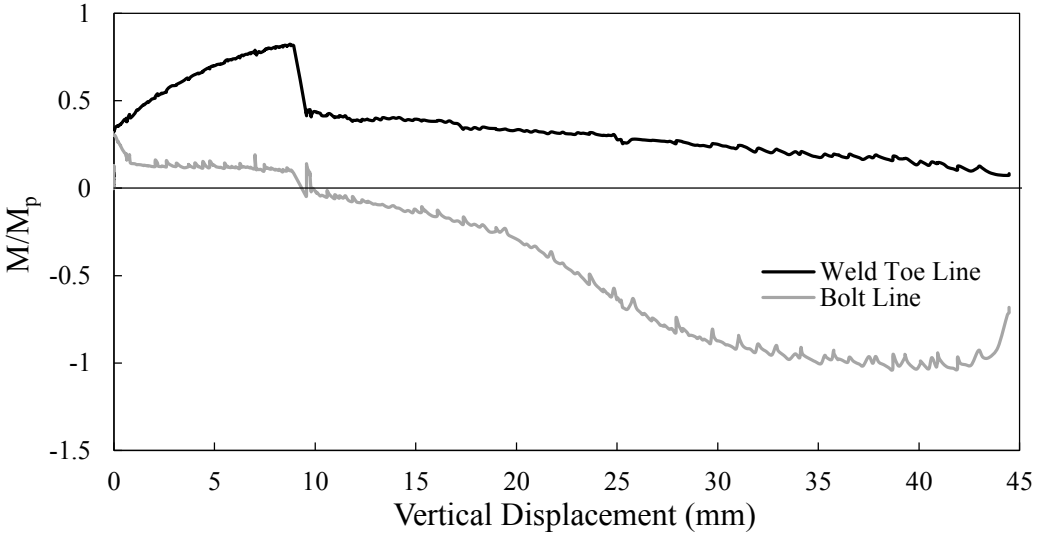

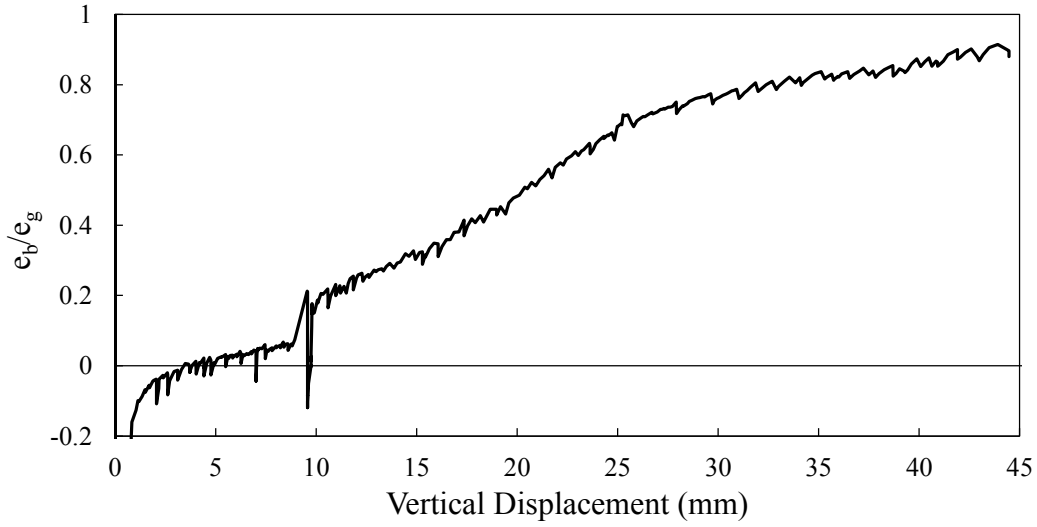

Figure B-16: Specimen 3BM-13-0

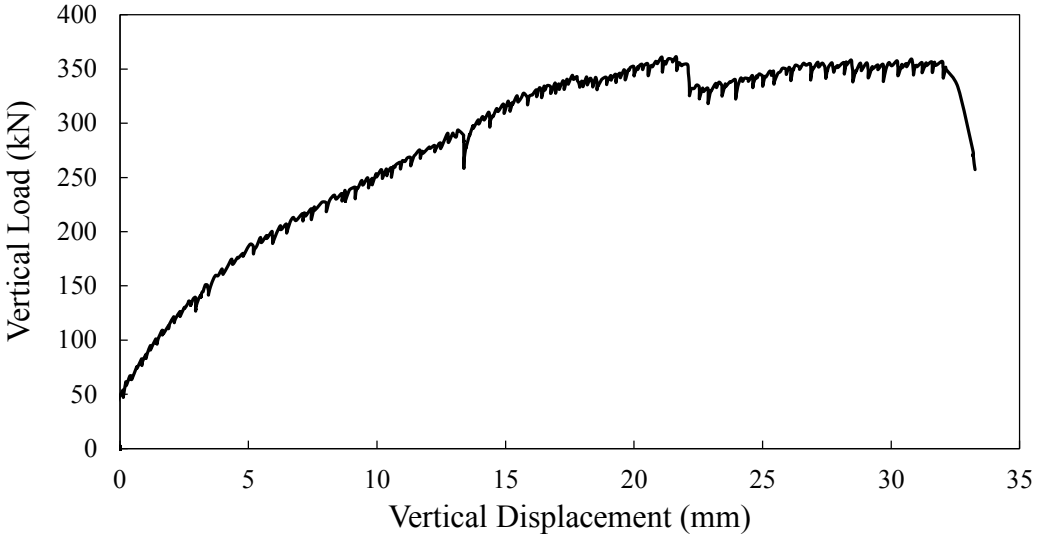

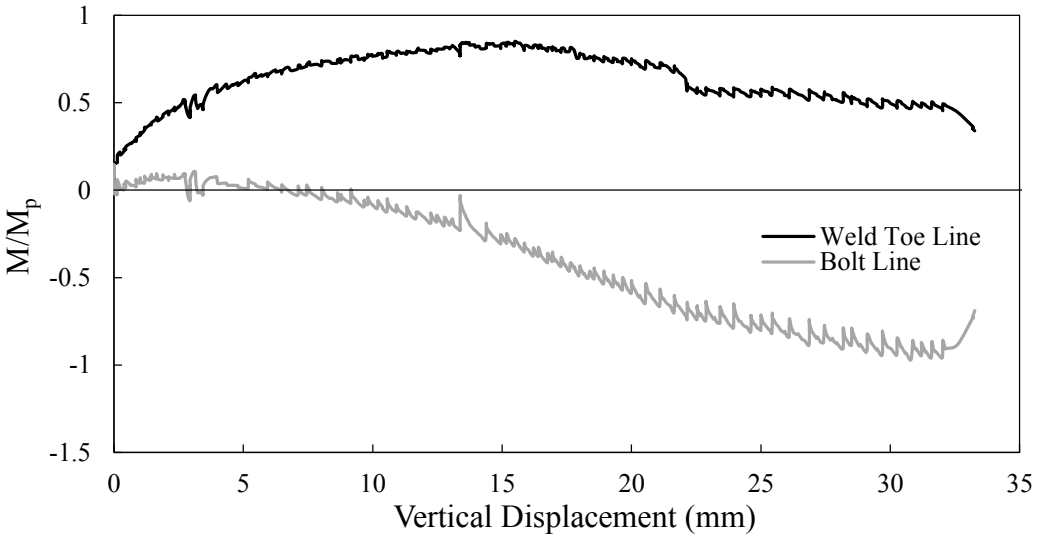

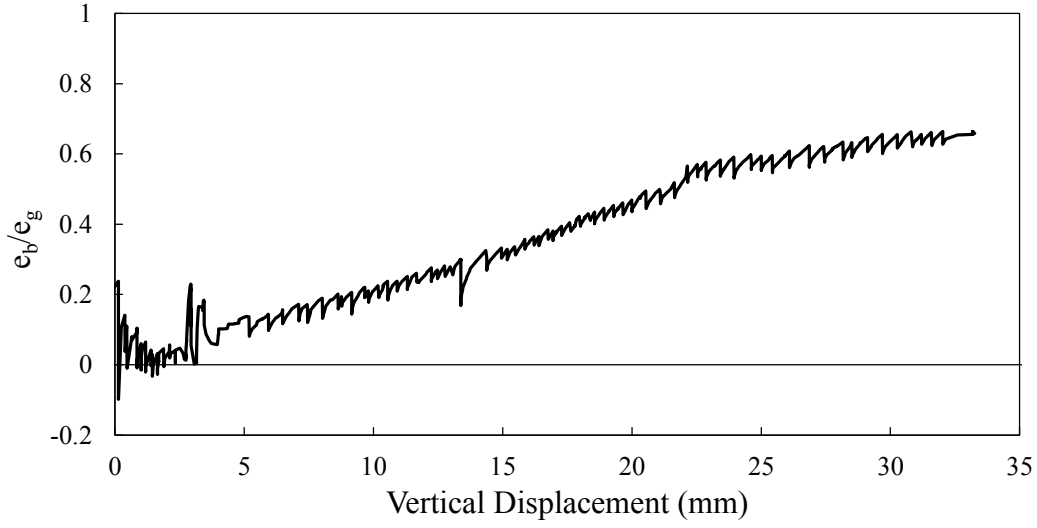

Figure B-17: Specimen 3BM-13-200C

Appendix C: Sample Finite Elements Analysis Response Curves for Extended Shear Tabs

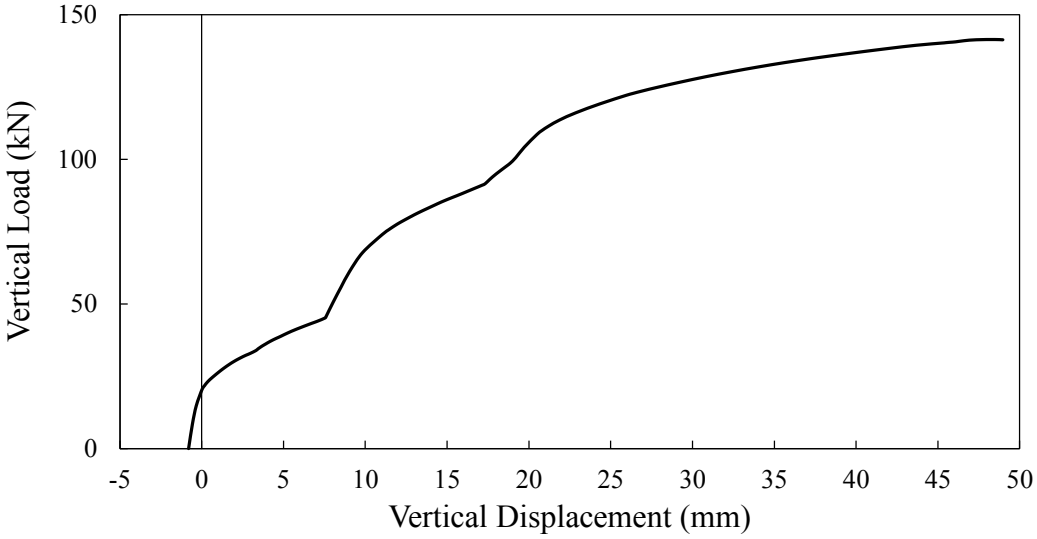

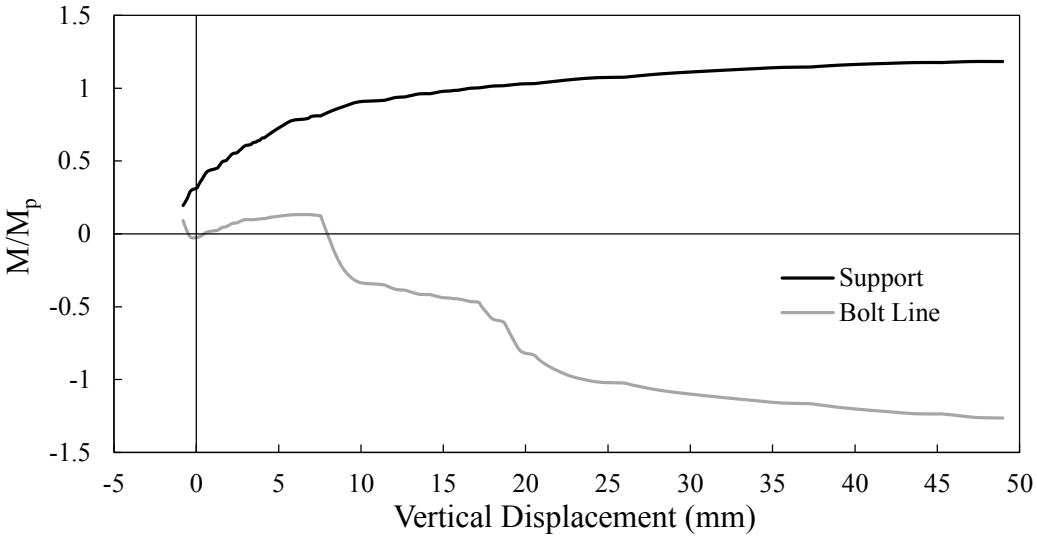

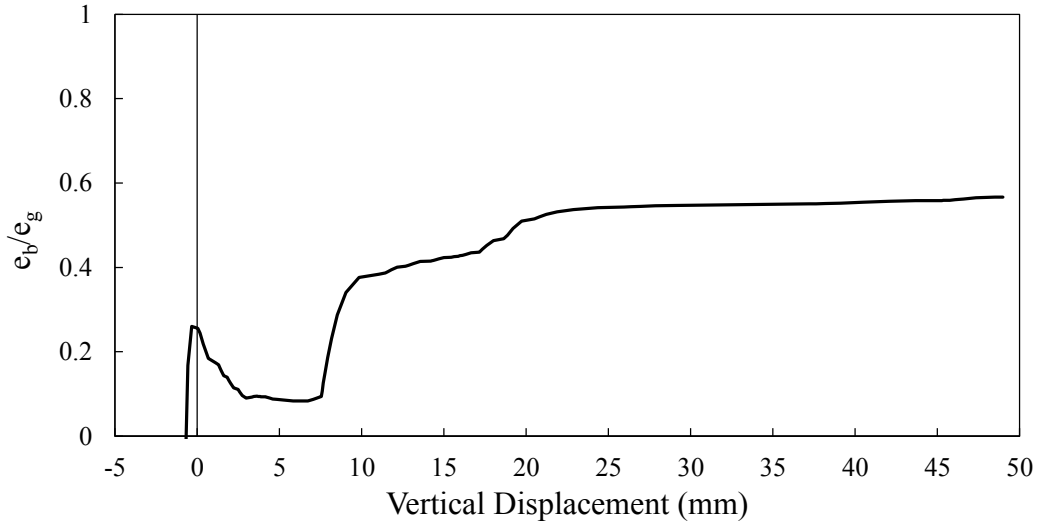

Figure C-1: Model 2BF-7

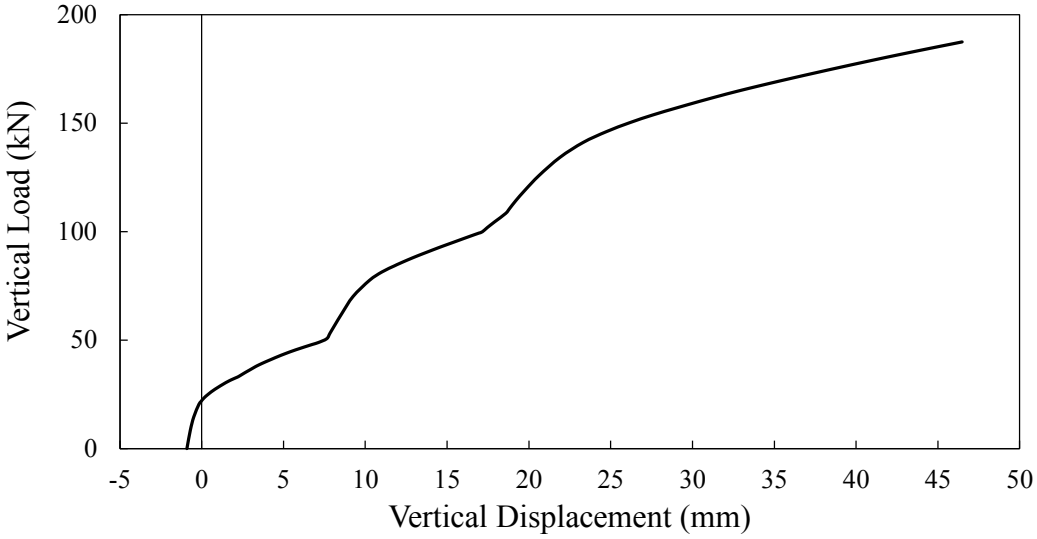

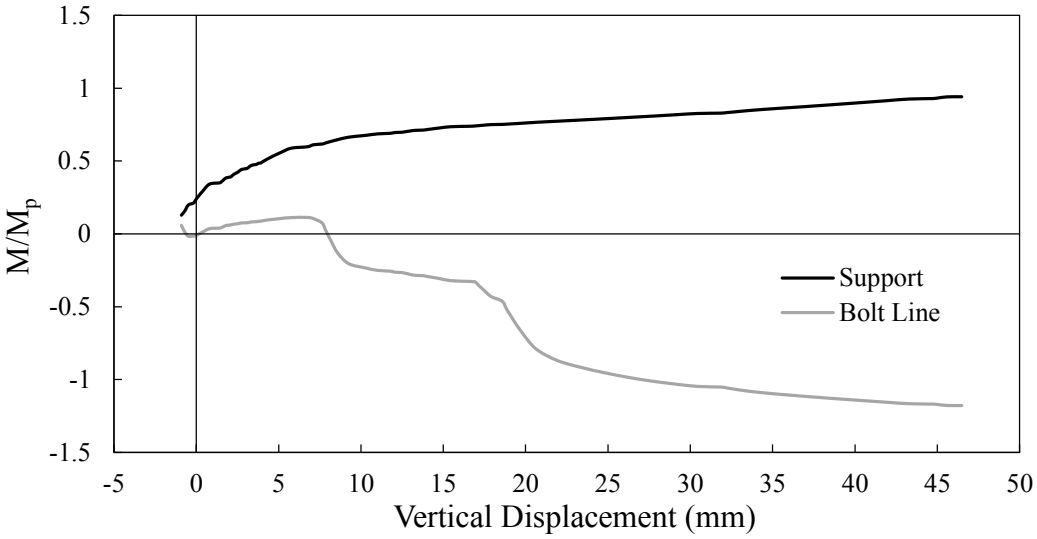

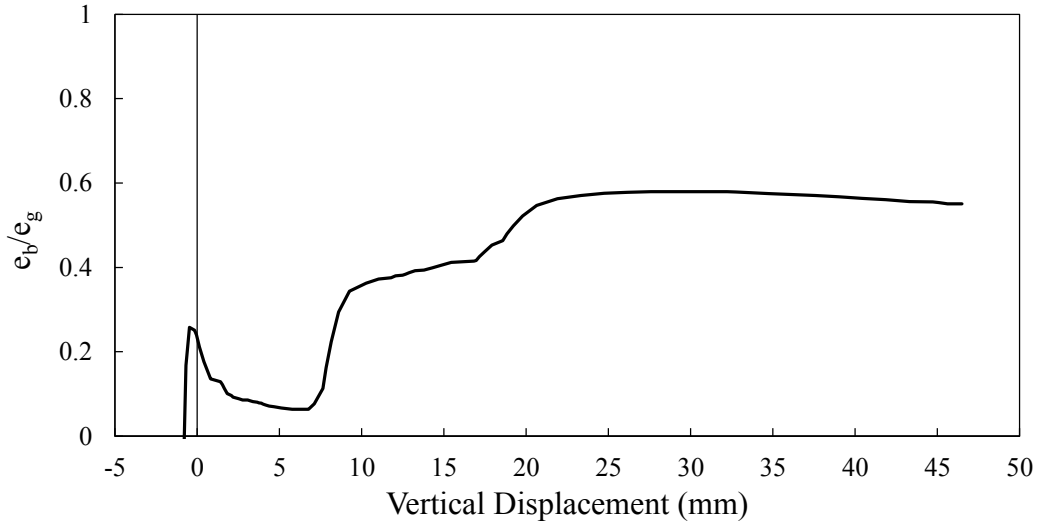

Figure C-2: Model 2BF-10

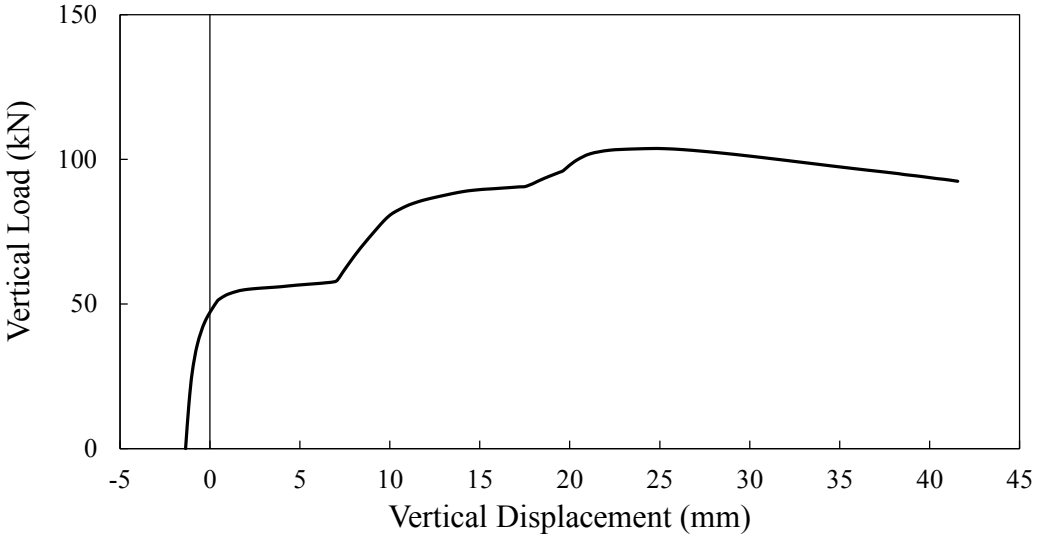

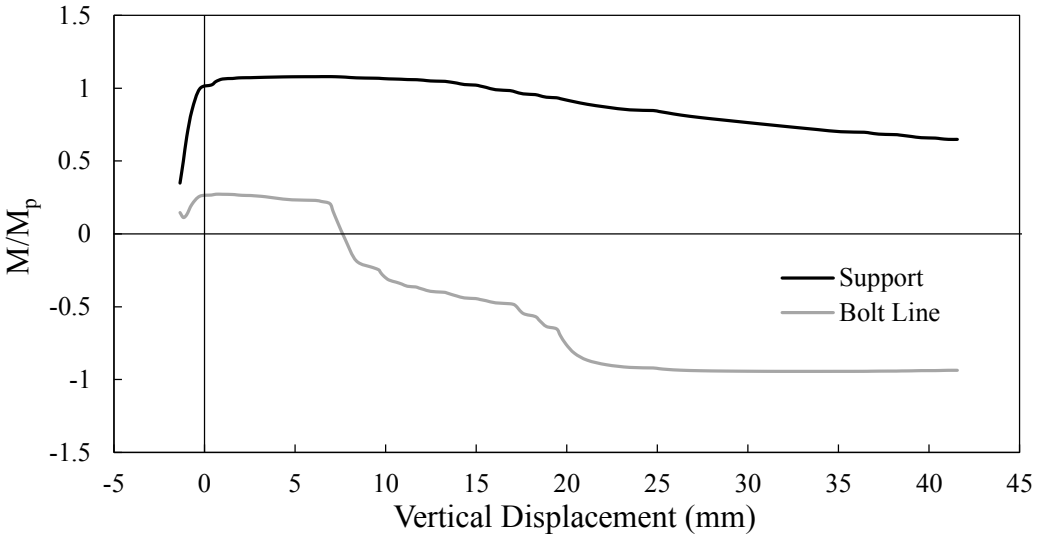

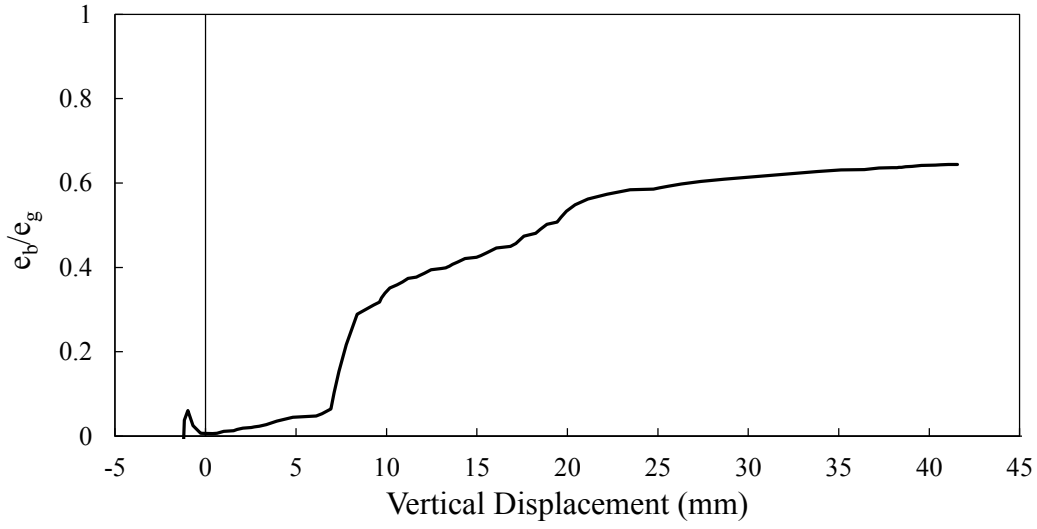

Figure C-3: Model 2BS-7

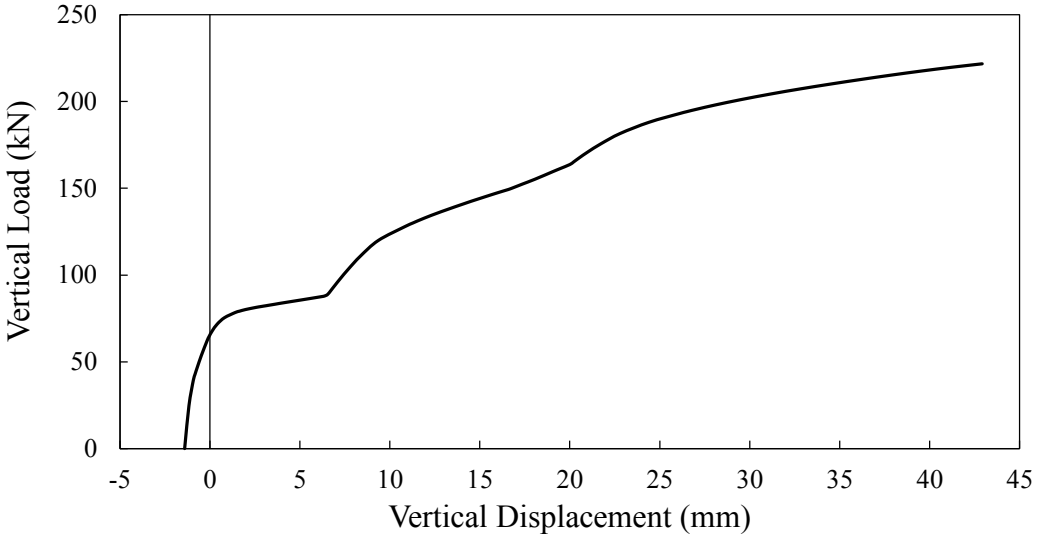

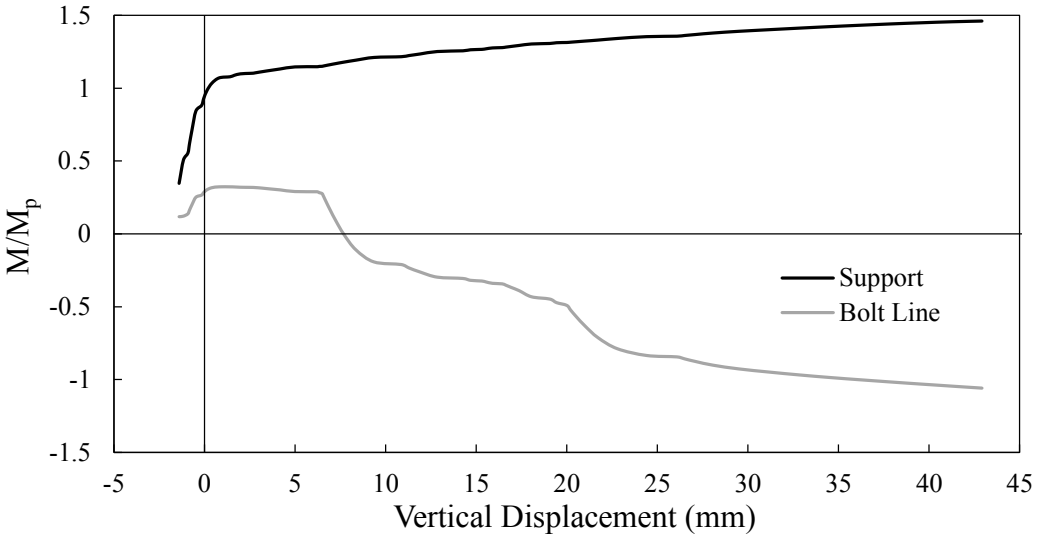

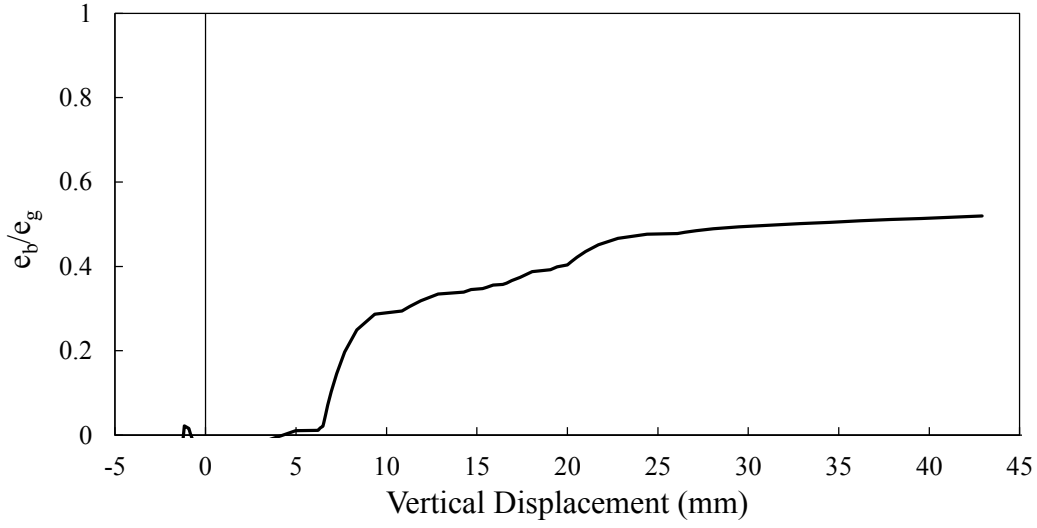

Figure C-4: Model 2BS-10

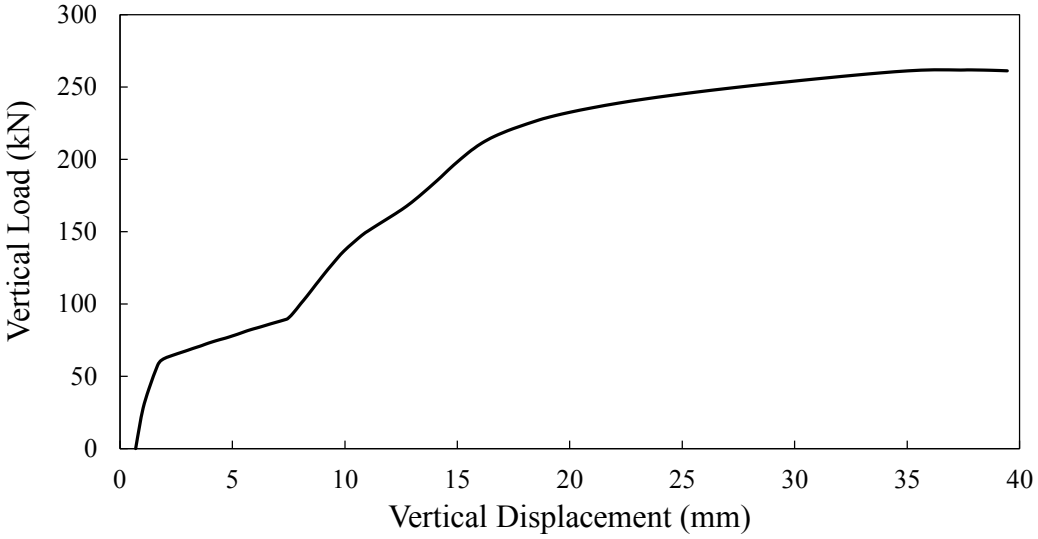

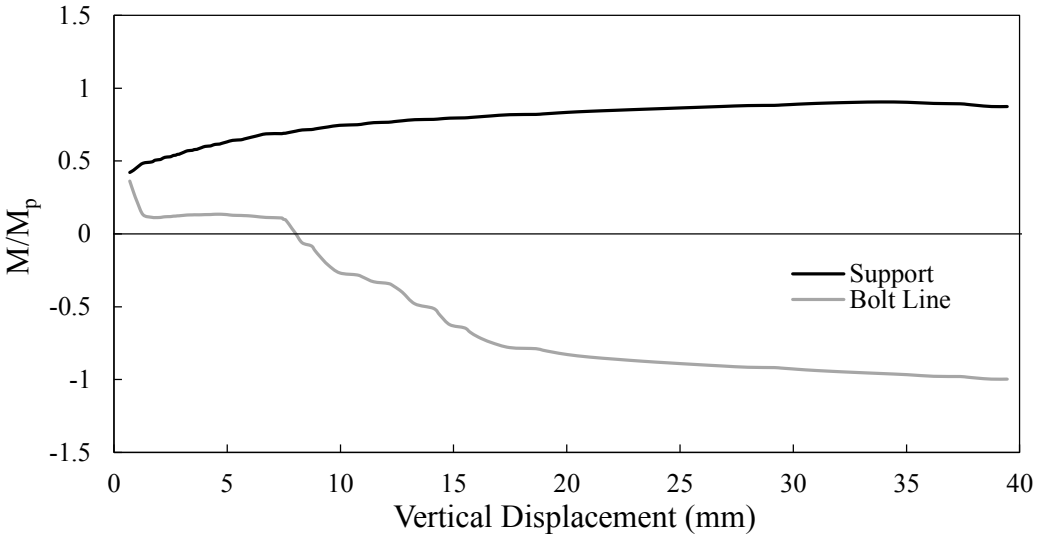

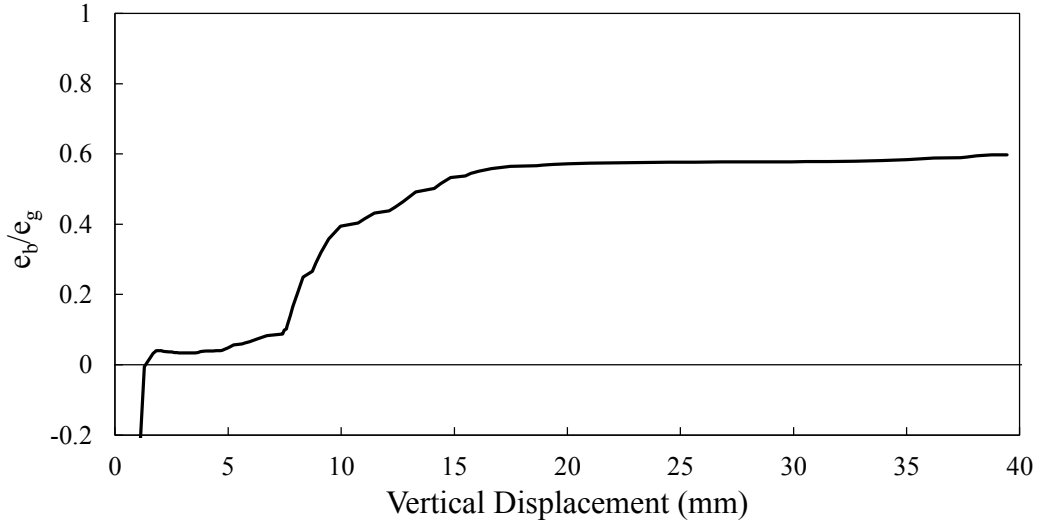

Figure C-5: Model 3BF-10

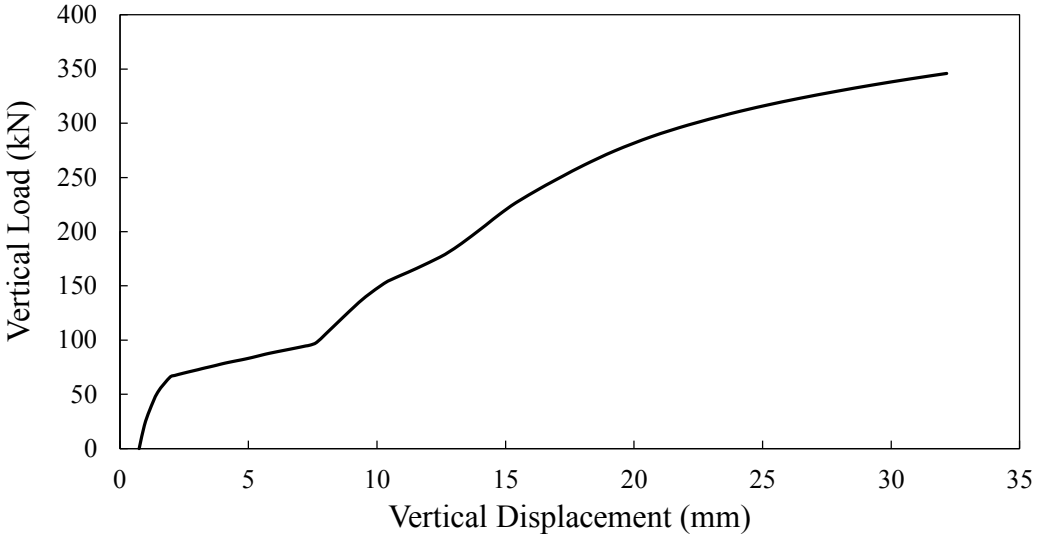

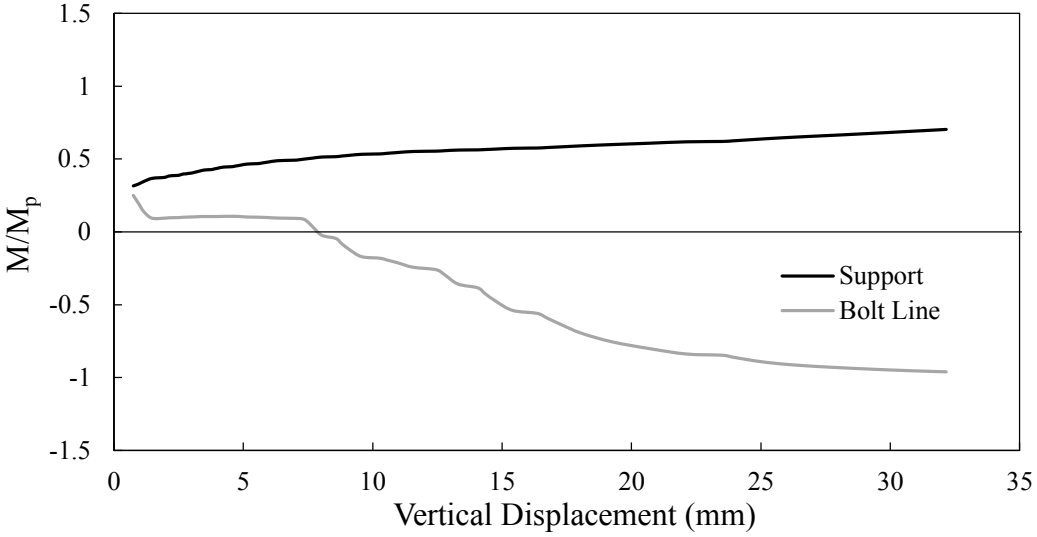

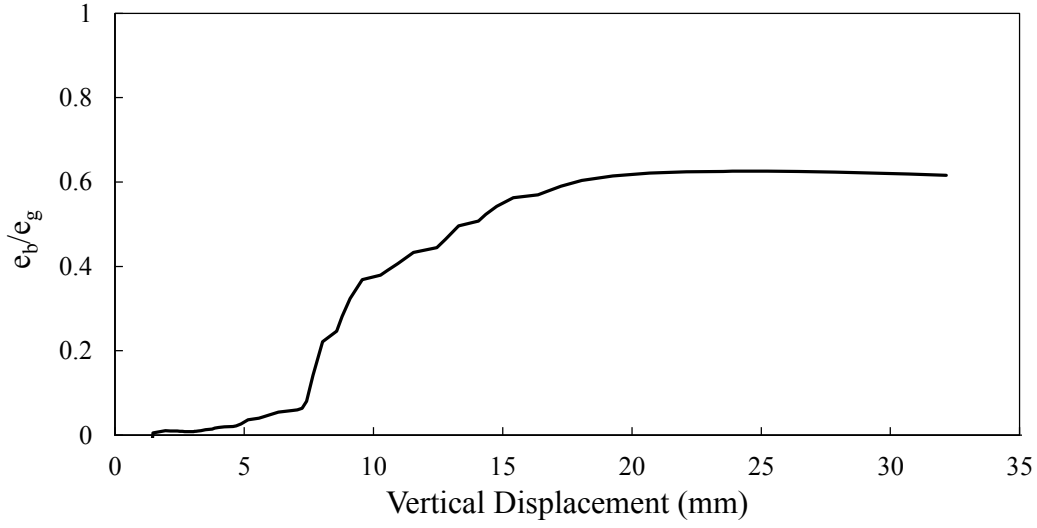

Figure C-6: Model 3BF-10

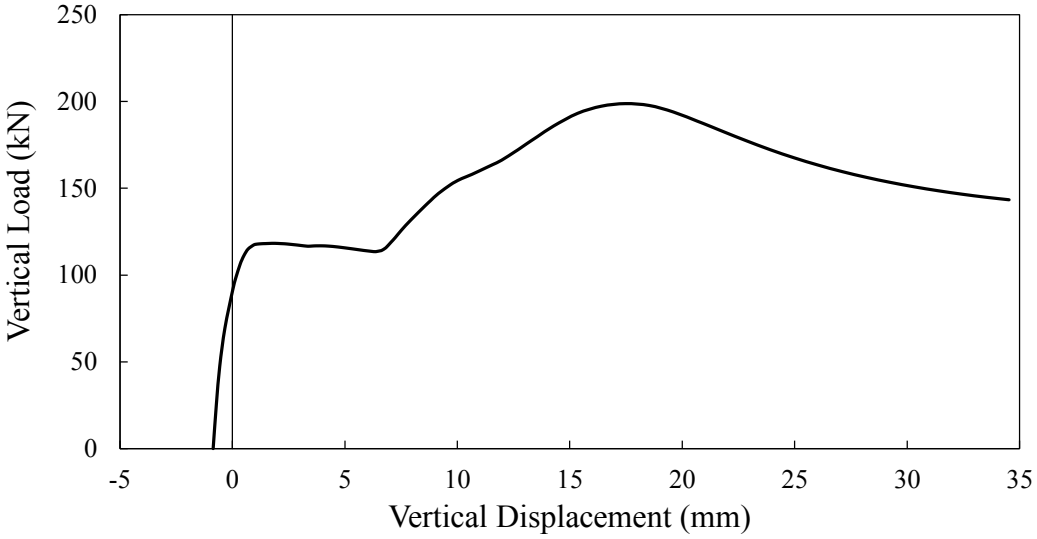

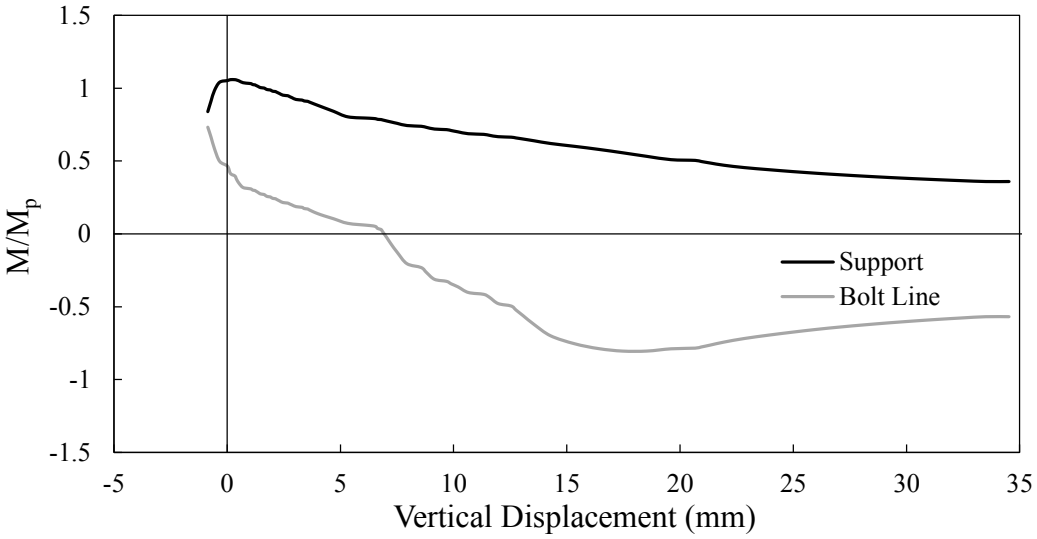

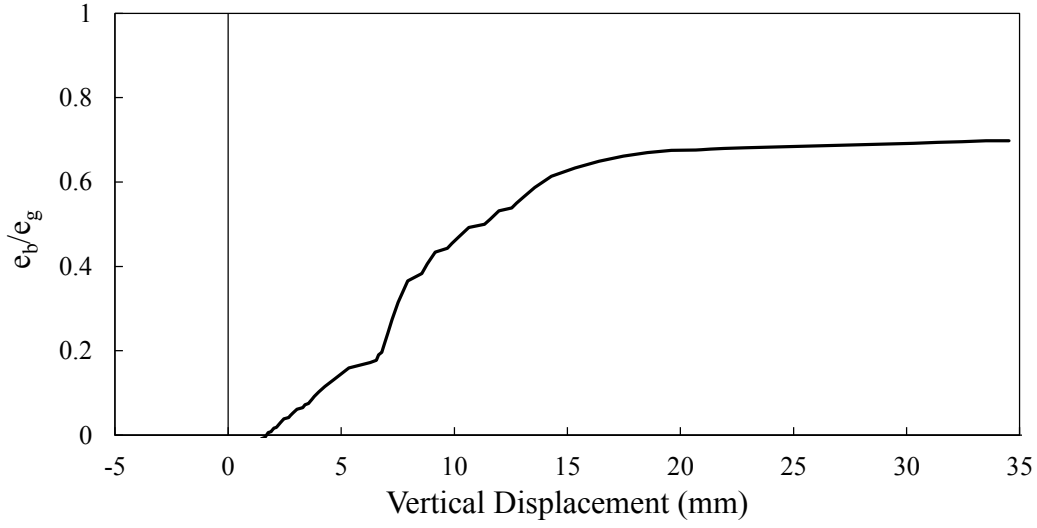

Figure C-7: Model 3BS-7

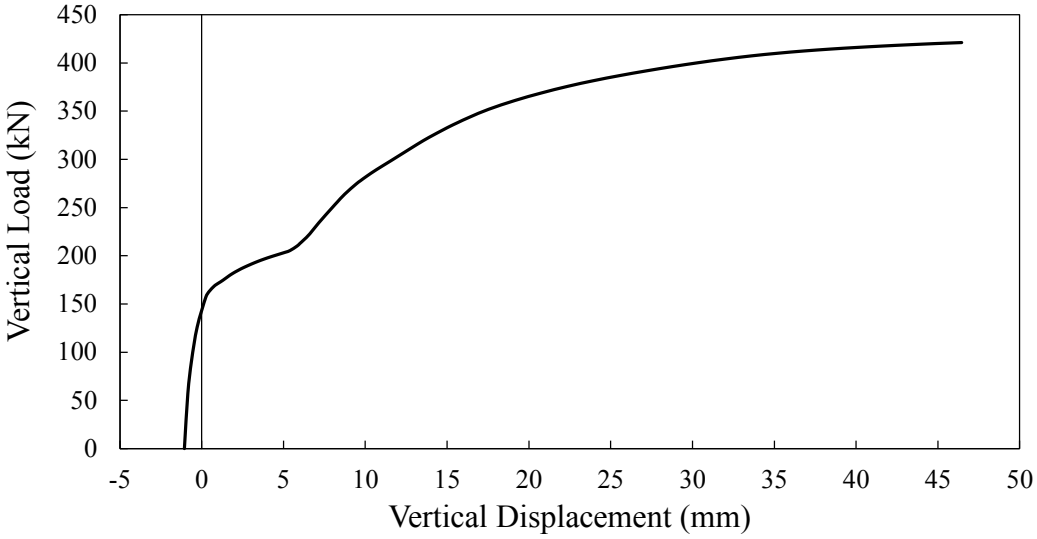

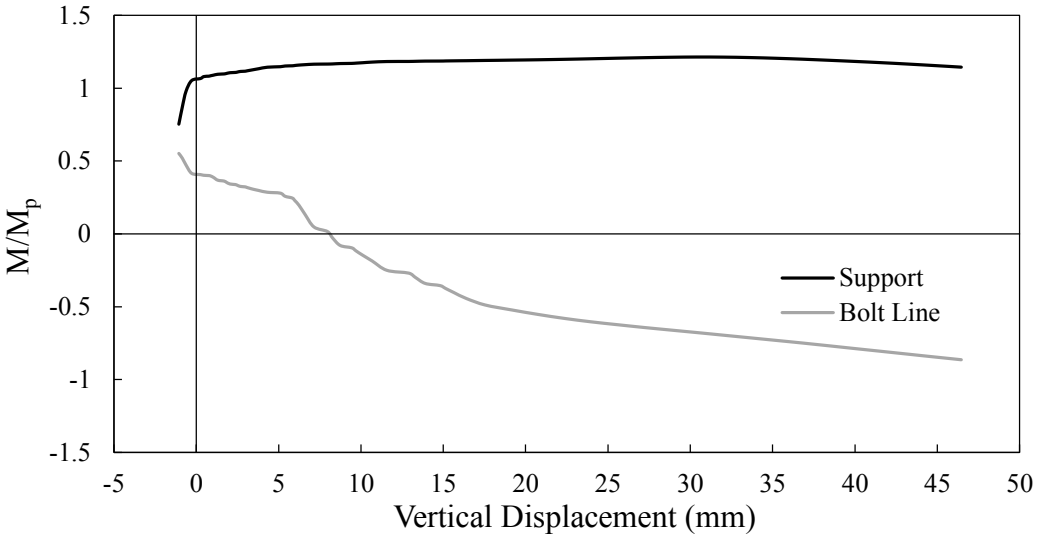

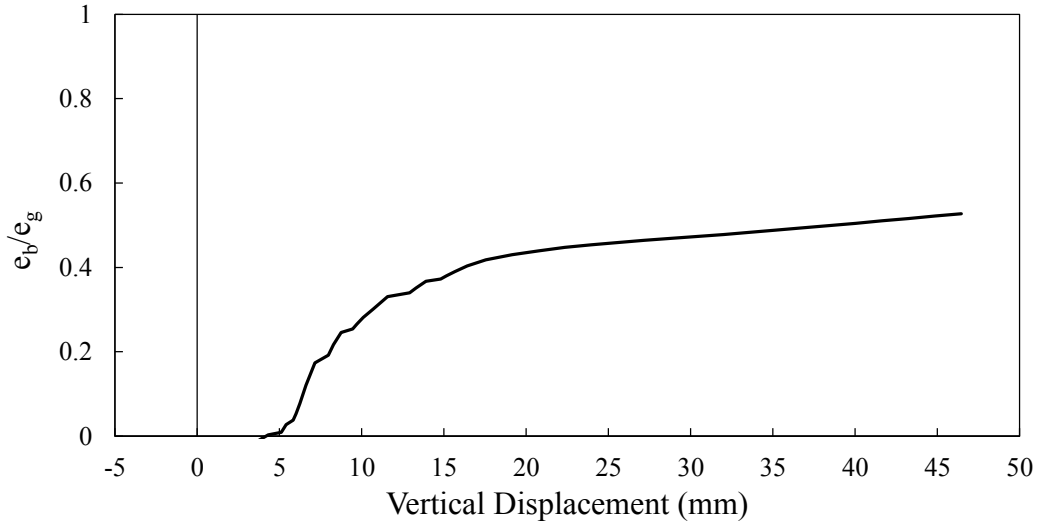

Figure C-8: Model 3BS-10

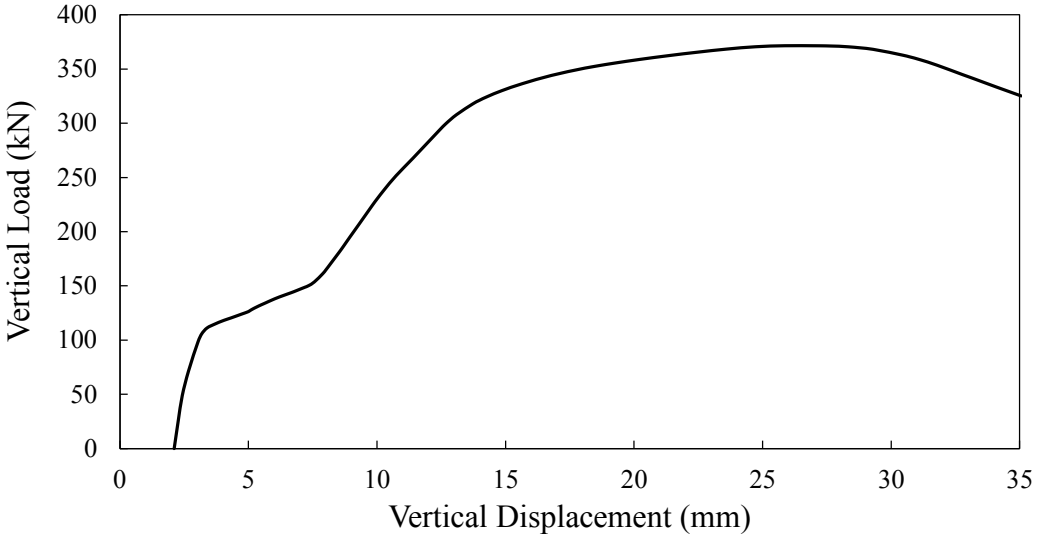

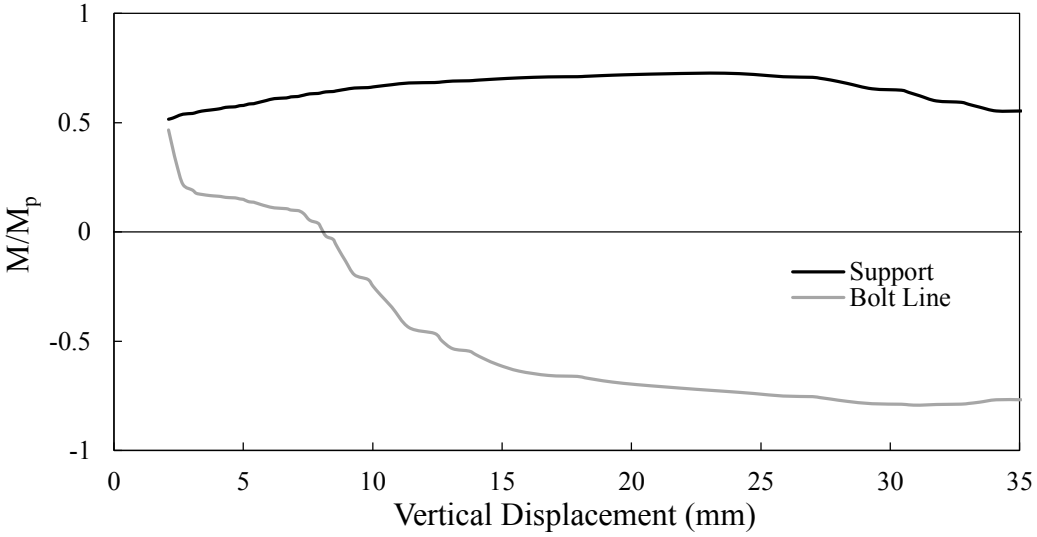

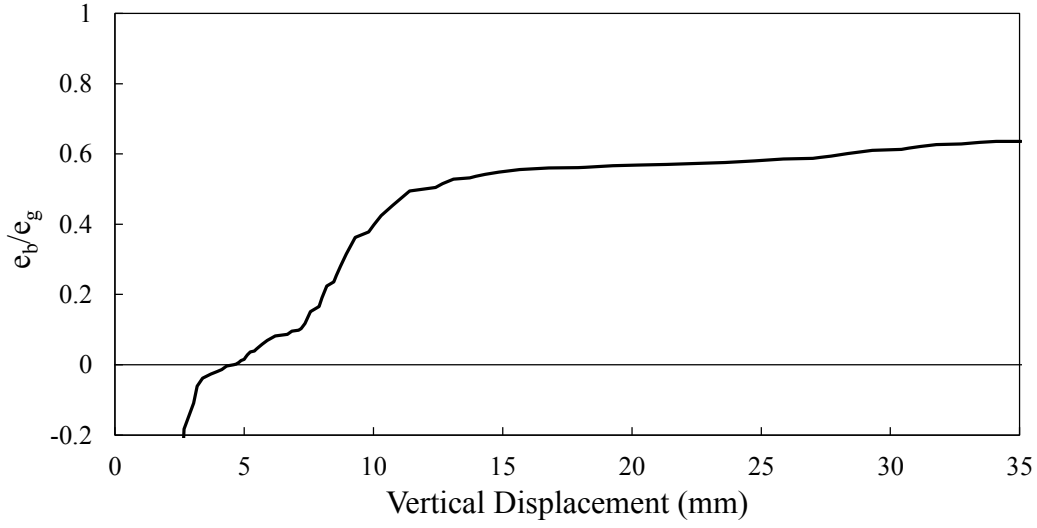

Figure C-9: Model 4BF-7

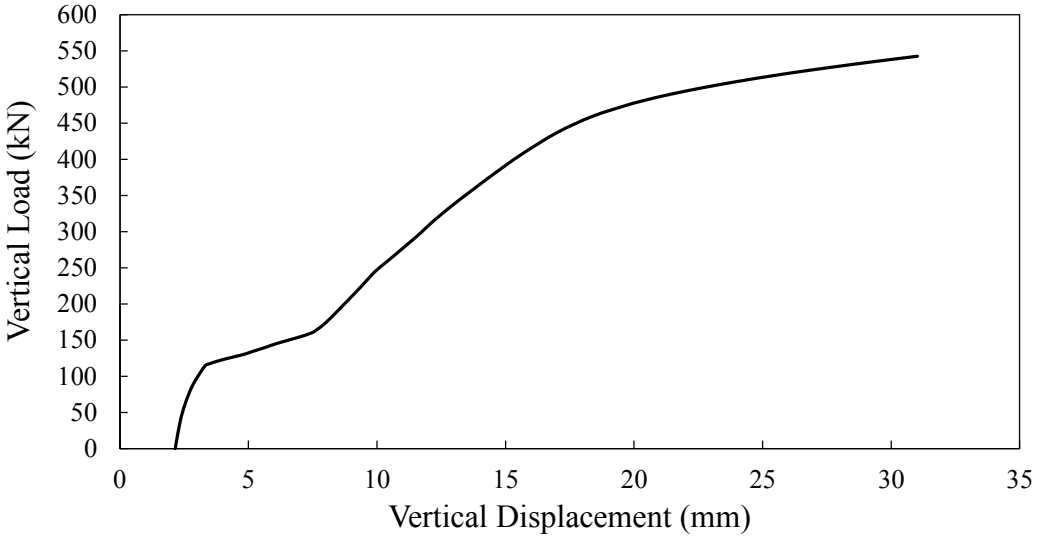

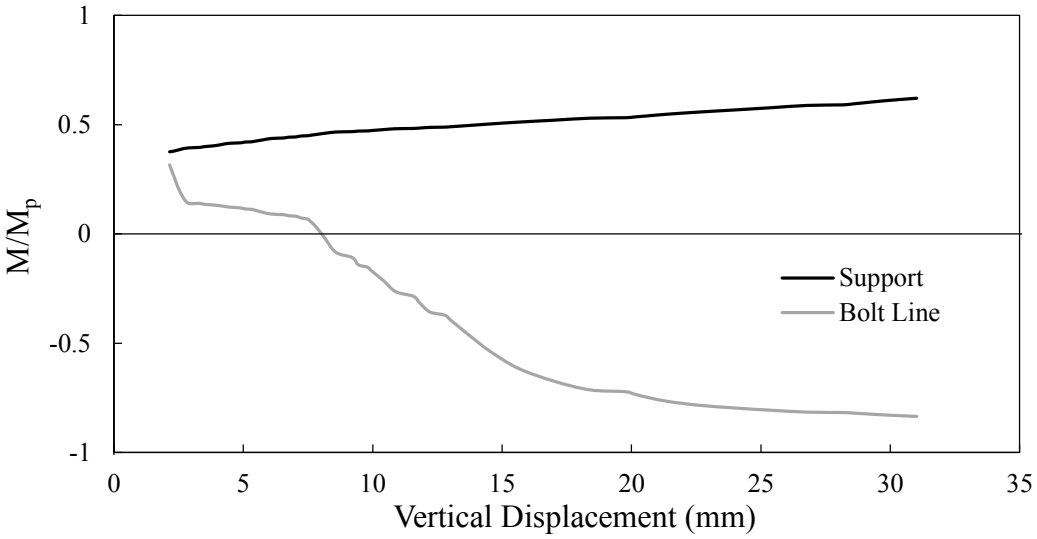

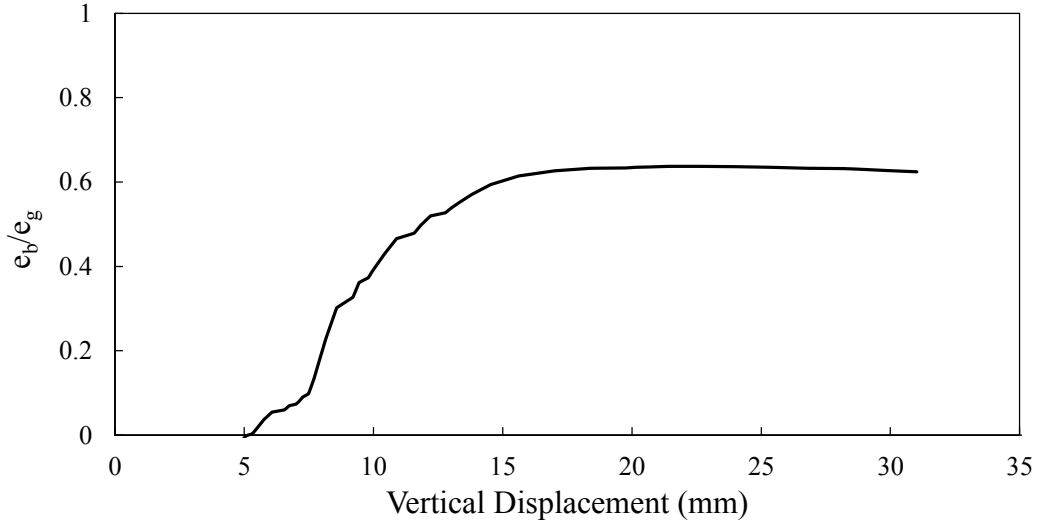

Figure C-10: Model 4BF-10

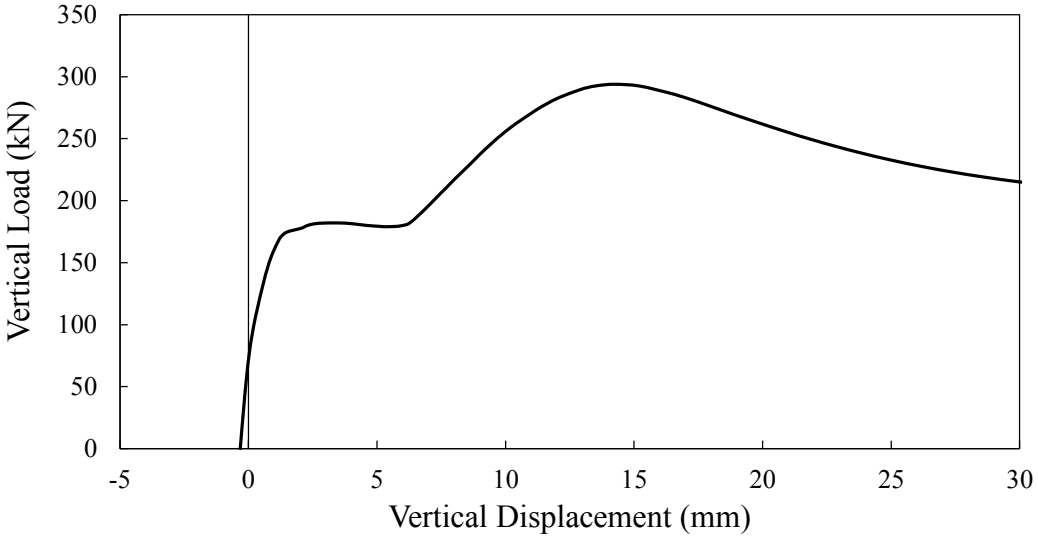

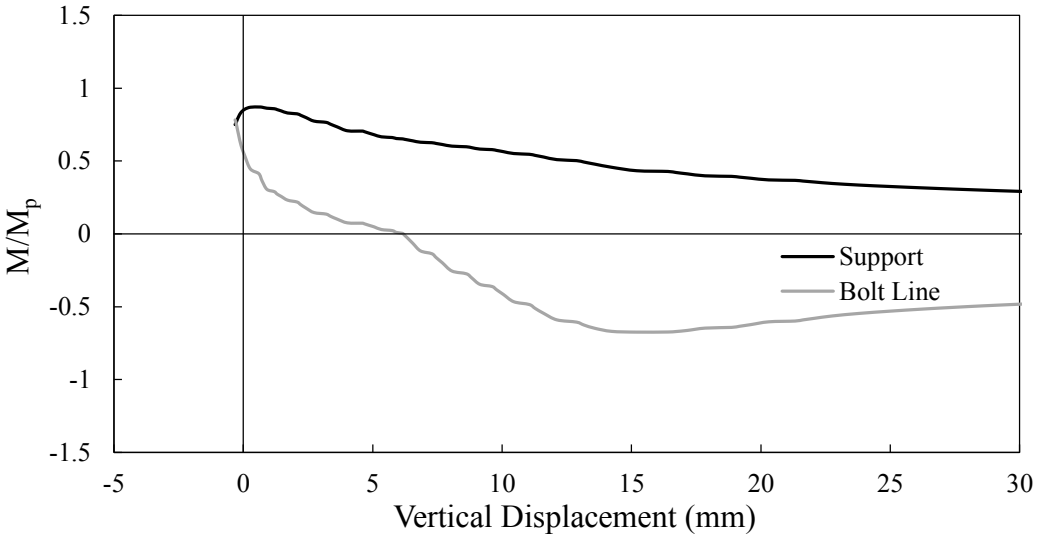

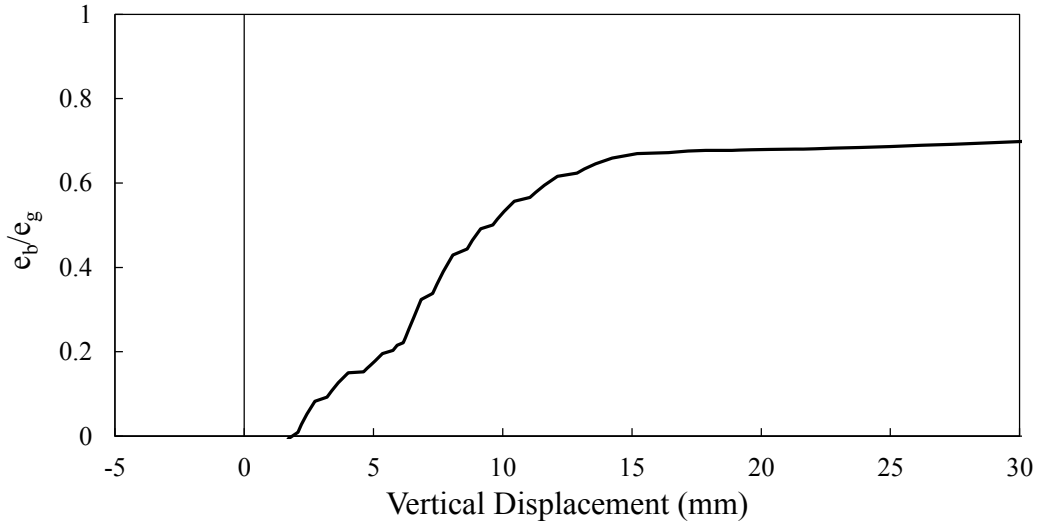

Figure C-11: Model 4BS-7

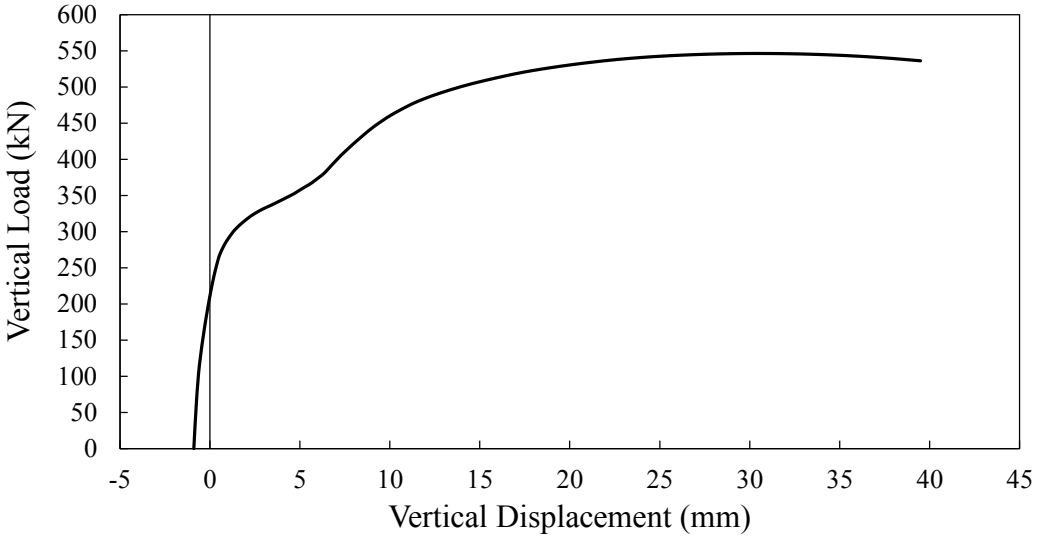

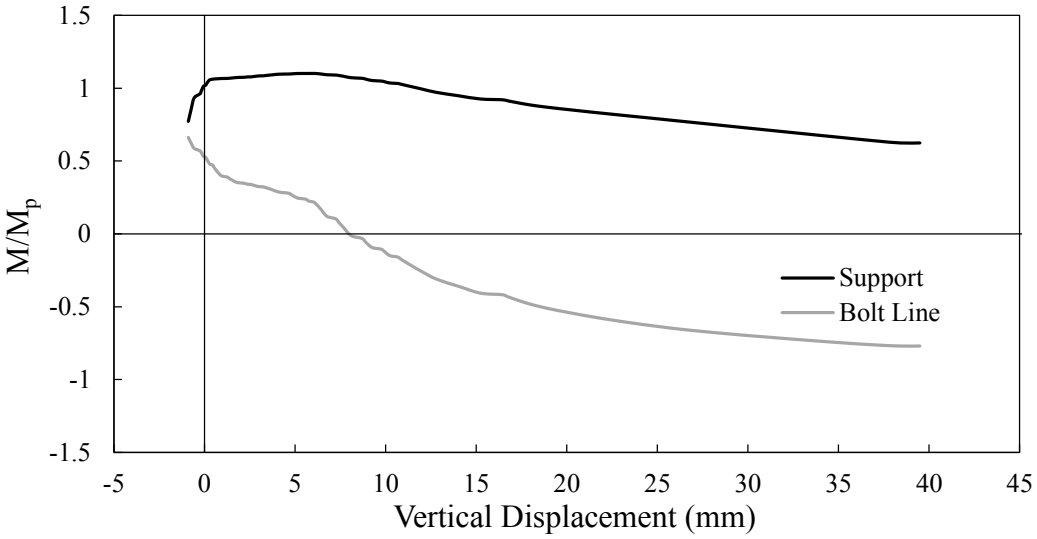

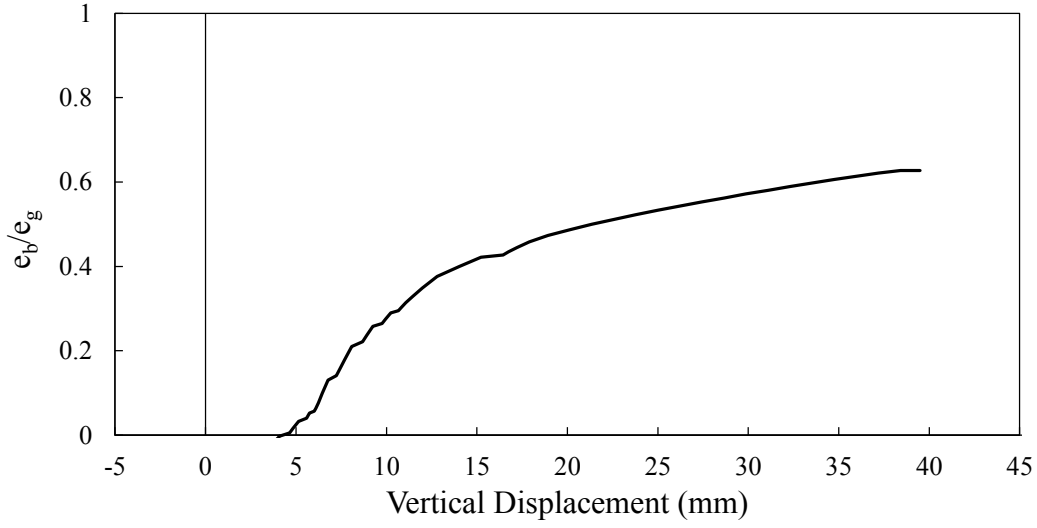

Figure C-12: Model 4BS-10

Appendix D: Sample Finite Elements Analysis Response Curves for Double-Coped Beams

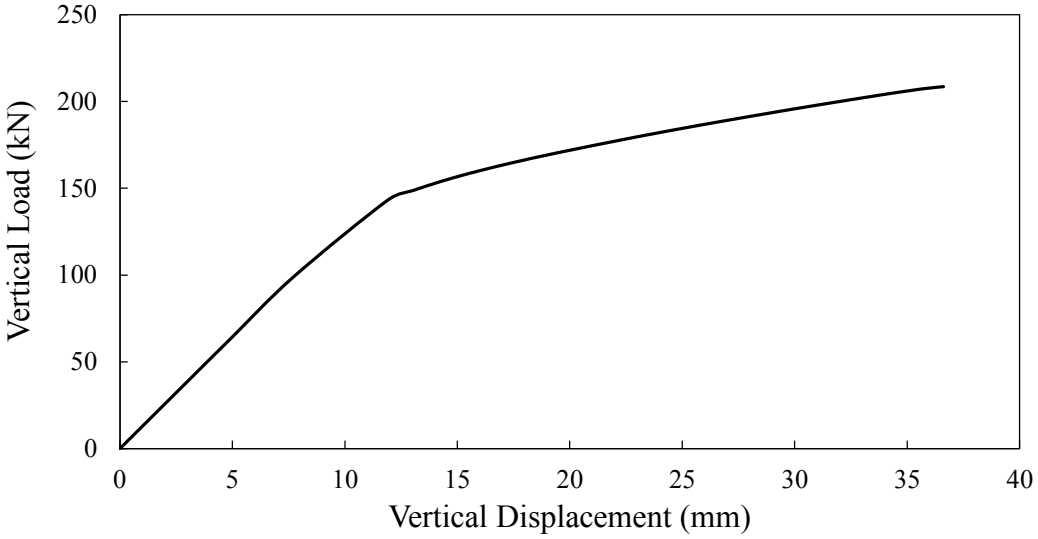

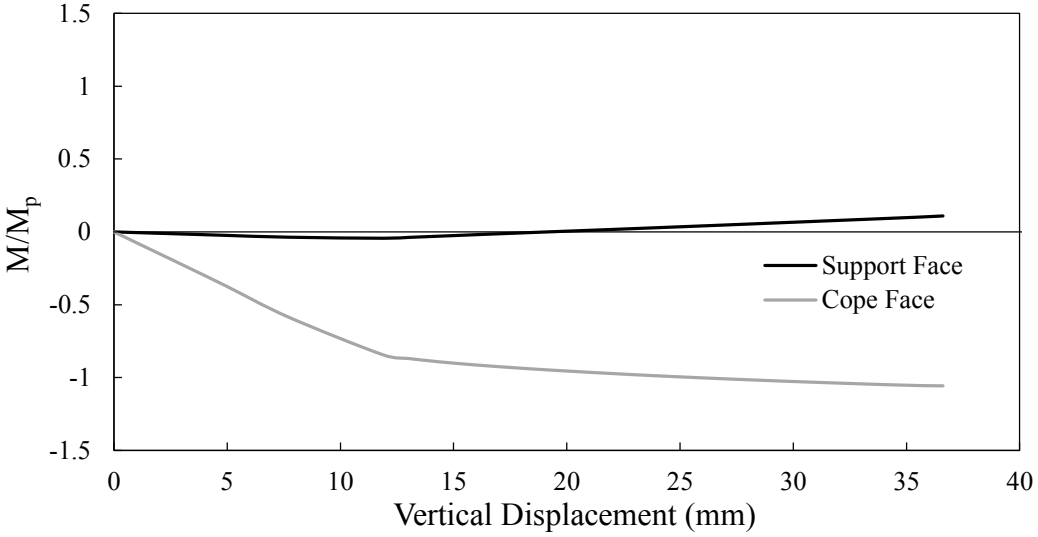

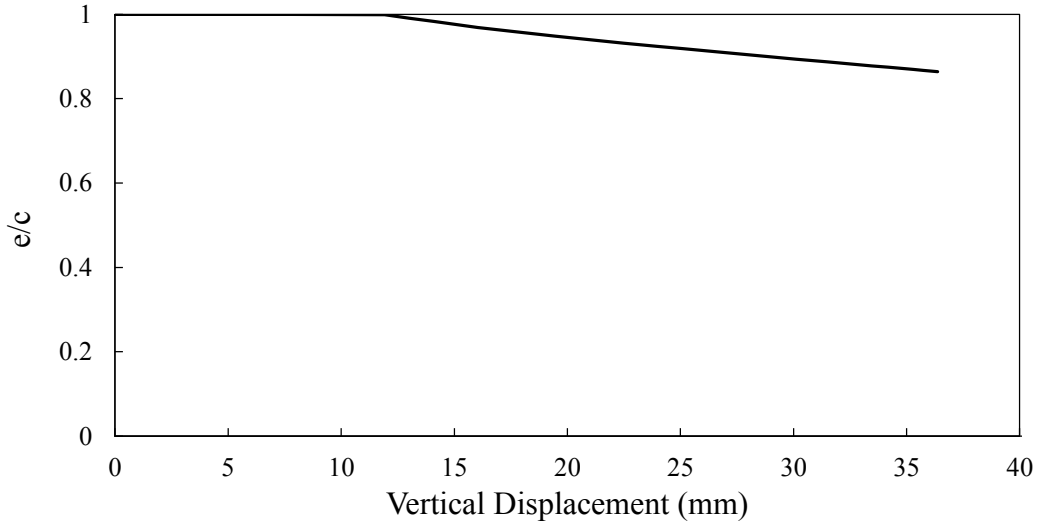

Figure D-1: Model h1-c1-t1-F

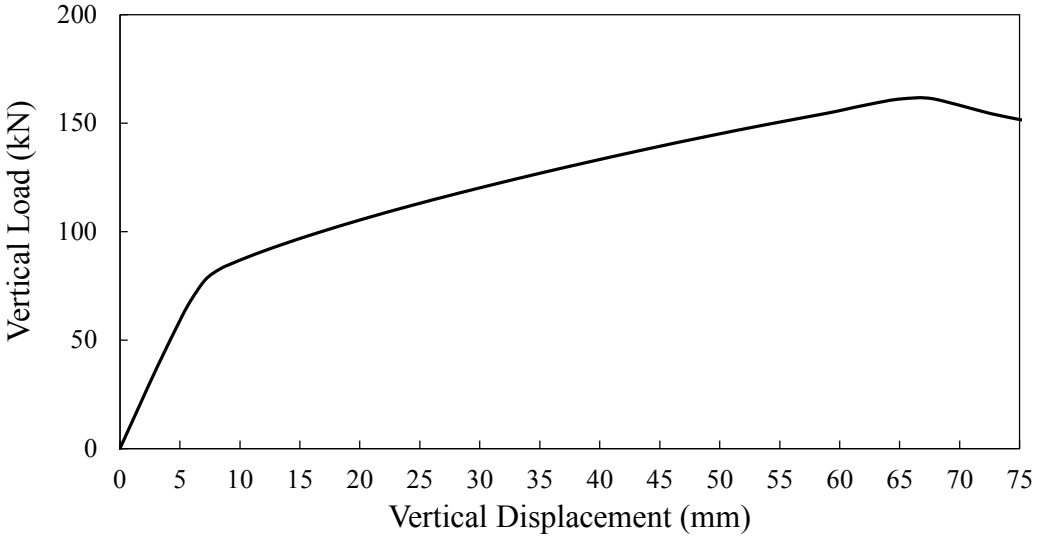

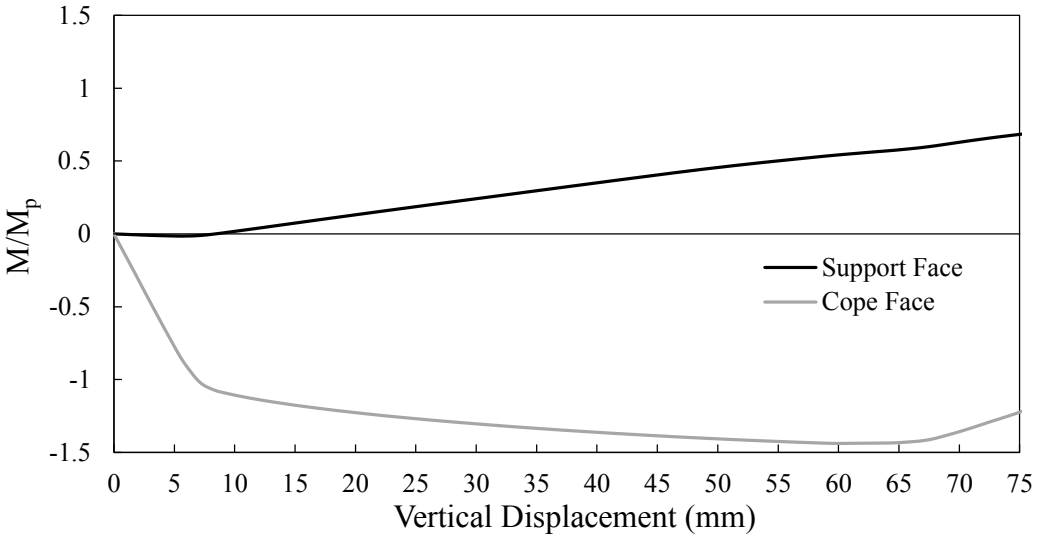

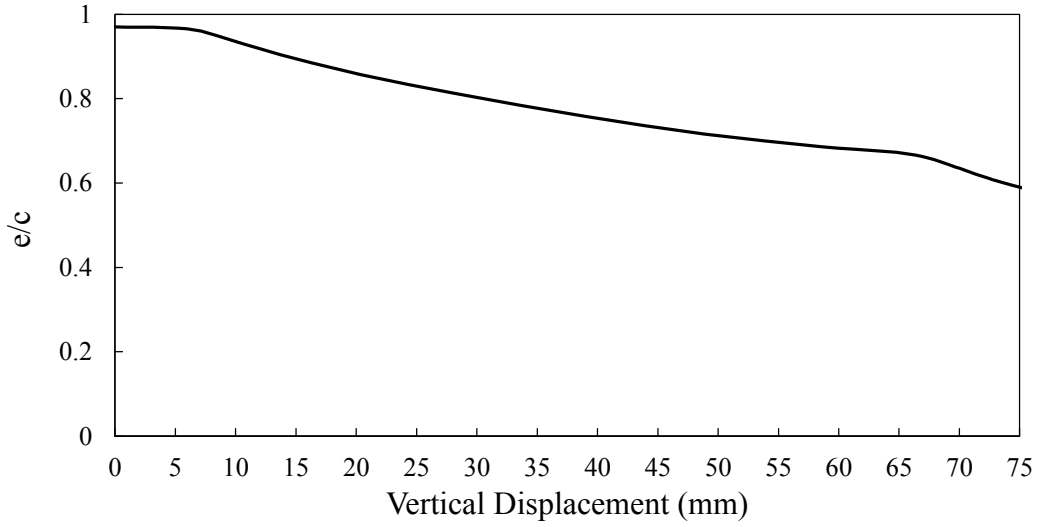

Figure D-2: Model h1-c2-t1-F

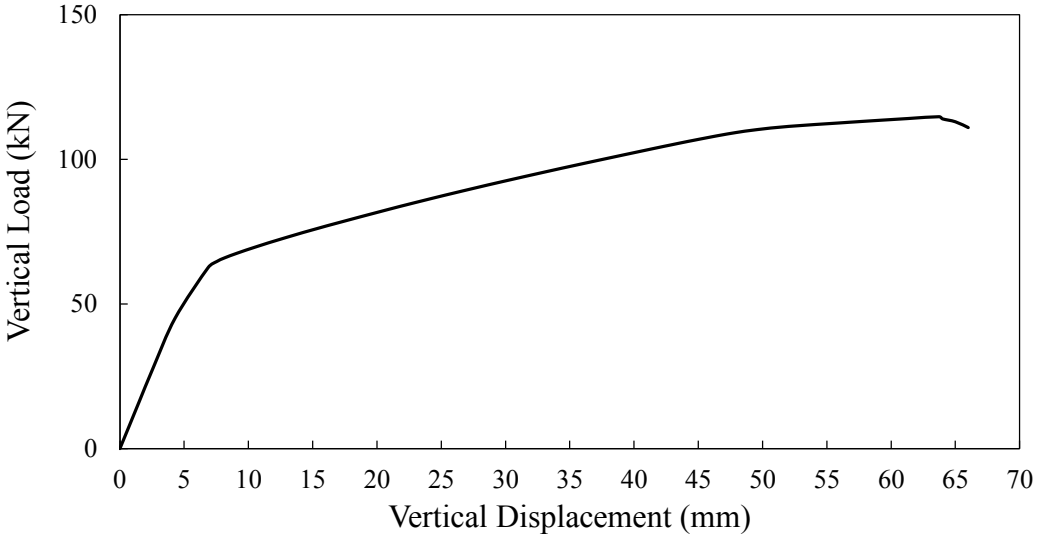

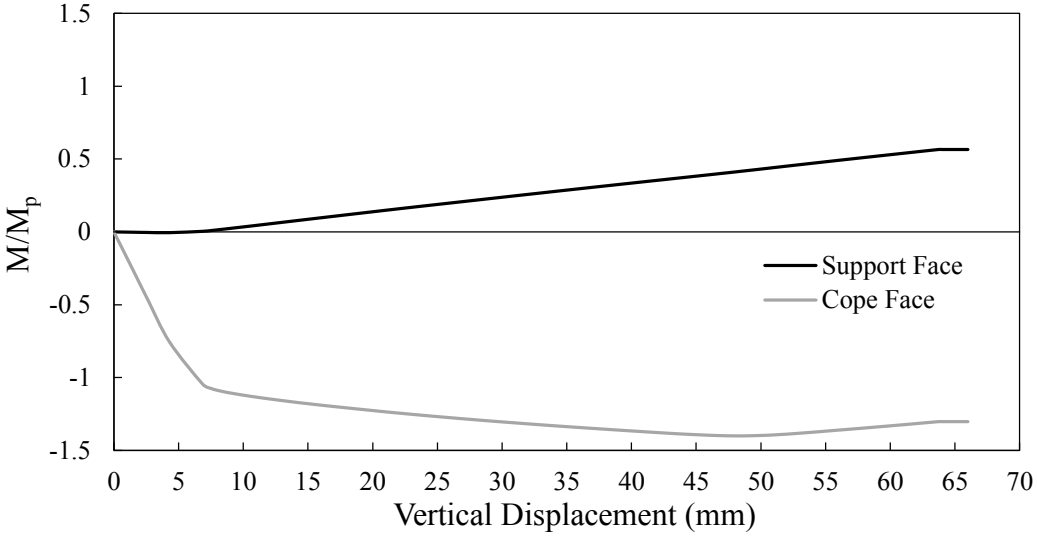

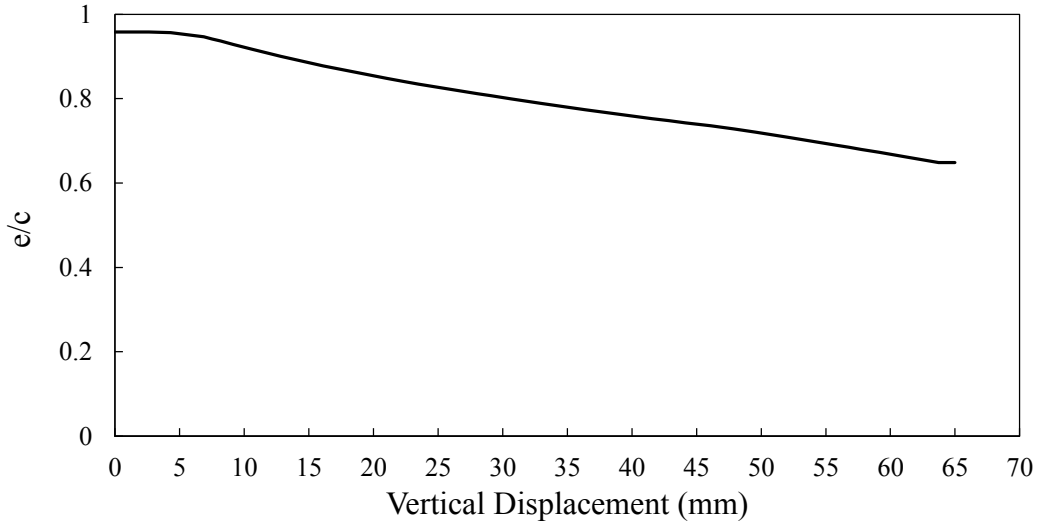

Figure D-3: Model h1-c3-t1-F

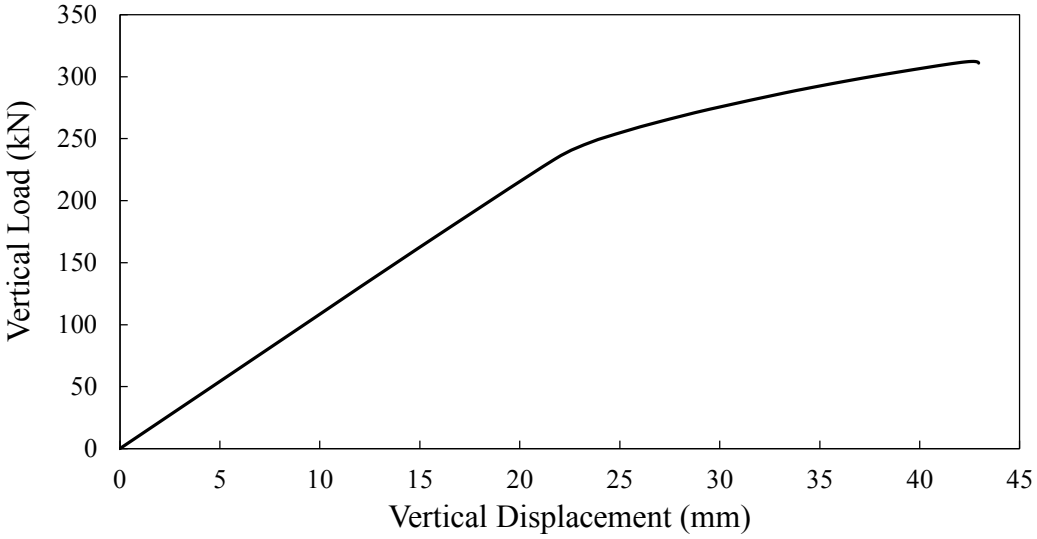

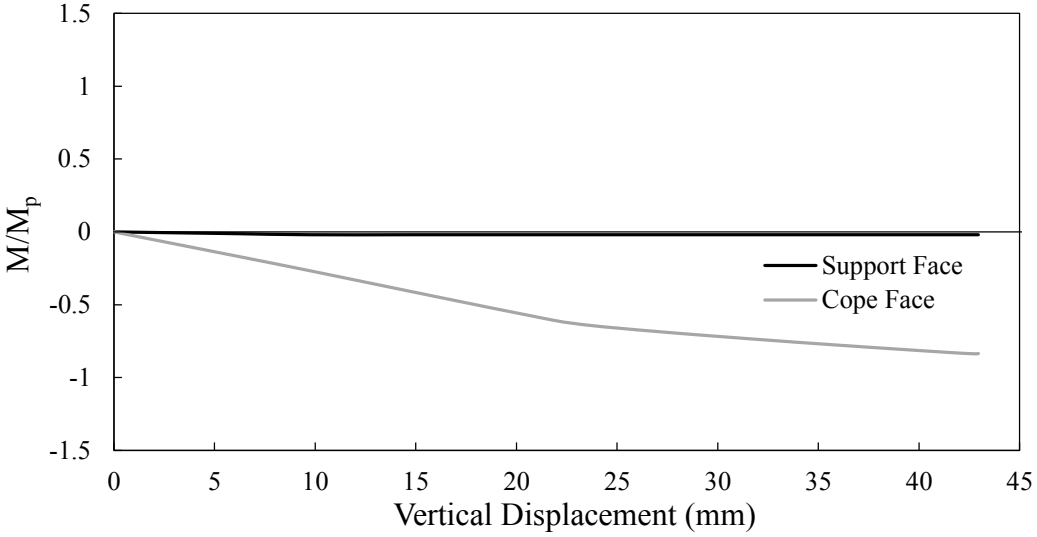

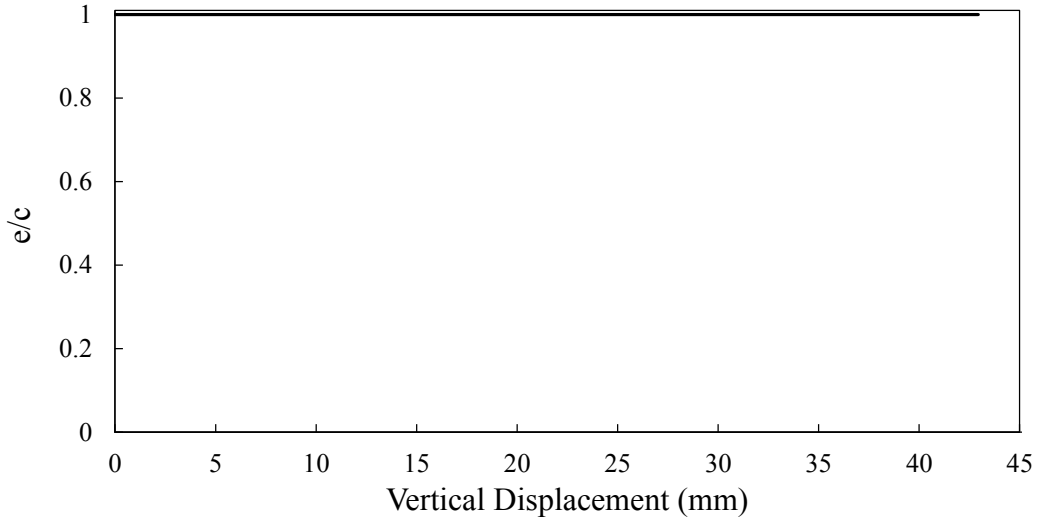

Figure D-4: Model h2-c1-t1-F

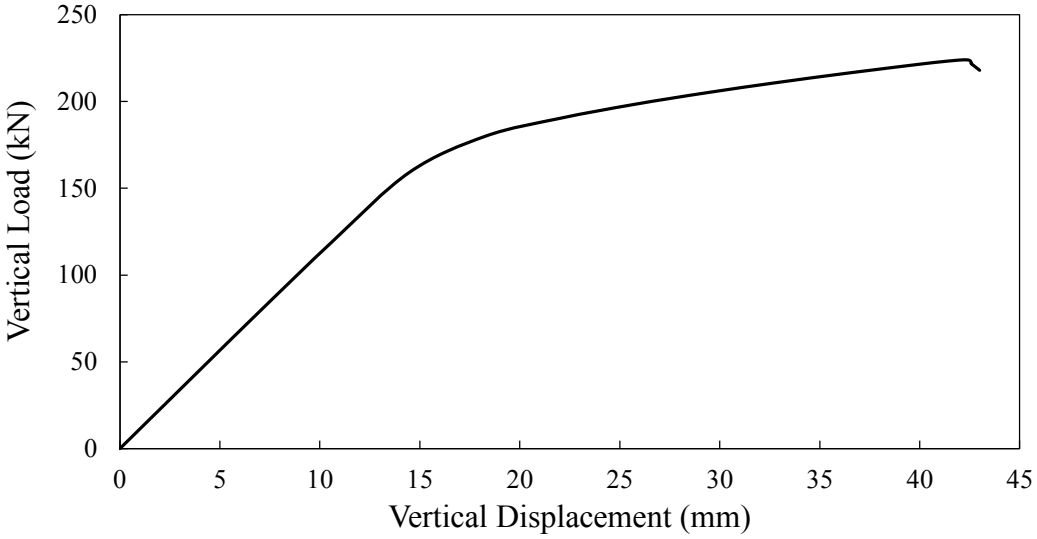

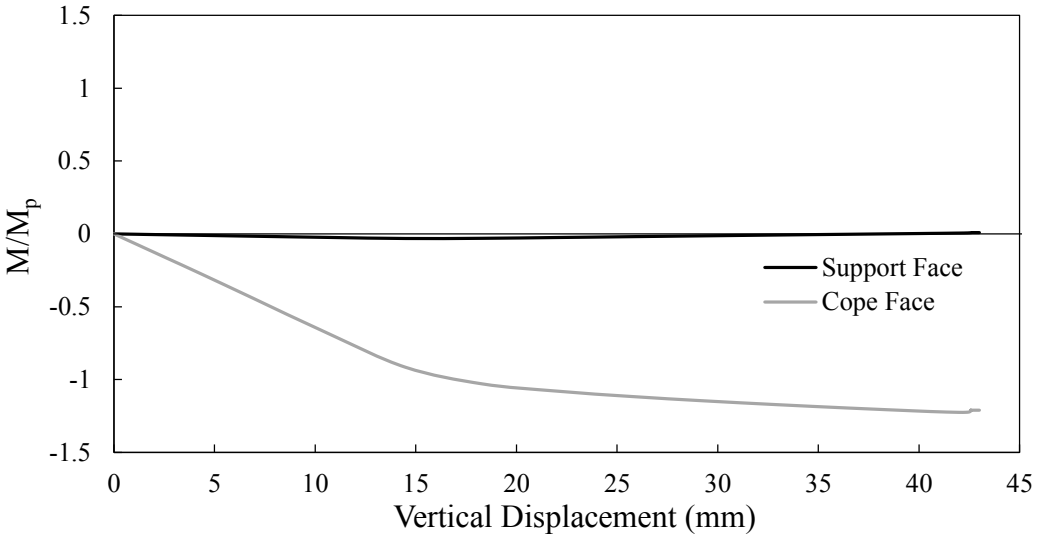

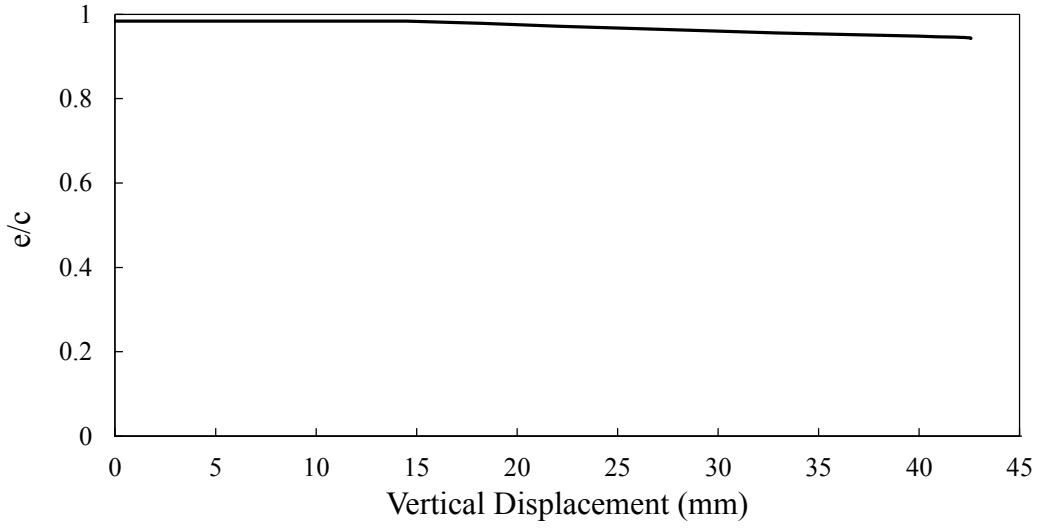

Figure D-5: Model h2-c2-t1-F

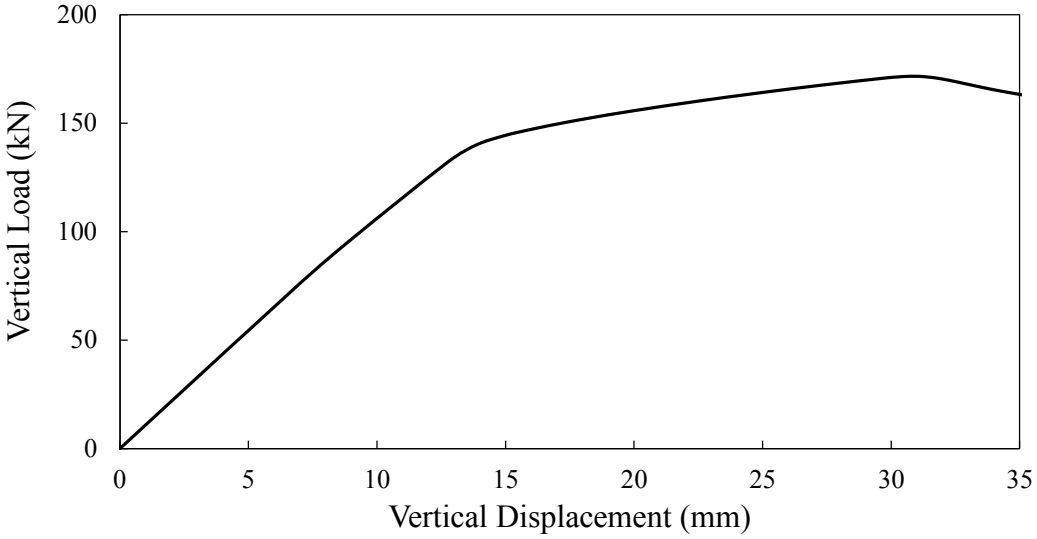

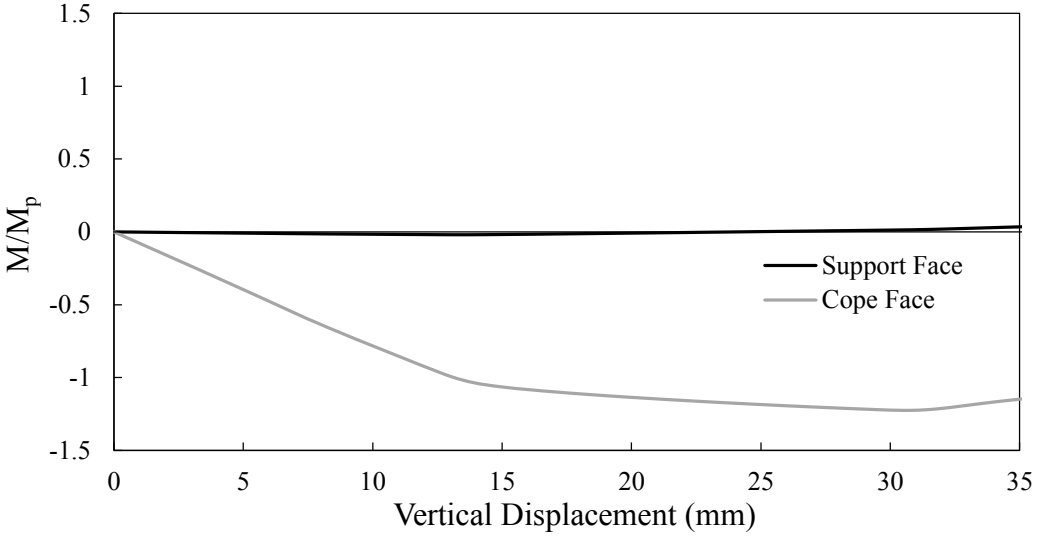

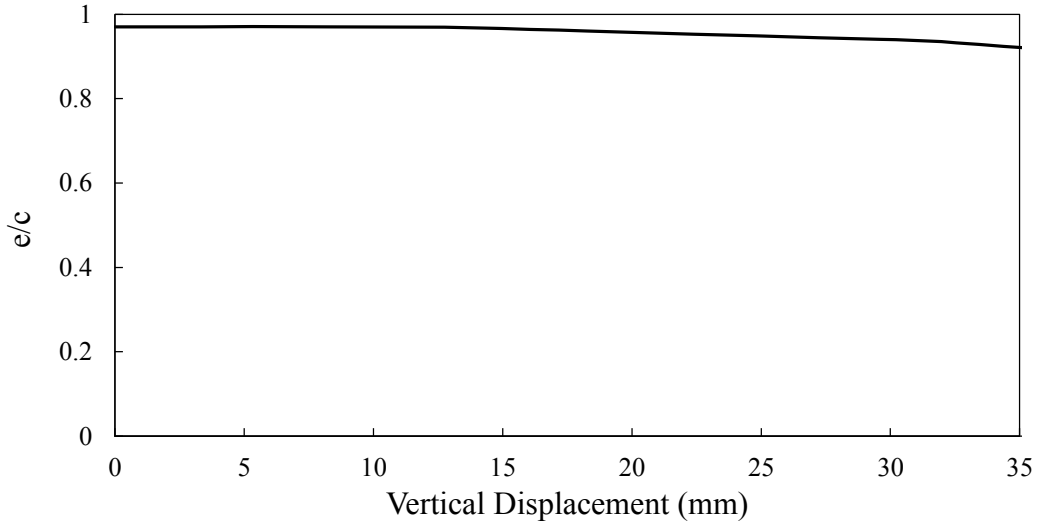

Figure D-6: Model h2-c3-t1-F

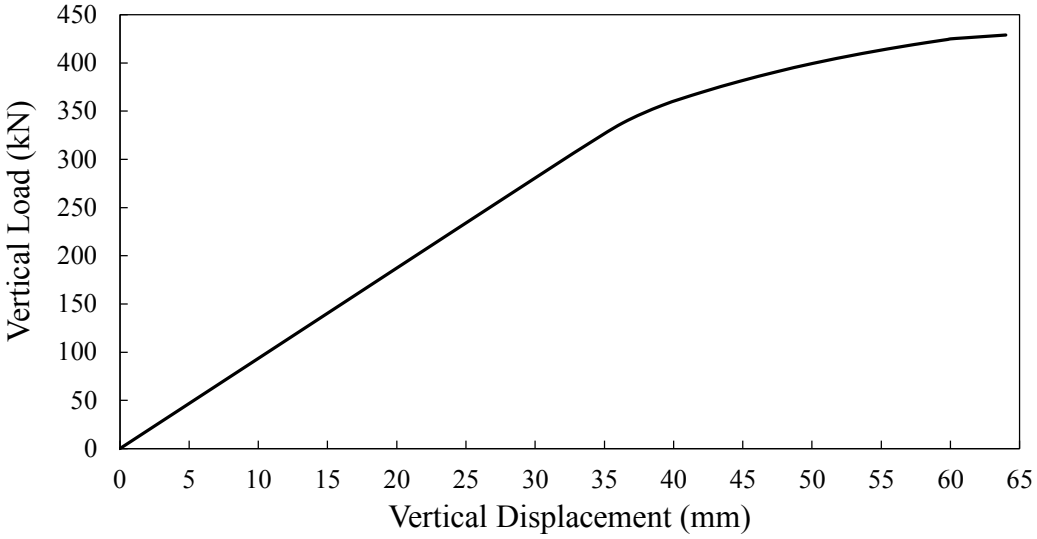

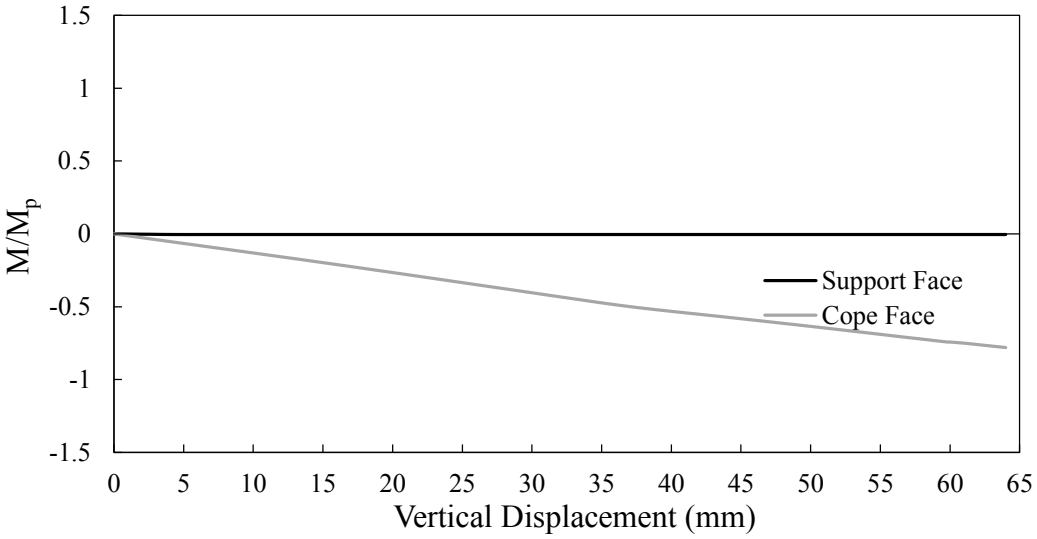

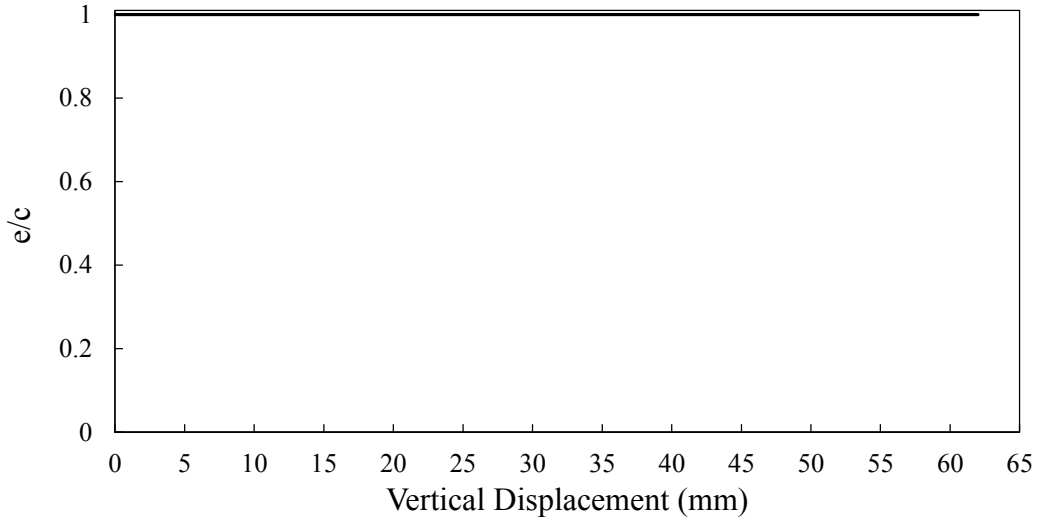

Figure D-7: Model h3-c1-t1-F

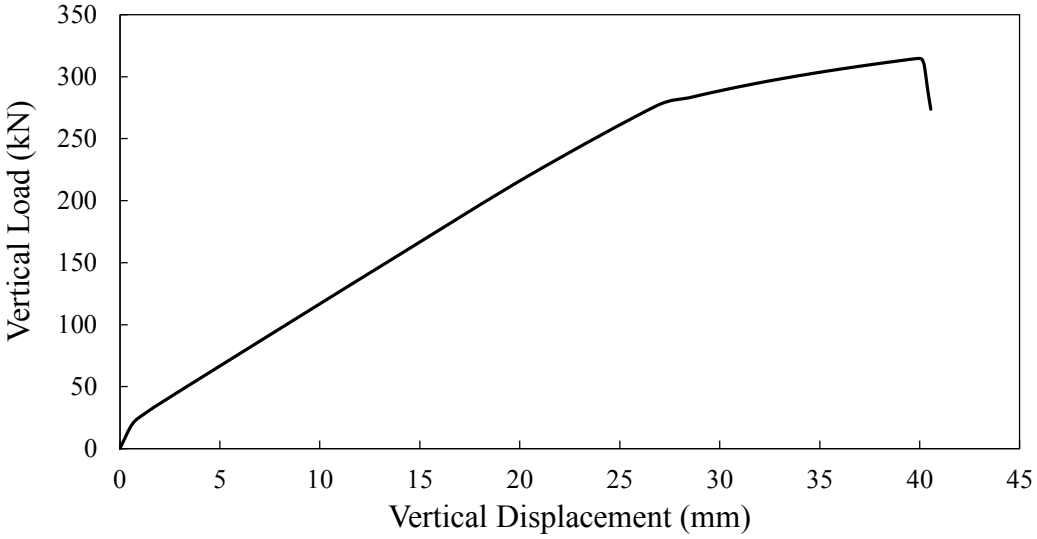

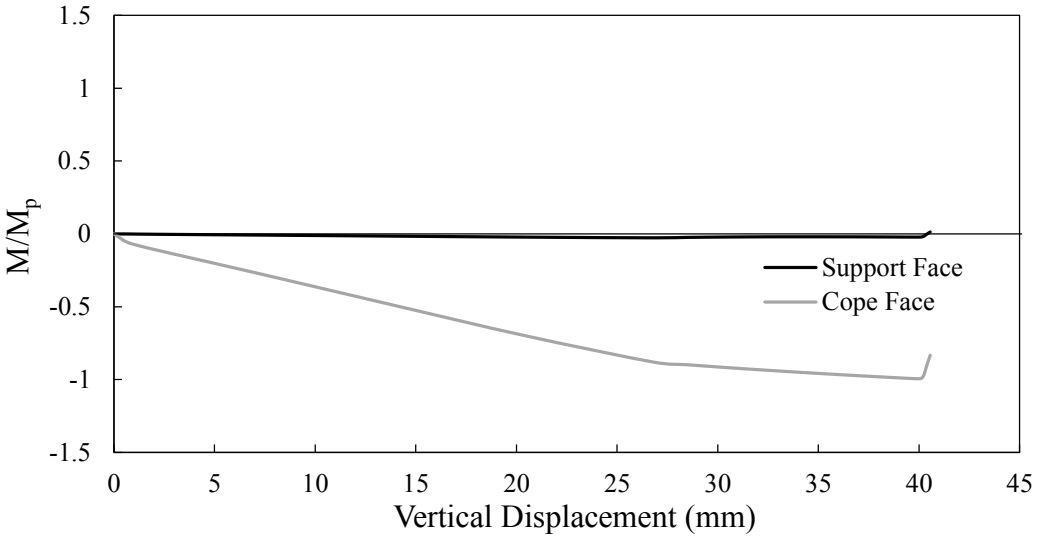

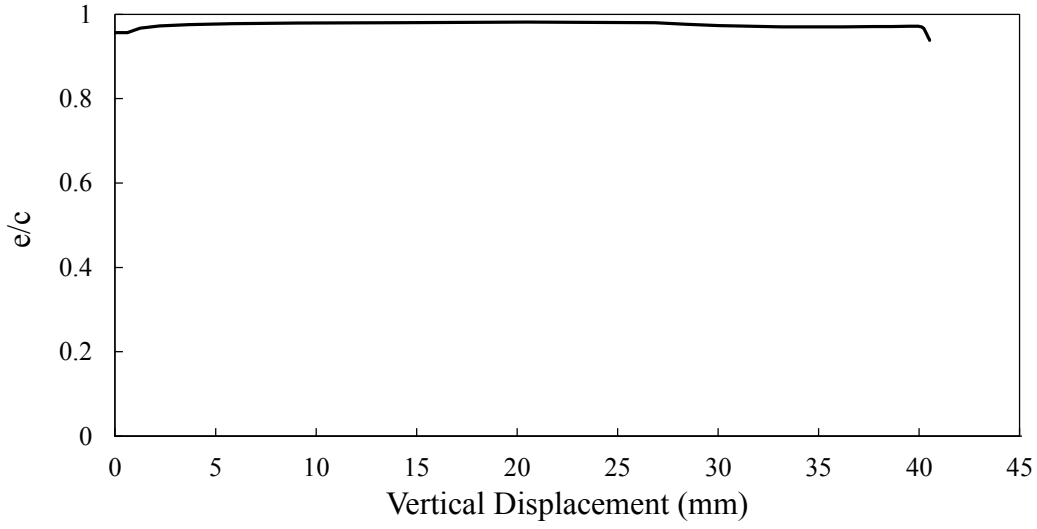

Figure D-8: Model h3-c2-t1-F

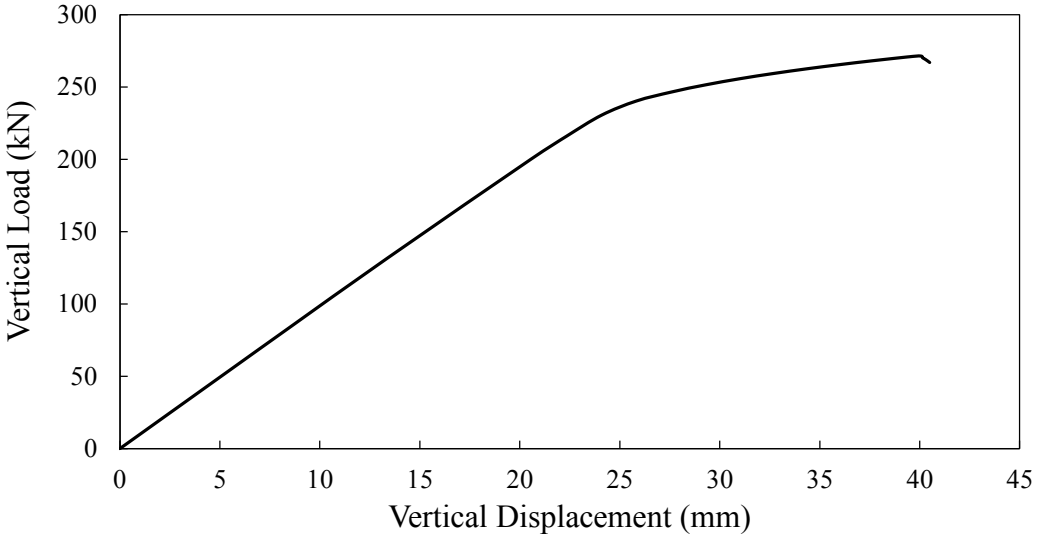

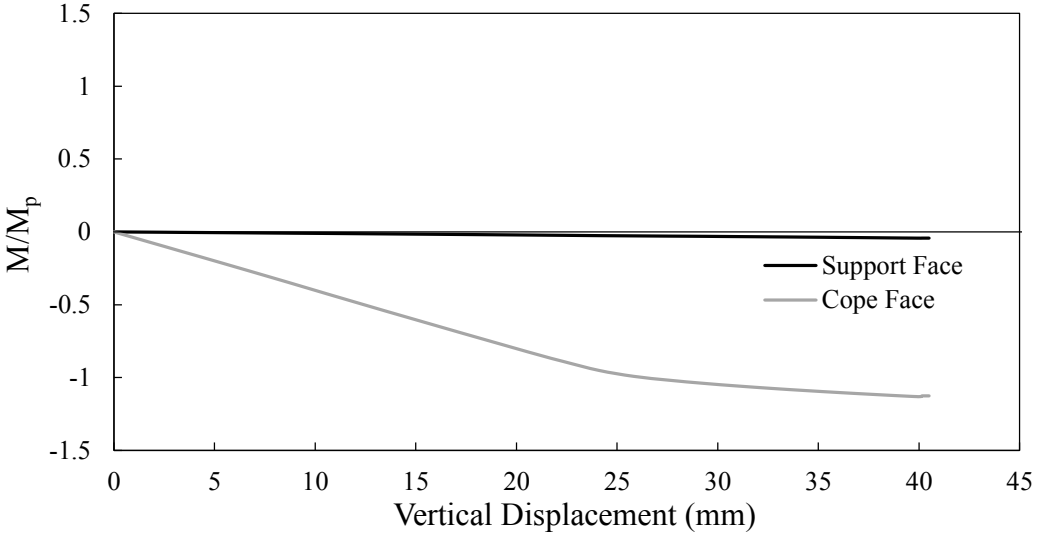

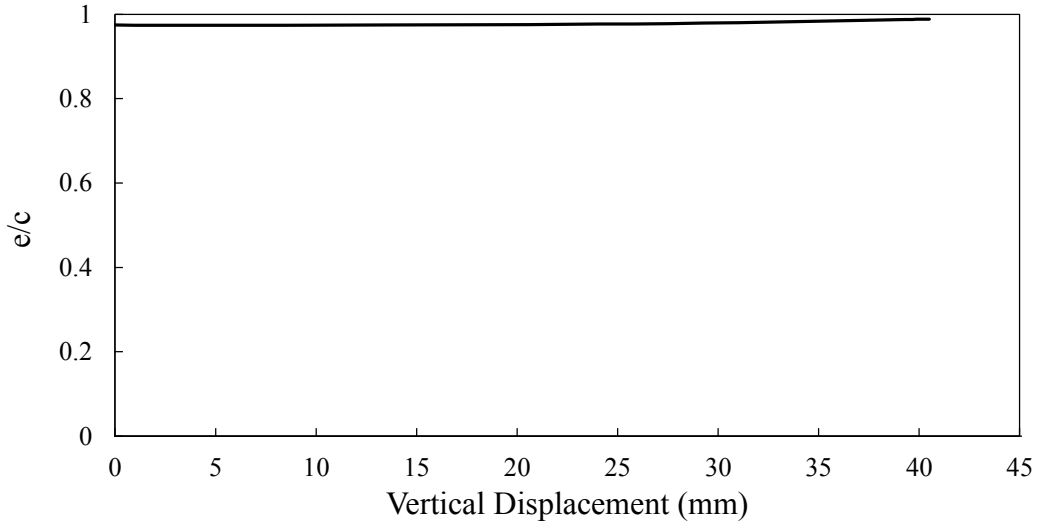

Figure D-9: Model h3-c3-t1-F

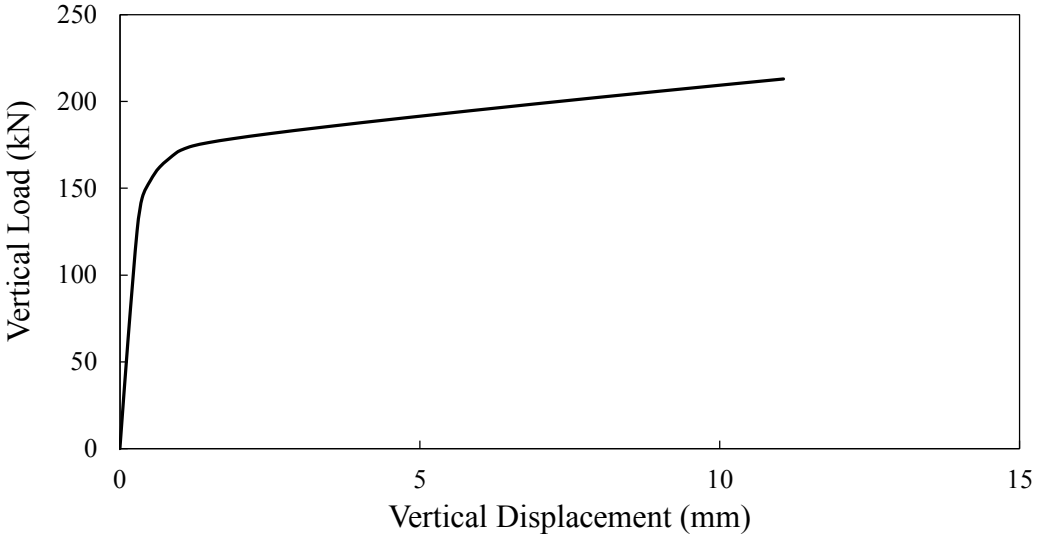

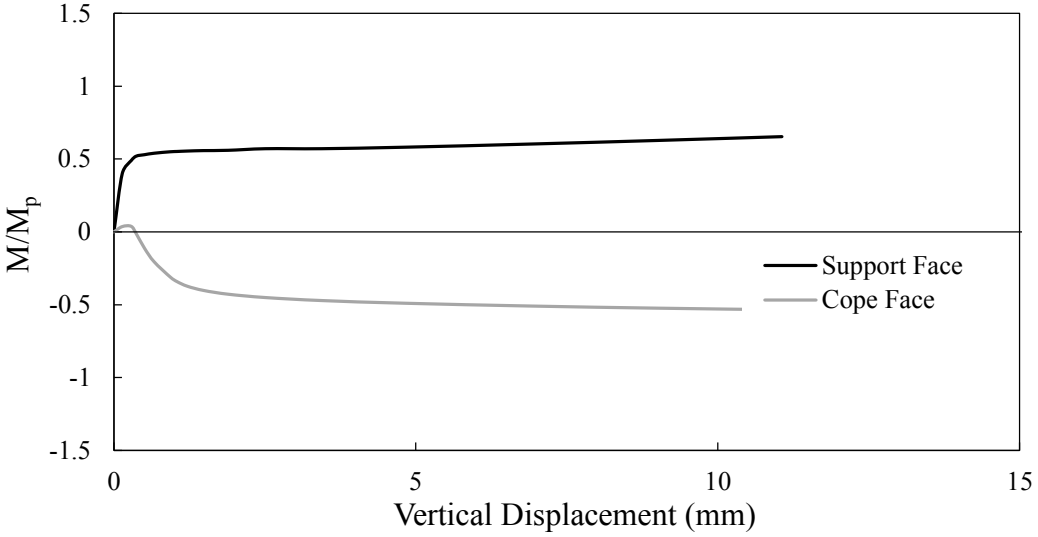

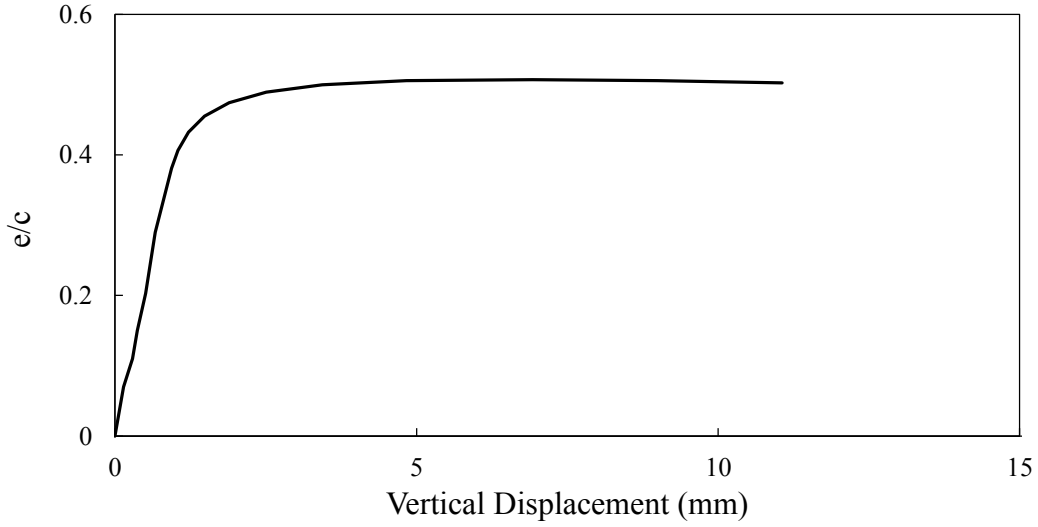

Figure D-10: Model h1-c1-t1-S

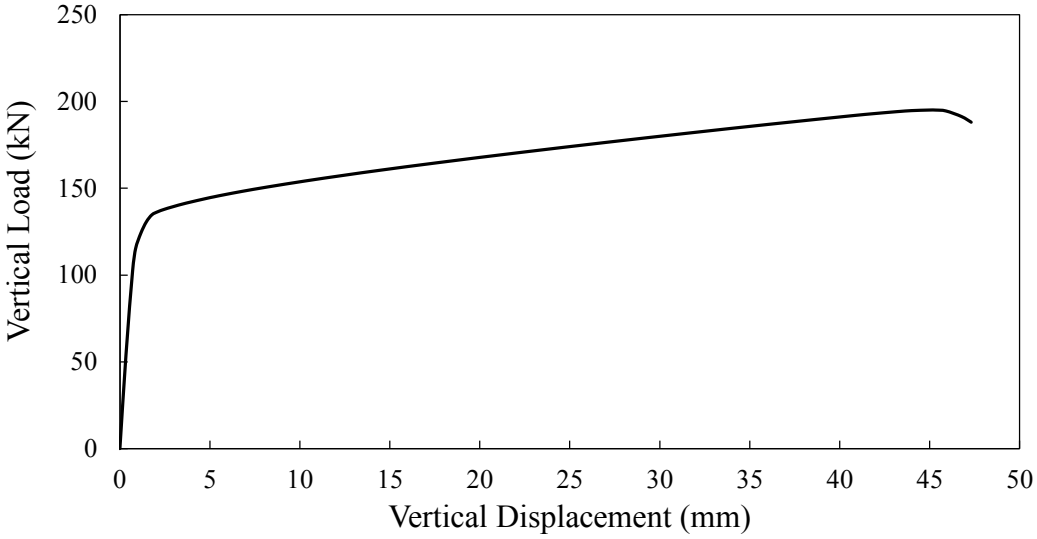

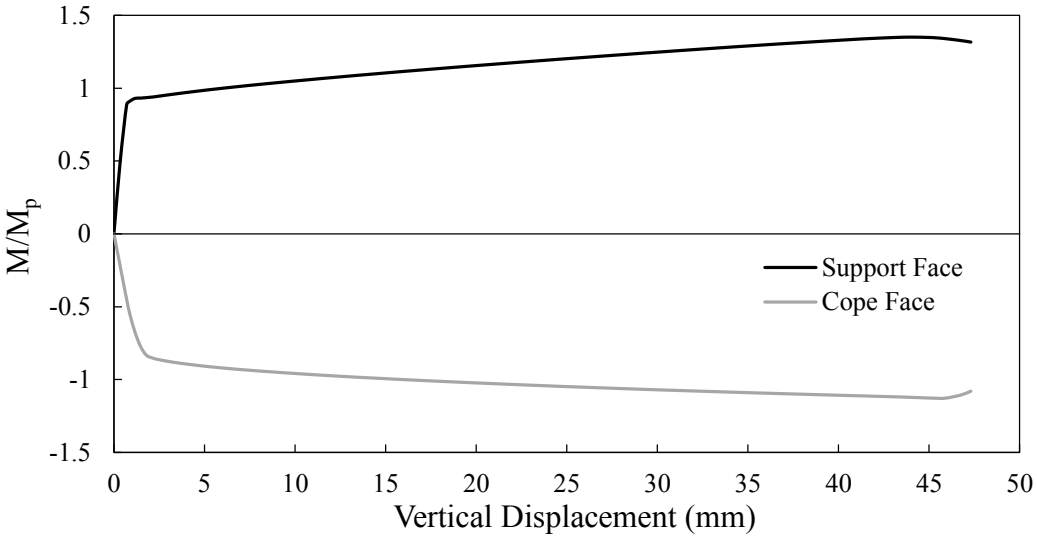

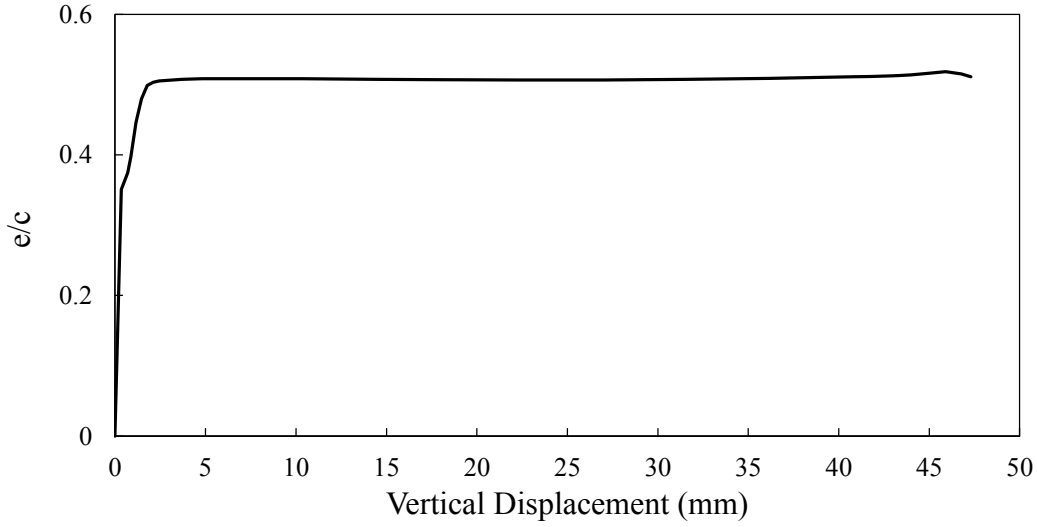

Figure D-11: Model h1-c2-t1-S

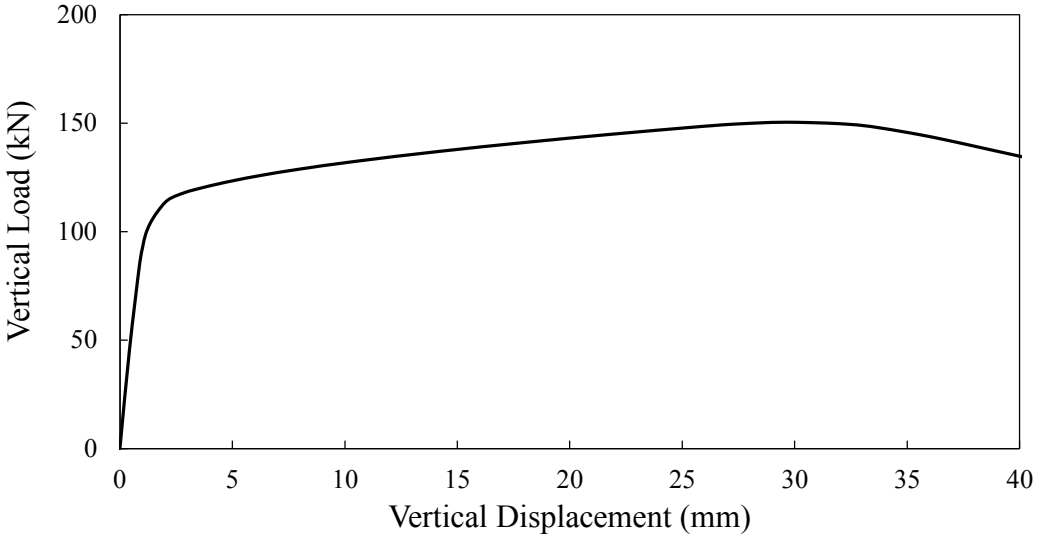

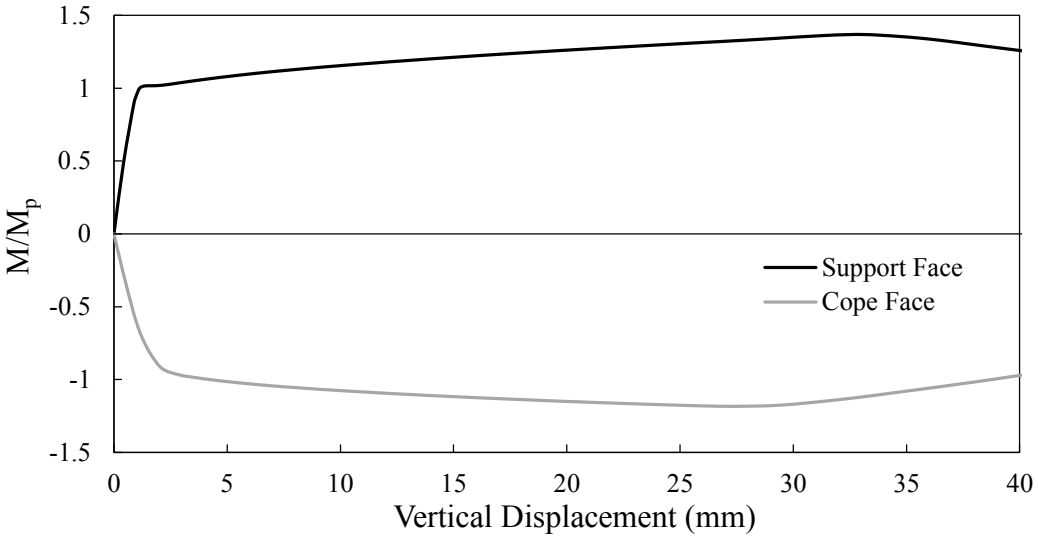

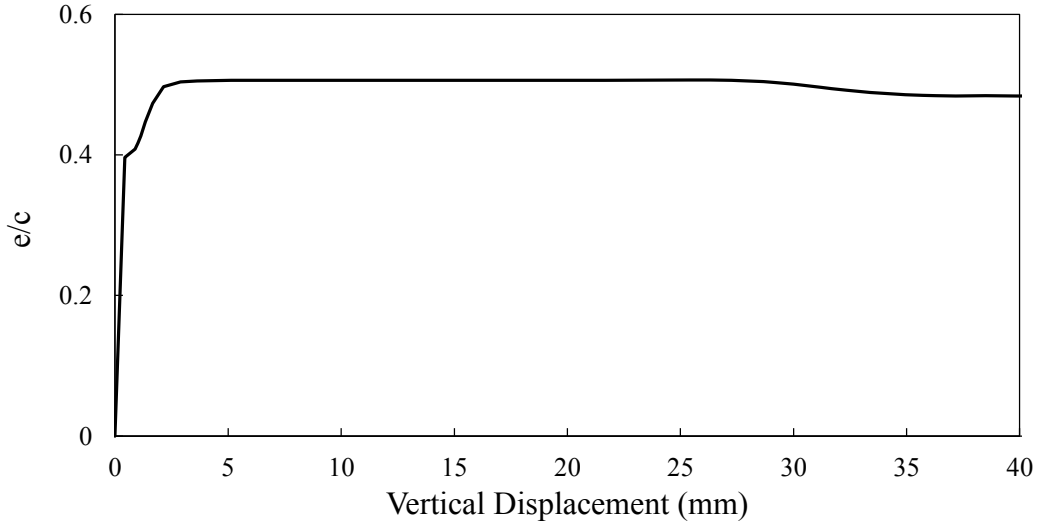

Figure D-12: Model h1-c3-t1-S

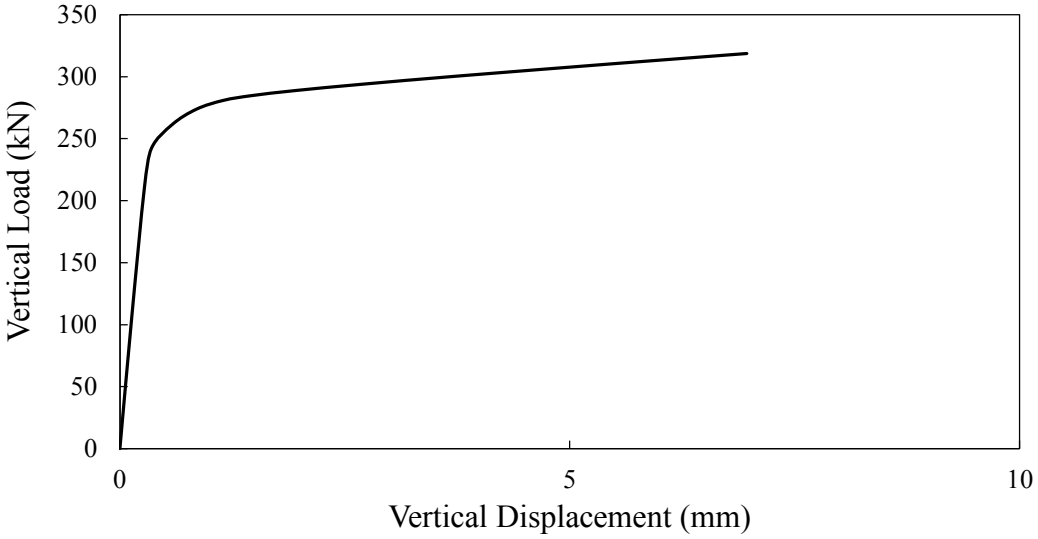

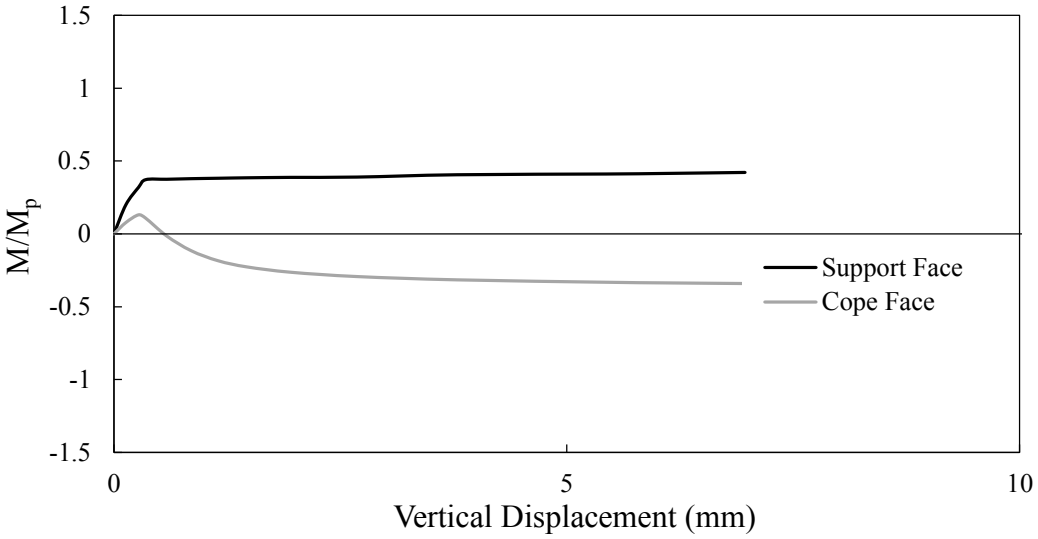

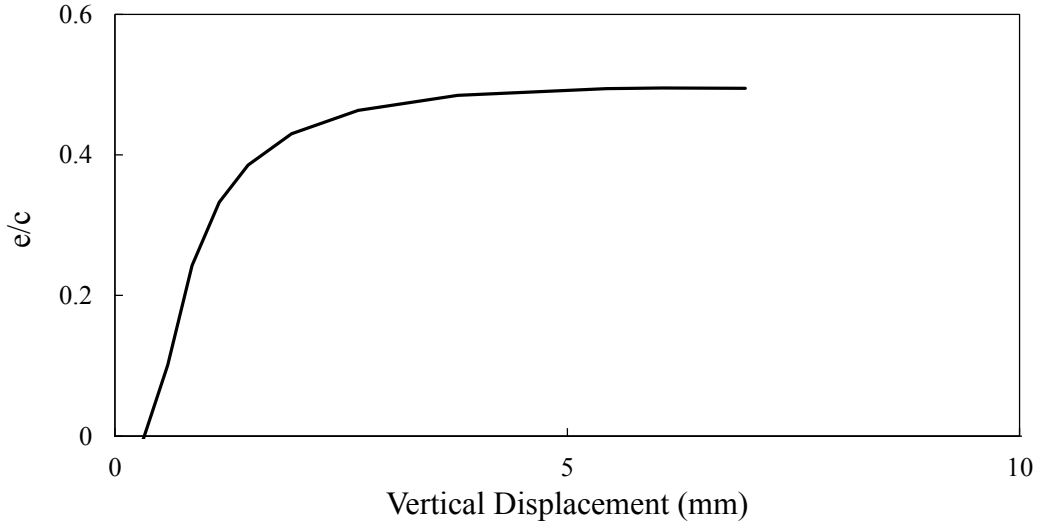

Figure D-13: Model h2-c1-t1-S

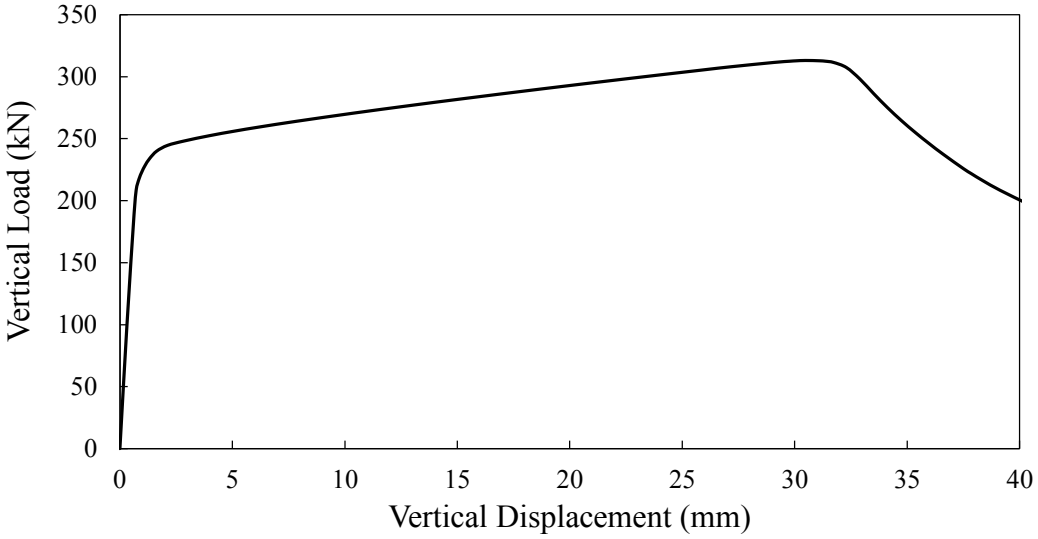

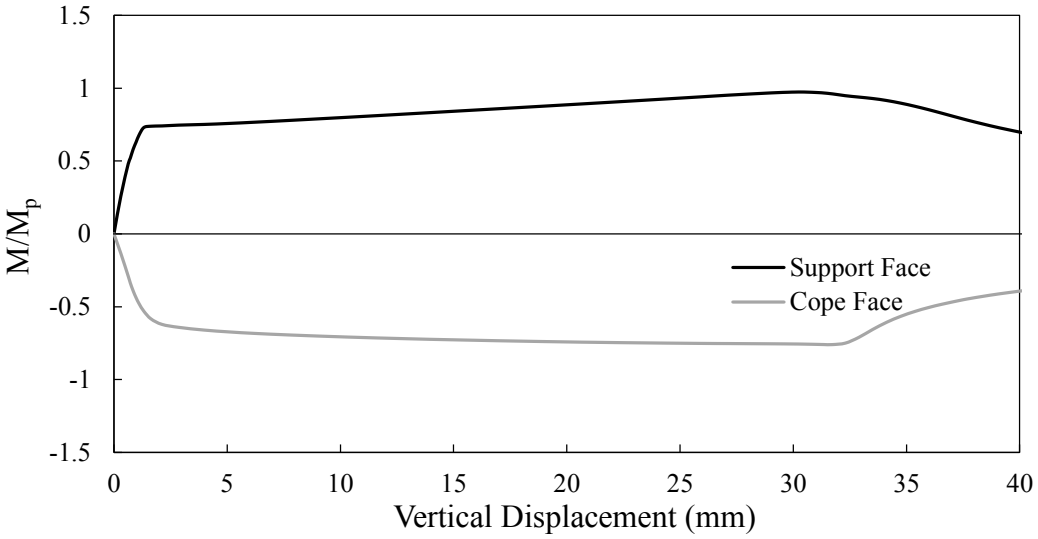

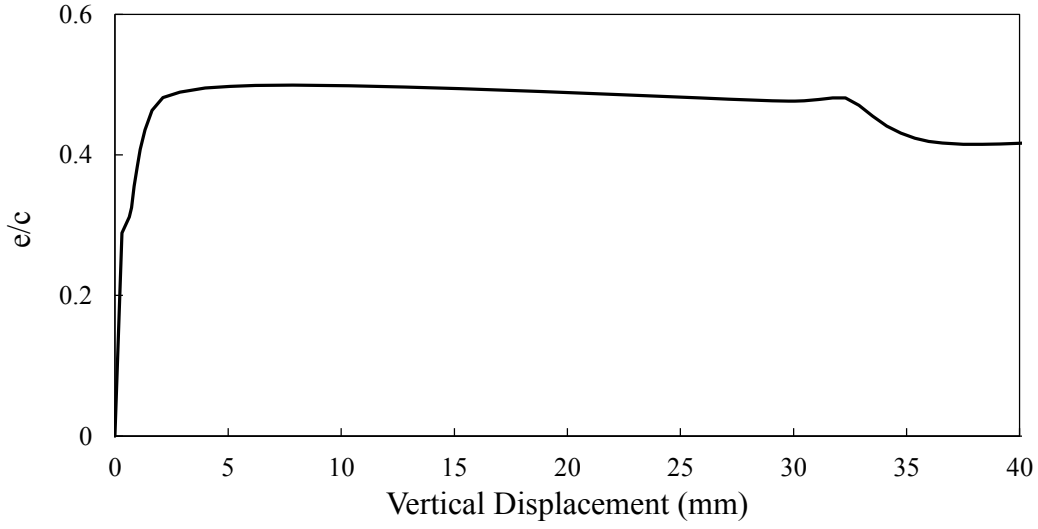

Figure D-14: Model h2-c2-t1-S

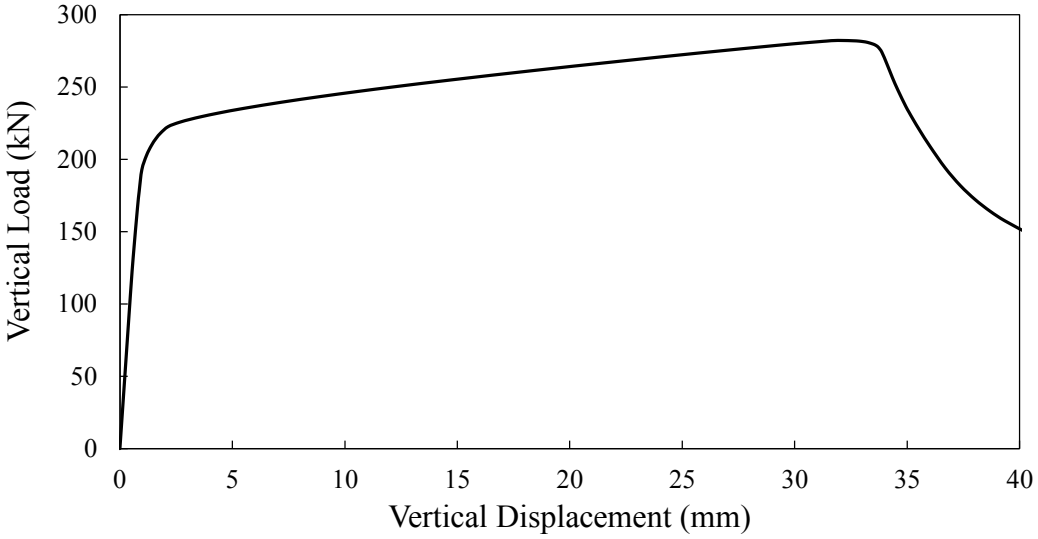

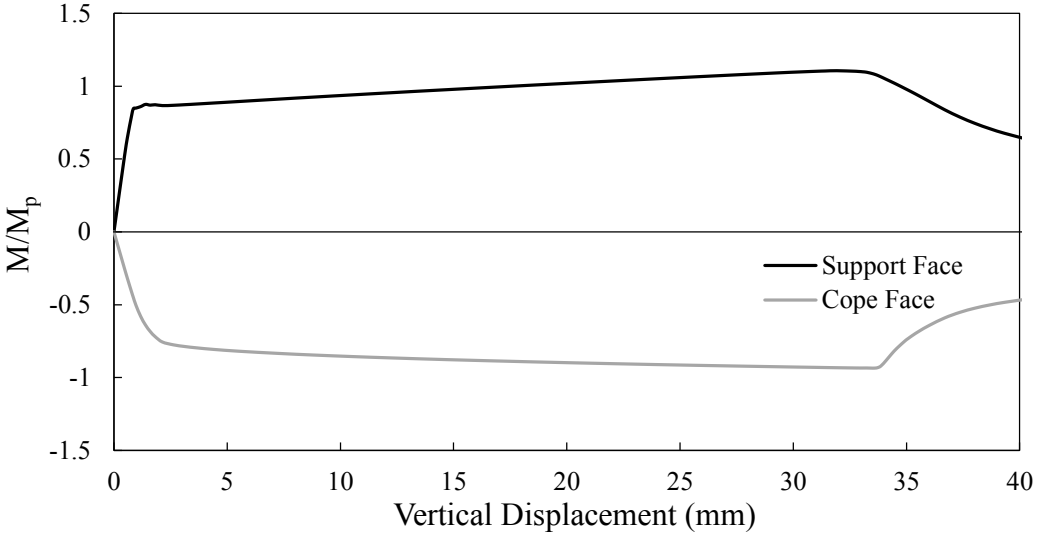

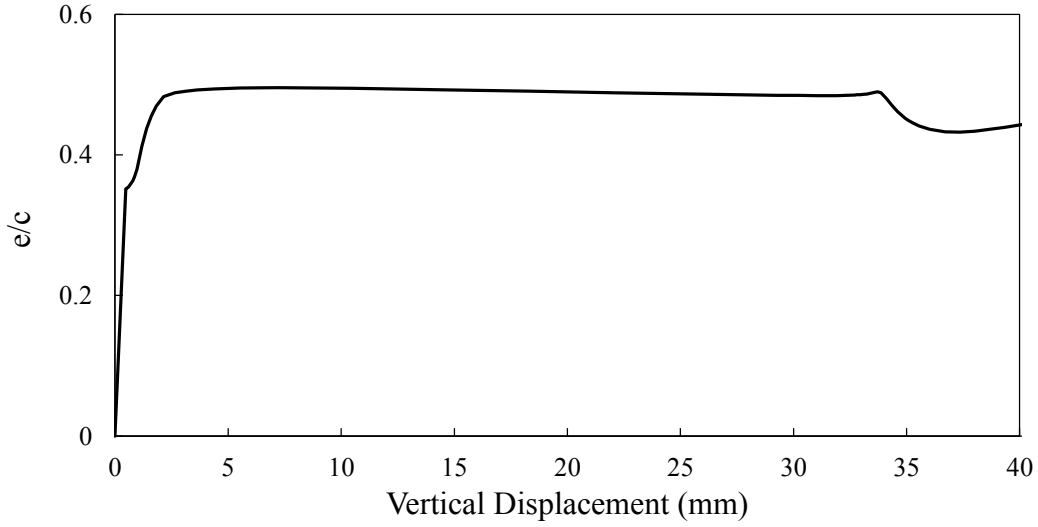

Figure D-15: Model h2-c3-t1-S

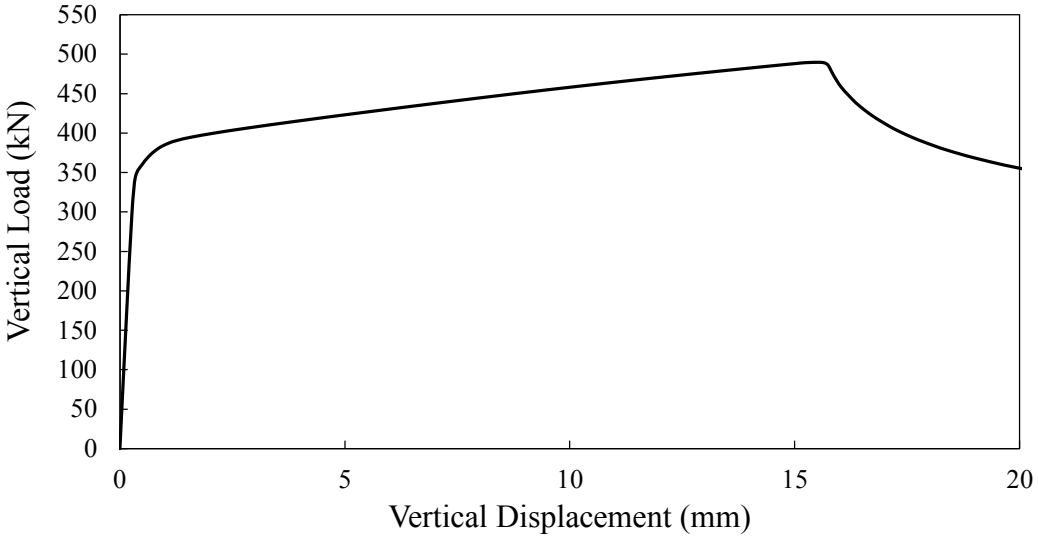

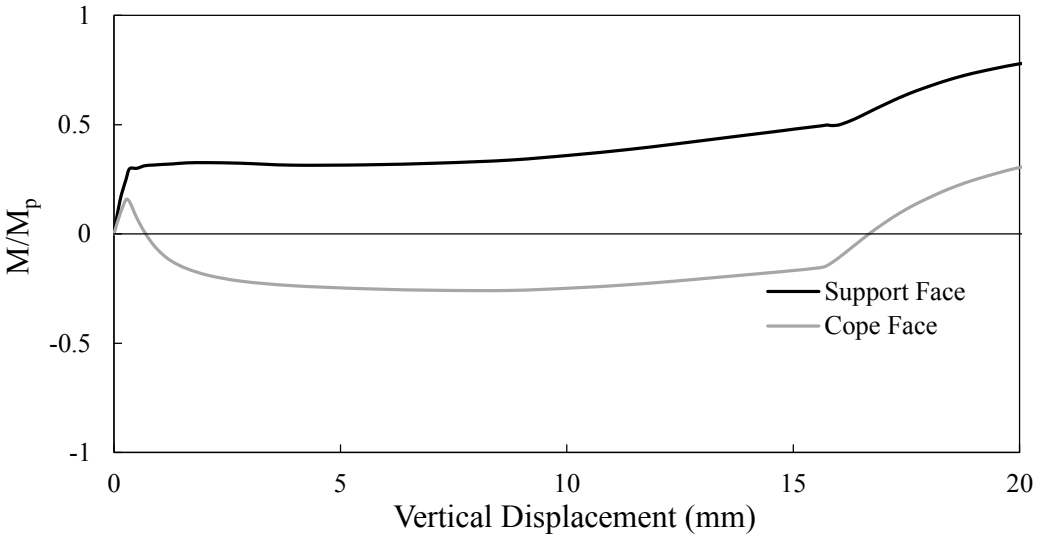

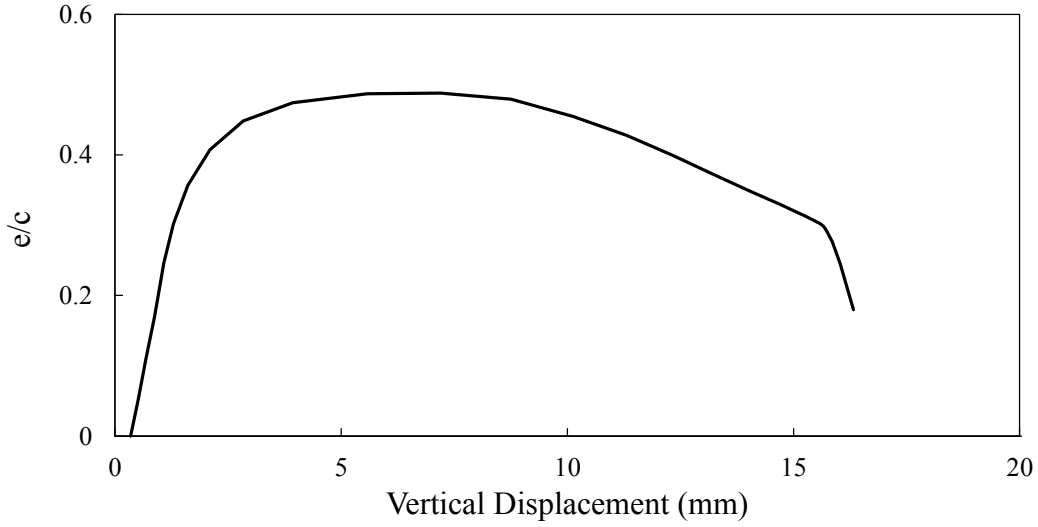

Figure D-16: Model h3-c1-t1-S

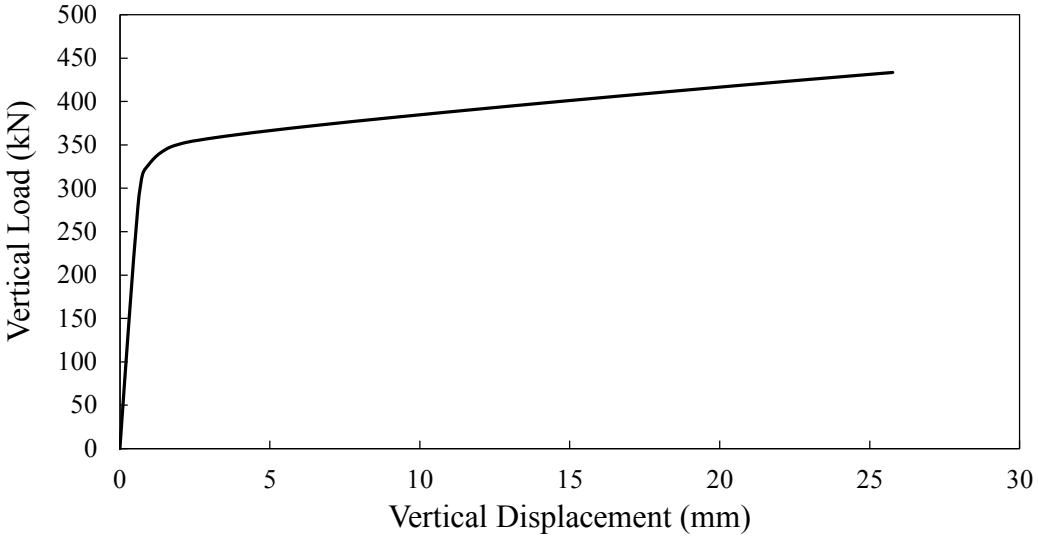

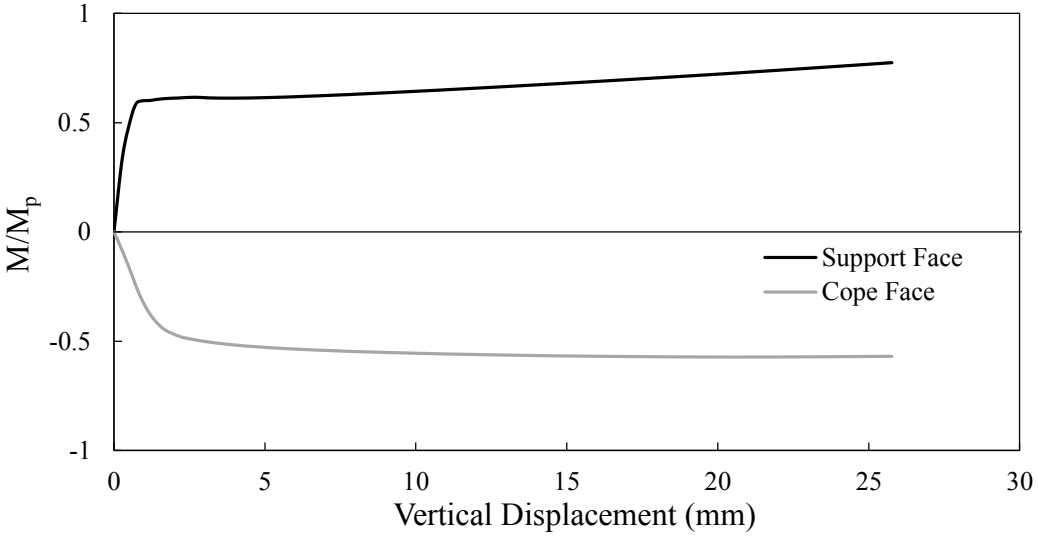

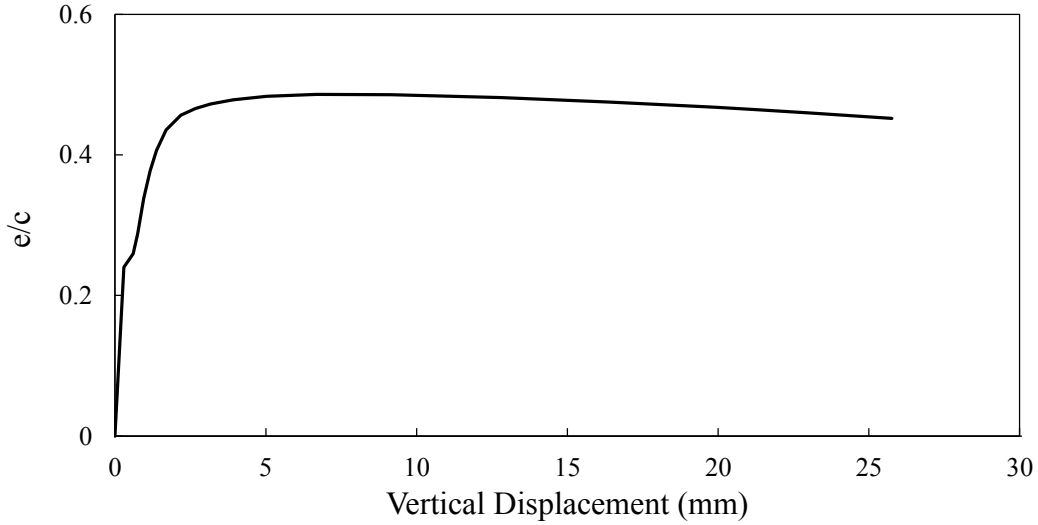

Figure D-17: Model h3-c2-t1-S

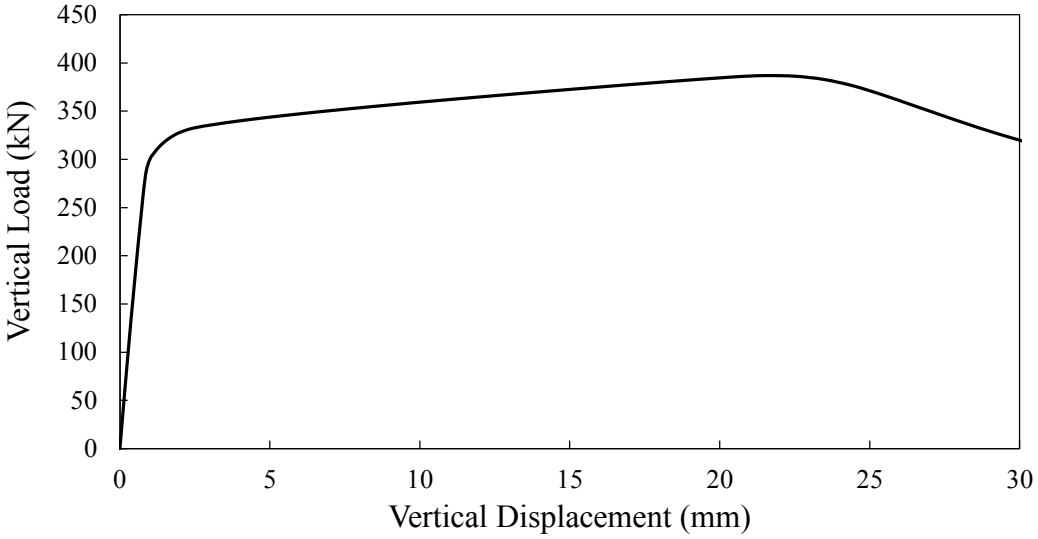

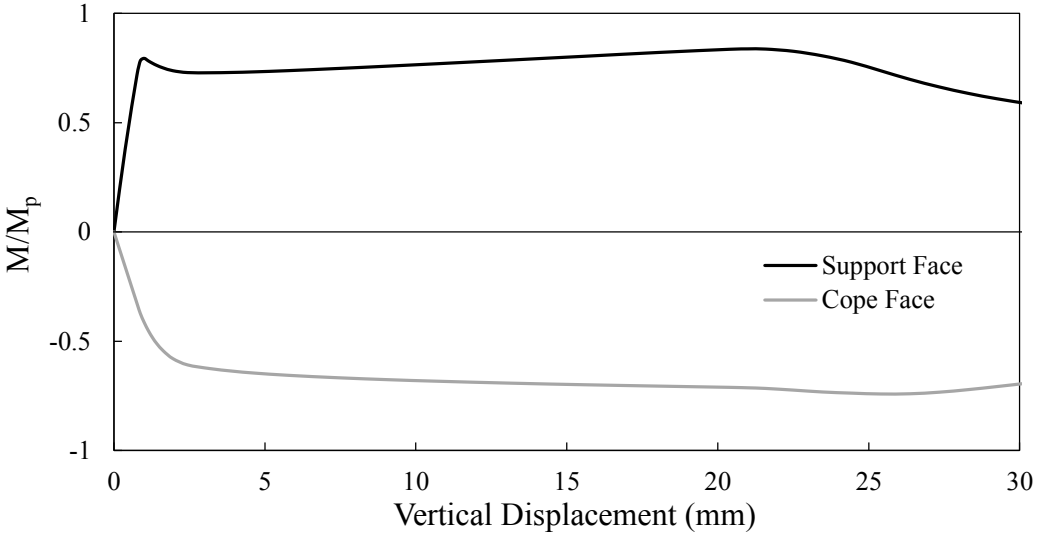

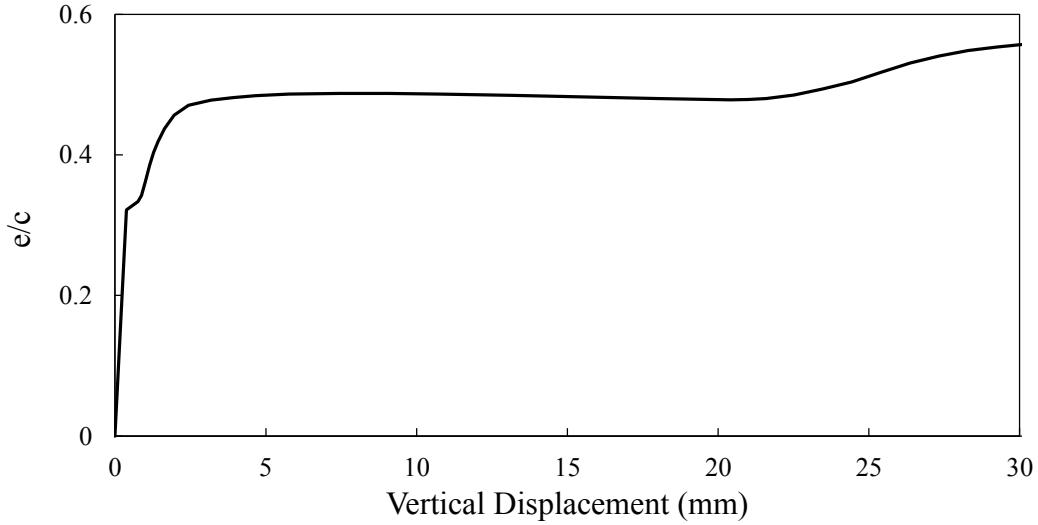

Figure D-18: Model h3-c3-t1-S